POLITECHNIKA LUBELSKA

MONOGRAFIE

# Safety Aspects of Modern Nuclear Power

*edited by*
*Elżbieta Jartych*

Lublin 2016

# Safety Aspects of Modern Nuclear Power

# Monografie – Politechnika Lubelska


Politechnika Lubelska
Wydział Elektrotechniki i Informatyki
ul. Nadbystrzycka 38A
20-618 Lublin

# Safety Aspects of Modern Nuclear Power

edited by
Elżbieta Jartych

Politechnika Lubelska
Lublin 2016

Recenzenci:
prof. dr hab. Mieczysław Budzyński
prof. dr hab. Bronisław Słowiński

Publikacja wydana za zgodą Rektora Politechniki Lubelskiej



ISBN: 978-83-7947-191-1

Wydawca: Politechnika Lubelska
ul. Nadbystrzycka 38D, 20-618 Lublin
Realizacja: Biblioteka Politechniki Lubelskiej
Ośrodek ds. Wydawnictw i Biblioteki Cyfrowej
ul. Nadbystrzycka 36A, 20-618 Lublin
tel. (81) 538-46-59, email: wydawca@pollub.pl
www.biblioteka.pollub.pl
Druk: TOP Agencja Reklamowa Agnieszka Łuczak
www.agencjatop.pl

Elektroniczna wersja książki dostępna w Bibliotece Cyfrowej PL www.bc.pollub.pl
Nakład: 100 egz.

**CONTENTS:**

# PREFACE

Safety of modern nuclear power plants is a key problem of world power engineering and includes many scientific, economic, and technical aspects. From the very beginning of existence of the nuclear power plants, there was a risk of possible accidents; therefore it was necessary to design countermeasures to protect the personnel and the public. There is a basic assumption that the risk associated with the nuclear power should be lower than the risk related to other methods of electricity generation. Despite the extensive experience gained since the beginning of nuclear "era", advanced techniques and tools for safety analysis, there is still a need for research and testing aimed at increasing the safety of nuclear power plants. This monograph has been prepared in order to familiarize the reader with safety problems of nuclear power plant operation and the protection of spent fuel.

In the first chapter the scaling problem was described as one of the most important issues in the safety assessment of the nuclear power plants. Safety assessment process can be achieved by performing numerous simulations using computer codes accepted by the nuclear safety authority. These codes should undergo validation and verification before the safety analysis is performed. The scope of scaling analysis is to define the discrepancy between the experiments and thermal-hydraulics calculations simulating the chosen experiment scenario. In the paragraph some results of the volume scaling analysis and calculations performed for the most dangerous accident, i.e. loss of coolant accident, were presented. To perform thermal-hydraulic analysis of the facilities the RELAP5, code dedicated to light water reactors, was used. The calculations were done on the supercomputer in Computing Centre of the National Centre for Nuclear Research (NCBJ) in Świerk near Warsaw, Poland. The proposed test facility and performed scaling analysis shown the adequacy of the chosen scenario, implemented boundary and initial conditions.

The next section of the monograph gives an overview of modern approaches to multi-physics and multi-scale problems in nuclear industry. Multi-physics problems consider many processes from neutron transport, thermal hydraulics, and nuclear fuel behaviour to the structural mechanics including mechanical loading, brittle fracture, inelastic behaviour, elevated temperatures, neutron irradiation, vibrations and seismic effects. Multi-scale problems relate to the scale from angstroms to kilometres in space and from femto-seconds to years in time. To solve these complicated problems, numerical computations based on superposition techniques and models at different scales are usually needed, this indicates that better mathematical algorithms, multi-resolution techniques for

multi-physics multi-scale problems and integration between different levels are necessary. Through the development of multi-core computer clusters in recent years, performing such advanced simulations of complex physical phenomena become possible. Overriding goal is to reduce the impact of uncertainties coming from the modelling of the physical processes as much as possible. In this paragraph approaches for simulating neutron transport phenomena, thermal hydraulics, structural mechanics, were described. Special attention was paid for thermal hydraulic analyses which cover wide range of scales and phenomena. Computational fluid dynamic was described as a basis of thermal-hydraulic codes with its problems of lack of methodology in the uncertainty quantification of the results and lack of good description of two-phase turbulence model. As an example a safety analysis of a medical facility for Boron-Neutron Capture Therapy (BNCT) was performed, namely analysis of the BNCT converter designed for the use in the MARIA Research Reactor at the NCBJ in Świerk. Thermal hydraulic system and modern computational fluid dynamics codes were applied using one- and three-dimensional approaches, i.e. model without and with consideration of the power distribution, respectively. The comparison and discussions of the results coming from different codes will allow the reader to understand the real challenges of multi-physics, multi-scale modelling.

The continuation of the multi-scale multi-physics problems is the next chapter devoted to neutron transport as the most important aspect of the nuclear core behavior. Hybrid methods which combine Monte Carlo simulations and deterministic methods were applied to solve the neutron transport equation in linear integral-differential form with appropriate boundary conditions. This equation was brought to the integral form which represents the fundamental neutron transport equation for a 3D system with energy dependence and is especially useful in the multiple collision approximation when absorption processes dominate. Then the integral neutron transport equation can be solved numerically with collision probability methods. Approximate methods, i.e. multigroup method, angular dependence approximation, spatial discretization for solving neutron transport equation were described. Existence, uniqueness, and non-negativity of transport equations solutions were also discussed. Multi-group neutron diffusion equations to simulate the whole reactor core with multi-level approach were presented as well. At the end of the paragraph the Authors considered the future and performance of the computational neutron transport methods, i.e. Monte Carlo, deterministic, and hybrid methods with their difficulties, disadvantages, weaknesses and limitations.

A very important issue of nuclear safety measures is taken into consideration in case of nuclear incidents or radiation hazards. The next two chapters are devoted to crisis management and risk assessment in the planning process of nuclear power plants. Firstly, a comprehensive decision support system RODOS installed in national emergency centres in several European countries was described. The system is able to support decisions about the introduction of a wide range of potentially useful countermeasures mitigating the consequences of nuclear accidents with respect to health, the environment, and the economy. Moreover, the major objective of the RODOS system is training and education in radiological protection and emergency management. The structure and functions of the system were described as well as the appropriate interfaces offered to plant safety, radiological and meteorological networks. On the basis of the on-line and prognosticated meteorological data RODOS system provides continuously updated fast and comprehensive assessments of the radiation situation after accidental releases of radioactive material into the atmosphere and/or the aquatic environment. Moreover, the system allows estimation of collective and individual doses via all external and internal exposure pathways of importance during and after the passage of the radioactive cloud. At the end of the section a special attention was paid for the inverse problem, namely finding a location of the release basing on the information coming from the monitoring network. Using the Bayesian approach and algorithm with Markov chain Monte Carlo sampling, the procedure of the contaminant source localization was presented as an example.

The next chapter is devoted to safety assessment during nuclear power plant designing process. The main aim of the modern nuclear power engineering is facing to ensure safety and security of the nuclear facilities and to convince people that the risks associated with nuclear installations are much lower than the risks to life and health arising from everyday lives. Until now Deterministic Safety Assessment (DSA) and Probabilistic Safety Assessment (PSA) methodologies were elaborated, used and developed. New methodology of an Integrated Risk Informed Decision Making (IRIDM) was proposed and described according to the recent documents of the International Atomic Energy Agency and U.S. Nuclear Regulatory Commission. The main features, advantages and limitations of IRIDM were presented. The major factors influencing a formal implementation of the IRIDM methodology within the regulatory organization were indicated and discussed.

The last part of the monograph concerns the problem of the nuclear radioactive waste. The main goal of radioactive waste management is to control and account for the radioactive waste to protect human health and the

environment as well as the future generations. Firstly, the metamict minerals as potential forms for immobilization of high-level nuclear waste (HLW) were described from their local structure point of view. In this purpose, the Mössbauer spectroscopy was applied as a very useful technique to study the local environment of $Fe^{2+}$ and $Fe^{3+}$ ions in iron-bearing metamict phases. Basics of Mössbauer spectroscopy were presented and then metamict minerals, i.e. allanite, perrierite, gadolinite, davidite, columbite, samarskite were described with their age, chemical composition and hyperfine interactions parameters. On the basis of the performed studies the mechanism of the metamictization process was explained and candidates as potential forms for immobilization of HLW were indicated.

Safety requirements on storage and disposal of radioactive waste in Poland were presented in the last chapter of this monograph. Fundamental principles of radioactive waste classification and management based on safety standards were described. Storage conditions for radioactive waste and spent nuclear fuel were quoted. Requirements for surface and deep of repositories were presented. At the end of the paragraph nuclear waste sources in Poland were described and the data concerning the amount of solid and liquid wastes in years 2001-2014 were collected and presented.

The monograph tried to bring some safety problems of modern nuclear power plants, is working on a team of specialists. I hope that this position of literature in some way contribute to the enrichment of knowledge on these important issues.

*Elżbieta Jartych*

# CHAPTER 1

# Integral Test Facilities Scaling Issue in the Safety Analysis of the Nuclear Power Plants

Eleonora Skrzypek, Maciej Skrzypek
National Centre for Nuclear Research (NCBJ)
Andrzeja Sołtana 7 Str., 05-400 Otwock, Poland
eleonora.skrzypek@ncbj.gov.pl

## Abstract

Scaling issue in safety analysis of the nuclear power plants (NPP) is very important and can be used at the various levels of the safety assessment, as well as while Integral Test Facility designing. The safety analysis is the key element for the approval of the NPP design by the national nuclear safety authority and the issuing operating license for it. The scaling analysis (similarity analysis) is implemented to confirm the correctness of the following issues: the prepared model, the thermal-hydraulic code, code user and performed analysis of the selected NPP. While performing the scaling analysis, few concerns appear, such as: the choice of the approach to the analysis: time-reducing scaling, volume scaling or idealized time-preserving scaling. In the performed analysis the reproduced scaled scenario for the Integral Test Facility is the LOFT (Loss of Fluid Test) facility. The scaling $K_V$ analysis should be in the agreement with the experimental results and parameters should be predicted within reasonable shifts estimated with known uncertainties coming from various sources. The accomplished scaling analysis is, when the judgement of the Relevant Thermal-hydraulic Aspects (RTAs) is achieved, with the acceptable results.

## 1. Introduction

### 1.1. Scaling analysis context

Scaling is one of the important issues, not only in the safety assessment of the nuclear power plants and code assessment, but also in the designing process of test facilities. It is used widely to determine the correctness of the results of thermal-hydraulics codes and to propose a proper geometry of the test facilities, in way to predict in the best manner the occurring phenomena during particular accident scenario. One of the possible scenarios is Large Break Loss of Coolant

Accident (LBLOCA) with the Double Ended Guillotine Break (DEGB). This kind of the accident scenario was part of the LOFT Project, which was held originally by the US Nuclear Regulatory Commission, and was continued as an international collaboration project under the aegis of the OECD Nuclear Energy Agency (NEA) in 1978 to 1982 [1].In this paper the way of obtaining results from $K_V$ scaling analysis (of the experiment L2-5 LOFT to the ZION nuclear power plant) will be given as an example of the scaling analysis application in the NPP assessment. This kind of procedure can be classified as a part of the uncertainty analysis method. Loss-of-Fluid Test (LOFT) was a project that was a part of the Three Mile Island Reactor Pressure Vessel Investigation Project and as a nuclear test facility was able to address several configurations of LOCA. The results were significant achievement and influenced the improvement of the international database of large-scale experimental data on reactor safety.

### 1.2. The history of the scaling analysis in nuclear engineering

Scaling was widely known in the nuclear reactor technology especially through the overall development of the test facilities in the thermal-hydraulic research field. All these activities were dedicated to the advancement in the design scaling methodology. The part of the licensing of a new-built or operating power plant is the demonstration of its safety mainly by means of the experiments and the usage/application of the computer codes. The codes in the past had capability to simulate the scenarios from the scaled down facilities with good accuracy, but meanwhile the issue of translating this knowledge to the NPP size appeared. That is why as a result in the field of the thermal-hydraulic codes there was a need for the formation of theirs scaling capability assessment. There was a successful programme carried out by the United States Nuclear Regulatory Commission (the equivalent of the Polish National Atomic Energy Agency – PAA) in 1980s which recognized the possibility to create the user guides for the code scaling assessment – Code Scaling, Applicability and Uncertainty (CSAU). This methodology in one chapter focuses on the possibility of the scaling usage for licensing in the safety analysis of the NPP. In the beginning the project referred to the specific accident scenario in NPP –BE LBLOCA (Best Estimate LBLOCA). It can also be successfully applied for the other types of the accidents. The study was focused on the capabilities of the computer thermal-hydraulic codes to scale up phenomena taken from the small-scale facilities to NPPs size [2].

## 1.3. Safety assessment and safety analysis as a part of the licensing process of nuclear power plants

Safety analysis of nuclear power plants (NPPs) is a part of the safety assessment process that can be achieved by performing numerous simulations using accepted by the nuclear safety authority computer codes. The codes predict the behaviour of the thermal-hydraulic parameters in the primary and secondary side of the nuclear power plant. The thermal-hydraulic parameters are evaluated and assessed by determining the safety margins, which define the difference between the calculated value and the safety limit, set by the national safety authority.

The base of the safety analysis is the use of the computer codes, which should undergo validation and verification, before the safety analysis of the NPP. The verification of the computer code is done in order "to demonstrate that the code design conforms to the design requirements" [3]. In general the verification is planned to show the efficiency of the translation of the ruling physical equations and data to the code language. The validation is a process outcome of which is to present the capability of the code to predict (in realistic or conservative manner) the system behaviour in terms of selected parameters. The process involves the execution of the test calculations:

a) *Basic tests*. These kinds of experiments are not always related in the direct way to the nuclear power technology but the results derived from them are transferred to the correlations development. In the correlations the relevance between parameters is investigated empirically.

b) *Separate effect tests*. Separate experiments address the specific phenomena which are predicted to be present during NPP operation or accident. These kinds of tests do not cover the whole spectrum of the phenomenon, but focus on the specific occurrences description. The idea of separate effect tests is to replicate the changes in the system in the full scale. Codes which are adequately representing the experiments results can be qualified to the determination of the correct solution, in the different scale systems, but with the same phenomena presence. The separate effect tests are designed to determine the laws and equations ruling specific phenomenon in the various parts of the NPPs.

c) *Integral tests*. Those experiments are dedicated to the nuclear power plants operation and transients. These tests are made usually in scaled down size with mainly preserved height and components simulators, because of the high

economic cost of the facility in full scale. The aim is to represent all of the processes in the chosen scenario with the highest achievable accuracy.

d) *Nuclear power plant level tests and operational transients*. These tests and experiments are highly valuable for the safety of the NPPs. The tests are performed with the reasonable margin of safety and are the key issues in the NPP model assessment [4].

These test calculations are performed in the two different situations. Firstly, they are performed by the code developer and secondly the code user. The second execution is an independent code assessment and it is a process undertaken by the code user to correlate the capabilities of the Integral Test Facilities (ITF) modelling in the specified code to the development of the NPP model, by means of the scaling analysis.

# 2. Scaling analysis

## 2.1. Scope and issues of scaling analysis

Whenever there is a necessity for usage of computer codes in the licensing of the NPPs the qualification and verification of the code, code use process and code user appear. That is why the scope and issues of the scaling analysis need to be formulated and deeply understood. Scaling analysis is a part of the process, scope of which is to define the discrepancy between the performed experiments in nuclear thermal-hydraulics and calculations simulating the chosen experiment scenario.

This part of the assessment of the code can be done by the independent code users that are why their abilities and experience are crucial in this particular part of the model qualification. The scope and aim of the scaling in the licensing process of the NPP is shown in the Figure 1.1.

The scaling is visibly beneficial and usable during all stages of the licensing process of the nuclear power plant, but with the restriction that the user of the code should be conscious about the code applicability to the specific domain and its capabilities to reproduce predicted phenomena [5].

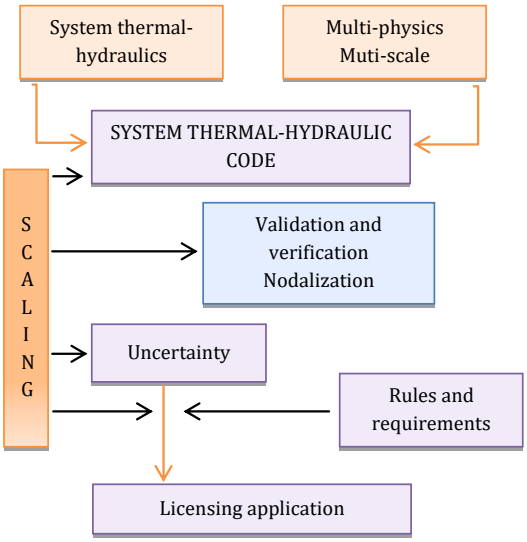


Figure 1.1 The definition of the aim of scaling [5].

The Figure 1.2. represents the process of the code assessment with the internal and external qualification, respectively by the code developer and the code user. The code is required to be able to perform the "similarity analysis" – the scaling analysis. The similarity check is the presentation of the correctness of the input NPP nodalization to undergo the scenario from the ITF experiment.

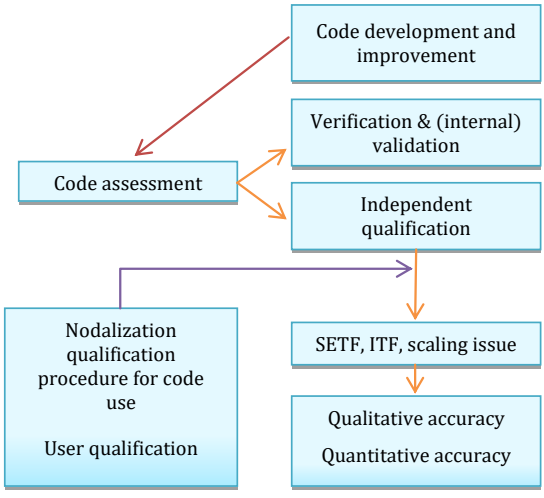


Figure 1.2 Internal and external code qualification [4].

In the scaling analysis there are some conditions that are obligatory to be met. These are in particular: the initial and boundary conditions taken exactly from the experiment and implemented to the NPP model, while the performance of the similar accident scenario, as done in the ITF. The input file with the defined safety systems especially HPIS (High Pressure Injection System), LPIS (Low Pressure Injection System) or accumulator is set for the conditions of the experimental facility. The NPP with its design and power is in all cases much larger than the test facilities created through the decades of the research in the nuclear technology. But the results from the scaled simulation should reproduce the relevant phenomenon in the experiment to the larger scale [4]. Those phenomena are called the Relevant Thermal-hydraulic Aspects (RTAs) and their examples are presented in the Table 1.1. These are the key elements that are indicating the agreement of the scaled calculation with the experiment and are judged by the independent expert qualitatively and quantitatively. In the table the phenomena for the current generation of the reactors are presented. These reactors are for example the evolutionary reactors: ABWR (General Electric), EPR (NPI, Parent Co.: Framatone and Siemens), passive reactors: AP–600 (Westinghouse), SBWR (General Electric) or other advanced reactors like CANDU-3 (Atomic Energy of Canada Limited) [6].

Table 1.1 Relevant thermal-hydraulic phenomena identified for the current generation reactors according to the [6].

| | | |
|---|---|---|
| 0 | Basic phenomena | 1. Evaporation due to depressurization<br>2. Evaporation due to Heat Input<br>3. Condensation due to pressurization<br>4. Condensation due to Heat Removal<br>5. Interfacial Friction in Vertical Flow<br>6. Interfacial Friction in Horizontal Flow<br>7. Wall to Fluid Friction<br>8. Pressure Drops at Geometric Discontinuities<br>9. Pressure Wave Propagation |
| 1 | Critical Flow | 1. Breaks<br>2. Valves<br>3. Pipes |
| 2 | Phase Separation/Vertical flow with and without mixture level | 1. Pipes/Plena<br>2. Core<br>3. Downcommer |
| 3 | Stratification In Horizontal Flow | 1. Pipes |
| 4 | Phase Separation At Branches | 1. Branches |

| | | |
|---|---|---|
| 5 | Entrainment/Deentrainment | 1. Core<br>2. Upper Plenum<br>3. Downcommer<br>4. Steam Generator Tube<br>5. Steam Generator Mixing Chamber (PWR)<br>6. Hot Leg with ECCI (PWR) |
| 6 | Liquid-Vapour Mixing with Condensation | 1. Core<br>2. Downcommer<br>3. Upper Plenum<br>4. Lower Plenum<br>5. Steam Generator Mixing Chamber<br>6. ECCI in Hot and Cold Leg (PWR) |
| 7 | Condensation in Stratified Conditions | 1. Pressurizer<br>2. Steam generator Primary Side (PWR)<br>3. Steam Generator Secondary Side (PWR)<br>4. Horizontal Pipes |
| 8 | Spray Effects | 1. Core (BWR)<br>2. Pressurizer (PWR)<br>3. Once-Through Steam Generator Secondary Side (PWR) |
| 9 | Countercurrent Flow/Countercurrent Flow Limitation | 1. Upper Tie Plate<br>2. Channel inlet Orifices (BWR)<br>3. Hot and Cold Leg<br>4. Steam generator Tube (PWR)<br>5. Downcommer<br>6. Surgeline (PWR) |
| 10 | Global Multidimensional Fluid Temperature, Void and Flow Distribution | 1. Upper Plenum<br>2. Core<br>3. Downcommer<br>4. Steam Generator Secondary Side |
| 11 | Heat Transfer | 1. Natural or Forced Convection (Core, Steam Generator, Structures)<br>2. Subcooled/Nucleate Boiling (Core, Steam Generator, Structures)<br>3. DNB/Dryout (Core, Steam Generator, Structures)<br>4. Post Critical Heat Flux (Core, Steam Generator, Structures)<br>5. Radiation (Core)<br>6. Condensation(Steam Generator, Structures) |
| 12 | Quench Front Propagation/ Rewet | 1. Fuel Rods<br>2. Channel Walls and Water Rods (BWR) |
| 13 | Lower Plenum Flashing | |
| 14 | Guide Tube Flashing (PWR) | |
| 15 | One and Two Phase Impeller-Pump Behaviour | |
| 16 | One and Two Phase Jet-Pump Behaviour (BWR) | |

| | |
|---|---|
| 17 | Separator Behaviour |
| 18 | Steam Dryer Behaviour |
| 19 | Accumulator Behaviour |
| 20 | Loop Seal Filling and Clearance (PWR) |
| 21 | ECC Bypass/Downcommer Penetration |
| 22 | Parallel Channel Instabilities (BWR) |
| 23 | Boron Mixing and Transport |
| 24 | Noncondensable Gas Effect (PWR) |
| 25 | Lower Plenum Entrainment |

The reason for the scaling is associated with the size of the experiments. This comes from the fact that all of the experiment could not be performed and designed at full scale. The main reason for this issue is the cost of the experimental facility, where according to the OECD-NEA [1] the budget of some exemplary project – the OECD/NEA LOFT Project was estimated to be US$ ~100.0 million. This facility was the biggest facility with the loaded nuclear fuel into the reactor core which made the experiment budget more expensive. Other work done for the correct use of the test facilities was done by OECD/NEA/CSNI by establishing the validation matrices from the SETF – Separate Effect Test Facilities (SETF-CCVM (Containment Code Validation Matrix)) and ITF (ITF-CCVM) for the thermal-hydraulic codes [7], [8]. This made the data gathered from the experiments systematized and possible to employ in the code validation as also the qualification of the model of the NPP. In addition this established the connection between the design of the test facilities and their usage for the purposes of the NPP licensing by means of the safety analysis with thermal-hydraulic codes.

## 2.2. Approaches to the scaling analysis

When the subject of the scaling of the nuclear technology appears, the approaches to the scaling design of the test facilities should be mentioned. The understanding of the ITF and SETF design is translated into the timing and occurrence of the phenomena characteristic to the Design Basis Accidents (DBAs) and transients. In the literature there are three different concepts of the design scaling [4], [5]:

a) The time-reducing scaling.

The objective is to scale the facility in such manner that all relevant phenomena in time-reduced scaling compared to the real size NPP are preserved. All geometrical dimensions are scaled by fixed factor, which is of the same value that factor for the time scaling between events. This solution is beneficial

while designing the test facility, which can be described “by the negligible body forces induced by the gravity acceleration” [4]. These forces need to have weaker impact on the phenomena occurrence than the local pressure differences.

b) Time preserving scale.

Time preserving scale is also called the volume scaling. The test facility in such installation is scaled down in volume with the conservation of height and as much as possible of length. In this type of scaling the scaling factor is equal to the ratio between the test facility volume and real volume of the NPP. The sources of the heat or the heat sink are also scaled by this factor (core power etc.). Of course due to the disorder of the ratio of the height and volume of the facility the heat transfer surface area is larger and the corresponding heat losses are consequently increasing.

c) Idealized time preserving modelling.

This type of scaling the nuclear test facility is depending directly on the equivalency of the geometrical components in the NPP and experimental facility. The agreement needs to be visible between conservation equations of volumes and separately homogenous flow paths of the fluid [4]. In this case the idealized time scaling is similar to the volume scaling but in this concept the height of the facility is not preserved.

All of given examples of the designing test facility are relevant to the scaling analysis. Although, in the most of cases the selected ITF is suitable for the demonstration of the correctness of the safety analysis for the NPP, there are always some discrepancies between the ITF and NPP design. In these cases the reversed scaling is used which means that the already made NPP model in the selected thermal-hydraulic code is adapted to the experimental facility conditions. The concepts of the scaling “in both ways” are called the – bottom-up and top-down approach [9]. Both approaches have different scopes and they are focusing on the other aspects of the phenomenon in the nuclear technology field. In the top-down scaling the idea is to “evaluate the global system behaviour and systems interactions from integral test facilities that can be shown to represent the plant-specific design under consideration” [9]. On the other hand, the bottom-up approach has the aim to investigate the problems raised in the operated NPP and to propose the design of the test facility that covers the phenomenon observed locally. In general the most suitable and reasonable concept for the purposes of the safety analysis for the NPPs is the volume scaling. In the volume scaling all of components remain untouched except for

the volume, boundary and initial conditions of the safety systems as well as the power, which has to be scaled by the volume factor.

### 2.3. Documents, procedures and methodologies

In the literature there are few documents and regulatory guides that mention the use of the scaling analysis in the safety analysis process with the use of the deterministic thermal-hydraulics codes. These are mainly the documents published by the nuclear safety authorities like U.S. Nuclear Regulatory Commission – methodology EMDAP - Evaluation Model Development and Assessment Process [9] and the methodology "Quantifying Reactor Safety Margins – Application of Code Scaling, Applicability and Uncertainty Evaluation" [2]. In these documents the objective is to present the methodology which focuses on the description of the obtaining uncertainty associated with the use of the thermal-hydraulic code. Therefore, in the presented methodologies the scaling analysis plays central role and is a major contributor to the evaluation of the uncertainties coming from the model nodalization, the imposed conditions and the code user. Through the decades the scaling analysis has become the issue strongly investigated and many articles and scientific journals were dedicated especially to the issue of scaling in nuclear technology [10].

## 3. Calculations

### 3.1. Description of the performed calculations

In the design basis accident the most dangerous accident is a loss of coolant accident (LOCA). This concept assumes LOCA as a postulated pipe break. Depending on safety systems availability, that is necessary to cool down the core, we distinguish small, medium and large break LOCA. In the first LOCA high pressure injection system is sufficient to keep coolant inventory at the safe level. Removal of the heat from core can be provided by the steam generator to the secondary side, assuming that the plant is shut down. Medium break LOCA is typically an event where the high pressure injection system is needed early in the event sequence. After that pressure goes down the low pressure injection systems and accumulators are necessary to ensure long-term cooling. Large break LOCA is the most severe scenario where water-coolant rapidly leaves the primary side and HPIS and LPIS have to be actuated to prevent the overheating of the core [11]. Double ended guillotine break loss of coolant accident is one of the largest break scenarios. In this event it is assumed that the pipe is promptly cut and water can leave primary side from both sides and through the largest flow area leak. Occurrence of the DEGB is an extremely unlikely event in

normal operation [12]. Therefore some organization (CSNI/NEA) postulated that LB LOCA should be ruled out as design basis accident (DBA). This statement is motivated by the fact that nowadays pipes material quality is higher and the operational experience shows that LOCA is only hypothetical accident [13].

During loss of coolant accidents many phenomena occur due to depressurization of the system. The rapid pressure drop in the system causes that the saturation temperature of the fluid is also decreasing and water starts to boil at lower temperatures. After reaching saturation temperature water evaporates and two-phase flow appears. It worsens cooling conditions of heated surfaces (fuel cladding), because vapour has lower heat transfer coefficient than water. As a consequence it can lead to severe accident during which following phenomena as oxidation of cladding, hydrogen production or rupture of reactor pressure vessel (RPV) can occur.

During normal operation, in PWR, many pressure losses take place, i.e. because of the friction between fluid and walls, in changes of the flow area, local pressure drop and due to differences of the elevation. If instead of the water in pipes the mixture of water and steam appears, total pressure drop in channel flow will increase. Additionally in two-phase flow new pressure loss has to be taken into account. Due to different densities of the phases (gas much smaller than fluid), vapour and water in mixture have different velocities (vapour much faster than water). As a result velocity of the mixture accelerates what causes additional pressure losses.

If the break appears in one of the legs, the pressure wave in primary side is rapid and extremely expected (highly anticipated). It may cause deformation of the core barrel, and as a result it decreases the cool ability of the core or clogs control rods outside of the core.

### 3.2. Description of the used tool - TH code - RELAP5

To perform thermal-hydraulic (TH) analysis of the facilities code RELAP5 was used. This code has been developed by Nuclear Regulatory Commission and a consortium consisting of several countries and domestic organizations. The code is dedicated to light water reactors to simulate steady-state and transient behaviour of the hydraulic part of the NPP and to perform analysis including loss of coolant, anticipated transients without scram and operational transients such as loss of feed water, loss off offsite power, station blackout and turbine trip. The flow is simulated as a single-phase (water, steam) or two-phase flow (mixture of water and steam). During two-phase flow calculation, code

solves conservation equations (mass, energy and momentum) for each phase separately. The conservation equations are as follows:

mass conservation equation for water:

$$\frac{\partial}{\partial t}[\rho_1(1-\alpha)A]+\frac{\partial}{\partial z}(\rho_1 j_1 A)=-\Gamma A \tag{1.1}$$

mass conservation equation for steam:

$$\frac{\partial}{\partial t}[\rho_V \alpha A]+\frac{\partial}{\partial z}(\rho_V j_V A)=\Gamma A \tag{1.2}$$

energy conservation equation for water:

$$\frac{\partial}{\partial t}[(\rho_1 i_i - p)(1-\alpha)A]+\frac{\partial}{\partial z}(\rho_1 i_1 j_1 A)=q_1^{''} P_H \tag{1.3}$$

energy conservation equation for steam:

$$\frac{\partial}{\partial t}[(\rho_V i_V - p)\alpha A]+\frac{\partial}{\partial z}(\rho_V i_V j_V A)=q_V^{''} P_H \tag{1.4}$$

momentum conservation equation for two phase mixture:

$$\begin{aligned}&\frac{\partial G}{\partial t}+\frac{1}{A}\frac{\partial}{\partial z}(\frac{G^2 A}{\rho_M})+\frac{\partial p}{\partial z}+[\Phi_{l_0}^2\frac{4C_{f,l_0}}{D_h}+\\&\sum_i \varsigma_i \Phi_{l_{0,i}}^2 \delta(z-z_i)]\frac{G^2}{2\rho_1}+\rho_m g\sin\varphi=0\end{aligned} \tag{1.5}$$

where: $\rho$ is density $[\frac{kg}{m^3}]$, $\Gamma$ is the volumetric mass exchange rate between phases $[\frac{kg}{m^3 s}]$, α is void fraction, A is cross-sectional area $[m^2]$, $j$ is superficial velocity $\frac{m}{s}$, $i$ is enthalpy $[\frac{kJ}{kg}]$, $p$ is pressure $[Pa]$, $q^{''}$ is heat flux $[\frac{W}{m^2}]$, $P_H$ is

wetted perimeter $[m]$, $G$ is mass flux $[\frac{kg}{m^2 s}]$, $\rho_M$ is dynamic mixture density $[\frac{kg}{m^3}]$, $C_{f,l_0}$ is Fanning friction factor for liquid, $\varsigma$ is local loss coefficient $[Pa]$, $\phi_{l_0}^2$ two phase friction multiplier, $D_h$ is hydraulic diameter, $\rho_m$ is static mixture density $[\frac{kg}{m^3}]$, $g$ is gravitation $[\frac{kg}{m^2 s}]$, $\varphi$ is slope of the channel. Each index *v* and *l* means vapour and liquid respectively.

Also equations for the non-condensable and solute mixtures are available. Inside of the code particular modules are included dedicated to nuclear reactors technology: point reactor kinetics, pumps (including jet pump for BWR), valves, pipes, separators, electric heaters, heat releasing or absorbing structures, accumulators or logic part responsible for system control.

While creating an input deck to RELAP5 code user has to assume good nodalization using generic components: time dependent and single volumes, time dependent and single junctions, branches, pipes, separators valve and pumps. In each control volume code calculates thermodynamic parameters depending on the type of a component. In volumes user can read pressure, void fraction, fluid and gas temperature, saturation temperature, density and fluid sub-cooling (gas overheating). In junctions RELAP5 calculates mass flow rate, enthalpy and flow area. Using given components user has to create system, i.e. hot and cold legs, RPV, pressurizer and steam generators. Each component has to have implemented initial conditions.

Equations are solved numerically using a finite-difference technique. Output data given in downstream node are input data for upstream node. Applying those techniques provides us with a possibility to run economical calculations of thermal-hydraulic systems during transients. In complex system calculations take time and need high computing power. In this case it is good to use supercomputer with many nodes and cores. Applying parallel calculation of the various scenarios needed for the safety analysis allows us to reduce calculation time and to speed up obtaining results. One of that supercomputer is formed in Świerk Computing Centre. The actual parameters of the Centre are as follow: 1920 computing cores, 7680 GB RAM, 560 TB disk storage which gives the computing power of 17.25 TFLOPS, also it is continuously developed.

It should be noted that RELAP5 does not analyse obtained results. For this purpose user has to employ engineering judgment and compare calculated results with real values in the system. In transient simulations assessment of the correctness has to be performed taking into account relevant thermal-hydraulic aspects (RTAs), sequence of main events and time trends.

### 3.3. Integral test facility LOFT, Large Break LOCA test L2-5

As it was mentioned in the previous section, to make the scaling analysis it is crucial to consider scaled facility and test facility where the test was performed. In this report the specified test facility is the Loss of Fluid Test (LOFT) facility. It is 50MW thermal power pressurized water reactor constructed in Idaho National Engineering Laboratories in the US. It allows us to study the engineered safety features in commercial PWR systems, especially concerning loss of coolant accident (LOCA). LOFT facility consists of two loops (Figure 1.3).

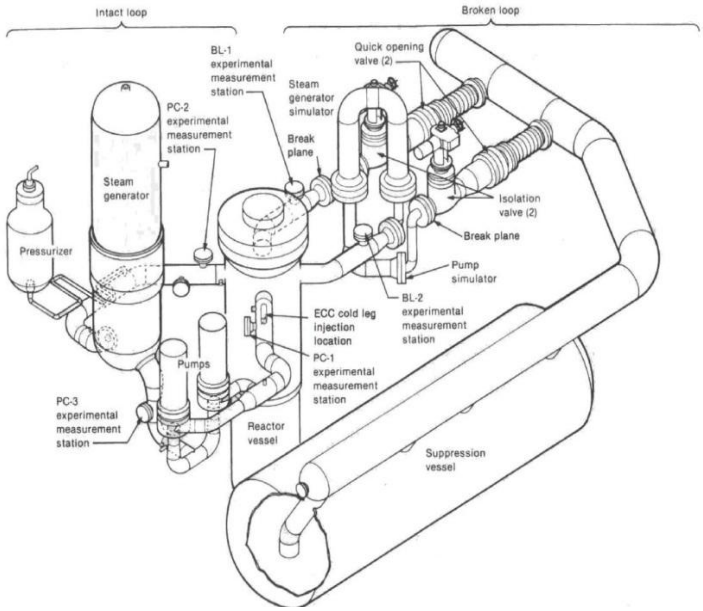


Figure 1.3 LOFT facility.

Intact loop, which represents three loops in primary side and second broken loop. Intact loop is typical PWR loop with steam generator, pressurizer and two pumps connected in parallel. In the broken loop the steam generator was replaced by the simulator and the break was placed at the cold leg. The break is simulated by quick opening valve and is connected to suppression vessel. To measure all of the relevant parameters in LOCA scenario during experiments, designer added additional measurement stations. Main part of LOFT facility is the reactor pressure vessel (RPV) where oxide uranium fuel was used. Core is simulated by 1300 nuclear fuel rods with active length of 1.676 m. RPV can be divided into annular downcommer, lower and upper plena, lower support plate and nuclear reactor core. Due to the presence of two loops in primary coolant system, RPV has four nozzles connected to cold and hot legs. Emergency core cooling system is simulated by two low pressure injection systems, two high pressure injection systems and two accumulators, each connected to intact loop. LOFT is a volumetrically scaled facility where heights of components are not preserved. It does not allow us to predict appropriate loss of pressure in gravity term as it is in idealized time preserving scaling. LOFT facility was constructed to carry out nonnuclear and nuclear experiments. Nonnuclear ones were simulated as those with isothermal conditions existing in primary side. It allows us to see how the coolant behaves, from the fluid dynamics point of view with elimination of the nuclear risk. Those simulations provided useful operating characteristics and system response during loss of coolant experiments. The nuclear experiments are those in which coolant temperature is changing across the core through produced power. We can distinguish following experiments: double-ended cold leg break, small and intermediate size breaks or steam generator tube rupture.

One of the nuclear experiments was L2-5 test. The configuration of the system was designed as double-ended 200 % cross section guillotine break (DEGB) represented by two quick opening valves on the cold leg. The flow break area equals to flow area of the pipe- 0.008365 $m^2$. Water can leave the primary side from the reactor side and from the SG simulator. Initiation of the break follows after steady-state in 0 s as a reference point. Almost immediately the reactor is scrammed and the coolant pumps coast down. Emergency core cooling systems, HPIS and LPIS, launch in 23.9 s and 37.32 s, respectively. Accumulator is dependent on pressure. If pressure drops below 4.29 MPa flow automatically begins. Table 1.2 shows a sequence of imposed events in transient simulations. In performed analysis time step changes during calculation, when transient occurs (after 400 seconds of steady state) RELAP5 calculates the transient with maximum time step of $10^{-4}$ instead of $10^{-2}$. It allows us to obtain more accurate results for 120 seconds transients.

Table 1.2 Sequence of imposed events

| EVENTS | SET POINTS |
|---|---|
| Experiment initiated - break opening (s) | 0 |
| Reactor scrammed (s) | 0.24 |
| Primary coolant pumps tripped (s) | 0.94 |
| Feedwater isolation start (s) | 0.3 |
| Feedwater isolation (s) | 2.5 |
| Steam line isolation start (s) | 0.35 |
| Steam line isolation (s) | 9.35 |
| Accumulator initiated (MPa) | 4.29 |
| HPIS injection initiated (s) | 23.9 |
| LPIS injection initiated (s) | 37.32 |
| LPIS injection terminated (s) | 107.1 |
| End of transient (s) | 120 |

## 3.4. Nuclear power plant ZION

While performing the scaling analysis, the user should be conscious if the design of the scaled NPP is suitable for the experiments from the ITF. In this section ZION NPP will be described, with its characteristics, and the agreement of the design to the experiment will be addressed. ZION is a pressurized water reactor in Illinois in the United States. This is a four loop Westinghouse design reactor with thermal power output of 3250 MW. This Station was decommissioned in 1998 after owners' decision that electricity prices on the market are not competitive. The same year a decision was taken that in 2010 dismantlement process will be started. This process is estimated to take at least 10 years and its cost will be about one billion USD [14].

The documentation of the ZION NPP was shared to R&D institutes. It gave a possibility to model entire installation focusing on primary side of the NPP. After that many thermal-hydraulic analysis could be performed, i.e. loss of coolant accident, loss of flow accident or station blackout. Making the model of nodalization which will be suitable for the projection of the L2-5 experiment it was necessary to implement some changes related to plant description and transient features. The primary side modelled in RELAP5 code was divided into three intact loops and a broken loop. Each of intact loops equipped in emergency core cooling systems (ECCS): LPIS and accumulator. There is no HPIS and

LPIS in broken loop due to changes related to the transient features. Safety systems were connected to the cold leg while the primary side has one pressurizer situated in the hot leg. Break on the broken loop is replaced by two quick opening valves able to simulate DEGB- LBLOCA. Reactor pressure vessel consists of four annular downcommers (components 315-318), lower plenum (323), core bypass (320), core channels (335, 334) and upper plenum (356). In the core a peripheral and average region can be distinguished, hot zone, hot fuel assembly and hot rod, what makes easier to see what is happening with the nuclear fuel during LOCA. Figure 1.4 represents the core nodalization where two core channels are vissible and each of them has multiple heat structures related to the specific core region. Model was created impementing RELAP5 modeling rules where for example the ratio between the height and flow area of the node is strongly advised. Bypass and core channels are divided into eighteen volumes on the same elevations (slices). The same number of heat sructures isrecommended. The recommendation for the RELAP5 users is to desing the nodalization in the manner where the lengths of two neighbouring volumes are not longer than two times.

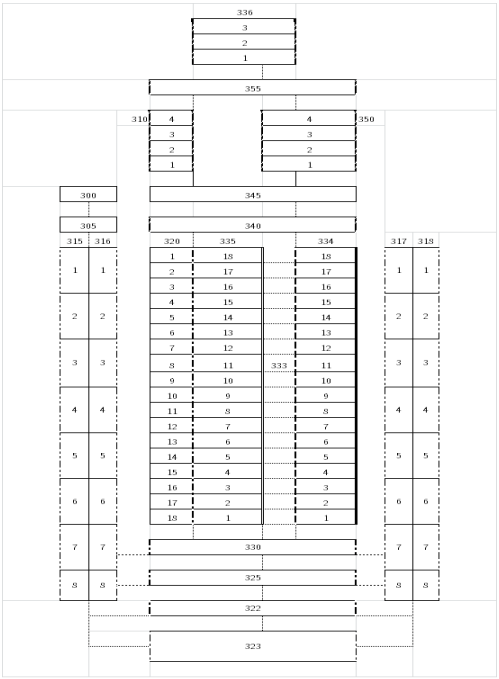


Figure 1.4 RPV nodalization.

## 3.5. Identification of the key issues in the analysed loss of coolant scenario

In the performed scaling analysis the most important issue is Relevant Thermal-hydraulic Aspects analysis. As mentioned above it allows us to evaluate obtained results and classifies results using four levels scale: E – excellent, R – reasonable, M – Minimal and U – unqualified. Last judgment disqualifies whole RTA and calculations have to be repeated. Aspects listed in Table 1.3 are classified to particular groups depending on what safety systems (HPIS, LPIS, and accumulator) or component (pressurizer) behaviour is analysed. Following types of parameters can be distinguished: integral parameter (IPA), non-dimension parameter (NDP), single valued parameter (SVD) and time sequence of events (TSE). During this analysis engineering judgment is request.

Table 1.3 Relevant Thermal-hydraulic Aspects

| RTAs | Type | UNIT | CALC | EXP LOFT | Judgment |
|---|---|---|---|---|---|
| Experiment L2-5 initiated | TSE | s | 0.00 | 0.00 | E |
| Break flowrate behaviour | | | | | |
| Subcooled break flow ended (cold leg) | TSE | s | 2.50 | 3.40 | R |
| Integral break flowrate at dryout time | IPA | kg | 13 043.252 | 493.00 | M |
| Integral break flowrate at ACC injection time | IPA | kg | 200 417.220 | 3 768.00 | R |
| Integral break flowrate at core quenching time | IPA | kg | 261 613.050 | 4 804.00 | R |
| Integral break flowrate at 100 s | IPA | kg | 258 526.560 | 5 160.00 | E |
| Pressurizer behaviour | | | | | |
| Time of emptying | TSE | s | 12.00 | 15.40 | R |
| PRZ pressure/primary pressure at 5 s | NDP | - | 1.6297 | 1.93 | R |
| PRZ pressure/primary pressure at 10 s | NDP | - | 1.4689 | 2.01 | M |
| PRZ pressure/primary pressure at emptying time | NDP | - | 1.0681 | 1.92 | M |
| Time of PRZ pressure - primary pressure equalization | TSE | s | 37.00 | 38.00 | E |
| Dryout occurrence | | | | | |
| Cladding temp initially deviated from saturation | TSE | s | 0.40 | 0.91 | R |

| | | | | | |
|---|---|---|---|---|---|
| Time of maximum cladding temperature | TSE | s | 4.70 | 28.47 | M |
| Peak cladding temperature | SVP | K | 1 039.17 | 1078.00 | E |
| Core cladding quenched | TSE | s | 74.00 | 65.00 | R |
| Upper plenum pressure behaviour | | | | | |
| Pressure at dry out time | SVP | MPa | 9.84 | 9.54 | E |
| Pressure at 10 s | SVP | MPa | 5.6467 | 5.76 | E |
| Pressure at 20 s | SVP | MPa | 2.4447 | 2.91 | R |
| Pressure at core quenching time | SVP | MPa | 0.3831 | 0.44 | R |
| Pressure at 100 s | SVP | MPa | 0.3067 | 0.42 | R |
| Accumulator behaviour | | | | | |
| ACC intervention time | TSE | s | 14.00 | 16.80 | R |
| ACC pressure 10 s after injection initiation | SVP | MPa | 3.4697 | 2.68 | R |
| ACC pressure 20 s after injection initiation | SVP | MPa | 2.6846 | 1.78 | R |
| ACC pressure at core quenching time | SVP | MPa | 1.5723 | 0.98 | R |
| Integral ACC flowrate at core quenching time | IPA | kg | 66 251.97 | 1504.00 | E |
| Integral ACC flowrate at 100 s | IPA | kg | 66 251.97 | 1506.00 | E |
| Accumulator emptied | TSE | s | 72.00 | 49.60 | M |
| HPIS behaviour | | | | | |
| HPIS intervention time | TSE | s | 24.00 | 23.90 | E |
| HPIS flowrate at core quenching time | SVP | kg/s | 32.91 | 0.74 | E |
| HPIS flowrate at 100 s | SVP | kg/s | 32.91 | 0.75 | E |
| Integral HPIS flowrate at core quenching time | IPA | kg | 1 768.84 | 33.30 | R |
| Integral HPIS flowrate at 100 s | IPA | kg | 2 625.05 | 59.50 | E |
| LPIS behaviour | | | | | |
| LPIS intervention time | TSE | s | 38.0000 | 37.32 | E |
| LPIS flowrate at core quenching time | SVP | kg/s | 89.1333 | 5.67 | E |
| LPIS flowrate at 100 s | SVP | kg/s | 91.7846 | 7.21 | R |
| Integral LPIS flowrate at core quenching time | IPA | kg | 10 060.64 | 146.80 | R |
| Integral LPIS flowrate at 100 s | IPA | kg | 17 142.75 | 379.66 | E |
| Accumulator + HPIS + LPIS behaviour | | | | | |

| | | | | | |
|---|---|---|---|---|---|
| Integral ECC flowrate at core quenching time | IPA | kg | 89 910.89 | 1685.00 | R |
| Integral ECC flowrate at 100 s | IPA | kg | 105 787.53 | 1945.00 | R |
| Primary System Mass behaviour | | | | | |
| Minimum mass / initial mass | NDP | - | 0.0735 | 0.27 | M |
| Primary mass at core quench time/initial mass | NDP | - | 0.2727 | 0.41 | M |
| Primary mass at 100 s/initial mass at 100 s | NDP | - | 0.3138 | 0.40 | M |

Obtained results are in good agreement with the experiment. Comparing calculated values with LOFT L2-5 experimental data we can see that LOFT scenario was implemented to ZION NPP correctly. Used time preserving and volumetric scaling way in this analysis is reflected in the obtained results. Almost all TSA type parameters are excellent because time of the actuation of systems was taken from experiment and preserved in the $K_V$ scaled calculation. Obtained volumetric factor was calculated making ratio of the ZION volumes to LOFT facility. All safety systems and power were scaled using this factor. The LOFT test facility is about 50 times smaller in volume than the ZION NPP.

### 3.6. Evaluation of the performed scaling analysis

During the evaluation of the performed scaling analysis beyond RTA the evaluation of time sequence plots becomes very helpful. It conveys comparison of experiment and calculated data in the function of time. The similarity analysis is carried out and all of the steps below need to be satisfied:

a) The scaling factor needs to be evaluated on the basis of the chosen scaling approach. The ratio is the $K_V$ factor that includes the comparison of the primary system's volumes of the ITF and the NPP.

b) To perform the correct transient calculation the achievement of the steady state needs to be confirmed. The relevant quantities (parameters) need to be scaled properly and be constant during the steady state.

c) The scaling analysis needs to be performed with the boundary and initial conditions corresponding to the experiment. At the end of the $K_V$ analysis the data and results need to be assessed and accepted, in other case the calculations need to be repeated [15].

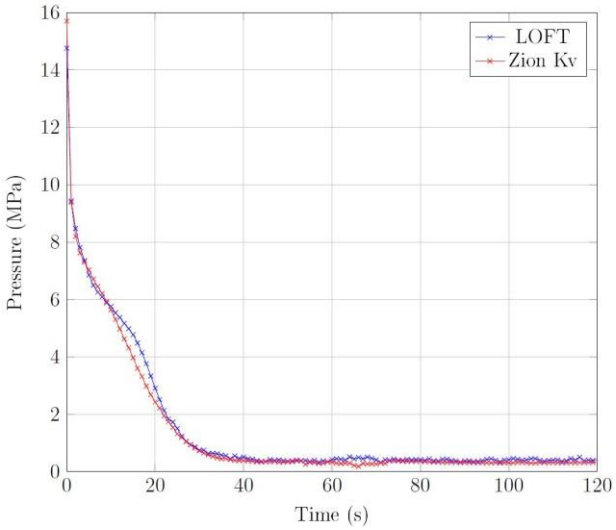


Figure 1.5 Time trends of intact loop 1 pressure in hot leg

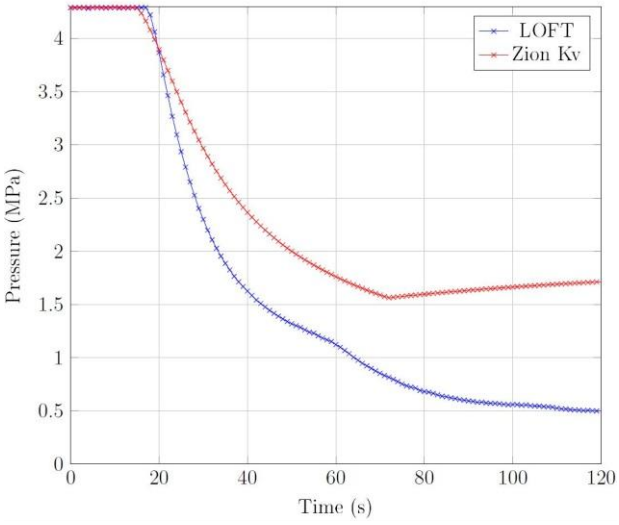


Figure 1.6 Time trends of accumulator 1 pressure

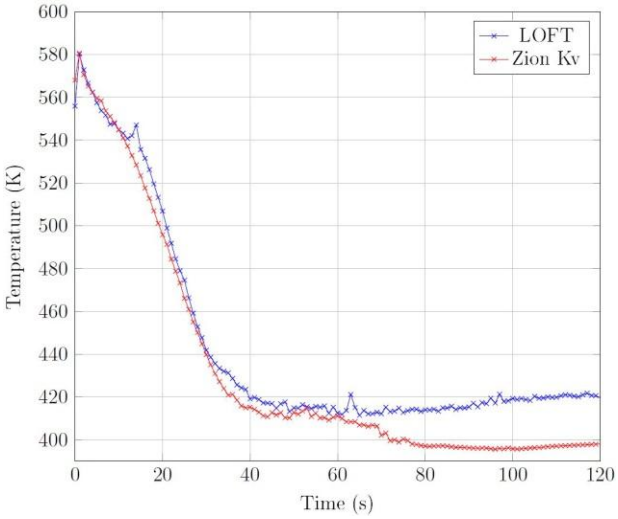


Figure 1.7 Time trends of coolant temperature in core inlet

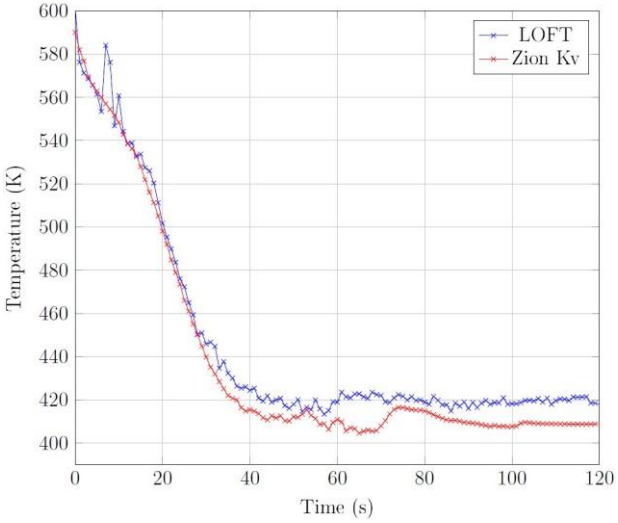


Figure 1.8 Time trends of coolant temperature in core outlet

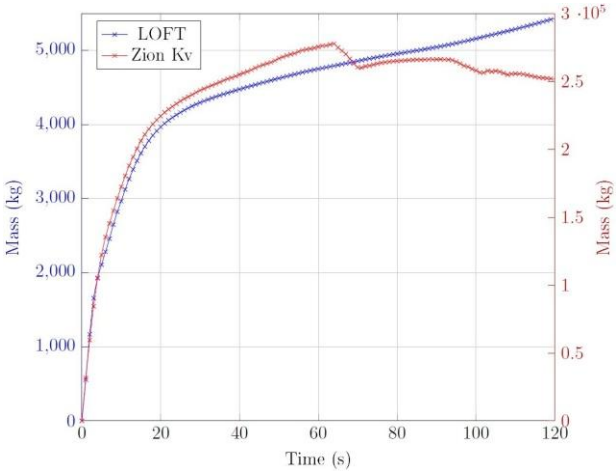


Figure 1.9 Time trends of integral break mass flow

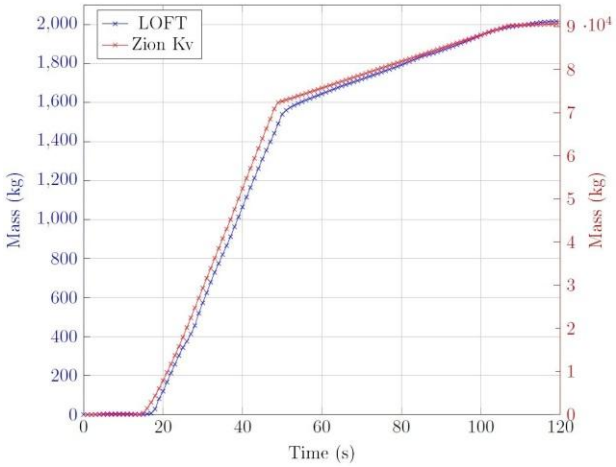


Figure 1.10 Time trends of ECCS integral mass flow

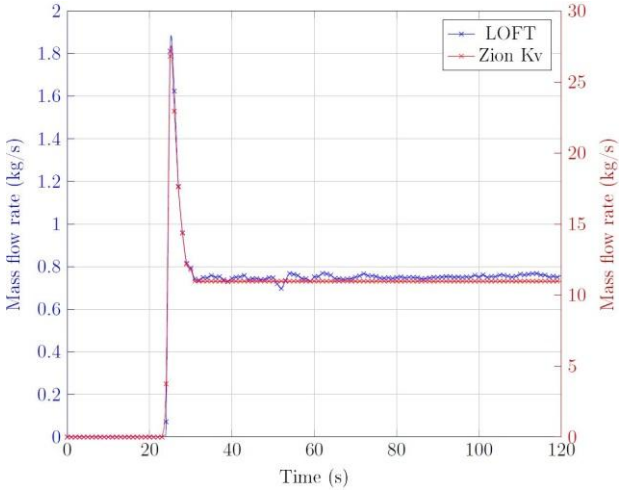


Figure 1.11 Time trends of mass flow rate in HPIS

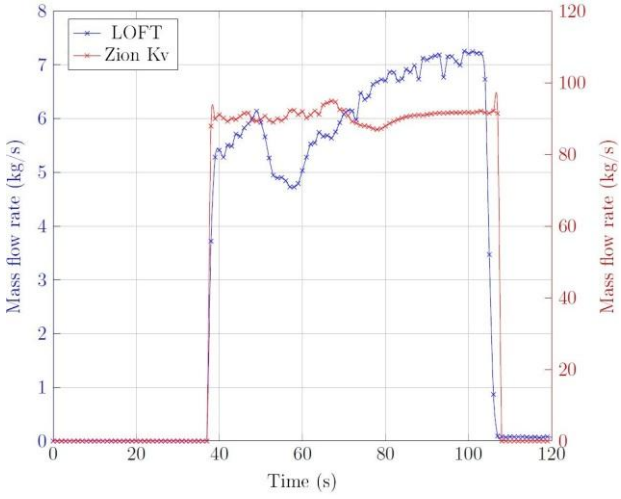


Figure 1.12 Time trends of mass flow rate in LPIS

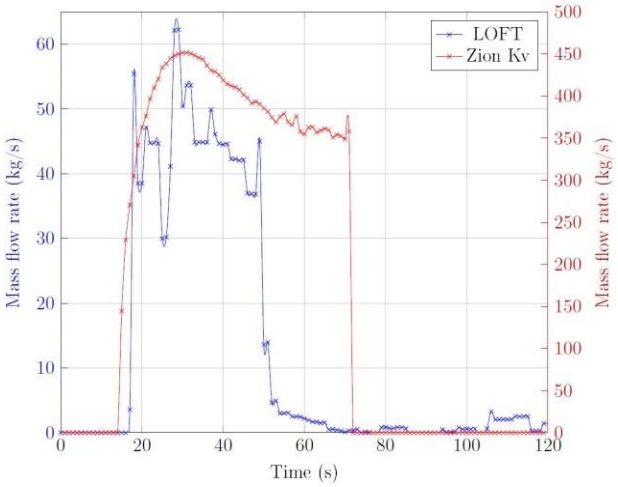


Figure 1.13 Time trends of mass flow rate in accumulator

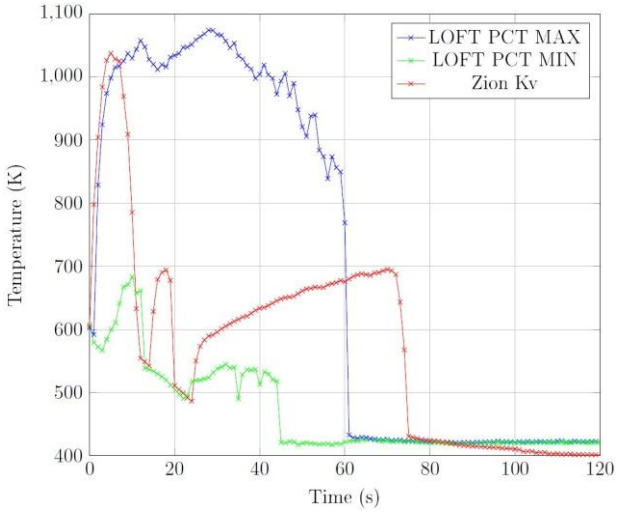


Figure 1.14 Time trends of maximum cladding temperature

Figures 1.5 to 1.14 show time trends of characteristic parameters, as follows: pressure in hot leg, pressure in accumulator, inlet and outlet coolant temperatures in the core, integral break mass flow rates and total ECCS integral mass flow rates, HPIS, LPIS, accumulator mass flow rates, and maximum cladding temperature. Some plots have double y-axis because the range of obtained result is scaled by $K_V$ factor which in this case equals to 44.45. It allows easy comparison between experiment and calculated values. Left Y-axis corresponds to experimental results of the LOFT L2-5 test and right Y-axis expresses scaled Zion model calculations.

On each plot it is easy to see that calculated time trends are in good agreement with experiment. It confirms correctness of the relevant thermal hydraulic aspects, even though the time trend of maximum cladding temperature was assessed as minimum (Table 1.3). As it was mentioned in the beginning of this paper the volume scaling was applied during calculation. In this way not all dimensions of the components are preserved, for example core and associated heat transfer surfaces. In the LOFT experiment design the heat transfer surfaces in the core are smaller which resulted with higher cladding temperatures. Additionally, in the ZION NPP calculation not every property was taken directly from the LOFT facility, like material properties which highly affect the heat transfer between the hot rods and coolant. As shown in the last Figure 1.14, the cladding temperature quenches quicker than in reference case.

## 4. Summary

The scaling of the Integral Test Facilities in the safety assessment process is an issue of great importance. The demonstration of the correctness of the performed safety analysis for the chosen NPP design is crucial. The scaling analysis not only comprises of the measure to qualify the results of the safety analysis but also of the nodalization development, the code or the code user. Each of the mentioned issues is a great contributor to the overall uncertainty of the results coming from the analysis that use thermal-hydraulic codes. This uncertainty became the important part of the safety assessment and was deeply studied throughout the decades and lead to the development of the methodologies for the uncertainty evaluation. The scaling analysis is the means for this accomplishment and is described in various documents (“Quantifying Reactor Safety Margins – Application of Code Scaling, Applicability and Uncertainty Evaluation” [2]).

While performing the scaling analysis there are steps that need to be fulfilled. The analysis can be performed with the sufficient test database for the selected scenario. The choice of the ITF scenario, the approach to the scaling, and in the end the proper results evaluation are necessary. This all processes need the engineering judgement, which is crucial to the achievement of the acceptable level of the safety for the analysed NPP. The proposed test facility, the NPP (LOFT L2-5 test and ZION NPP) and performed scaling analysis shown the adequacy of the chosen scenario, implemented boundary and initial conditions.

The work was supported by the EU and MSHE grant no. POIG.02.03.00-00-013/09.

## References

[1] OECD Nuclear Energy Agency, [Online]. Available: http://www.oecd-nea.org/jointproj/loft/. [Accessed 12 03 2013].
[2] B.Boyack, R.Duffey, P.Griffith and G.Wilson, "Quantifying Reactor Safety Margins, Application of CSAU Methodology to LBLOCA," EG&G Idaho, Idaho Falls, December 1989.
[3] International Atomic Energy Agency, "Deterministic Safety Analysis for Nuclear Power Plants, Specific Safety Guide No. SSG-2," International Atomic Energy Agency, Vienna, 2009.
[4] A. Petruzzi and F. D'Auria, "Thermal-Hydraulic System Codes in Nulcear Reactor Safety," vol. Volume 2008, no. 10.1155/2008/460795, 8 November 2007.
[5] F. D'Auria, M.Lanfredini and N.Muellner, "Scaling analysis in BEPU licensing of LWR," *Nuclear Engineering and Technology,* pp. pp.611-622, August 2012.
[6] N.Aksan and F. D'Auria, "Relevant thermal-hydraulic aspects of advanced reactor designs," OECD, Paris, November 1996.
[7] N.Aksan, F. D'Auria, H.Glaeser and R.Pochard, "OECD/NEA-CSNI Separate Effects Test Matrix for Thermal-Hydraulic Code Validation," Issy-Ies-Moulineaux, September 1993.
[8] N.Aksan, D.Bessette, I.Brittain and e. al., "Code validation matrix of thermal-hydraulic codes for LWR LOCA and transients," OECD/CSNI, March 1987.
[9] U.S. Nuclear Regulatory Commision, "Regulatory Guide 1.203 Tansient and accident analysis methods," U.S. NRC , Washington, December 2005.
[10] Elsevier B.V., *Nuclear Engineering and Design, Volume 186,* pp. 1-306, 1 November 1998

[11] B.O.Y.Lydell, “Strategies for Reactor Safety: Preventing Loss of Coolant Accidents,” NKS, Vista, CA, USA, 1997.
[12] A. Andrews and P. Folger, “Nuclear Power Plant Design and Seismic Considerations,” 2012
[13] U.Schmocker, “Redefining the Large Break LOCA,” in *Technical basis and its implications*, Zurich, 2003.
[14] N. Jackson, [Online] “http://finance.yahoo.com/news/Lessons-From-Zion-How-atlantic-4087270317.html,” 20 June 2011.
[15] D.Araneo, A. D. Novo, F. D'Auria and G.M.Galassi, “Scaling of small break LOCA in VVER 1000 system,” in *International Conference Nuclear Energey for New Europe 2005*, Bled, Slovenia, 2005.

# CHAPTER 2

# Overview of modern approaches to multi-physics, multi-scale problems in nuclear technology

Mieczysław Borysiewicz, Tomasz Kwiatkowski, Sławomir Potempski,
Piotr Prusiński, Michał Spirzewski
National Centre for Nuclear Research (NCBJ)
Andrzeja Sołtana 7 Str., 05-400 Otwock, Poland
piotr.prusinski@ncbj.gov.pl

## 1. Introduction

Multi-physics and multi-scale simulations of physical phenomena reflects the concept of modelling based on taking into account all the processes which are coupled one to the other by establishing appropriate interfaces between them, and treating the system as a whole, as far as possible. The elements of such system can describe processes that occur in various spatial and temporal scales.

This section gives an overview of approaches used for different aspects of multi-physics and multi-scale issues along the lines presented in NEAMS (Nuclear Energy Advanced Modelling and Simulation) program and are based mostly on the white paper [1].

Huge variations in time and spatial scales in reactor physics pose mathematical and computational challenges. Models of full fuel cycle should comprise reactor physics, fuel design, processing and reprocessing, waste repository and so forth. The physical processes have ranges in scale from angstroms to kilometres in space and femtoseconds to years in time — from electronic structures computation for separation chemistry to the material models of dislocation, brittleness, corrosion and cracks propagation for the fuel, concrete and metal, to the thermal hydraulics of the full reactor and seismic effects on the reactors.

For proper treating multi-physics one should consider both interfaces among neutron transport, thermal-hydraulics, nuclear fuel and structural mechanics on one hand, and between different scales within each process and component to be modelled, on the other side. One of the main problems, in this respect, is to transfer appropriate information from one to the other level, so the treatment on

all the levels is scientifically justified, while the continuity, consistency and accuracy of the solution should be maintained. Numerical computations based on different techniques are usually needed for this purpose and then additional problems for linking various approaches, like deterministic and stochastic ones, may arise. Such situations happen, for example, when solving deterministic differential equations would be very time consuming due to the necessity of using high resolution mesh for complex geometries and therefore the Monte Carlo methods are applied.

Multi-scale modelling can be realised via superposition techniques and models at different scales – for example, more accurate techniques like computational fluid dynamics for thermal-hydraulics simulations are used only for regions of particular interest in order to obtain better information of local behaviour of temperature, pressure or other parameters. Similarly in the area of material physics it is possible to start with *ab inito* methodology to describe microstructures at atomic scale in order to find macroscopic defects caused by irradiation.

Generally, two approaches for multi-physics simulations can be applied. The first one is based on incorporation of all needed physics via a number of different simulators into one single code. The other approach relies on the development of individual models and common interfaces for integrating them. Then the following modules can be considered [2]: neutronics, thermal-hydraulics, structural mechanics, fuel performance, chemistry, reactor systems, multi-resolution geometry, mesh adaptation and management. Such an approach is applied, among others, in NURESIM (Nuclear Reactors Simulation) project within EU framework programs.

However, most currently used codes in nuclear industry and by regulatory bodies are dated back to 1970s and 1980s, representing a conglomerate of tools that are uneven in terms of accuracy and validation and are only loosely coupled (often by human intervention). They were developed for supporting decision making and were designed to model all important safety aspects starting from individual fuel pellets to severe accidents for the whole plant. This includes neutronics, fluid and heat transfer, thermo-mechanics, chemistry, fuel behaviour and balance of the plant. These codes were built, first of all, basing on experimental data, simplified models and applying the concept of aggregate parameters. The basic methodology relies on bench-top experiments leading to prototype operation and afterwards to full-scale demonstration. Such costly experiments were important for ensuring consistency. Conservative design margins were then established after some operation of the full size system. The

uncertainty of the key parameters and validation of the data and models were not obtained via well understanding of science underlying but rather by expert judgment. It seems that design margins can be essentially improved when more advanced models will be applied.

Historically, scientific research has been carried out in two main ways: modelling based on theory and on experimentation. With the advent of computers, simulation has found a role as a third complement to this historical approach.

There are a lot of problems related to safety of traditional reactors, which need better physical modelling, like nucleate boiling, critical heat flux, pressurised thermal shocks, re-flooding and fluid structure interactions. This means also that better mathematical algorithms, multi-resolution techniques for multi-physics multi-scale problems and integration between different levels are necessary. It has been pointed out in [1] that two areas are critical: development of second order in time coupling methods and simultaneously supporting sensitivity analysis, data assimilation and optimisation coupled with partial differential equations (PDE). Among the most promising methods that can be applied one can mention: Strang splitting, predictor-corrector methods, implicit-explicit schemes and Jacobian free Newton-Krylov algorithms.

Incredible progress in computer technology, in particular development of multi-core clusters in recent years, allows for performing advanced simulations of complex physical phenomena.

As a consequence, predictive science has progressed as a complement to empiricism, with key experiments as the essential instruments to validate the models and simulation tools. Because of the high cost and long time associated with experimentation, simulation has gained more ground in the scientific research process. In particular for nuclear systems, the improvement in understanding of fundamental processes and the progress in simulation capabilities through integration and multi-physics and multi-scale approaches, when linked to the significant advances in computational power, make significant technological breakthroughs achievable.

This needs, however, development of new generation of computer codes based on parallel paradigm and therefore is more difficult to implement than standalone sequential computing programs. That was one of the main reasons for creation of the Interoperable Technologies for Advanced Petascale Simulations

(ITAPS) centre within the Scientific Discovery through Advanced Computing (SciDAC) program of the United States Department of Energy (DoE).

The main purpose of this centre is to provide a number of interoperable tools for manipulation of geometry and meshes including adaptive mesh refinement (AMR), and well defined services both for basic numerical solvers and system tools like dynamic load balancing.

In order to assure neutral access to mesh and geometry common interfaces and data structures have been defined. Basic services include, among others, efficient libraries for solving partial differential equations by different approximation techniques like finite difference, finite volume, finite and spectral elements, and discontinuous Galerkin methods. Application of such packages will allow for effective implementation of multi-physics and multi-scale solvers in multi-processor environment.

The ultimate goal of these efforts is a design minimizing the uncertainties as much as possible. In principle, there are two major sources of uncertainties: input physical data and modelling. For the first, one can mention nuclear cross sections, physical characteristics of materials (e. g. heat capacity, thermal conductivity, viscosity, etc.), fabrication data, chemical reactions rates, etc. In general, these quantities can be improved either by measurements or by a better industrial process (fabrication data), but often a limit exists in the level of improvement that can be achieved. On the other hand the uncertainty related to modelling comes from approximations made in the computational methodology used in the design process. That is the area where advanced simulation can provide a major benefit. The hope is to reduce the impact of uncertainties coming from the modelling of the physical processes as much as possible.

Such a move to predictive modelling needs improving [1]: 1) geometric fidelity by using 3D domain; 2) numerical fidelity, by applying finer resolution and higher-order schemes; 3) application performance and physics fidelity by improving models (for example, using transport instead of diffusion models and large-eddy simulation instead of k-epsilon, etc.). In the area of geometric fidelity, some improvements include predicting how nuclear waste evolves in a geochemical, repository environment or the rate of radionuclide migration in highly-inhomogeneous, geological media. For numerical fidelity better uncertainty quantification methods for models and simulations are needed, as well as the elimination of homogenization. This would result in explicit up-scaling of macro-scale to meso-scale models. Such improvements would allow scientists to model the simulated evolution of pin assembly and deformation in

fuels of detailed peak fuel pin fluxes and temperatures to a one percent uncertainty level of reactor transient conditions with loss of flow and of the up-scaling of bench-level technologies to the plant level. Improved physics should enable predicting material thermo-mechanical responses, damage, and, ultimately, failure under extreme conditions in fuels, cladding material, pin assemblies, and reactor vessels, a key objective of any reactor simulation.

Such concepts are the basis of a dedicated program NEAMS (Nuclear Energy Advanced Modelling and Simulation) that has been established by US DoE [3]. One of the main purposes of this program is to build new generation of computing codes and systems for science based understanding of nuclear energy systems. This should result in faster innovation cycle and better apprehension of the performance, safety and reliability of the current and new reactors. In particular the main attributes of this program, among others, have been defined as follows [3]:

- approach based on first principles and high dimensionality (i.e. 3D),
- adequate modelling of space and time: multi-scale issues properly resolved,
- appropriate verification, validation with sensitivity and uncertainty analysis,
- usage of integrated systems.

The NEAMS program has been organized in five areas:

1. Integrated Performance and Safety Codes (IPSC): for better understanding the detailed integrated performance of nuclear systems including:

- Nuclear Fuels,
- Reactor Core and Safety,
- Separations and Safeguards,
- Waste Forms and Near Field Repositories.

2. Fundamental Methods and Models (FMM): for modelling in smaller length scale and performing atomistic to continuum multiscale simulation. This element can be also applied for generating the data needed for physical and engineering models.

3. Verification, Validation and Uncertainty Quantification (VU): development of methodologies to be used by IPSC and FMM program elements in order to estimate inherent uncertainties in modelling and simulation. This element is considered as a principal interface with US Nuclear Regulatory Commission.

4. Capability Transfer (CT): turning scientific codes into engineering tools to be used by industry and licensing body – this is a key element for the success of the program.

5. Enabling Computational Technologies (ECT): this element is to ensure that the technologies are available to make the first four program elements possible.

The NEAMS program can be considered as an indicator of currents trends in further development of nuclear industry knowledge-based and innovative.

It is obvious that integrating performance and safety codes requires very detailed simulations based on coupling various physics for a wide range of spatial and temporal scales. The most important areas are neutron transport, fluid flow, fuel behaviour and the problems related to structural mechanics.

Basing mostly on the paper [1] prepared for NEAMS program we shortly introduce the main problems and perspectives for the development of new generation of codes to deal with multi-physics and multi-scale issues.

### 1.1. Neutron transport

One of the most common applications of radiation transport is the calculation of nuclear reactors and one of the biggest problems in its practical implementation is related to multiple scales in the different independent variables, namely: time, direction, position and energy:

- Time: from nuclear feedback effects ($\sim 10^{-7}$s) to fuel depletion ($\sim 10^{12}$s),
- Direction: from complete isotropy (fission emitted neutrons) to complete anisotropy (beams),
- Position: from pin cell internals ($\sim 10^{-3}$m), to full the extent of full reactor cores ($\sim 10^{1}$m),
- Energy: from resonance widths ($\sim 10^{-3}$eV) to neutron emission energies ($\sim 10^{7}$eV).

To cope with these problems, averaging methods like cell homogenization and multi-group spectrum collapse have been developed.

Concerning geometrical scales for a typical reactor physics problem it ranges from the size of the nuclear radius ($\sim 10^{-14}$m) to the external size of the core ($\sim 10^{1}$m). Although the smaller scales (up to the material structure, $\sim 10^{-4}$m) are usually taken into account in the cross section processing the remaining five or-

ders of magnitude cause the problem of finding the solution computationally costly.

Starting from the coarsest level one can identify the following hierarchy of levels (Figure 2.1):

- full core level (~$10^{1}$m), with external boundary conditions that represent the effect of other materials and structures surrounding the core;
- fuel assembly level (~$10^{-1}$m), which represent the smallest unit in terms of fuel movement in, out and within the core;
- fuel pin level (~$10^{-2}$m), with the surrounding moderator and coolant represents the smallest repeated unit in terms of reactor analysis;
- fuel pin and absorbing components internals (~$10^{-4}$- $10^{-3}$) represent the smallest scale of interest in reactor analysis. They are still important for the spatial self-shielding effects that take place at this scale, but at the same time the effect is usually problem dependent to be introduced as a parameter in the cross section library.

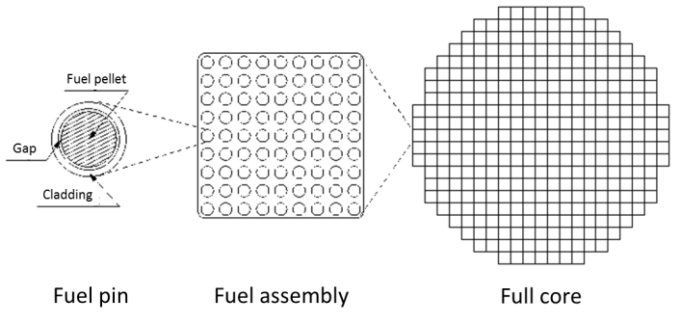


Figure 2.1 Hierarchical geometrical structure present in a nuclear power reactor. Source [1].

Typical methods to deal with this problem is to average the properties on a region using as a weighting function the solution of an approximate problem solved with approximate boundary conditions. For multi-grids, the averaged properties can be either obtained by homogenization or by application of the operators used for mapping from one grid to the other. Anyway, the transport equation is solved exactly only in the coarsest scale using average properties and a source given by the projected residual of the equation in a finer grid. In all finer levels the only operations required are the applications of a relaxation steps for smoothing the solution and using interpolation/relaxation operators to communicate the levels.

In general there are two approaches for simulating neutron transport phenomena: deterministic and stochastic. Starting from the first principles one has to solve seven-dimensional linearized Boltzmann transport equation (space: 3, direction: 2, energy:1, time:1).

At present mostly nodal (coarse-mesh) two group diffusions methods are applied. They are based on pre-computed cross sections and assembly discontinuity factors, which can be computed for single assembly and reflective boundary conditions. However, with the appearance of more complex reactor core designs like partially loaded cores with mixed-oxide fuel or high burn-up loadings, there is a need for using more advanced methods in order to obtain proper accuracy. Hence, new methods have been developed based on fine-mesh (pin-by-pin), higher order neutron transport model or multi-group approach. In order to apply the latter instead of two group diffusion nodal code, the discrete ordinates (SN) or spherical harmonics (PN) approximations are mostly used. The simplified SP3 model has become very popular as it is more accurate than diffusion approximation and demands less computing power than SN or PN methods. In order to achieve performance at the petascale level in principle new algorithms have to be developed. Current adaptive methods, related to spatial dimension should be extended for angular variable. In case of energy it seems that sub-grid models could treat the energy dependence properly.

The Argonne National Laboratory (ANL) has developed UNIC (Ultimate Neutronic Investigation Code) software [4] containing two solvers based on the second order even-parity transport equation, utilizing spherical harmonics and a discrete ordinates approximation for the angular variable. The third solver is based on a first-order method of characteristics, thus providing a more efficient capability for geometry modelling. The code utilizes an unstructured mesh, and taking into account that in order to represent properly complex geometry of a reactor core, billions of spatial elements, hundreds of angles, and thousands of energy groups are needed, this leads immediately to the problem of petascale size ($10^{15}$). ANL has already evaluated the performance of the code and applied higher fidelity techniques for two representative fast reactor problems (PHENIX and ZPR-6).

The other approach for reactor analysis relies on Monte Carlo simulation, also based on first principles with possible application of parallel algorithms implemented via particle tracking methods. Various events, like collision, absorption, fission, escape are recorded for each particle thus constituting the history of particles. The continuous Monte Carlo method enables high accuracy modelling, but because of its statistical origin typically large computing times

are required in order to obtain the results both for integral parameters and local distributions. Traditionally, Monte Carlo codes have been applied for determining reactivity coefficient or multiplication factor. However, in case when detailed information on local behaviour of quantities like power density is required, it is much more difficult to perform the simulations and achieve sufficiently accurate results in reasonable computational time. It is not expected that full core simulation by Monte Carlo techniques with enough good statistics will be available for multi-physics problems on non-orthogonal grids in next ten years [1]. In the meantime a promising approach has been proposed by Oak Ridge National Laboratory (ORNL), where hybrid deterministic/Monte Carlo MAVRIC code is under development. It links a new, three dimensional, discrete ordinates transport code (Denovo), with a modern Monte Carlo transport solver (Monaco) – the current version can be applied for nuclear shielding and radiation dose assessments. It seems that hybrid method will allow for efficient computation of the spatial distribution of neutrons (with complex reactor geometry) taking into account requirements for multi-physics coupling. The Monte Carlo techniques require also estimation of uncertainties for reactivity parameters, for example, by error propagation methods during depletion and kinetics processes. This can be achieved by adjoint methods, however currently there are no models with continuous energy capabilities. Similar problem exists for cross-section sensitivity analysis.

Another observed tendency is to link Monte Carlo neutronics with thermal-hydraulics in order to obtain three dimensional power and thermal-hydraulic solution, particularly for steady state simulations. The important issue here is efficient accumulation of high precision fluxes on non-orthogonal mesh which is a key point for proper treatment of multi-physics.

### 1.2. Thermal Hydraulics

Thermal hydraulic analyses constitute critical elements both for the design optimization and safety analyses of reactors. Simulation of flow and heat transfer can be used not only for core modelling but other elements like steam generators, pipes, pumps and condensers. Thermal-hydraulic simulations are very demanding calculations, in particular when detailed temperature distribution is needed in order to predict hot spots. Full understanding of heat transfer, mixing processes, turbulence and multi-phase multi-fluid flows for steady and unsteady flows as well as local phenomena such as thermal striping, fretting, and flow induced vibration is necessary for these purposes. Additionally, complex geometries causes the number of unknown variables can be huge. There is a need for improvement in four areas [1]:

- Direct solving of Navier-Stokes equations (DNS) which corresponds to first principle approach for front tracking, diffuse interface models, particle methods and lattice Boltzmann models;
- Large Eddy Simulation (LES) for high Reynolds numbers in open media for performing high accuracy calculation for one channel or within plena;
- Computational fluid dynamics (CFD) in porous media for multi-channel analysis;
- System scale for the whole plant.

Even for non-boiling flows first-principles based DNS is not possible even for the fastest computational clusters currently available. Direct solving of Navier-Stokes equations can be performed only for simple domains and by no means can be applicable to the whole reactor system. In fact, application of DNS even for single channel (with the Reynolds number of the order of ten to hundred thousands) is still beyond reach the existing computing cluster capabilities. Due to complexity of geometry and multi-scale issues also LES approach is of very limited application – typically such models are used for small domains. Therefore CFD techniques are utilised mainly for determining the mean flow effects in more complex domains by means of Reynolds Averaged Navier-Stokes (RANS) simulations, which need less computational effort than LES. This leads to the hierarchy of simulation capabilities, each operating at differing scales.

A number of various CFD codes are used in real applications: both commercial general purposed (like CFX and Fluent of ANSYS, STAR-CD of CD-Adapco or TransAT of Ascomp) and more specific, developed originally for safety reactor problems (Trio_U, Saturne, Neptune or Nek5000).

This means that in such situation the multi-scale approach should be applied in order to model thermal-hydraulic effects. It can be based on coupling CFD codes with system codes.

Other situations where multi-scale technique is required arise in case of modelling of complex phenomena. Consider for example simulation of convective boiling described in [5]. Four scales should be taken into account:

- Macro-scale (a few centimetres – one or more sub-channels): responsible for cross-sectional distributions of global variables, like void fraction, temperature, heat fluxes, fluid velocities and pressure. In order to model this scale one can use generally purposed CFD code, preferably based on two-fluid RANS or Lagrangian particle tracking LES;

- Meso-scale (millimetres): the scale of the growing bubbles and detaching from the wall – thermal and velocity fields immediately adjacent to the bubble and the wall are fully resolved. In this case DNS code coupled with interface tracking method to simulate life cycle of bubbles;
- Micro-scale (micrometres): movement of the triple interline (vapor/liquid/wall) during the bubble life cycle and the evaporation of the thin liquid film (micro-layer). Few theories based on film theories or contact angle can be applied to resolve these problems;
- Nano-scale (nanometres; molecular scale): this scale can be used to analyse processes occurring at the interface between vapour and liquid, or at the triple contact line between solid, vapour and liquid in order to provide important parameters in the regions important for the overall mass transfer problem. This scale requires molecular technique type of modelling.

In general the following scales can be considered [2]: system, component, mesoscale, microscale and atomic, corresponding respectively to application of the system codes, sub-channel or porous 3D models, CFD RANS/LES, CFD DNS with interface tracking and molecular dynamics or direct simulation Monte Carlo methods.

### 1.3. Nuclear fuel modelling

Taking into account multi-scale issues, simulation of nuclear fuels is particularly demanding. The related processes which should be modelled have ranges of 10 orders of magnitude in size from the sub-atomic nuclear to the structural component level, and 22 orders of magnitude in time, from the sub-picosecond level of nuclear collisions to decade-long component service lifetimes. A lot of quantities describe nano- or micro-structures which are formed when irradiation degrades the physical and mechanical properties of nuclear fuels, cladding and structural materials. In this respect initial material composition and microstructure, the thermo-mechanical loads, and the irradiation history are particularly important.

Thus simulation of complex systems in materials science and condensed matter physics includes a chain of models for: macro-scale continuum mechanics, defect evolution in meso-scale, classical mechanics molecular scale, and quantum-mechanical effects (Figure 2.2). The following models then can be considered: *ab initio* electronic structure calculations, molecular dynamics; accelerated molecular dynamics; kinetic Monte Carlo; phase field equations or rate theory simulations with thermodynamics; and kinetics by passing information about the controlling physical mechanisms between modelling techniques over the relevant length and time scales.

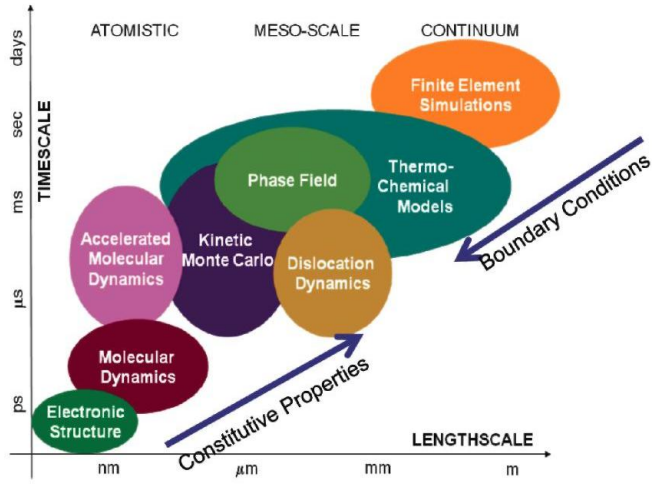


Figure 2.2 Multi-scale materials modelling paradigms, showing simulation techniques that address events at specific length scale and time scales. Reproduced from [6].

Apart from complexity of actinide components and loading conditions the following quantities have impact on material behaviour: temperature, neutron flux and fluency. Chemical interactions at the fuel cladding or between structural materials and the coolant can lead to the corrosion, which can be also caused by stress occurring with irradiation. Initial formation of defect cluster on the electronic structure level is related to times starting from femtoseconds. At the level of single crystals, cladding and fuel interaction is described in nanoseconds. Then for crack formation on the polycrystalline level one needs microseconds, while swelling and species migration can be observed in milliseconds. Three dimensional fuel assembly modelling relates to minutes and finally at whole plant scale, operations are described in years (Figure 2.3). Despite of the fact that many fundamental problems at atomic scale are still not

resolved, in any case modelling of nuclear fuel in full scale is far beyond reach the power of existing high-end computational clusters. Therefore currently accurate atomic scale physics is not present in fuel performance codes. Nevertheless increasing computing capabilities should allow us to apply micro-scale models in simulations. Such models can be developed basing on fundamental physics experiments.

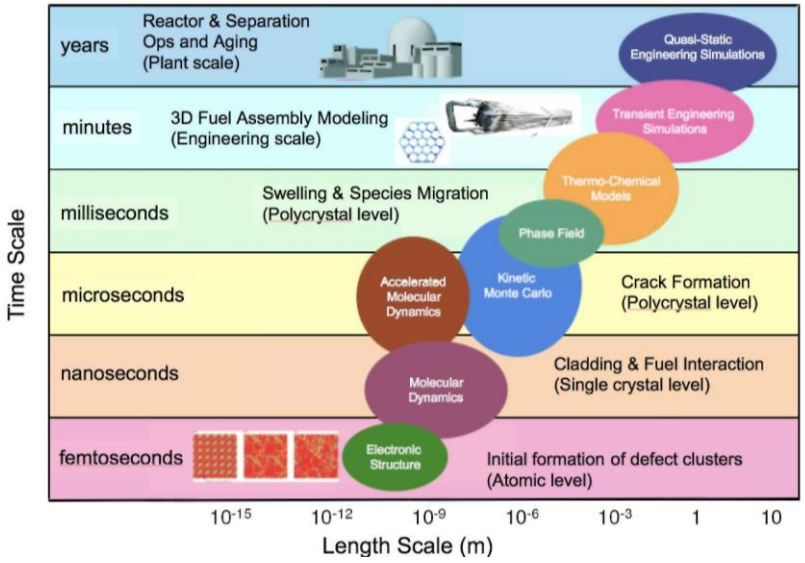


Figure 2.3 Multi-scale nuclear fuel modelling. Source [1].

According to [1] the main challenges for nuclear fuel modelling are the following:

- radiation induced micro-structural evolution,
- electronic structure methods for actinides,
- thermodynamic quantities in $UO_2$, $PuO_2$ and mixed-oxide fuels,
- mesoscale simulation of micro-structural evolution of fuel and the effects on thermo- mechanical response of fuel,
- modelling of fuel cladding and core structure,
- integral fuel performance code,
- integration of validation, verification and uncertainty quantification.

Taking into account these needs, there is a number of computational techniques that should be considered – the most important ones are [1]:

development of high order *ab initio* data and their automatic extraction for inter-atomic potential determination, solvers for long range forces, discretization methods for dynamics taking into account microstructural heterogeneity, coupling heat transport with species diffusion, models determining global ground states of multicomponent systems, linking front tracking with continuum field technique and parallel algorithms for long-time behaviour simulations.

### 1.4. Structural mechanics

The role of structural mechanics is to show adequacy of component design by combining mechanics techniques with the models of material behaviour. This includes, among others, such elements as: mechanical loading, brittle fracture, inelastic behaviour, elevated temperatures, neutron irradiation, vibrations and seismic effects. Similarly, as in nuclear fuel modelling, some of the processes can be described at microscopic level particularly those related to fuel pin design. Multiscale issues are related to scaling from materials to structures to deal with processes for the entire structure. This should allow for determination of vibrational response in heat exchangers or soil-structure interaction in case of earthquake. For large structural mechanics simulations this however requires application of adaptive mesh refinement and development of new parallel algorithms ensuring load balancing that can be applied to finite element modelling. Such models should allow for simulation of brittle materials and proper treatment of smoothened materials.

### 1.5. Repository modelling

The main aim of repository modelling is to produce a realistic assessment of the long-term performance of an arbitrary waste form for a complex geochemical environment. This should include estimation of uncertainties in the whole process basing on individual uncertainties inherent in the long-time scales of the problem. The spatial scale is of the order $10^{-2}$-$10^{3}$m (Figure 2.3), while temporal from 10s to $10^{8}$s.

The following fundamental physical and chemical processes are typically modelled [1]:

- multi-phase flow and multi-component transport in saturated porous media,
- mass and heat transfer within the waste emplacement drift,
- thermal geo-hydrology in host geologic medium that surrounds the waste,
- evolution of chemical environment,
- degradation of engineered systems,

- transport of radionuclides,
- impact of disruptive geological events.

For performing such simulations an integrated package of physical models including uncertainty propagation would be probably the best solution. This however needs development of software platform supporting various complex multi-physics models and appropriate infrastructure to ensure required performance.

Currently, the most advanced is a total system performance assessment (TSPA) model designed for the analysis of the proposed Yucca Mountain repository in USA (Figure 2.4). It integrates several physical and chemical processes for calculating long-term prognosis. The main components are the following [1]:

- Limiting water contacting waste package: for dealing with processes affecting water movement above the repository horizon (climate, net infiltration and unsaturated zone hydrology) and possible ingress of water into the emplacement drifts by seepage;
- Prolonging waste package lifetime: for dealing with processes affecting the degradation rate of the engineered barriers, including the environments in the emplacement drifts and the corrosion processes that affect the lifetime of the drip shield and waste package;

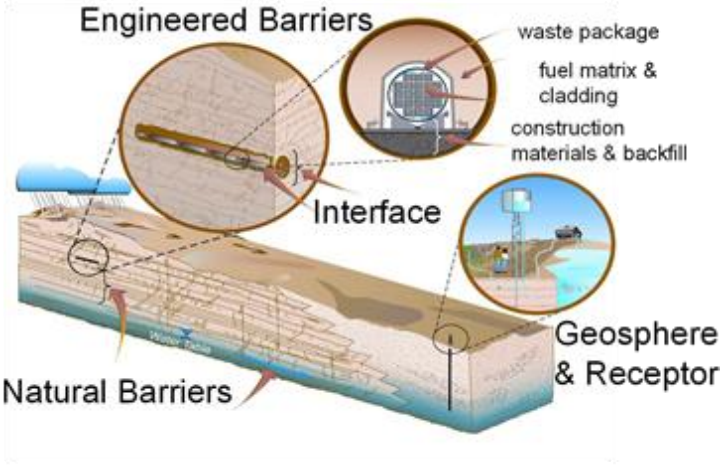


Figure 2.4 Multiple natural and engineered barriers contribute to ultimate performance of a geologic repository. Modified from DOE/OCRWM image in [1].

- Limiting radionuclide mobilization and release: for dealing with processes in the waste package such as the degradation of the spent fuel cladding and the alteration of the waste form when it is exposed to moisture, as well as the mobility and transport characteristics of the different radionuclides contained in the waste;
- Slowing radionuclide migration away from the engineered barrier system: for dealing with processes in the drift, the unsaturated zone and the saturated zone that tend to delay or disperse the radionuclides that may be released from the engineered barriers;
- Addressing the effects of potentially disruptive processes and events: for dealing with analysis of the potential significance of low probability events such as igneous activity.

The current system includes these processes as loosely coupled simplified models that are either abstracted from physics-based process models or are based on empirical correlations derived from experimental data. However, it is planned to build a tightly integrated package of physics-based models of the fundamental processes with a rigorous treatment of uncertainty propagation.

### 1.6. Seismic analysis and design

Historically, the main fields of investigation associated to earthquake are probabilistic seismic hazard assessment, interaction between soil and the structure, structural mechanics and dynamics. In case of earthquake seismic wave propagation in heterogeneous 3D media must be modelled while the response of the structure can be very complex. According to [1] the following areas need improvement:

- Nonlinear structural mechanics: this should allow for better understanding of structural system designs by defining clearly the goals taking into account extreme rare seismic events. For this purpose nonlinear material and structural element models have to be developed;
- Three-dimensional, time-domain interaction between soil and structure: currently limits due to computational power allows for a coarse mesh for relatively small soil domain surrounding the plant. Therefore, usage of massively parallel simulations would enable applying 3D coupled system response. Another important element is related to secondary equipment systems of NPP, which are sensitive to dynamic motions in the frequency range of 25-30 MHz. In order to model it properly, it is necessary to use fine mesh resolution for the structure and soil. Implicit time integration is the best

method when elastic wave speed is high and explicit ones vice versa. This means that hybrid schemes would be optimal;

- Three-dimensional regional seismic wave propagation: recent developments in the seismological community have shown that massively parallel computations of regional seismic wave propagation can be utilized;
- Simulations of fault to structure: this should allow for providing full 3D simulations of possible fault ruptures to structural response system.

## 1.7. Mesh management

For CFD or structural mechanics, a generation of good quality mesh can be problematic and time consuming, particularly when adaptive mesh refinement techniques are applied. It is natural that the models for different physics need various computational grids; therefore appropriate mapping between the results obtained from different modules must be assured. Typical examples are: upscaling microscale simulation data to meso- and macro-scale; molecular dynamics for ionic fluids for determining thermodynamic and transport parameters; extracting defects and grain boundaries from molecular dynamics simulations. For this reasons, automation methods should be developed with generation of multi-resolution grids and the tools allowing for removing non-important details from CAD data. Additional complication arises when sensitivity analysis has to be carried out. In this case also quantification of uncertainties due to operation on various meshes should be taken into account.

Currently a number of software tools can be used to deal with complex geometries of the computational domain including mesh generation tools, adaptive techniques and tools for dynamic partitioning for effective usage of parallel algorithms. However, the problem of integration of these tools is difficult and requires a lot of efforts. Therefore, as it has been already mentioned, a dedicated centre ITAPS (Figure 2.5) has been established in order to develop tools allowing for manipulation with interoperable and interchangeable meshes, geometries, etc.

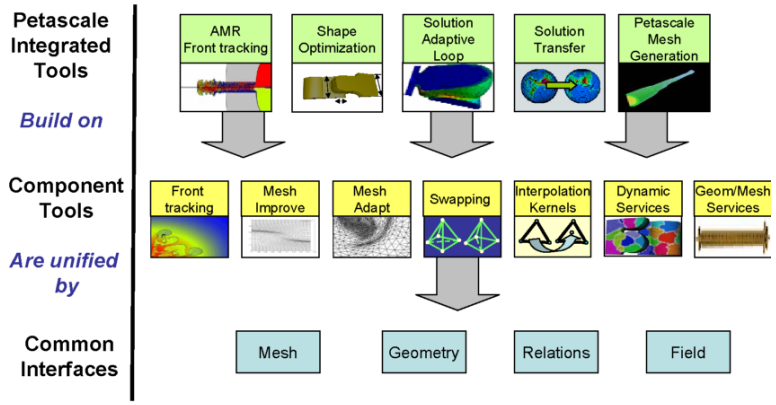


Figure 2.5 The ITAPS center is developing integrated services that build on multiple component services and common interfaces for geometry, mesh and field

The general idea is as follows: starting from the definition of the problem with the description of the geometric and temporal domain (annotated by attributes), decomposition into a set of piecewise components is done, (thus creating the mesh) and the continuous PDEs are then approximated on that mesh using some numerical schemes. By automatizing, the computing process simulation provides often feedback to the domain, which means that adaptive methods are applied which allows for obtaining more accurate solution. The ITAPS is based on data model consisting of three basic types: geometric, mesh and field data. These core data types are associated with each other through data relation managers, which control the relationships among two or more of the core data types. Then the building blocks are the concepts of entities, entity sets and tags, as follows:

- Entities represent atomic pieces of information such as a vertices in a mesh or edges in a geometric model;
- Entity sets are arbitrary collections of entities (ordered or unordered). The two primary supported relationships among entity sets are contained in and parent/child to allow for sub-setting and hierarchical applications;
- Tags are containers for attaching user-defined data to ITAPS entities and entity sets.

Then the common interfaces have to be defined within this data model. This can be implemented typically in C language, but some additional flexibility can be obtained by utilizing SIDL/Babel technology provided by the Common Component Architecture Forum (CCA).

## 1.8. Multi-physics, multi-scale methods, algorithms and codes

The spatial ranges of physical phenomena are from angstroms to kilometres, temporal one - from femtoseconds to years. The models are generally based on coupled PDEs, ODEs or integro-differential equations, describing various physic processes at different scales. The following areas which need further improvement have been identified in [1] as the most important:

- Monte Carlo techniques: there is a need for scalable and accurate algorithms to deal with high-dimensional functions. Neutronics calculation for Boltzmann's equation is a typical example;
- Multi-scale physics: information exchange between multi-scale models is a crucial point for effective implementation of model's chain;
- Coupling models for different time scale: very often time step is determined by the processes at finest scale – then adaptive time stepping and integration methods can be applied. As an example for the need of such solution is transient analysis for reactor safety;
- Improved solution time for coupled models: in this respect, time splitting of operators and proper treatment of boundary conditions at different levels and scales are required. In particular for transient analysis solvers for stiff time evolution problems needs more effective algorithms;
- Mathematical techniques for complex multiscale and multilevel boundary conditions: this is important to keep accuracy of the solution;
- Adaptive methods for multi-physics approach: coupling core neutron transport with thermal-hydraulics. New methods will be necessary to deal with Newtonian and non-Newtonian flows in complex geometries. This includes: phase change, particle interactions, bubble development turbulence, chemical reactions, free surface problems, front tracking and interaction between fluid and structure;
- Multi-scale methods for constrained optimisation: effective methods are required, among others, for reliability and safety analysis for reactor design, operations and seismic analysis;
- Code coupling: this is a complicated problem requiring appropriate mathematical representation of data that should be exchanged between different codes. For example, the coupling of codes representing the reactor core and vessel with the models simulating the balance of plant piping, pumps, structures, and other important components generally cannot be done without enormous investment of time and effort. Similarly, detailed fuel rod performance codes providing high-fidelity response cannot be easily used to provide information to full-core simulations. This can be achieved by

building dedicated software platforms with well-established interfaces in order to develop and test the models and then perform effective parallel simulation utilizing high performance computing resources. Additional needs are related to have a possibility of propagation of uncertainty between the codes;

- Development of high order numerical schemes for complex geometries with adaptive mesh refinement and front tracking techniques, which can be effectively implemented on high performance clusters basing on parallel computing algorithms.

## 1.9. Ongoing developments

The NEAMS Toolkit, being under development, will be served as a basic tool for researchers, so they can develop computational models, validate it and verify against experimental data, and finally, estimate its uncertainties. At present few applications are already available [3]. Some of them are described shortly below, together with other systems being under development based on similar approach.

The present version of NEAMS tools include: MARMOT and BISON code for fuel, and RELAP7 and SHARP for reactors.

The aim of MARMOT code it to simulate how nuclear fuel and its cladding change in time basing on micron scale. In particular, it enables to model how the microstructures evolve under irradiation by receiving inputs from atomic scale simulations. It is possible to generate new material properties and irradiation behaviour and pass the results to engineering scale codes BISON. The purpose of the latter is to easily incorporate new material property and irradiation behaviour taken from MARMOT under normal, off-normal and accident conditions. Hence, both codes constitute the basic models for nuclear fuel.

The thermal-hydraulic RELAP-7 system analysis module provides one dimensional lumped parameter system performance and safety analysis capability. It will address a broad range of phenomena at a plant scale, hence localized phenomena cannot be analysed in great detail at every point in the plant.

The Simulation-based High-efficiency Advanced Reactor Prototyping (SHARP) [8], developed at Argonne National Laboratory is a suite of physics simulation software modules and computational framework components aiming at assessment of the impact of design decisions on performance and safety of nuclear reactors or their components. It consists of models enabling advanced

reactor simulation, in particular coupled neutronics and thermal-hydraulics, and structural mechanics modules. The thermal-hydraulic part includes a hierarchy of CFD models starting from detailed turbulence computations, performed by DNS and LES, to full core analysis based on RANS and sub-channel models.

Initially, the package was applied for sodium-cooled fast reactors to demonstrate their passive safety characteristics, resulting from multi-physics thermal-structural-neutronics phenomena. Later, a number of components have been integrated, for example simulations of steady state conditions for some assembly types were performed by using the following modules: mesh generation MeshKit, the PROTEUS neutronics, CFD Nek5000, the Mesh-Oriented DataBase (MOAB) mesh management, and the COUPÉ driver. The MeshKit was also used for generating computational meshes for a very high-temperature gas-cooled reactor and applied in PRONGHORN multi-dimensional reactor analysis code. A number of specific modules was then applied for different types of fuel assembly and reactors, and various simulations were performed, finally leading to essential improvements of used modules. Among the most important ones, one can mention a number of improvements made in Nek5000 CFD code, integration of the structural mechanics module Diablo with the SHARP framework (in particular with Nek5000), coupling RELAP-7 with PRONGHORN, and extending functionality of neutronics module PROTEUS (neutron and gamma transport solvers, cross-section processing tools, and tools for depletion and fuel cycle analysis).

Another comprehensive modelling and simulation suite for nuclear safety analysis and design - SCALE has been developed at ORNL [9]. The main domains of SCALE are: criticality safety, radiation shielding, cross-section processing, reactor physics, sensitivity and uncertainty analysis, and characterization of spent fuel. In high performance computation SCALE provides solutions to model complex systems, high fidelity shielding, reactor physics and sensitivity analysis in continuous energy. The structure of SCALE is modular enabling for automation via control modules some standard analytical sequences. One of such control module, is for example, TRITON (Transport Rigor Implemented for Transient Depletion with ORIGEN) enabling depletion calculations by coupling SCALE functional modules, which perform problem dependent multi-group cross-section processing, neutron transport calculations, and isotopic depletion and decay. Accurate neutron transport calculations can be made by NEWT or KENO models. Finally, one can get an accurate first-principles approach for depletion and lattice physics analysis of a broad spectrum of fuel designs.

Electricite de France (EDF) has also developed a number of codes that can be used within one framework [10]. In this respect, one can mention Saturne, the general purpose CFD code that can be applied both for incompressible and expandable flows and with or without turbulence and heat transfer. It contains dedicated modules for combustion, Lagrangian particle tracking and radiative heat transfer. Both RANS and LES models are included in Saturne.

The ASTER code based on finite element method can be applied to structural analysis and contains modules for simulating mechanical processes like: fatigue, damage, fracture, contact, geo-materials, porous media, and multi-physics coupling.

The SYRTHES code is designed to perform transient thermal simulation in complex solid geometries, and can treat the following problems: heat and mass transfer, conduction and radiation.

All the codes can function on Salome platform, serving for pre- and post-processing for numerical simulation.

In the next sections of this article, one will learn more on one specific subject, namely thermal hydraulic analyses. The use of words “one specific subject” may be misleading, because the topic itself covers wide range of scales and phenomena, which cannot be solved by one type of codes.

For this reason, next chapters will present, first, the basis on which these codes rely and then their practical use, by means of applying different class of codes to the same experimental example. Finally, the comparison and discussions of the results coming from different codes will allow the reader to understand the real challenges of multi-physics, multi-scale modelling.

## 2. Computational Fluid Dynamics

One of the most important aspect of nuclear business, after radiation maintenance (or protection), is a proper heat management and for this reason thermal-hydraulic analyses are necessary. In general, they are conducted at any stage of nuclear power plant life cycle - from the blueprints to the decommissioning phase - accounting for fuel fabrication, long-term spent fuel facilities etc. Normally, the thermal-hydraulic (TH) analyses comprises either single components or whole systems, the issue of research may be flow passing feedwater pump, but it may be also a flow circulating in a primary circuit. Depends on needs, TH analyses provide system performance parameters and can

answer a question: how the system will react upon any undesired distortion in the coolant flow.

There are several types of codes that resolve TH issues in nuclear facilities among which computational fluid dynamic (CFD) codes will be discussed first due to the scale they cover.

CFD codes are designed to solve the Navier-Stokes equations, i.e. conservation equations for mass (2.1) and momentum (2.2a-2.2c) in the cases of 2D or 3D flows. For flows involving heat transfer or compressibility, an additional equation for energy conservation (2.3) is solved. For flows involving species mixing or reactions, a species conservation equation is solved or, if the non-premixed combustion model is used, conservation equations for the mixture fraction and its variance are solved. Additional transport equations are also solved when the flow is turbulent.

Governing equations for the 3D unsteady flow of a compressible Newtonian fluid including heat transfer should be as follows:

$$\frac{\partial \rho}{\partial t} + div(\rho U) = 0 \qquad (2.1)$$

$$\frac{\partial (\rho u)}{\partial t} + div(\rho u U) = -\frac{\partial p}{\partial x} + div(\mu\, grad\, u) + S_{Mx} \qquad (2.2a)$$

$$\frac{\partial (\rho v)}{\partial t} + div(\rho v U) = -\frac{\partial p}{\partial y} + div(\mu\, grad\, v) + S_{My} \qquad (2.2b)$$

$$\frac{\partial (\rho w)}{\partial t} + div(\rho w U) = -\frac{\partial p}{\partial z} + div(\mu\, grad\, w) + S_{Mz} \qquad (2.2c)$$

$$\frac{\partial (\rho i)}{\partial t} + div(\rho i U) = -p\, div\, U + div(k\, grad T) + \Phi + S_i \qquad (2.3)$$

where:

$U = [u,v,w]$ – velocity,

$\mu$ – dynamic viscosity,

$S_M$ – momentum source,

$i$ – internal energy,

$k$ – thermal conductivity,

$\Phi$ – dissipation function.

In other words, CFD codes can handle flows which may be steady or unsteady, laminar or turbulent, incompressible or potentially dilatable/compressible, isothermal or not, single-phase or multiphase, either non-mixable or undergoing phase change. Scalars and turbulent fluctuations of scalars can be taken into account. CFD codes can treat lagrangian particle tracking, radiative transfer, pulverized substances or gas combustion or even electricity effects. All these features and many others make CFD of a multipurpose use [11, 12, 13].

CFD bases mostly on Finite Volume Method (FVM), which means discretization of a flow domain usually "encapsulated" in a complex geometry. A process of discretization is commonly known here as a meshing and yields typically millions of cells. CFD engineering practice shows that the medium size of a domain is about 10-30 millions of cells, while the characteristic length of a single cell can range from fractions of millimetres up to tens of centimetres, i.e. $10^{-12}$ $m^3$ – $10^{-3}$ $m^3$ when 3D case is considered. When NPP comes as a TH issue it appears that CFD can handle only single components, i.e. fuel pellets with their cladding, fuel bundle, pump or at best reactor pressure vessel with its internals, rather than whole systems or circuits and that comes from the hardware limitations. One needs to keep in mind that the set of equations mentioned above has to be solved for each cell! For example, Figure 2.6 depicts model of VVER-1000 reactor pressure vessel made of 85 mln cells [14]. Since thermal effects are of the main concern here, a part of continuity and momentum equations, it is necessary to solve energy equation. Moreover k-ε model was involved to track flow turbulence effects, which impose a need for another six equations. In total it is (at least) 11 equations for every single cell. This is 935 mln of equations for one time/iteration step!

Although expensive, CFD is a powerful technique providing information on very local phenomena, like surface hot spots, flow turbulences affecting negatively heat transfer etc. These high resolution results are essential not only when designing or optimizing particular components, but also to indicate fracture points of whole system that they could be easily omitted at the bigger scale.

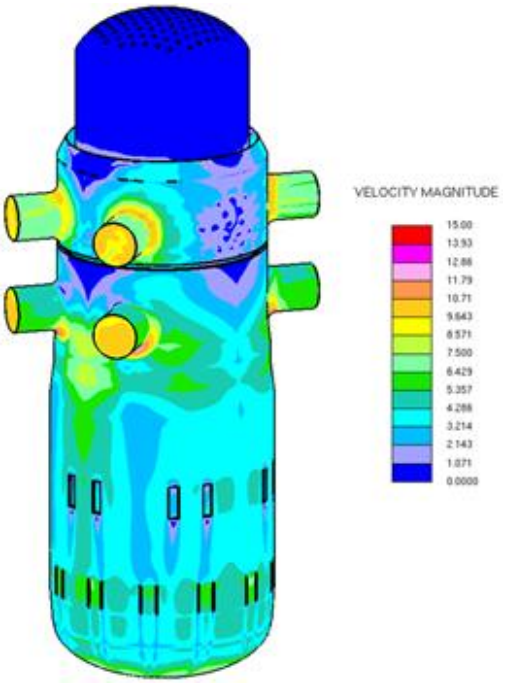


Figure 2.6 Velocity magnitude distribution in VVER-1000 reactor pressure vessel [14].

Even though physical basics of this technique have been given by Claude-Louis Navier and George Gabriel Stokes in XIX century, CFD had to wait over a century for its first software implementation. At the beginning only in the aerospace industry, now CFD is widely used, i.e. in weather prediction, air-conditioning design, chemical process engineering or even in biomedical engineering e.g. to track blood flow patterns and many more. Development of CFD is strongly related to progress in the field of numerical analysis and computer hardware, particularly High Performance Computing (HPC). Due to the latter one, the rise in speed of CFD calculations following growth in features and number of models became a fact in the last decade and is still on-going.

Unfortunately, this progress is still too slow for the nuclear industry, where CFD is treated as an “immature” technique. It is because limited hardware capabilities force simplifications in models. These simplifications are hidden usually in solver implementation which is based likely on empirical correlations instead of being derived from *ab initio* rules. Those correlations have limited scope of applications, not necessarily fitting all the needs posed by the real case. Moreover, there are lots of alternatives and that creates a space for a situation,

where more than one solver can simulate the same phenomenon, giving slightly different results, though all are still best estimates – with some uncertainties - of the real parameter of interest. The problem here lies in the lack of (uniform) methodology in uncertainty quantification of the results, so important from the nuclear safety point of view. The diversity of approaches to the solution and the number of intermediate options without proper assessment are, in general, not acceptable for nuclear engineers, who like straight and clear procedures.

The main problem of CFD is a lack of good description of turbulence model. Actually, there is no one good model for all the cases and instead each code offers set of models with different range of applicability, e.g. ANSYS Fluent provides over 20 different turbulent solvers. These models can be, however, divided into 3 main categories, i.e. RANS, LES and DNS, according to their level of simplification.

In 90% of cases, CFD engineers successfully apply Reynolds-Averaged Navier-Stokes (RANS) solver to their research. RANS is focused on mean flow and the effects of turbulence on mean flow properties. Prior to the application of numerical methods the Navier-Stokes equations are time averaged. Extra terms appear in the time-averaged (or Reynolds-averaged) flow equations due to the interactions between various turbulent fluctuations. These extra terms are modelled with classical turbulence models: among the best known ones are the k-ε model and the Reynolds Stress Model. Since the computing resources, required for reasonably accurate flow computations, were and still are rather modest, this approach has been the support of engineering flow calculations for over the last three decades [15].

Another - intermediate form of turbulence calculations which tracks not only the mean flow, but also the behaviour of the larger eddies is called Large Eddy Simulation (LES). The method involves space filtering of the unsteady Navier-Stokes equations prior to the computations, which passes the larger eddies and rejects the smaller eddies. The effects on the resolved flow (mean flow plus large eddies) due to the smallest, unresolved eddies are included by means of a so-called sub-grid scale model. Unsteady flow equations must be solved, so the demands on computing resources in terms of storage and volume of calculations are large, but this technique is currently starting to address CFD problems with complex geometries.

From the nuclear engineering point of view the best choice would be the Direct Numerical Simulation (DNS). This kind of simulation computes the mean flow and all turbulent velocity fluctuations. The unsteady Navier-Stokes

equations are solved on spatial grids that are sufficiently fine that they can resolve the Kolmogorov length scales (at least 4 cells covering the smallest eddy in one dimension) at which energy dissipation takes place and with time steps sufficiently small to resolve the period of the fastest fluctuations. These calculations are highly costly in terms of computing resources, so the method is not used for industrial flow computations yet.

Finally, big international effort is currently devoted to improve understanding of the relevant phenomena involved in the incidents and/or accidents of NPPs, also in developing their numerical representations, in order to increase the realism of plant behaviour assessment and to improve the accuracy of safety margin assessment. Just to mention programs and projects within the framework of NURESAFE [16] or NUGENIA [17].

## 3. System Thermo-Hydraulic codes

From the very beginning of the nuclear era there was always a need for knowledge of the parameters of the system – in our particular case – steam generation system. Regardless of what kind the nuclear power plant was (PWR or BWR), for it safe operation it was necessary to have sufficiently efficient safety systems which where actuated in case of unexpected behaviour or transient or in case of emergency. Effectiveness of these safety systems depends on, indirectly, the knowledge of the plant behaviour during various transients – expected and unexpected as well as during design basis accidents and beyond design basis accidents. The answer to these concerns lies within system scale calculations.

These kinds of calculations or simulations are mainly focused on thermo-hydraulic aspects of the system. In a nutshell, its main concern was the radiation protection against the public. That goal was achieved through assuring the core was constantly sub-critical (neutronic scale/analysis) and it was under no circumstance uncovered to the steam [18].

System scale codes are defined as codes that provide an answer/reaction of the whole thermo-hydraulic system of the nuclear power plant with its safety systems to any discrepancy from normal operation that may occur. This goal is achieved through introduction of a generalization and averaging of some effects and phenomena.

Generally, whole reactor and steam circuit is modelled by roughly one thousand elements. Usually they solve three balance equations as follows [19]:

- mass balance equation:

$$\frac{\partial}{\partial t}(A\alpha\rho_G) + \frac{\partial}{\partial z}(A\alpha\rho_G V_G) = A\Gamma + \sum_{i=1}^{4} S_i + S_v \tag{2.4}$$

- momentum equation:

$$A\alpha_k\rho_k\left[\frac{\partial V_k}{\partial t} + V_k\frac{\partial V_k}{\partial z}\right] + A\alpha_k\frac{\partial P}{\partial z} + Ap_i\frac{\partial \alpha_i}{\partial z} +$$
$$A\beta\alpha_g\alpha_l\rho_m\left[\frac{\partial V_G}{\partial t} - \frac{\partial V_L}{\partial t} + V_G\frac{\partial V_G}{\partial z} - V_L\frac{\partial V_L}{\partial z}\right] \tag{2.5}$$
$$= \sum_{i=1}^{2} A\Gamma_i(W_i - V_k) + A\tau_k - \frac{1}{A}\chi_f C_k\frac{\rho_k}{2}V_k|V_k| + A\alpha_k\rho_k g_z + \frac{R\alpha_k}{4}p_i\frac{\partial A}{\partial z}$$

- energy equation:

$$A\frac{\partial}{\partial t}\left(\alpha\rho_k\left[H_k + \frac{V_k^2}{2}\right]\right) + \frac{\partial}{\partial z}\left(A\alpha_k\rho_k V_k\left[H_k + \frac{V_k^2}{2}\right]\right) - A\alpha_k\frac{\partial P}{\partial t}$$
$$= Aq_{ge} + \chi_c q_{pg} + \sum_{i=1}^{3} A\Gamma_i\left[H_i + \frac{W_i^2}{2}\right] + A\alpha_k\rho_k V_k g_z \tag{2.6}$$

In aforementioned equations numbers of different parameters are used, such as:

- interfacial mass transfer,
- rate of entrainment,
- rate of stratification,
- interfacial friction,
- interface velocity.

It should be highlighted that all calculations and equations are solved mainly in one-dimensional manner and all elements (volumes/nodes) of such codes are treated one-dimensionally – which is very important to remember.

These three equations are written for two phases of water, additionally for each incondensable gas if one or more are present in the system. For some system codes (i.e. CATHARE) fluid always is comprised of two phases which yields six equations – for single phase fluid, a residual phase treatment is used,

meaning the void fraction coefficient equals to $10e^{-5}$ for liquid only or $10e^{-6}$ for vapour only.

Two-fluid and six-equation model was used for very specific reasons. Thanks to this it is possible to easily model various phenomena that may occur in nuclear power plant normal or unexpected operation:

- phase separation,
- stratification,
- co-current and counter-current flows,
- CCFL – counter-current flow limitation,
- critical flow,
- cold water injection,
- reflooding, etc.

Moreover, all kinds of different flow regimes and all heat transfer regimes can be simulated (see Figure 2.7). System codes are design to model whole systems of nuclear power plants. Although, their biggest advantage is that models of the system, which are hundreds of meters of piping, should simulate the pre-defined accident in less than twelve hours.

To achieve this goal it is somewhat necessary to employ some level of averaging. Method of that kind brings some advantages and disadvantages. Before discussing pros and cons the idea itself will be explained.

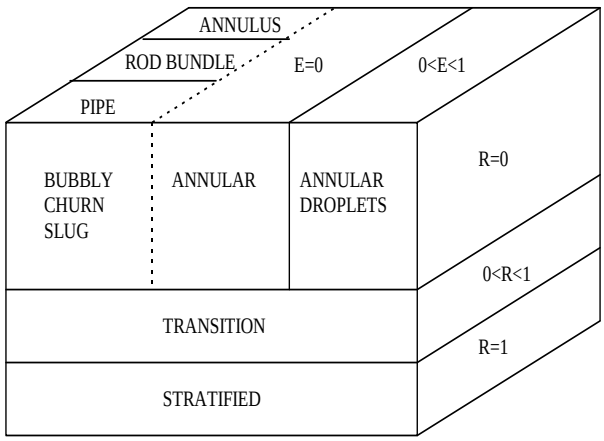


Figure 2.7 Flow regimes. Depending on different parameters of the flow, respective flow regime model is applied [19].

Averaging – in the essence it means expressing for example entire BWR upper plenum by single volume. The implication coming from this is as follows: upper plenum in its extensiveness is characterised by single pressure (volume is divided in two sub-volumes – one for liquid phase and one for vapour phase) that is stored in software's memory. The same is applied to the temperatures and other parameters of state which results in somewhat omitting the effects of the pressure gradient along vertical axis. Fortunately, that happens only to volumes itself. Such effects as pressure stratification are taken into consideration in nodes that connect volumes to other elements of the model. In Figure 2.8 one can see typical volume with connections – port *i* and *j*. However, the volume consists only of two scalars describing its behaviour (two round white circles) which do not take into account phenomena mentioned above, upon the connection of two ports, two additional scalars(red circles) are implemented so this phenomenon's effect is calculated.

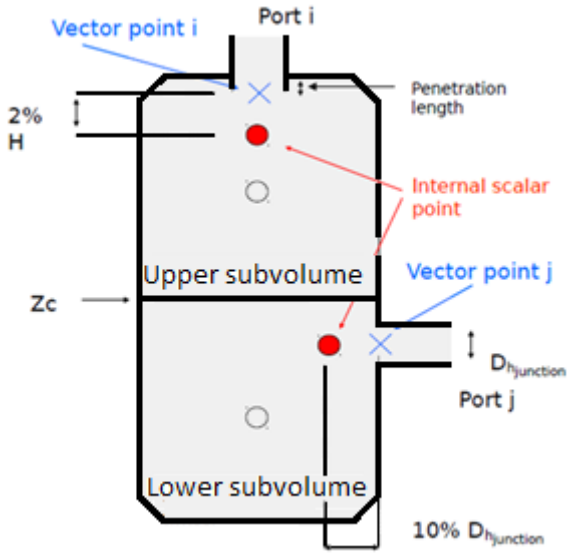


Figure 2.8 Volume element. White circles represent scalar points of lower and upper (liquid and vapour, respectively) plena of the volume. Between them there is no vector point which does not mean these 2 points do not exchange mass and energy. Blue crosses and red circles are vector and scalar points coming from adjoined elements – port i and port j.

Slightly different approach is incorporated to all kind of pipes or core region. Depending on the calculation power in disposition and on resolution of the results one can divide pipes in roughly twenty volumes/nodes (volumes in a sense that the part of a pipe's volume is parameterized to a single node at which all parameters are stored – both for liquid and vapour – see Figure 2.9).

Taking all these features (one-dimensional models/solvers, averaging approach) we receive a code that can model all systems of the nuclear power plant with entire reactor pressure vessel, safety system and all major components in relatively small amount of time. This feature plays very important role in the accident analysis. The main reason for this is that accident analysis requires time of the order of magnitude of tens of hours of transient.

In spite of averaging, these codes produce very good results within acceptable criteria that is required in the nuclear industry. Large amount of effort was put to assure the accuracy of that type of codes through the verification process on integral test facilities as well as separate effect test facilities. The main concern of the nuclear industry is to obtain reliable tool that can provide a sufficiently acceptable time trends of mass flow rates, pressure of the system, heat transfers, core water level, vapour fraction, critical flows etc.

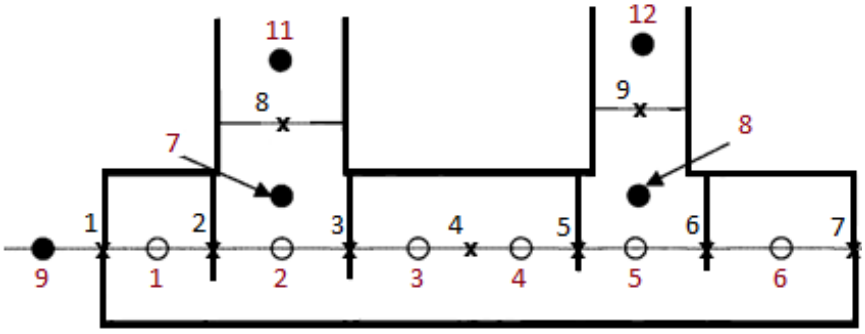


Figure 2.9 Axial element. Here it is depicted a pipe with 2 tees. Scalars (circles, red numbering) from 1 to 6 are internal axial points. Scalars 7 & 8 are internal points coming from connections with other elements. Scalars from 9 to 12 are external points of axial for connection with other elements. Vector points are marked as crosses. They are created between scalars [20].

As far as computation is concerned, such codes do not require high performance computers. Regular desktop computers are enough to perform system calculation. In general that software run sequential calculations (mainly due to architecture of the code). However, CATHARE, which is constantly under development, can also be executed using parallel computing.

The most important drawback coming from averaging method is the resolution of the results. Due to the fact that large area and volume are averaged means that we lose the possibility to see details of some elements. For example, we would not know the temperature of the specific fuel rod mainly due to the fact, the temperature of that particular rod was taken with other rods for averaging. For purposes such as presented best suited are components codes and CFD codes which deal with very fine meshes and do not employ such level of averaging.

The description of the usage of the code from the phenomenological, analytical and numerical point of view was presented. But the range of use of these types of code does not end here. Both codes, CATHARE and RELAP5, were used as a basis to build simulators for operators of the nuclear power plant.

There are many applications of RELAP5 in simulators, but in this text only one will be described, namely RELAP5-HD created in Idaho National Laboratory. Its thermo-hydraulic engine was RELAP5-3D that was integrated into SimExec - real time simulator executive. This framework makes the interactive interfacing with the outside world straightforward. Due to the architecture of the RELAP5 code it is very complex to apply it to simulators. This problem is solved by sharing the parameters in common memory. Thanks to this the outside world may be the simulator, users or tools to monitor results or interfaces with boundary conditions [21].

For CATHARE2 there is a simulator called SOFIA that stems from Simulator for Observation of Functioning during Incidental and Accidental situations. The project has been divided into 2 phases. The first phase was to use TRACAS+ as a TH code with about 300 mesh cells. The simulation is allowed both in real time and accelerated time, with a possible simulation from the maximum nominal power to cold shutdown. The real time of simulations is allowed except in the case of large break on the circuit [22].

SOFIA can perform simulations in normal operation and in incident and accident operation, such as start-up and shutdown, load following, house load, loss of power, loss of heat sink, loss of feedwater systems, primary and

secondary circuit breaks, 100% power to cold shutdown states for maintenance (primary circuit opened), just before the reactor vessel opening, accident up to cladding temperature ~1200°C. Moreover, it can simulate both the nuclear and the conventional island: neutronics and/or TH processes using design codes; operational and safety I&C; electrical distribution, containment [22].

As concluding remarks it should be noted that averaging in the system codes is their most important advantage and at the same time their biggest drawback. As long as system codes are used in field they were designed to give correct and precise answer of the system (system scale). In the case of the more detailed calculations – component scale or CFD scale – respective computational codes should be employed (such as FLICKA4 or TRIO-U/NEPTUNE CFD).

# 4. Example: BNCT converter

From the very beginning of existence of the nuclear power plants, one was aware of the potential risks and had to design necessary countermeasures to protect personnel and the public from the effects of the possible accidents. There is a basic assumption that the risk associated with the nuclear power should be lower than the risk related to other methods of electricity generation. Over the years, advanced techniques and tools for safety analysis were developed and they are still evolving. Nowadays, safety analysis methodology is routinely employed in the field of nuclear engineering, but that knowledge is also applied to derivative issues, such as nuclear medicine or chemical industry.

The example, that is going to be presented in this paragraph, concerns safety analysis of a medical facility. The main part of it – somewhat similar to commercial nuclear fuel bundles - will be installed in the core of the MARIA Research Reactor at the National Centre for Nuclear Research (NCBJ Poland) and due to this; the safety analysis has to be conducted.

## 4.1. Problem description

The Boron-Neutron Capture Therapy (BNCT) is an experimental medical technique used to treat high-grade gliomas (specifically glioblastoma multiforme - GBM), because they are immensely resistant to all common forms of therapy including: surgery, radiotherapy, chemotherapy, immunotherapy and gene therapy. Based on statistics, the median survival of glioblastoma patients is typically 9-10 months and furthermore the 5-year survival rate is less than a few percent [23]. Glioblastoma is considered the most malignant and intractable of brain tumours. Usually, it occurs in the white matter of the brain, grows rapidly

and diffusely infiltrates both the white and grey matter, thus surgical resection of the tumours is not an effective method of the treatment. As a result, GBM must be regarded as whole-brain diseases. In theory, BNCT - in a selective way - destroys malignant cells while saves normal cells [24]. Physical concept of the method is based on reaction of thermal neutron capture by boron nucleus ($^{10}$B), which is non-radioactive constituent of natural boron:

$$ {}_0^1n + {}_5^{10}B \rightarrow {}_3^7Li + {}_2^4\alpha \tag{2.7} $$

A boron compound is injected into a patient, in whom it is attracted by malignant tumours tissue. Afterward, the tumour is irradiated with low-energy neutrons, which activate the boron solution and dissipate most of energy within the volume of a single cell. The cancer can be destroyed, because the boron concentrates in the tumour cells, while the normal cerebrum cells nearby receive the safe radiation dose [25].

To date, clinical trials of BNCT for patients with GBM have been carried out at few reactors in USA, Japan and Europe. This medical therapy needs the specific energy spectrum, thus it can be adopted only at some existing reactors. The BNCT, to be effective, needs a sufficient dose of epithermal neutrons, with negligibly low background of high energy neutrons. Kind of solution of this problem may be the use of fission converter facility, which modifies the energy spectrum of the primary neutron beam. Such a converter was designed for the use in the MARIA Research Reactor at the National Centre for Nuclear Research (NCBJ) in Świerk near Warsaw, Poland.

Figure 2.10 presents the facility for BNCT, which will be installed in the basket-vessel of the MARIA Research Reactor, properly it is a set of fuel rods placed in a specially adopted fuel separator. Flux density of the epithermal neutrons from the MARIA Research Reactor is too low to be directly used for the treatment. Therefore, the construction of the fission converter, which results in the production of fast neutrons, was required. Next, this flux through a suitably designed moderator/filter system will create the required therapeutic epithermal beam of spatial homogeneity and low contamination.

From the technical point of view, the BNCT converter consists of one measurement probe and 98 fuel rods with a height of 0.588 m and the fuel active zone equal to 0.5 m. The measurement probe, devoted to monitor temperature and neutron flux, is located in the one of the corner rods, which is the closest to the reactor core (bottom-right corner of the lattice presented at Figure 2.10b). The fuel is a dispersion of $UO_2$ within metallic magnesium. It is low-enriched

uranium – 10% U-235. Generally, the converter can be seen as a box-shaped reactor fuel assembly, which will be located in the graphite matrix instead of one of the reflector blocks with the active zone at half-height of the real core. The converter box walls are made of aluminium – the same as the cladding of graphite blocks. The block was equipped with a special feature – so called "foot" – holder, which allows to place it in the right position. The converter core itself is a triangular rod matrix with a step of 12 mm (Figure 2.10b) [26].

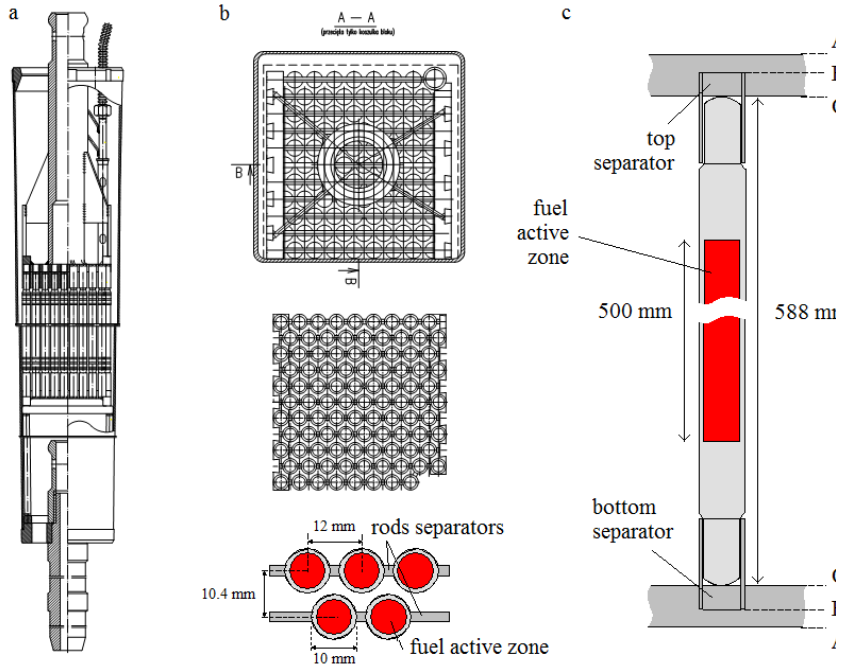


Figure 2.10 Details of the BNCT converter geometry (a) side cross-section view of converter box with internals, (b) top cross-section view, (c) the fuel rod installation [26].

The BNCT converter placed in the graphite matrix (side reflector) provides significant intensity of epithermal and fast neutrons, but from the other hand there is a need to ensure adequate cooling conditions. This is one of the most important and crucial safety conditions that must be fulfilled absolutely. In order to prove the existence of sufficient safety margins, the safety analyses were performed and summarized in the Safety Assessment Report [26]. Particularly, it was important to determine the maximum temperature of the rod wall surfaces (excessive increase of temperature may cause melting of fuel shield). The safety

document indicate that the maximum temperature of the most thermally loaded rod will never exceed 85°C (358K) for steady state and 136°C (409K) for transient emergency cases. Following assumptions where taken into account when performing the analytical calculation of BNCT converter heat transfer:

- inlet water temperature: 50°C (323K),
- pressure drop along the core matrix: 1400 mm $H_2O$,
- the height of the rod with the sleeves of separators: 0.59 m,
- thermal power of the 'hottest' rod: 5 kW (this rod replaces measurement probe for simplicity sake),
- the extrapolated height of fuel: 0.65 and 1.15 m.

Taking into account a number of limitations and difficulties of appropriate estimation of the temperature distribution over the rods by the analytical calculation, study of the heat transfer was performed only for one, though the most thermally loaded rod (see: red top in Figure 2. 11). In fact, this implies the existence of 99 rods instead of 98. This assumption was applied to all further studies.

Apart of the analytical calculation of the reactor safety-related margins, the study with the use of System Thermal Hydraulic (System TH) code (CATHARE) and modern Computational Fluid Dynamics (CFD) code (ANSYS Fluent v.13/14) were performed. CATHARE is intended to model fullscale problem rather than component scale issue. Thus, first the CATHARE analysis was carried out in order to determine general, averaged boundary conditions, which then were used to CFD analysis. This approach (full scale 3D study) allowed the use of more realistic input data, especially when one will take into account the fact that each of the 99 (98 in real) fuel rods in the converter has its own unique heat flux spatial distribution (Figure 2.11), what was not possible with analytical computation.

## 4.2. Scale definition

- *System scale approach*

The BNCT (Boron Neutron Capture Therapy) converter is a fuel bundle one meter in length and roughly ten by ten centimetres in cross-section. From the system scale point of view this is not the most suitable study, however, the converter itself may be the part of the larger system which can be affected by its behaviour.

For the sake of the correctness of the deterministic analysis, very specific guidelines were produced in order to achieve lowest possible input error. According to the IAEA publication: Accident Analysis for Nuclear Power Plant [28] (the final application of the system codes is the evaluation of the Nuclear Power Plant) first step is to gather the documentation of the design of the converter. This should consist of technical specification of the equipment. Additionally, documentation regarding the start-up of the installation and operation of the plant should be included.

Having this completed, an engineering handbook creation is in order. The engineering handbook needs to be developed in parallel with the development of the code input deck. The handbook is a document containing full description and records of how the database has been converted into and input deck for the particular computer code.

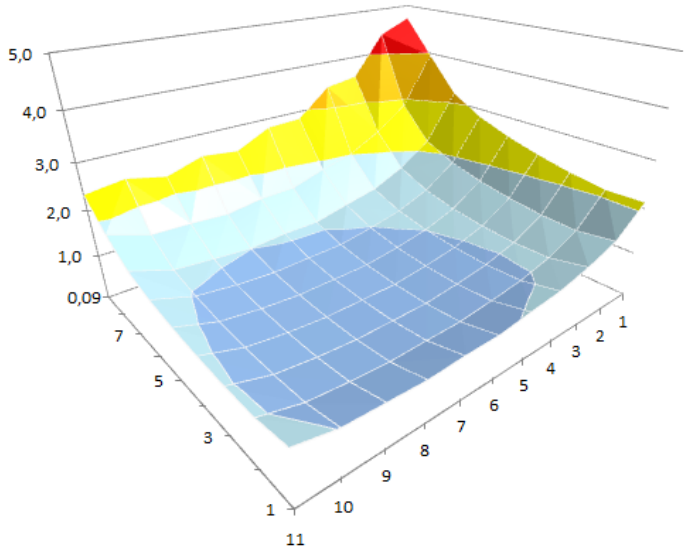


Figure 2.11 The power distribution over BNCT core lattice [kW]. Source [27].

The document contains details of:

- Methods and simplifying assumptions used to convert the technical plant data into the code input data;
- All calculations made to convert the technical plant data to the necessary format for the input deck;

- Nodalization schemes used for a single component as well as for the complete system being modelled;
- All modelling assumptions made, adequately described and explained.

For the particular case of BNCT, analysts had access to the blue-prints of the converter, blue-prints of the reactor MARIA (in which the converter will be installed) and the safety report.

The CATHARE2 code fidelity has given two possible approaches to the analysis of the BCNT converter, namely one-dimensional and three-dimensional and both approaches were performed for the sake of comparison analysis. Two input deck files were prepared for this need; both have its own engineering handbook.

Next two steps of the analysis are the verification and validation of the input data. Verification of the input is meant to find and correct possible errors with respect to the documentation supplied while validation of the input aims at calculation correctness. Namely, one must run the calculation to compare the results with the experiment. Validation of the input data file is an iterative process by means of which the correctness and adequacy of the models are confirmed with the reflection in the results compared with real model.

Firstly, the experiment of the BNCT converter will be described with its initial and boundary conditions, furthermore one- and three-dimensional approaches will be presented with respect to the BNCT converter model and lastly the results of both approaches will be shown and discussed. Since the description of the geometry of the BNCT converter was mentioned in previous chapter, the CATHARE model implementation will be discussed.

The BNCT converter will be positioned vertically in the reactor periphery due to the need to direct the flux of neutrons out of the reactor. The experiment assumes the flow to be coming from top to bottom with water velocity of 1.26 m/s and temperature of 50°C. The heat generation of the fuel is set to be ~100 kW in total. It must be noted that heat generation is not the same for every rod but due to positioning in reactor and nature of neutron distribution the heat generation is as it is presented in Figure 2.11.

As it was mentioned before two cases of BNCT converter were discussed. The one-dimensional model of the converter has not taken into account the power distribution. As it can be expected the one-dimensional model takes all power of rods and treats it as one medium delivering whole power to water. This

approach was applied as a fast calculating one and aimed only at cumulative effect of the converter in terms of temperature and pressure. The nature of the flow did not indicate any unusual phenomenon, hence such averaging and generalization could have been applied. However, this model was “sliced” quite finely (125 mesh cells) in order to measure the effects of sudden contraction and sudden enlargement. As it will be shown later the model simulates this quite accurately.

In the instance of three-dimensional model, the heat distribution over the rods was implemented although not to the very same extent as it is in real case scenario. This stems from the fact that CATHARE can implement only a limited amount of mesh cells in the three-dimensional element that was used. Hence, the converter bundle was divided in 25 layers along the axis *Z* and in 3 and 4 mesh cells in *X* and *Y* axis, respectively. As a result, the model was constructed with 300 mesh cells (Figure 2.12). Having said that the cross-section was divided in 12 elements which convey the fact that 99 rods were divided in 12 groups. Due to irregular geometry and mounting of the fuel bundle in casing, mesh was divided very uncommonly. The exact division can be seen in the Figure 2.13 with detailed geometry.

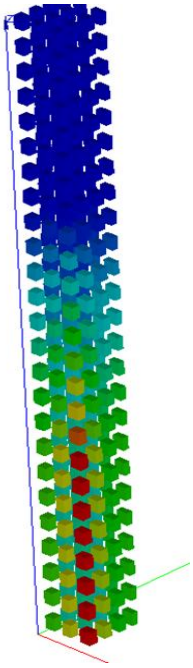

Figure 2.12 View of the converter 3 dimensional model – constructed of 300 mesh cells.

While applying the boundary conditions on the converter the main disadvantage of the CATHERE code emerged. Namely, the element called "Boundary condition" can be connected to only one mesh cell which implied adding 24 (inlet and outlet – 12 each) boundary conditions to use. However, this problem was solved by using the "volume" element that is provided with possibility to connect as many mesh cells with it as it is required. These actions yielded following model (Figure 2.13).

The results coming from both models were in exact match. This proves that averaging process and employed model in CATHARE work very well. The temperatures of the liquid at the outlet of the converter calculated with both methods are the same. The main difference between these two models is the effect of the power distribution which can be seen in different water density distribution. As a result it will produce different velocities which may cause a shift in inside the pressure. However, there is no evident proof of that, most probably due to low velocity of the flow. The observed effect was the cross flow in the converter from regions heated least to regions heated most, although the order of magnitude of the mass flow was $10^{-2}$. These effects were not observed when unified heat distribution was applied.

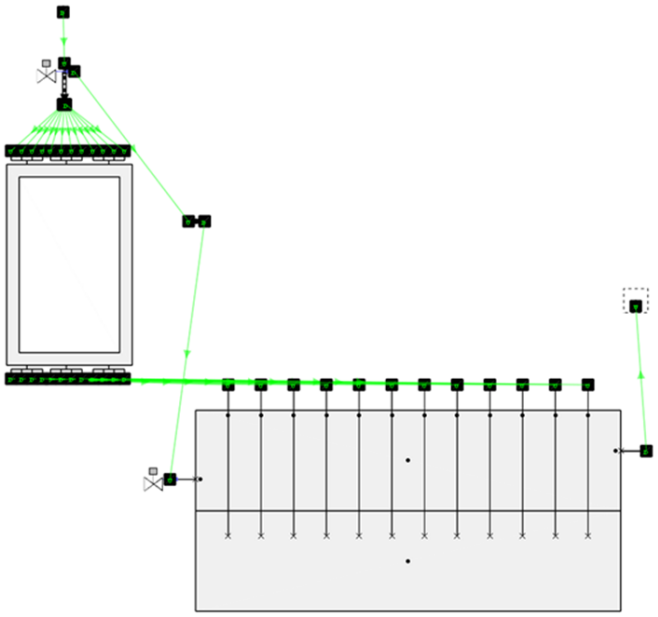

Figure 2.13 View of the converter with system it has been modelled - reactor cooling pool.

When one considers pressure drop along the converter, one may distinguish different factors that are constitutive of the pressure difference. First and most important one is the frictional pressure drop which is a product of fluid's interaction with wall which is expressed in sheer stress. The formula for this is as follows:

$$-\chi C_K \rho_K \frac{|V_K| V_K}{2} \tag{2.8}$$

$$C_K = c_K \cdot f_K \tag{2.9}$$

$$f_K = Max\left\{\frac{16}{\mathrm{Re}_K},\ \frac{0{,}079}{\mathrm{Re}_K^{0,25}},\ 0{,}003\right\} \tag{2.10}$$

Second factor that is strongly affecting the pressure change is geometry change. For a converter flow it can be generalized to the following formula:

$$\varepsilon_{out} = (1 - \frac{A_1}{A_2})^2 \tag{2.11}$$

$$\varepsilon_{in} = (\frac{A_2}{A_c} - 1)^2 \tag{2.12}$$

and lastly the factor coming from energy balance which is a direct effect of geometry change. For a converter flow it can be generalized to the following formula:

$$dp_{out} = \frac{\rho\left(\left(\frac{G}{\frac{\rho}{A_1}}\right)^2 - \left(\frac{G}{\frac{\rho}{A_2}}\right)^2\right)}{2} \tag{2.13}$$

$$dp_{in} = \frac{\rho\left(\left(\frac{G}{\frac{\rho}{A_2}}\right)^2 - \left(\frac{G}{\frac{\rho}{A_1}}\right)^2\right)}{2} \tag{2.14}$$

for outlet and inlet, respectively.

Contrary to methodology applied to CFD modelling, one needs not to choose definite model for flow/turbulence calculation. CATHARE system code was made in the manner, where this step is omitted for user's sake. The code applies proper calculation methods accordingly to the flow/heat regime map.

When calculations are initiated, the initial state of all components is first to be obtained. This is achieved by the initial conditions being extrapolated over components using the same path that flow of the system would go. In the case of BNCT converter, the initial point is the junction that connects boundary condition element with a header that will distribute the flow over all inlet cells in the 3D converter model (or junction connecting boundary condition element with 1D converter model accordingly). The initial state of the system checks if the parameters are in reasonable range of values for current model. That means the flow will change correspondingly to the change of flow area, and so on. It also checks whether the heating of the converter does not yields superheated steam. If any of the requirements are not converged the calculation will not be started. Achieving the initial state of the model, the steady state is calculated. It must be noted that range of parameters of the initial guess will not necessary be the same every time calculations are run, meaning that steady state will be achieved despite different initial guess conditions. However, for the sake of calculation time, it is best to set the initial conditions as close to desirable steady state conditions as possible. Then transient calculation are actuated and last as long as it was set in the command block of the input file. When steady state of the system is achieved time step takes values of tens of seconds

The calculations' time resolution is based on NEWTON approximating method (Figure 2.14).

X0 solution at time t, equation to be solved:

$F(x) = 0$ at time t+dt.

Building the series:

$$X_{k+1} = X_k + \frac{F(X_k)}{F'(X_k)} \tag{2.15}$$

at each iteration, the system solves:

$$F'(X_k) \cdot dX = -F(X_K) \tag{2.16}$$

$$X_{k+1} = X_k + dX \tag{2.17}$$

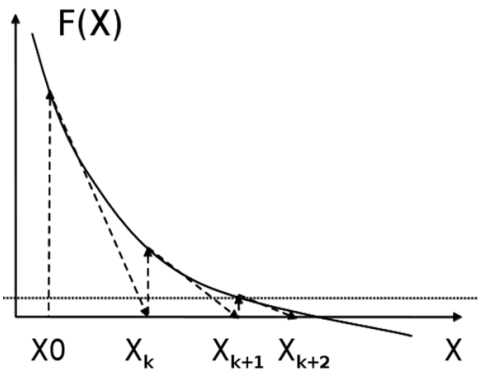


Figure 2.14 Newton approximation method represented in graphical manner.

For the BNCT converter calculations, performed in CATHARE, it was necessary to run transient phase of calculations despite the fact that no transient is happening. For the sake of gaining the results, the transient calculations phase had to be present and set to 30 seconds.

When one compares the general scheme and approach to calculations of the CATHARE (or any similar system code), it becomes clear that system code provide only one physical model, only with small possibilities of enabling or disabling some of the factors (phenomena) or models (i.e. 2 phase pressure drop due to contraction – possibility of RELAP5 to calculate this phenomenon with 2 different models). This comes with some benefits and drawbacks and the view on those depends on the reviewer. First feature for that is it does not allow user to commit a mistake while constructing the model and applying incorrect physical package that should be used in that case. The code chooses the

appropriate scheme from the flow/heat regime map. However, this prevents the user from applying the model that produces very accurate results for the very specific case of flow. The difference between CFD codes (which provide you with broad set of physical models for different kinds of flow) is that system scale codes are created for very specific applications which are flows of highly pressurized water of high temperature and nothing else. These codes do not support flows of other fluids as main fluids in the system, however gases such as oxygen, nitrogen, helium etc. are treated as incondensable gases. Moreover, they are validated by their creators with multiple integral test facilities and separate effect tests and such.

- *CFD approach*

Since spatial heat distribution is highly non-uniform and since the specific geometry, causing turbulences in a stream, may lead to impaired heat transfer, one may expect that local phenomena will play here an important role. Thus the results given by the System TH code need an in-depth review, by means of extra validation. This can be done if CFD approach is applied. Although demanding, the CFD technique is capable to provide robust high resolution case analysis.

Before the BNCT converter fuel assembly (BNCT CFA) CFD simulation starts to run it is necessary to prepare appropriate setup, according to the well-defined steps:

1) Mesh generation,
2) Time frame (steady or transient mode),
3) Model definitions (energy, turbulence, species…),
4) General operating conditions,
5) Boundary conditions specification,
6) Choice of proper numeric algorithm and scheme and preparation of a set of factors constituting a stable simulation run,
7) Run & post-processing,
8) Verification and validation.

The very first action in the way to the simulation is a mesh generation, in other words splitting the domain, either 2D or 3D, into smaller elements called cells in order to apply Finite Volume Method. The domain itself or its shape is prepared in CAD software earlier. In most of the industrial cases, when complex geometry is an issue, CFD engineer has to clean-up the geometry by removing its details meaningless from an experimental point of view, somehow simplifying the model. In case of BNCT CFA, the domain was created the other

way round, by extracting 3D model from 2D blueprints. Thus, instead of simplifying, the project aims to move slowly toward more complicated geometry, carefully tracking an influence of every single change applied.

In general, it is recommended to minimize the number of cells in the domain due to hardware limitations. It can be achieved by cutting off the domain along the symmetry axis and removing the rest of repeating parts or even convert the 3D to 2D model. However, the analysis of BNCT CFA cannot be conducted this way. The problem comes from the fact that each fuel rod is characterized by unique heat production rate; simply there is no physical symmetry axis.

Another thing is a cell scale problem. For CFD purposes, a relative increase in size of two neighbouring cells (growth rate) should not exceed 1.2. The CFD model of BNCT converter fuel assembly is of a size 118x120x700 mm. The most important here is, however, the minimal cell size that could be multiplied afterwards by a factor 1.2. The shortest length between two surfaces appears between the rods and it is equal to 2 mm. Nevertheless, one needs to take into account that it is important to cover all the heat structures with the appropriate number of cell boundary layers. For rods in the BNCT converter, this number was estimated to 7; however, due to hardware limitations this number was decreased to 5 with minimal negative influence. This means that at the distance of 2 mm there has to be at least 10 cells, but in real this value is not less than 11 and in turns 2 mm divided by 11 is about 0.18 mm (when growth rate is not considered)!

There are certain rules and factors that should be obeyed in order to obtain mesh of a good quality, which are not going to be discussed here, but it is worth to mention that in case of the CFD model of BNCT converter channel, it is hardly possible to decrease the number of cells below 10 million and to keep those factors at recommended level.

When the mesh is ready (Figure 2.15), one can apply time frame of the experiment, meaning steady state or transient. The steady state is used to convert boundary conditions information into realistic initial conditions in every single cell before transient is run. Transient, in turn, is used to evaluate the continuous change of flow parameters in time. For the BNCT CFA, the steady state was achieved after 11h.

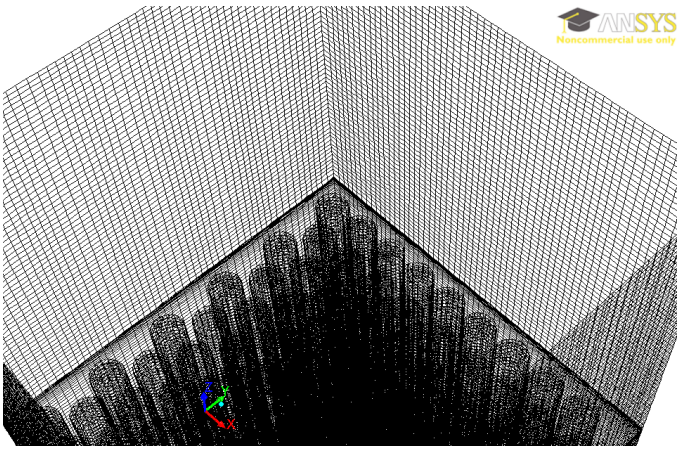


Figure 2.15 CFD mesh details of the BNCT converter fuel assembly.

Next step in the CFD analysis is to choose appropriate model of physics. The number and the diversity of models depend on a code applied to the experiment. For the purpose of this simulation, the ANSYS Fluent 14.0 [11, 29] was used for its reach set of turbulence models.

The most popular turbulence model among CFD engineers for its range of applicability and rapidity is 2 equations RANS model called k-ε model, at least in the first approach to a case. This solver provides valid solution mainly for a free stream in complex ducts or when it meets simple obstacles in a far field. However, it is very sensitive in the area of boundary layers and thus difficult to apply in case of the BNCT CFA. As it was recognized, another RANS model, namely Shear-Stress Transport (SST) k-ω, suits the needs better (Figure 2.16).

The shear-stress transport (SST) k-ω model was developed by F. Menter [30] to effectively blend the robust and accurate formulation of the k-ω model in the near-wall region with the free-stream independence of the k-ε model in the far field. To achieve this, the k-ε model is converted into a k-ω formulation. The SST k-ω model is similar to the standard k-ω model, but includes the following refinements:

- The standard k-ω model and the transformed k-ε model are both multiplied by a blending function and both models are added together. The blending function is designed to be one in the near-wall region, which activates the standard k-ω model, and zero away from the surface, which activates the transformed k-ε model;

- The SST model incorporates a damped cross-diffusion derivative term in the ω equation (2.19);
- The definition of the turbulent viscosity is modified to account for the transport of the turbulent shear stress;
- The modelling constants are different.

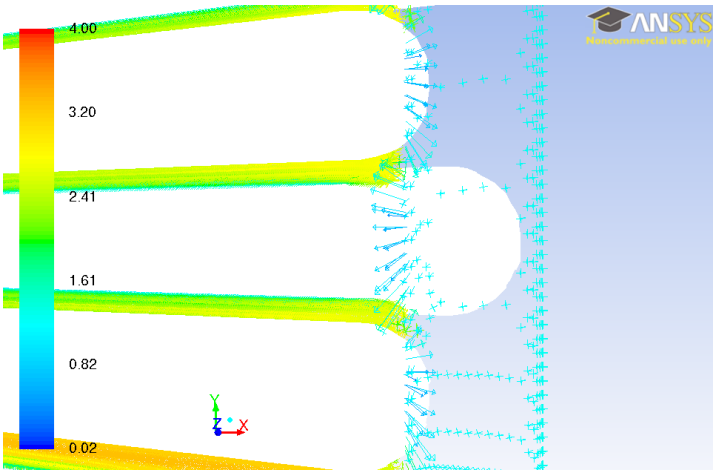


Figure 2.16 Flow velocity vectors (slice made along the channel) at the entrance of the fuel rods zone.

These features make the SST k-ω model more accurate and reliable for a wider class of flows (e.g., adverse pressure gradient flows, airfoils, transonic shock waves) than the standard k-ω model.

Transport equations for the SST k-ω model.

$$\frac{\partial}{\partial t}(\rho k)+\frac{\partial}{\partial x_i}(\rho k u_i)=\frac{\partial}{\partial x_j}(\Gamma_k \frac{\partial k}{\partial x_j})+\tilde{G}_k-Y_k+S_k \qquad (2.18)$$

$$\frac{\partial}{\partial t}(\rho \omega)+\frac{\partial}{\partial x_i}(\rho \omega u_i)=\frac{\partial}{\partial x_j}(\Gamma_\omega \frac{\partial \omega}{\partial x_j})+G_\omega-Y_\omega+D_\omega+S_\omega \qquad (2.19)$$

where:

$k$ – turbulence kinetic energy,

$\omega$ – specific dissipation rate,

$\Gamma_k$, $\Gamma_\omega$ – effective diffusivity of k and ω,

$\tilde{G}_k$ – turbulence kinetic energy generation (due to mean velocity gradients),

$G_\omega$ – specific dissipation rate generation,

$D_\omega$ – cross –diffusion term: $D_\omega = 2(1-F_1)\rho \frac{1}{\omega\sigma_{\omega,2}} \frac{\partial k}{\partial x_j} \frac{\partial \omega}{\partial x_j}$ (2.20)

$Y_k$ , $Y_\omega$ – dissipation of k and due to turbulence,

$S_k$ , $S_\omega$ – user – defined source terms,

At this point, one should specify physical properties of the fluid and conditions under which it flows. According to the assumptions made in the Safety Assessment Report [26], it is a single phase water flow driven by the pressure difference with no phase change expected. However, since the water plays here a role of a coolant for hot fuel rods, one should expect at least slight change in its density, i.e. when using ANSYS Fluent 14.0, one should replace constant density value with a function of temperature. One should also define boundary conditions, i.e. inlet, outlet, channel walls and 99 rods. Although it is rather trivial task in case of BNCT CFA, it takes couple of hours on typical desktop PC to define all of them due to hardware (i.e. RAM) requirements for processing more than 1GB-sized case-files.

Finally, it is necessary to set up numeric algorithm and schemes. The scheme is used to describe the way how differential equation should be translated into discretized form and then those discretized equation are gathered in a form of algorithm to solve physical problem, i.e. to find distributions of physical properties. According to the logic of ANSYS Fluent, one should define algorithm first and then schemes. The same logic is preserved here.

There are two categories of algorithms in ANSYS Fluent: Pressure-Based Navier-Stokes (PBNS) and Density-Based Navier-Stokes (DBNS). The use of the first approach is effective when one deals with low-speed incompressible flows, and since water, in general, may be treated as incompressible and its velocity in the experiment is relatively low, i.e. expected velocity is in a range of 1-3 m/s, the PBNS seems to be the ideal choice. In this approach, the pressure field is extracted by solving a pressure or pressure correction equation, which is obtained by manipulating continuity and momentum equations.

The ANSYS Fluent platform provides four segregated algorithms for solving PBNS equations. These are SIMPLE, SIMPLEC, PISO and FSM. However, in general, the use of SIMPLE or SIMPLEC algorithms is recommended for steady-state calculations. Moreover, experiments done in this research [27] have shown no difference between the results obtained using SIMPLE and SIMPLEC, so the first one was applied. By definition, the ANSYS Fluent uses the SIMPLE algorithm in a modified form, i.e. adding under-relaxation factors $\alpha_i$ to the correction equations given in STEP3 on Figure 2.17.

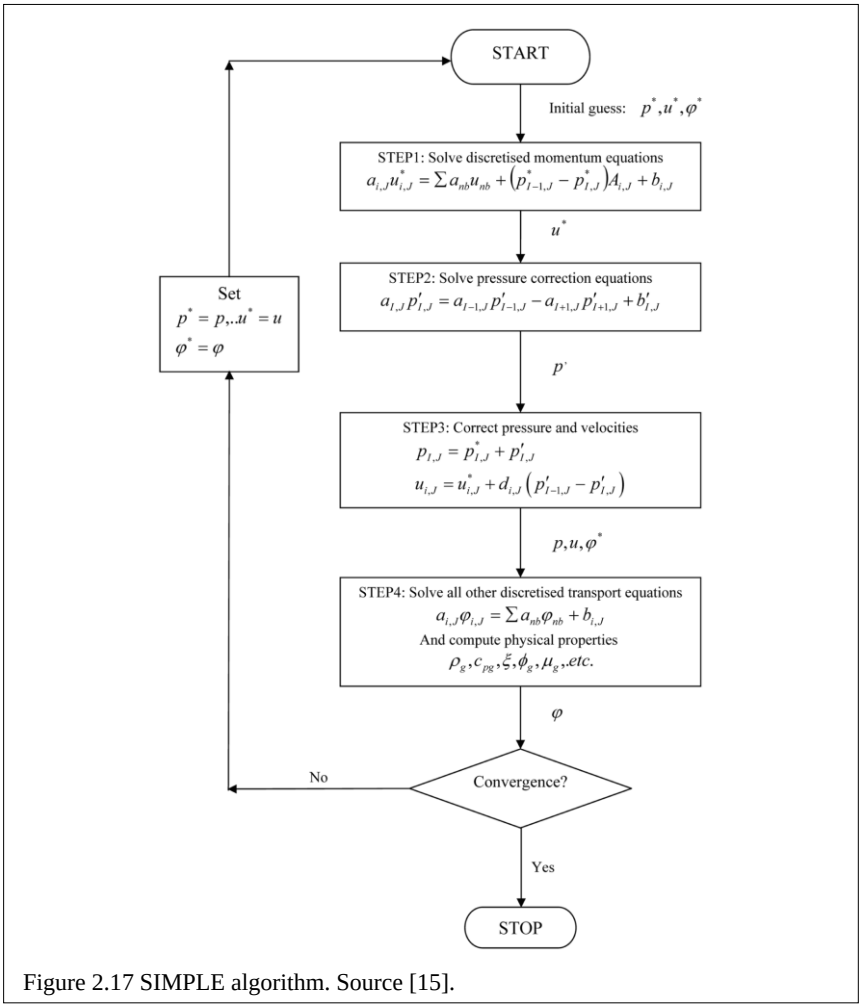

Figure 2.17 SIMPLE algorithm. Source [15].

Under-relaxation factors in the correction equations:

$$p_{I,J}^{new} = p_{I,J}^{*} + \alpha_p p_{I,J}^{'} \tag{2.21}$$

$$u_{i,J}^{new} = \alpha_u u_{i,J}^{'} + (1-\alpha_u) u_{i,J}^{(n-1)} \tag{2.22}$$

Such a trick ensures stable computation, e.g. when $\alpha_p$ is equal to 1 in the pressure correction equation (2.6) the guessed pressure field $p^*$ is corrected by $p'$. However, the corrections $p'$, in particular when the guessed field $p^*$ is far away from the final solution, is often too large for stable computations. A value of $\alpha_p$ equal to zero would apply no correction at all, which is also undesirable. Setting $\alpha_p$ between 0 and 1 allows us to add to guessed field $p^*$ a fraction of correction field $p'$ that is large enough to move iterative process forward, but small enough to ensure stable computations.

A bit more complicated, here, is an under-relaxation factor application to velocity field. The thing is that there is one intermediate step required, namely before one apply under-relaxation factor as it is shown in equation (2.7), he has to, first, correct guessed value of velocity basing on pressure difference (STEP3 in Figure 2.17). This comes from the fact that the pressure and the velocity are coupled in the momentum equation (2.2a-2.2c).

However, apart of this algebra, one should remember that the choice of satisfying values for under-relaxation factors is not trivial and bases on repetitive process of adjustments. The longer experience of CFD engineer or the better his intuition is, the shorter is the process.

As it was mentioned, one should not forget to define schemes, e.g. the SIMPLE algorithm, presented above, assumes the use of Backward Differencing Scheme. The ANSYS Fluent offers couple of schemes from among which the most popular are Upwind, QUICK, MUSCL etc. Moreover, it allows us to set schemes separately for every major variable, i.e. in case of BNCT converter the scheme must be defined for pressure, momentum, for both of k and ω due to two extra turbulence equations and one for energy. Apart of pressure, which is set to Standard, the rest uses Second Order Upwind by default.

Almost the last step in the procedure is to define monitors and limits. The monitors are the fixed values to control behaviour of residual values for every equation in the set. The residual values are simply the differences between preceding and current step of iteration. The solution is considered to be

converged when the residual value drops down below the monitor value. The limits, in turn, are physical limits for indirect (derived) flow parameters, i.e. temperature.

When all above is done, one can start his simulation. For BNCT CFA the steady state was achieved after about 15000 steps and around 11h of 192 cores (2.5-3.1GHz@AMD Opteron 6276) of HPC cluster.

Although the results are going to be discussed in the next section, it is worth to mention that each post-processing procedure leads to some minor or major adjustments in the model and then to another run, of course up to the point when the results are satisfactory enough.

### 4.3. Comments on results

The aim of all of the thermal hydraulic analyses done for BNCT converter, both analytical and numerical, was to check relevant flow and heat transfer parameters in terms of safety margins. These safety margins, here, are related to the coolant pressure difference between inlet and outlet as well as the wall temperature of the most thermally loaded (‘the hottest’) rod. The threat and the most undesired scenario would be one with partial or complete loss of flow due to pressure difference decrease which could impaired heat transfer, increasing coolant boiling, leading to rods uncovering and consequently to fuel element melting.

One of the issues, when preparing the model, is the choice of proper tools, namely computer codes. Since they are always limited due to the hardware capabilities certain compromise has to be made. The overall rule; however, should be always not to lose the scope/perspective of the modeled problem.

Previous sections have already shed light on the different approaches to the same matter, but the question still remains if the results are different and if so, on which we can rely. Although the experiment with real equipment, which could solve this problem easily, has not been performed yet, there is one thing worth to mention at this point. All of the computations yield the results that stay in compliance with each other.

The very first check was related to the coolant velocities pattern. Figure 2.18 depicts good match between the results coming from CATHRE and Fluent. The CATHARE's solution is exactly in the middle of bounds given by Fluent. The only difference is the outlet velocity where the turbulence affects CFD solution. However, longer outlet space in the model could resolve this issue.

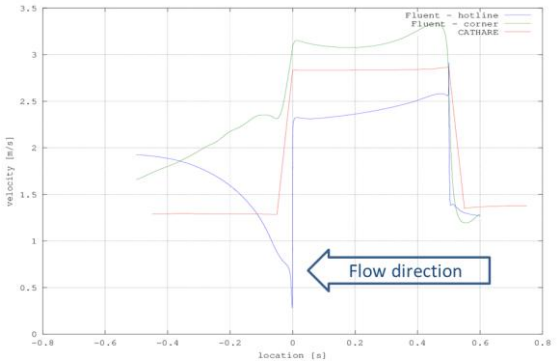


Figure 2.18 Flow velocities calculated in Fluent (measured in two extreme positions around the hottest rod) and CATHARE (measured in a column of cells containing hottest rod).

Another issue was the coolant temperature (Figure 2.19). When the highest fluctuation (in the vicinity of 'the hottest' rod) of the CFD simulation is compared with the averaged system code solution, it becomes obvious that there is no difference between two models when inlet and outlet are considered. Nevertheless, such local temperature phenomenon revealed by Fluent may have and indeed do have a strong contribution to the impaired heat transfer.

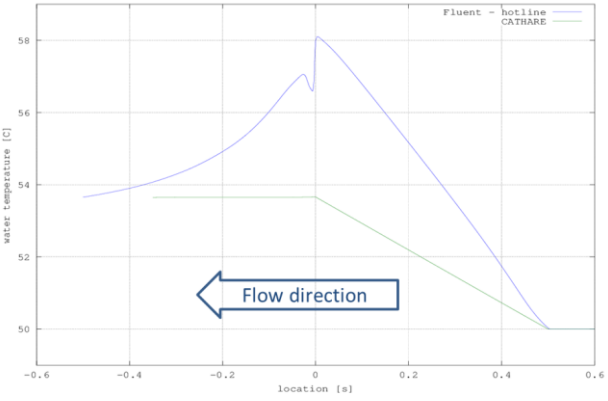


Figure 2.19 Coolant temperature increase along the channel by Fluent and CATHARE.

The effect of averaging is well-presented in the Figure 2.20. Here, the heat distribution at the cross-section of the outlet from a fuel active zone is compared.

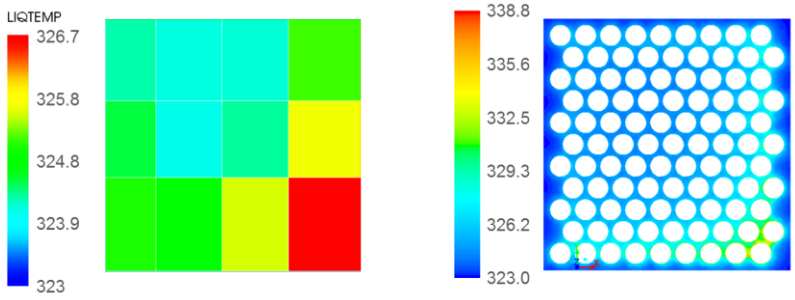


Figure 2.20 Coolant temperature cross-sectional distribution at the end of rods. The difference in resolution between CATHARE (left) and Fluent (right).

Eventually, when comparing the temperature of 'the hottest' rod, it is clear that results coming from system code are by a little underestimated in regard to CFD, which is the visible effect of averaging (Figure 2.21). The discrepancies at inlet and outlet of the CFD simulation results are caused by the low quality mesh at these regions and are treated as numerical errors. For further studies, it was estimated that the maximum temperature of the rod surface is equal to 84°C (357 K). Although the CFD value is by a 10 degrees higher than the one from the system code and even by a 20 degrees compared to analytical solution, it is still below the safety margin (85°C).

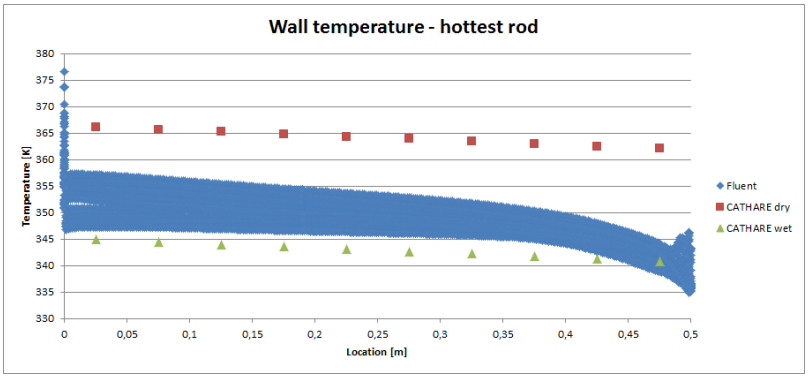


Figure 2.21 The temperature of the most thermally loaded rod. The blue bound depicts the result coming from Fluent and the green indicators – results given by CATHARE, both measured on surface. The brown points represent CATHARE results of rod's centreline temperature.

This is the most important remark of this study, because it shows how relevant is a role of high resolution best estimate code, i.e. CFD, at the design stage. The real benefit, here, is a knowledge about the real distance from the margin. Such result says which improvements or optimization of flow domain geometry would be advised.

This conclusion leads to another. CFD codes demands tens of hours and hundreds of CPUs available to achieve such resolution, while system codes need one typical desktop CPU to give demanded answer in a couple of seconds (sometimes minutes, and hours in case of complicated two-phase critical flow). This is also the reason why the system codes are used for licensing or during an emergency/accidental conditions in NPP. When the fast response of the whole circuit is necessary to be known, in order to decide what countermeasures to apply, system codes are more advantageous compered to CFD.

It should be mentioned that nowadays trend is to couple both system and CFD codes into a one mechanism to gain all the benefits, for scope and resolution's sake of the simulation. However, this is still an early stage of development and as for the moment one should simply use both type of thermal hydraulic codes wisely.

In general, when modeling any physical phenomenon, an appropriate dose of conservatism and engineering judgment aided by the best estimate codes are advised in order to avoid exceeding the safety margins. Also, a scope of the model and its range of applicability should be clearly defined.

## Acknowledgments

The presented work was supported by the EU and MSHE grant no POIG.02.03.00-00-013/09.

## References

[1] T. Downar, A. Siegel, C. Unal, White Paper on Integrated Performance and Safety Codes, http://neams.ne.anl.gov
[2] P. Turinsky, Advances in multi-physics and high performance computing in support of nuclear reactor power systems modelling and simulation, Nuclear Engineering and Technology, vol. 44 no 2, pp. 103-112, 2012.
[3] NEAMS webpage, http://neams.ne.anl.gov
[4] G. Palmiotte et al, UNIC: Ultimate Neutronic Investigation Code, Proc. of M&C + SNA, 2007 .

[5] B. Niceno, Y. Sato, A. Badillo, M. Andreani, Multi-scale modeling and analysis of convective boiling: towards the prediction of CHF in rod bundles, Nuclear Engineering and Technology, vol. 42 no 6, pp. 620-635, 2010.
[6] W. J. Phythian, R. E. Stoller, A. J. E. Foreman, A. F. Calder, D. J. Bacon, A comparison of displacement cascades in copper and iron by molecular-dynamics and its application to microstructural evolution, Journal of Nuclear Materials vol. 223, pp. 245-261, 1995.
[7] L. Diachin, A. Bauer, B. Fix, J. Kraftcheck, K. Jansen, X. Luo, M. Miller, C. Ollivier-Gooch, M. S. Shephard, T. Tautges, H. Trease, Interoperable mesh and geometry tools for advanced petascale simulations, 2007.
[8] ANL webpage, http://www.ne.anl.gov/capabilities/sharp/
[9] SCALE webpage, http://scale.ornl.gov
[10] EDF webpage, http://research.edf.com
[11] ANSYS Inc., ANSYS Fluent Theory Guide, Release 14.0, 2011.
[12] EDF R&D, Code Saturne version 2.0.6 practical user's guide, 2012.
[13] OpenFOAM Foundation webpage, http://www.openfoam.com/features/
[14] O. Kudryavtsev, Russian national presentation (Gidropress - Russia) The IAEA Regional Workshop on Advances in DSA including the Application of CFD Codes, Ljubljana, Slovenia, 2011.
[15] H. Versteeg, W. Malalasekera, An Introduction to Computational Fluid Dynamics The Finite Volume Method, Prentice Hall, 2007.
[16] NURESAFE project webpage, http://www.nuresafe.eu/
[17] NUGENIA webpage, http://www.nugenia.org/
[18] IAEA, Deterministic Safety Analysis for Nuclear Power Plants, IAEA, Austria, 2009.
[19] CEA, Description of the base revision of physical laws used in the 1D, 0D and 3D modules, CEA Grenoble, France, 2008.
[20] CEA, Description of the Axial module, CEA Grenoble, France, 2011.
[21] KSG | GfSSimulatorzentrum webpage, Simulator for Gundremmingen Nuclear Power Plant receives Reactor Pressure Vessel and Reactor Core Model with Design Code Quality, Germany, 2012.
[22] M. Sepielli, E. Negrenti, C. Parisi, M. Cappelli, Proceedings of the International Conference Nuclear Energy for New Europe 2011. The Role of Thermal-hydraulic System Codes in NPP Engineering Simulators, Italy, 2011.
[23] R. F. Barth, J. A. Coderre, M. G. H. Vicente, T. E. Blue, Boron neutron capture therapy of cancer: Current status and future prospects, Clinical Cancer Research 11 (11), pp. 3987-4002, 2005.
[24] Y. Nakagawa, K. Pooh, T. Kobayashi, T. Kageji, S. Uyama, A. Matsumura, H. Kumada, Clinical review of the Japanese experience with boron neutron

capture therapy and a proposed strategy using epithermal neutron beams, Journal of Neuro-Oncology 62, pp. 87-109, 2003.
[25] N. Golnik, K. Pytel, Irradiation facilities for BNCT at Research Reactor MARIA in Poland, Polish Journal of Medical Physics and Engineering 12 (3), pp. 143-153, Poland, 2006.
[26] K. Pytel, W. Mieleszczenko, M. Dorosz, T. Kulikowska, Z. Marcinkowska, Safety analyses of BNCT converter, IEA (NCBJ) Internal Report, Poland, 2010.
[27] P. Prusiński, S. Potempski, M. Borysiewicz, K. Kowal, T. Kwiatkowski, A. Prusiński, CFD analysis of the safety related thermal hydraulic parameters describing a flow domain of an experimental medical installation (BNCT converter) inside of the Research Reactor MARIA, Journal of Power Technology vol. 4, pp. 227-240, Poland, 2012.
[28] IAEA, Accident Analysis for Nuclear Power Plants, IAEA, Austria, 2002.
[29] ANSYS Inc., ANSYS Fluent User's Guide, Release 14.0, 2011.
[30] F. R. Menter, Two-Equation Eddy-Viscosity Turbulence Models for Engineering Applications, AIAA Journal. 32(8), pp. 1598–1605, USA, 1994.

# CHAPTER 3

# Multi-scale multi-physics in neutronic analyses

Mieczysław Borysiewicz, Rafał Możdżonek, Anna Wasiuk
National Centre for Nuclear Research (NCBJ)
Andrzeja Sołtana 7 Str., 05-400 Otwock, Poland
mieczyslaw.borysiewicz@ncbj.gov.pl

Reactor core behaviour is driven by many physical phenomena. For this reason reactor core modelling and simulations involve neutronics, thermal-hydraulics, thermo-mechanics, fuel behaviour and chemistry, as well as the balance of the whole plant – all with feedback effects. One of the most important aspects of the core behaviour is related to the neutrons propagation and their interactions with a nuclear fuel and other materials inside a core. Physical phenomena in the neutronic scale are characterised by such quantities as neutrons diameter (ca. $10^{-15}$ m), velocity varying between 1 and 10000 km/s and average distance before their interaction with matter varying between several tens to a couple of cm.

In the early days neutronic calculations were performed in analytical way, for example by determining the multiplication of a nuclear chain reaction in a finite medium via six-factor formula (DOE 1993):

$$k_{eff} = \eta \varepsilon p d \Lambda_f \Lambda_t ,$$

where parameter $\eta$ stands for reproduction factor, $\varepsilon$ for fast fission factor, $p$ for the resonance escape probability, $d$ for thermal utilization factor, $\Lambda_f$ for fast non-leakage probability and $\Lambda_t$ for thermal non-leakage probability. Additionally, the multiplication factor $k_{eff}$ is defined as:

$$k_{eff} = \frac{numbers\ of\ \ neutrons\ in\ \ one\ \ generation}{numbers\ of\ \ neutrons\ in\ \ preceding\ \ generation}.$$

For the detailed description of the subject's basis the reader should refer to (DOE 1993). This method unfortunately did not allow prediction of neutron flux (power) spatial distributions inside the reactor core, and therefore all information related to that data (e.g. core material ageing and fuel burnup) were unavailable.

Nowadays neutronic calculations are performed using much more sophisticated methods thanks to the computational power of present computers.

Research on computational methods for the Boltzmann transport equation has been actively pursued from the 1950s up to the present (Adams and Larsen 2002; Carlson and Lathrop 1968; Carter and Cashwell 1975; Haghighat and Wagner 2003; Kalos and Whitlock 1986; Larsen 1992; Larsen and Morel 2009; Lewis and Miller 1993; Lux and Koblinger 1991; Marchuk and Lebedev 1981; Sanchez and McCormick 1982; Spanier and Gelbard 2008; X-5 Monte Carlo Team 2003).

We can distinguish two types of modelling and simulation strategies in case of neutronic codes:

- Monte Carlo (MC) methods, based on tracking the "life" of neutrons;
- deterministic methods, based on solving of the Boltzmann neutron transport equation or diffusion equation.

Stochastic (or Monte Carlo) methods are based on a probabilistic interpretation of the transport process. Deterministic methods instead are based on (i) discretizing the Boltzmann transport equation in each of its independent variables, resulting in a (typically very large) algebraic system of equations, and then (ii) solving this algebraic system.

Monte Carlo and deterministic methods are viewed as complementary. However, during the past 10 years, it has become understood that hybrid methods - which combine aspects of both Monte Carlo and deterministic methods - can be used to enhance the strengths and overcome the weaknesses of the individual approaches.

Neutronic codes, based on MC transport methods are very accurate but also require very CPU intensive techniques. In this approach transport process is seen from the viewpoint of single neutron. Simulation can be described as a chain of events that at each step depends only on neutron coordinates and energy. In each such step neutron during propagation in medium interacts with encountered materials. Outcome of each interaction is randomly sampled from probability density functions based on continuous isotopes microscopic cross-sections for neutron interactions such as absorption, scattering and fission. The whole simulation consists of a large number of steps. After that, statistical methods are used to estimate the final result. In reality, MC codes do not solve the neutron

transport equation (see eq. (3.2)), instead they do stochastic estimations for integrals of the form:

$$R = \int_V \int_{4\pi} \int_0^{\infty} \Phi(r, \Omega, E) dV d\Omega dE \qquad (3.1)$$

where *f(r, Ω, E)* stands for arbitrary response function which may depend on any of the variables (e.g. a reaction cross section). As a result of these steps, MC simulation produces random variables with statistical precision dependent on running time. Essentially MC codes consist of three main parts:

1) ray-tracing algorithm which aims to determine material encountered by neutron at certain position (*x*, *y*, *z*) and its distance to the nearest boundary in certain direction (α, β, γ) ;
2) module used for sampling an outcome for neutron interactions with materials based on probability distributions characterizing these processes;
3) statistical algorithms used for collecting results from events taking place during neutron propagation in the medium and calculating statistical mean values and associated with them statistical errors.

Monte Carlo methods are widely used because of their relative ease of implementation, their ability to treat complex geometries with great fidelity, and their ability to solve problems accurately with cross-sectional data that can have extremely complex energy-dependence. However, Monte Carlo simulations can be costly, both to set up and to run.

MC neutron transport codes can be used for: reactor analysis (mostly in criticality calculations), detector response, modelling, dosimetry calculations and validation of deterministic neutronic codes.

Monte Carlo methods have certain basic advantages. If the geometry of the system and its cross sections are known, then the results of the Monte Carlo simulation contain only statistical errors. By processing a sufficient number of Monte Carlo particles, it is possible to reduce the probable statistical error below any specified level.

According the *central limit theorem*, for any Monte Carlo simulation, the statistical error in the estimation of a given quantity is, with probability 0.68, bounded by:

$$Statistical\ \ error \leq \frac{\sigma}{\sqrt{N_{MC}}},$$

where $\sigma$ (the *standard deviation)* is specific to the given problem and the quantity estimated, This estimation holds only for $N_{MC}$ sufficiently large. It indicates that as $N_{MC}$ increases, the statistical error will, with high probability decrease. The negative feature is that the rate of decrease of the statistical error is slow - to decrease the statistical error by a factor of 10, it is necessary to increase $N_{MC}$ (and hence the computational expense) by a factor of 100.

To accomplish the Monte Carlo process, the code user must input a (generally) large number of *biasing parameters* that successfully "encourage" Monte Carlo particles to migrate from the source to the specified detector region. These parameters are strongly problem-dependent, and generating them can be a slow and laborious task. For difficult problems, a lengthy process of trial and error maybe necessary, and there is no guarantee that at the end of this process, the code user will have been successful.

Because they are all-purpose tools and are designed without any specific approximations concerning physics and geometry of the problem, they are used for cases for which deterministic codes cannot be applied easily. MC codes require a lot of computational power as well as computer memory, and therefore now they are developed with the aim of running them on powerful computing clusters with parallel processing capabilities. Fortunately, the MC algorithms are parallel in nature as each neutron can be traced independently, and for this reason the codes simulation speedup should theoretically increase linearly. In reality the speedup is limited by the memory bandwidth because these codes require the transfer of large amount of data (materials properties) between cluster nodes.

Although deterministic methods are much faster than Monte Carlo ones particularly for one and two-dimensional problems, both methods are slow for realistic three-dimensional modelling. Additionally, deterministic methods are multi-stage and involve complicated computing techniques. Neutronic codes that use these techniques can be divided into two main groups:

- codes solving multi-group equation of transport in space and energy, for example by the collision-probability method (integral equation) or by using $S_n$ methods (integral differential equation) – e.g. (Marleau 2001; Le Mouel and Soldevila);

- codes solving the equation of the dynamic, or static, diffusion of neutrons in two or three dimensions, in a reactor core using the finite elements, the finite differences with acceleration by coarse mesh, and the nodal methods – e.g. (Downar; Baudron).

Both deterministic approaches deal with entire neutron population, instead of dealing with neutrons separately as it is in the case of MC methods. Codes representing the first group mostly have been used for reactor core lattice calculations called lattice codes, in the process to calculate neutron flux distribution and multiplication factor of the whole reactor core. They take as an input the multi-group library of isotopic nuclear data (microscopic cross sections for neutrons interaction with certain isotopes as a function of neutron kinetic energy divided into groups – usually 172 and more), as well as a description of the fuel assembly lattice (Figure 3.1), and for this data with applied specific boundary and initial conditions solve the set of the neutron transport equations.

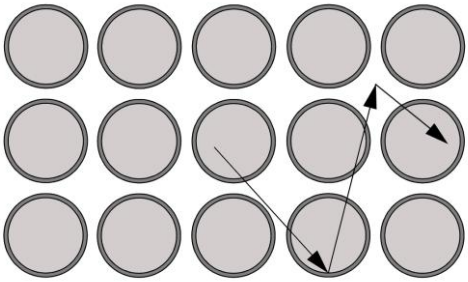

Figure 3.1 Regular lattice of fuel pins in a fuel assembly with highlighted path fallowed by single neutron between its emission and absorption points.

## 1. Neutron transport equation

The time-dependent form of neutron transport equation can be written in the following form (Rozon):

$$\begin{aligned}\frac{1}{v(E)}\frac{\partial\Phi}{\partial t}(r,E,\Omega,t) &= -\Omega\cdot\nabla\Phi(r,E,\Omega,t)-\sum(r,E,t)\Phi(r,E,\Omega,t)\\ &+\frac{1}{4\pi}\int_{R^+}\int_{S^2}\sum_S(r,E',E,\Omega',\Omega,t)\Phi(r,E',\Omega',t)d\Omega' dE'\\ &+\frac{x_f(E)}{4\pi}\int_{R^+}\int_{S^2}v_f(r,E')\sum_f(r,E',t)\Phi(r,E',\Omega',t)d\Omega' dE\\ &+\sum_{i=1}^{N}\frac{\chi_{d_i}(E)}{4\pi}\lambda_i C_i(r,t)+S(r,E,\Omega,t)\end{aligned} \tag{3.2}$$

where:
$R^+$ - non-negative real numbers,
$r=(x,y,z)^T\in V\subset R^3$ - position vector in volume *V*,
$E\in R^+$ - energy,
$\Omega\in S^2=\{\Omega\in R^3:\|\Omega\|_2=1\}$ - direction,
$t\in R^+$ - time,
*v(E)* - neutron velocity,
*N* - number of delayed neutron precursors,
$C_i(r,t)$ - concentration of delayed neutron precursors in group *i*,
$\lambda_i$ - decay constant of group i precursors,
$v_f(r,E')$ - average number of neutrons produced per fission.

Above equation describes the neutron flux Φ at a certain position, energy, direction, and time, and can be derived by considering how the flux changes with time. This change in time is determined by measuring the difference between neutrons gained and neutrons lost. The loss of neutrons is described by the first two negative terms on the right-hand side of the equation (3.2), while the gain in neutrons is described by the next three positive terms. The negative terms represent the neutron losses occurring due to streaming and neutrons colliding with the underlying nuclei. When a collision occurs the neutrons may be captured, scattered, or they may cause fission. In any of these cases the collided neutrons no longer travel in the same direction Ω with the same energy *E* and are therefore lost from the considered angular flux Φ. The probability that

neutrons interact in any way with medium is described by the total cross-section $\sum(r,E,t)$. The third term on the right side of the equation stands for the increase of the flux Φ when neutrons are scattered from a previously different direction Ω' and energy level *E'* into the direction Ω and energy *E*. The probability for this process is determined by the scatter cross-section $\sum_S(r,E',E,\Omega',\Omega,t)$. The next (fourth) term is the gain of neutrons from fission processes, while the fifth term is the production of neutrons due to delayed neutron precursors (i.e. unstable nuclei which undergo neutron decay). $\chi_f(E)$ and $\chi_{d_1}(E)$ functions represent the distribution of neutrons produced in certain reactions. The first function describes neutrons produced by fission reactions in energy group *E* and the second one the distribution of the neutrons produced by delayed neutron precursors (also in energy group *E*). The last term tells us about neutrons that are gained from non-fission sources such as radioactive materials that decay and emit neutrons without a neutron-nucleus collision. Solution of eq. (3.2) for 3D models demands huge computational power because the problem has seven dimensions: three in space, two in direction, and one in each energy and time.

The eq. (3.2) represents the most popular linear integro-differential form of neutron transport equation and is unsolvable without additional information such as boundary and initial conditions. Initial conditions can be incorporated in the equation for example by assuming that all nuclear data are time independent and $\lim_{n\to\infty}\Phi(r,E,\Omega,t)=0$. After integration over all time, the time dependent neutron transport equation simplifies to the time independent steady state form (without delayed neutrons):

$$[\Omega\cdot\nabla+\sum(r,E)]\Phi(r,E,\Omega)=\frac{1}{4\pi}\int_{R^+}\int_{S^2}\sum_S(r,E',E,\Omega',\Omega)\Phi(r,E',\Omega')d\Omega'\,dE'$$
$$+\frac{\chi_f(E)}{4\pi}\int_{R^+}\int_{S^2}\nu_f(r,E')\sum_f(r,E')\Phi(r,E',\Omega')d\Omega'\,dE+S(r,E,\Omega)$$

(3.3)

$$\Phi(r,E)=\int_0^\infty\Phi(r,E,t)dt$$

with this form of equation, steady state condition is described by steady state source distribution term *S(r, E, Ω)* and appropriate boundary conditions.

## 2. Boundary and continuity conditions

A number of different boundary conditions which can be applied for the transport equation (3.3) are as follows. We assume, that the domain *V* where the particles move maybe surrounded by a boundary $\partial V$ where *boundary conditions* are imposed. We also introduce $N(r_s)$, the outward normal at. $r_s \in \partial V'$. Solution of the transport equation in *V* requires the knowledge of the angular flux $\Phi(r_s, V, E, \Omega)$ for $\Omega \cdot N(r_s) < 0$.

***The zero-flux boundary condition (no incoming neutron boundary conditions)***

$$\Phi(r_s, V, E, \Omega) = 0 \text{, for } \Omega \cdot N(r_s) < 0 \text{ .}$$

***Albedo boundary condition***

The albedo boundary condition is used to relate the incoming flux with the known outgoing flux. This condition is written as

$$\Phi(r_s, V, E, \Omega) = \beta\Phi(r_s, V, E, \Omega')$$

with $\Omega \cdot N(r_s) < 0$ the solid angle $\Omega'$ representing the direction of the outgoing particle. The albedo is equal to zero and one for a vacuum and reflective boundary condition, respectively. Intermediate values can also be used.

Specular reflection corresponds to the case where

$$\Omega \cdot N(r_s) = -\Omega' \cdot N(r_s) \text{ and}$$
$$(\Omega x \Omega') \cdot N(r_s) = 0 \text{ .}$$

The white boundary condition is a reflective condition where all particles striking the boundary turn back to $V$ with an isotropic angular distribution. In this case,

$$\Phi(r_s,V,E,\Omega)=\beta\frac{\int_{\Omega'\cdot N(r_s)>0} d^2\Omega'[\Omega'\cdot N(r_s)]\Phi(r_s,V,E,\Omega')}{\int_{\Omega'\cdot N(r_s)>0} d^2\Omega'[\Omega'\cdot N(r_s)]}$$

with $\Omega\cdot N(r_s)<0$ and where $\beta$ is the albedo, defined as before the above ) simplifies to

$$\Phi(r_s,V,E,\Omega)=\frac{\beta}{\pi}\int_{\Omega'\cdot N(r_s)>0} d^2\Omega'[\Omega'\cdot N(r_s)]\Phi(r_s,V,E,\Omega')$$

Inside the domain $V$, the angular flux $\Phi(r_s,V,E,\Omega)$ must be continuous across all internal interfaces in *V* the direction $\Omega'$ of the moving particle. Discontinuities along $\Phi$ can occur only if the source density contains Dirac delta contributions. The continuity condition is not required along directions which are not parallel to the path of travel.

## 3. Integral transport equation

Eqs. (3.2) and (3.3) are in linear integro-differential form; however, there exists a lot of other equivalent forms with different mathematical properties, each appropriate for specific models with specific assumptions. Thus, we can distinguish such forms as: integral, even/odd parity, invariant embedding, pseudo flux, multiple collisions, Green's function, adjoint form and others. For example multiple collision form is appropriate for highly absorbing media, invariant embedding for half-space problems, the Green's function for highly heterogeneous 1D plane media in the multi-group approximation, the pseudo flux form for isotropic scattering in multi dimensions and adjoint form for estimation of changes in the neutron multiplication caused by small changes in material properties (perturbation theory).

Integral transport equation can be described as integration along characteristic curves defining the neutron paths. Conveniently, the characteristics of the linear Boltzmann equation are straight lines in the flux directions Ω along which the differential operator reduces to a total derivative. Neutron position can be parameterised by $r=r'+s\Omega$, where *s* is the assumed distance from the reference position *r* of the particle on its characteristic (magnitude of the vector *r* – *r'*) (Figure 3.2).

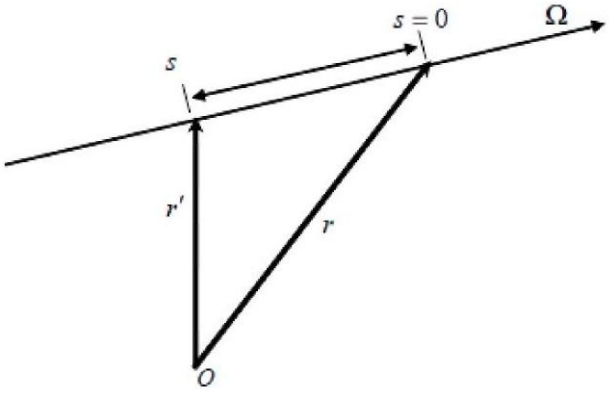


Figure 3.2 Graphical representation of characteristics. Neutron moves along direction Ω. Source [16].

Derivative along neutron path is described by:

$$\frac{d}{ds} = \frac{\partial r'}{\partial s} \cdot \nabla_{r'},$$

hence evaluation of eq. (3.3) gives:

$$[\frac{d}{ds} - \sum(r', E)]\Phi(r', \Omega, E) = -s(r', \Omega, E), \tag{3.4}$$

where:

$$s(r', \Omega, E) = \frac{1}{4\pi}\int_{R^+}\int_{S^2}\sum_S(r, E', E, \Omega', \Omega)\Phi(r, E', \Omega')d\Omega' dE'$$
$$+\frac{\chi_f(E)}{4\pi}\int_{R^+}\int_{S^2}\nu_f(r, E')\sum_f(r, E')\Phi(r, E', \Omega')d\Omega' dE + S(r, E, \Omega)$$

is the collision source. After defining the mean free path as:

$$\tau(r, r', E) = \int_0^{|r-r'|}\sum(r'(s'), E)ds'$$

and assuming that collision source is known, the solution of eq. (3.4) can be presented as:

$$\Phi(r,\Omega,E)=\Phi(r',\Omega,E)e^{-\tau(r,r',E)}+\int_0^S e^{-\tau(r,r'(s'),E)}q(r'(s'),E)ds'. \quad (3.5)$$

Integral form represents the fundamental neutron transport equation for a 3D system with energy dependence and is especially useful in the multiple collision approximation when absorption processes dominate. Integral neutron transport equation can be also solved numerically with collision probability methods.

## 4. Second-order forms

For simplicity of the method presentation we start with the first-order form of the stationary transport equation for one energy group, that can be written in the form:

$$\hat{\Omega}\cdot\vec{\nabla}\Phi(\vec{r},\hat{\Omega})+\sum(\vec{r})\Phi(\vec{r},\hat{\Omega})=\sum_s(\vec{r})\int d\hat{\Omega}'\Phi(\vec{r},\hat{\Omega}'+s(\vec{r}),\vec{r}\in V) \quad (3.6)$$

where $\vec{r}$ is the spatial location, and $\hat{\Omega}$, is the direction of neutron travel; $\sum$ and $\sum_s$ are the macroscopic total and scattering cross sections, respectively, *s* is the group source, and we normalize the angular integrals such that $\int d\Omega=1$.

Integrating over angle yields the neutron conservation equation and defining the even- and odd-parity flux components as

$$\Phi^{\pm}(\vec{r},\hat{\Omega})=1/2[\Phi(\vec{r},\hat{\Omega})\pm\Phi(\vec{r},-\hat{\Omega})] \quad (3.7)$$

We may evaluate eq. (3.6) at $\hat{\Omega}$ and $-\hat{\Omega}$ and add and subtract the results to obtain a set of coupled first-order equations

$$\hat{\Omega}\cdot\vec{\nabla}\Phi^{-}+\sum\Phi^{+}=\sum_s\phi+s \quad (3.8)$$

and

$$\hat{\Omega}\cdot\vec{\nabla}\Phi^{+}+\sum\Phi^{-}=0 \quad (3.9)$$

A pair of second-order equations may then be obtained. Eliminating $\Phi^{-}$ between eqs. (3.8) and (3.9) yields the even-parity equation

$$-\hat{\Omega}\cdot\vec{\nabla}\sum^{-1}\hat{\Omega}\cdot\vec{\nabla}\Phi^{+}+\sum\Phi^{+}=\sum_{s}\phi+s \tag{3.10}$$

while eliminating $\Phi^{+}$ yields the odd-parity equation

$$-\hat{\Omega}\cdot\vec{\nabla}\sum^{-1}\hat{\Omega}\cdot\vec{\nabla}\Phi^{+}+\sum\Phi^{+}=\sum_{s}\phi+s \tag{3.11}$$

These two equations contain only $\Phi^{+}$ and $\Phi^{-}$, respectively; since the scalar flux and current may be expressed as

$$\phi=\int d\Omega\Phi^{+} \tag{3.12}$$

and

$$\vec{J}=\int d\Omega\hat{\Omega}\Phi^{-} \tag{3.13}$$

Finally, we may also write a second-order equation for the angular flux by first solving eq. (3.6) for

$$\Phi=-\sum^{-1}(\hat{\Omega}\cdot\vec{\nabla}\Phi-\sum_{s}\phi-s)$$

and substituting into eq. (3.6) to obtain

$$-\hat{\Omega}\cdot\vec{\nabla}\sum^{-1}\hat{\Omega}\cdot\vec{\nabla}\Phi+\sum\Phi=(1-\hat{\Omega}\cdot\vec{\nabla}\sum^{-1})(\sum_{s}\phi+s) \tag{3.14}$$

## 5. Weak forms

The starting point for most space-angle approximations is the weak form of the forgoing equations. To obtain the weak forms of the coupled equations (3.8) and (3.9) we multiply the two by even- and odd-parity test functions, $\tilde{\Phi}^{+}$ and $\tilde{\Phi}^{-}$, respectively and integrate over angle and space:

$$\begin{aligned}&\int dV\int d\Omega[-(\hat{\Omega}\cdot\vec{\nabla}\tilde{\Phi}^{+})\Phi^{-}+\sum\tilde{\Phi}^{+}\Phi^{+}-\tilde{\phi}(\sum_{s}\phi+s)]\\&+\int d\Gamma\int d\Omega\hat{\Omega}\cdot\hat{n}\tilde{\Phi}^{+}\Phi^{-}=0\end{aligned} \tag{3.15}$$

$$\begin{aligned}&\int dV\int d\Omega[\sum^{-1}(\hat{\Omega}\cdot\vec{\nabla}\tilde{\Phi}^{+})(\hat{\Omega}\cdot\vec{\nabla}\Phi^{+})+\sum\tilde{\Phi}^{+}\Phi^{+}-\tilde{\phi}(\sum_{s}\phi+s)]\\&+\int d\Gamma\int d\Omega\hat{\Omega}\cdot\hat{n}\tilde{\Phi}^{+}\Phi^{-}=0\end{aligned} \tag{3.16}$$

The surface terms in the above equations determine the form of the boundary conditions.

It is the incoming angular flux that is known on the boundary. Hence

$$\Phi^{+}(\vec{r},\hat{\Omega})+\Phi^{-}(\vec{r},\hat{\Omega})-\Phi_{\lambda}(\vec{r},\hat{\Omega})=0,\vec{r}\in\Gamma,\hat{n}\cdot\hat{\Omega}<0 \tag{3.17}$$

and in particular the vacuum boundary $\Phi_{\lambda}(\vec{r},\hat{\Omega})=0,\vec{r}\in\Gamma,\hat{n}\cdot\hat{\Omega}<0$ is the homogeneous form of this condition.

With the incoming flux boundary conditions, eq. (3.16) becomes

$$\begin{aligned}&\int dV\int d\Omega[\Sigma^{-1}(\hat{\Omega}\cdot\vec{\nabla}\tilde{\Phi}^{+})(\hat{\Omega}\cdot\vec{\nabla}\Phi^{+})+\Sigma\tilde{\Phi}^{+}\Phi^{+}-\tilde{\phi}(\Sigma_{s}\phi+s)]\\&+\int d\Gamma\int d\Omega\,|\hat{\Omega}\cdot\hat{n}\,|\,\tilde{\Phi}^{+}\Phi^{+}+2\int d\Gamma\int_{\hat{n}\cdot\hat{\Omega}<0}d\Omega\hat{\Omega}\cdot\hat{n}\tilde{\Phi}+\Phi_{\lambda}=0\end{aligned} \tag{3.18}$$

where for vacuum boundary conditions we set $\Phi_\lambda = 0$. For most computations, the problem domain is bounded by some combinations of reflected and vacuum boundaries. We indicate this by dividing the boundary as $\Gamma = \Gamma_r + \Gamma_v$. Then, instead of eq. (3.18), we have

$$\begin{aligned}&\int dV\int d\Omega[\Sigma^{-1}(\hat{\Omega}\cdot\vec{\nabla}\tilde{\Phi}^{+})(\hat{\Omega}\cdot\vec{\nabla}\Phi^{+})+\Sigma\tilde{\Phi}^{+}\Phi^{+}-\tilde{\phi}(\Sigma_{s}\phi+s)]\\&+\int_{v}d\Gamma\int d\Omega\,|\hat{\Omega}\cdot\hat{n}\,|\,\tilde{\Phi}^{+}\Phi^{+}=0\end{aligned} \tag{3.19}$$

since no surface integral appears for $\Gamma_r$, where the essential reflected conditions are applied.

A full account of mathematical problems related with the variational formulations for first and second order of stationary neutron transport equation with continuous energy dependence can be found respectively (Borysiewicz and Stankiewicz 1979 A and B). In the paper (Borysiewicz 1981) the author basing on motion of stiff variational problems for neutron transport equations derived an asymptotic relation between integral-differential form of transport equations with diffusion equations and various approximate methods used for solving stationary neutron transport problems.

# 6. Approximate methods for solving neutron transport equation

Neutron transport equation in the integro-differential form even in the time-independent form (3.3) (with applied boundary conditions) cannot be solved due to the three main reasons:

- cross-sections change with neutron energy in a complicated way;
- streaming and scattering source terms are angular dependent;
- complex geometry of spatial regions with highly heterogeneous material properties.

For these reasons all deterministic transport codes use methods based on three approximations (Sanchez 2012):

- continuous energy dependence of cross-sections is reduced to the number of discrete energy groups;
- angular dependence of streaming and scattering source terms is handled by functional expansions or discretization using discrete ordinates ($S_N$) or projection ($P_N$) methods, respectively;
- spatial discretization of the transport equation in the most cases is based on a partition of the spatial domain into homogeneous regions and a coherent approximation of the flux and the source in each region.

## 6.1. Multigroup method

The multigroup method is based on partitioning the energy spectrum into G energy groups, such that:

$$\Delta E_g = [E_g, E_{g-1}], g = 1,2,..., G,$$

where the highest group $g$ = 1. After expressing the energy integrals of the scattering fission parts as sums over energy groups and introducing multi-group approximation such that:

$$\Phi(r, E, \Omega) = f(E)\Phi_g(r, \Omega)$$
$$S(r, E, \Omega) = g(E)S_g(r, \Omega)$$

$$\int_{\Delta E_g} f(E)dE = 1, \int_{\Delta E_g} g(E)dE = 1$$

the neutron transport equation becomes:

$$[\Omega\cdot\nabla+\sum(r)]\Phi(r,\Omega)=\frac{1}{4\pi}\int_{S^2}\sum_s(r,\Omega'\Omega)\Phi(r,\Omega')d\Omega' + \frac{1}{4\pi}\chi_f[\nu_f(r)\sum_f(r)]^T\Phi(r)+S(r,\Omega) \quad , \qquad (3.20)$$

where:

$$\sum(r)=diag\{E_g(r),\ g=1,...,G\}$$
$$\nu_f(r)\sum_f(r)=\{\nu_{f_g}(r)\sum_{f_g}(r),\ g=1,...,G\}$$
$$\sum_s(r,\Omega'\Omega)=\{\sum_{s_{g,g'}}(r,\Omega',\Omega),\ g'=1,...,G\}$$
$$\chi_f=\{\chi_{f_{g'}}\ g=1,...G\}$$

and:

$$\sum_g(r)=\int_{\Delta E_g} f(E)\sum(r,E)dE$$
$$\sum_{s_{g,g'}}(r,\Omega',\Omega)=\int_{\Delta E_g}\int_{\Delta E_{g'}} f(E')\sum_s(r,E',E,\Omega'\Omega)dE'dE$$
$$\nu_{f_g}(r)\sum_{f_g}(r)=\int_{\Delta E_g} f(E)\nu_f(E)(r)\sum_f(r,E)dE$$
$$\chi_{f_g}=\int_{\Delta E_g}\chi_f(E)dE$$

Additionally, for numerical algorithms, it is possible to reformulate the multi-group approximation as a series of one-group equations. The multi-group approximation is one of the most widely used approximations and is applied in almost all deterministic neutronic codes.

## 6.2. Angular dependence approximation

The other approximation related to the angular dependence of streaming and scattering source terms of the neutron transport equation is usually introduced by using $P_N$ or $S_N$ methods. In the $P_N$ method transport equation is projected over a set of angular functions such as spherical harmonics or, recently, partial-range angular functions such as wavelets. In spherical harmonics approach, a set of

spherical harmonics span a subspace which is invariant with respect to orthogonal transformations:

$$P_N = \{A_m(\Omega), k(m) \le N\}$$

The $P_N$ equations in 3D case contain $M = (N+1)^2$ unknown angular flux moments $\Phi_m(r)$ for $k(m) \le N$. $P_N$ projection approximation diagonalizes the scattering term via the truncation in the order *N* on the streaming part.

The $S_N$ approximation also called discrete ordinates approximation is used to solve neutron transport equation for a finite set of directions. The directions are associated with set of quadrature weights which enables to write the scattering source in terms of the angular fluxes in the prescribed directions. This procedure yields a system of equations for the angular fluxes in the selected angular directions, which are then discretized in the spatial variable using discontinuous finite element (DFE) or method of characteristics (MOC). The $S_N$ approximation, contrarily to the $P_N$ approximation, diagonalizes the streaming term by which equations are coupled.

### 6.3. Spatial discretization

The spatial discretization of the transport equation in the most cases is based on a partition of the spatial domain into homogeneous regions and a coherent approximation of the flux and the source in each region. We can distinguish two main approaches: traditional and advanced ones. In traditional approach regular orthogonal structured grid is used. It forces use of a huge number of elements (several millions) and curved boundaries approximated by orthogonal grid. In recent, advanced approach unstructured tetrahedral cells are used. In this case much fewer elements are needed to achieve accurate solution and curved boundaries are accurately represented.

In the early years, relatively simple finite difference (diamond difference and weighted diamond difference) methods were favored. Later, more sophisticated finite element, nodal, characteristic, and corner balance methods were introduced (Larsen and Morel 2009). Each of these types of methods tends to have its own advantages and disadvantages (Azmy 1992; Duo and Azmy 2007). For example, finite difference and (to a certain extent) nodal methods are relatively easy to implement on Cartesian (orthogonal, or box-like) spatial grids, while finite element, characteristic, and corner balance methods are better adapted to non-Cartesian (triangular, tetrahedral, or unstructured) spatial grids.

The description of DFE and MOC methods as well as $P_N$ and $S_N$ ones one can find in (Sanchez 2012).

A major issue in discretizing the spatial variable is the number of unknowns that must be calculated (and stored) per spatial cell. Methods that require a minimum amount of storage are generally less accurate on a specified grid, but the storage demand of particle transport problems is so high that in many problems, the simpler methods are preferred.

In addition to the issue of storing and processing the unknowns in the discretized Boltzmann equation, there is the fact that a linear algebraic system of equations with N >> 10 equations and unknowns cannot be solved by direct matrix inversion. For most practical problems, it is necessary to use iterative methods to calculate solutions.

The simplest iteration strategy is based on sweeping, which itself is based on the observation that with standard discretization schemes, problems with no scattering or fission can be solved directly and noniteratively by marching through the spatial grid in the direction of particle flow. (Different directions of flow can require a different direction of marching, or sweeping.) The angular flux solution of such a problem is termed the uncollidedflux; it consists of all particles that have not experienced a collision.

For problems with scattering, the source iteration strategy consists of performing sweeps and iterating on the scattering source. If the first sweep is performed with the scattering source $\Phi^{(N)}$

$$\Phi^{(N)} = \sum_{n=0}^{N} \Phi_n$$

where $\Phi_n$ is the angular flux of particles that have scattered exactly n times If a physical system is small and “leaky,” or has significant absorption, then particles will generally have short histories, and the series (298) will converge rapidly. However, if a problem has a subregion which is many mean free paths thick and dominated by scattering (rather than capture), then particles in that subregion will have long histories, and the above series will converge slowly (Carlson and Lathrop 1968; Larsen and Morel 2009).

To speed up the convergence of source iterations for problems with optically thick, scattering-dominated subregions, iterative acceleration strategies have been devised.

- *Chebyschev acceleratio*n - the earliest technique based on concepts from matrix algebra. This method worked to a limited extent, but it was not sufficiently efficient for many problems.

- *Rebalance method* - developed and used widely for a number of years. This method operates by calculating and applying, at the end of each sweep, rebalance factors on a fine or coarse space-energy grid. The rebalance method tends to become unstable when used on a fine space-energy grid, and to become stable but inefficient when used on a very coarse grid. The optimal (intermediate) grid is problem-dependent and must found by trial and error. Even when the optimal grid is found, the resulting method is often not as efficient as desired (Adams and Larsen 2002).

- *Diffusion synthetic acceleration (DSA)* - developed to speed up the convergence of source iterations. DSA is based on the following concept. At the end of a transport sweep, an exact transport equation is derived for the iteration error (the difference between the latest iterate and the converged solution). This equation is just as difficult to solve as the original transport equation for the angular flux. In DSA, this exact transport equation for the iteration error is replaced by an approximate diffusion equation (Adams and Larsen 2002; Alcouffe 1977). In practice, DSA is highly efficient for optically thin spatial grids. Unfortunately, unless great care is taken in the discretization of the diffusion part of the algorithm, it can become inefficient or unstable for optically thick spatial grids (Adams and Larsen 2002; Azmy 1998).

- *Krylov methods* - used, often in conjunction with DSA. Although Krylov methods require significant extra storage, they can be remarkably effective at stabilizing and speeding up the iterative convergence of methods based on source iterations, or on DSA (Adams and Larsen 2002; Faber and Mantueffel 1989).

## 6.4. k-Eigenvalue Problems

In numerical computations, transport equations are usually rewritten to the form in which time dependence is not treated explicitly. For non-fission systems with nonnegative time-independent external sources transport equation

simplifies to a form for which we can always find a nonnegative solution. For systems with fission materials such as reactor core, the problem is more complicated and the criticality problem needs to be considered.

When operating a nuclear reactor, the aim of the engineer is to achieve a controlled sustainable chain reaction where the number of neutrons that are produced is equal to the number of neutrons that leave the system through the outer boundary or are absorbed. Physically, such reactor system is called critical if a controlled sustainable chain reaction is time-independent and there is no presence of external sources of neutrons. In that case the mentioned balance between production and losses of neutrons occurs and we are dealing with time-independent asymptotic neutron distribution in the reactor core. If the equilibrium cannot be achieved, the asymptotic neutron distribution will be time-dependent and will (increase or decrease exponentially). Reactor core in these cases is said to be subcritical or supercritical, respectively. If external time-independent neutron source exists, only a subcritical system will eventually come to equilibrium with time-independent neutron flux distribution. For critical and supercritical systems such equilibrium is not possible and neutron flux distribution will increase with time. Fixed source calculations with imposed known source are usually used in shielding calculations to determine neutron distribution in the system and to minimalize the neutron dose while minimising amount of shielding material used.

Neutron transport equation with time-independent source in general is used to describe the period of time when neutron flux distribution inside the core is not constant, for example during the start-up period. In that situation a reactor core will not be exactly critical until fine adjustments have been made in composition and core geometry (via control rods movements and fuel burnup processes) or application adequate safety measures in case of an accident (Figure 3.3). When the reactor reaches an operating stage in which neutron distribution does not change with time then neutron transport equation can be reduced to the time-independent source-free form. Nevertheless, usage of the source-free transport equation is problematic. If we try to solve the source-free neutron transport equation and find that such solution doesn't exist, we know nothing about the criticality of the system. This is the reason for which criticality calculations are usually reformulated to the form of eigenvalue problem, where the eigenvalue measures the criticality level (provides quantitative information whether the system is subcritical, critical or supercritical). There are in use two most common formulations of eigenvalue problem:

- time-absorption eigenvalue, referred to as *k*-eigenvalue
- multiplication eigenvalue, referred to as α-eigenvalue.

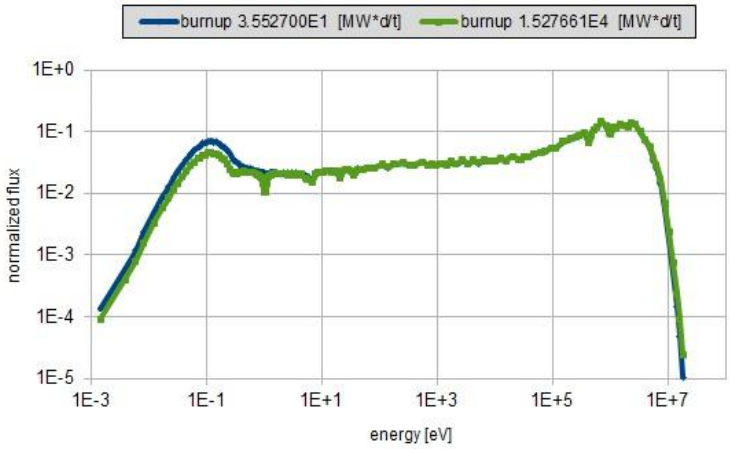


Figure 3.3 Example of neutron flux spectrum for homogenized fuel assembly in function of neutron kinetic energy. The figure presents two spectra with different burnups.

In *k*-eigenvalue calculations, one often sees the following version of (the transport equation in which the inhomogeneous source S(r,E,Ω) and the boundary source are set to zero, and the fission source is modified by a constant factor 1/*k*:

$$
\begin{aligned}
&[\Omega\cdot\nabla+\sum(r,E)]\Phi(r,E,\Omega)= \\
&\frac{1}{4\pi}\int_{R^+}\int_{S^2}\sum_S(r,E',E,\Omega',\Omega)\Phi(r,E',\Omega')d\Omega'dE' \\
&+\frac{\chi_f(E)}{4\pi k}\int_{R^+}\int_{S^2}\nu_f(r,E')\sum_f(r,E')\Phi(r,E',\Omega')d\Omega'dE \\
&\Phi(r,E,\Omega)=0, r\in V,\Omega\cdot n<0, 0<E<\infty
\end{aligned}
\qquad (3.21)
$$

These equations always have the zero solution: Φ = 0. The goal is to find the largest value of *k* such that a nonzero solution Φ exists. This *k* is called the criticality (or criticality eigenvalue) of the system *V*; the corresponding Φ is called the eigenfunction or fundamental mode.

If a system $V$ has a fissile region, then it can be shown that the criticality eigenvalue $k$ always exists, and the corresponding eigenfunction $\Phi$ is unique (up to a multiplicative constant) and positive. (If V has no fissile region, then we adopt the convention that $k = 0$.)

The motivation for defining $k$ in the above manner is as follows. In any system V with fission, neutrons are lost due to capture and leakage, and are produced by fission. If the production of neutrons due to fission exactly balances the loss of neutrons due to capture and leakage, then a nonzero, steady-state neutron flux is possible. (This concept underlies a steady-state power reactor.) By adjusting the magnitude of the fission source through the eigenvalue $k$, one can make this exact balance occur. If $k < 1$, the fission source must be increased for a steady-state solution to exist; this implies that capture and leakage dominate fission, and the reactor is sub- critical. If $k > 1$, the fission source must be decreased for a steady-state solution to exist; this implies that fission dominates capture and leakage, and the reactor is supercritical. If $k = 1$, capture and leakage exactly balance fission, and the reactor is critical. The calculation of $k$ for differing reactor configurations is one of the most important and ubiquitous calculations in the design and operation of nuclear reactors.

In some problems (in particular, the field of reactor kinetics), the criticality $k$ is replaced by the reactivity $p$, defined by

$$\frac{1}{k} - 1 = \rho$$

A reactor is subcritical if $\rho < 0$, critical if $\rho = 0$, and supercritical if $\rho > 0$.

## 7. Existence, uniqueness, and nonnegativity of transport solutions

Briefly, each time-dependent neutron transport problem, with or without precursor densities, *always* has a unique nonnegative solution. Steady-state neutron transport problems (in which precursor densities are neglected) do not always have a unique nonnegative solution, but when they do not, there is a physical explanation. (A classic theoretical discussion of the existence of solutions of time-dependent transport problems is given in (Borysiewicz and Spiga 1974; Borysiewicz and Kruszyńska 1978).

To discuss the connection between solutions of time-dependent and steady-state neutron transport problems, we consider time-dependent and steady-state

problems without precursor densities in which the internal source and the prescribed incident boundary fluxes are nonnegative and independent of *t*. We then have:

1. If $V$ is subcritical ($k < 1$), the time-dependent neutron flux limits as $t \to \infty$ to a steady-state neutron flux, which is the (unique, nonnegative) solution of the steady-state neutron transport problem.

2. If $V$ is critical ($k = 1$) and the internal source and prescribed incident boundary fluxes are nonzero, the time-dependent neutron flux grows linearly in $t$ as $t \to \infty$ . In this situation, no limiting ($t \to \infty$ ) steady-state solution of the time-dependent problem exists, and no solution of the corresponding steady-state neutron transport problem exists.

However, if the internal source and prescribed incident boundary fluxes are zero, then the time-dependent neutron flux limits as $t \to \infty$ to a steady-state neutron flux of the form:

$$\Phi(x,\Omega,E,t) \approx C\Phi(x,\Omega,E) \text{ for } t \approx \infty \tag{3.22}$$

where $\Phi$ is the $k$-eigenfunction for the critical system and $C$ is a constant that depends on the initial condition $\Phi$ of the time-dependent problem. In this situation, the steady-state neutron transport problem has an infinite number of solutions, all given by (3.22), with the constant $C$ arbitrary.

If $V$ is supercritical ($k > 1$), the time-dependent neutron flux grows exponentially in $t$ as $t \to \infty$. If the internal source and prescribed incident boundary fluxes are nonzero, the corresponding steady-state neutron transport problem either has a unique nonpositive solution, or no solution exists.

If the internal source and prescribed incident boundary fluxes are *zero*, then the steady-state neutron transport problem will either have the solution $\Phi = 0$, or an infinite number of solutions of the form of (3.22), where $\Phi$ is now some other (than the $k = 1$) eigenfunction of the system; this eigenfunction is nonpositive (nonphysical).

In all cases, a unique, positive solution of the time-dependent neutron transport problem exists. Also, a positive solution of the steady-state neutron transport problem exists if and only the solution of a corresponding time-dependent problem has a steady-state limit as $t \to \infty$, and if the steady-state limit of the time-dependent problem does exist, it is a solution of the steady-state problem. Issues of the existence and uniqueness of the solutions for the time

dependent neutron transport equations and *k*-eigenvalue problems were thoroughly analyzed in the papers (Borysiewicz 1970, 1978; Borysiewicz and Mika 1969,1972).

## 8. Smoothness of the angular flux

This often poorly understood topic, dealing with the continuity and differentiability properties of the angular flux, has major implications in the accuracy of approximation schemes and numerical methods for simulating transport problems. It is not possible to discuss this subject fully here; instead we give some illustrative examples (see Borysiewicz and Spiga 1974; Borysiewicz and Kruszyńska 1978, for a more thorough discussion). The basic facts are as follows:

1. Solutions of planar-geometry transport problems with vacuum boundaries and finite isotropic internal sources are *smooth* (continuous with continuous first derivatives) functions of $x$ and $\mu$, except at outer boundaries and material interfaces between regions with different cross sections and internal sources. At such interfaces, $\Phi$ is: (i) continuous in $x$ with a discontinuous first derivative, and (ii) discontinuous in $\mu$ at $\mu = 0$. This *boundary-layer* behavior occurs only at the interface between different material regions, and at the outer boundary of the system.

2. Angular flux solutions of multidimensional transport problems with vacuum boundaries exhibit the same boundary-layer behavior as described above at material interfaces and the outer boundary of the system. However, because of geometrical effects, multidimensional angular fluxes also lack smoothness away from boundary layers. Generally, multidimensional transport solutions are continuous functions of $r$ and $\Omega$ but have discontinuous first derivatives. Occasionally, these solutions can even be discontinuous. Thus, multidimensional transport solutions are inherently not "smooth"; they lack even one continuous derivative in $r$ and $\Omega$. The lack of smoothness of the transport solution is an impediment to the calculation of accurate numerical solutions of multidimensional neutron transport problems.

3. Solutions of problems with nonzero but smooth prescribed incident boundary fluxes have the same smoothness properties as described above. However, if the incident boundary fluxes are not smooth, then the uncollided flux component of $\Phi$ can be nonsmooth throughout $V$. For example, an incident monodirectional (delta function) beam of neutrons on $\partial V$ creates a delta function component of $\Phi$ that propagates entirely through $V$.

This simple problem applies to the uncollided angular flux in any source-driven problem. In general, when the fight path $r - s\Omega$ passes through a "corner" of a source region, $\Phi$ ($(x, \Omega, E)$ is continuous with a discontinuous derivative (with respect to $x$, $y$, or $\omega$). When the fight path passes through a corner of a material region that does not contain a source, $\Phi$ has a weaker singularity (a continuous first derivative but a discontinuous second derivative). And, as we showed above, when the fight path traces along the planar edge of a source region, $\Phi$ is discontinuous. For problems with scattering, the statements in this paragraph hold for each $n$th collided flux $\Phi_n$, and for $\Phi$ itself. For problems driven by boundary sources, similar results also follow.

In general, for multidimensional, multiregion problems, $\Phi$ is generally a function with weak smoothness properties (Borysiewicz and Spiga 1974; Borysiewicz and Kruszyńska 1978). This basic fact has not stopped practitioners from employing numerical methods that require the exact solution to be smoother than it actually is to achieve the theoretically optimal accuracy. However, the lack of smoothness of $\Phi$ negatively affects the accuracy and convergence rates of the resulting numerical solutions. For example, methods that would be second-order accurate if the solution is unrealistically smooth exhibit convergence rates that are less than second order when applied to realistic problems (Duo and Azmy 2007; Larsen 1982). (However, numerical experiments also show that certain integrals of the flux actually do converge with second-order accuracy (Larsen 1982). The topic of the lack of smoothness of the angular flux and how this affects multidimensional numerical simulations is only qualitatively understood.

## 9. Diffusion neutronic codes

The neutron flux (see Figure 3.3) calculated by neutron transport lattice codes can be used to obtain sets of macroscopic cross sections characterising specific homogenised sub-region of the reactor core in a function of energy groups (energy spectrum is usually divided into 2 to 8 intervals). After that the generated macroscopic cross sections may be used as materials' properties library in the input for codes solving diffusion equation (representing the second group of the deterministic neutronic codes). While the lattice codes solving neutron transport equation are usually used to model only a small part of the reactor core (for example one fuel assembly), diffusion neutronic codes aim to simulate whole reactor core. In the neutron diffusion theory neutrons diffuse from regions of high concentration to the regions of low concentration, similarly to gas molecules diffusing to reduce spatial variations in concentration (Scheben

2011). The process can be described by the multi-group neutron diffusion equations (Al-Malki et al. 2012):

$$\frac{1}{v_g}\frac{\partial}{\partial t}\phi_g(r,t) = \nabla \cdot D_g(r)\nabla\phi(r,t) - \Sigma_{a_g}(r)\phi(r,t) - \sum_{g'>g}^{G}\Sigma_{s_{g,g'}}(r)\phi(r,t)$$
$$+\sum_{g=1}^{G}[\chi_g \nu\Sigma_{f_{g'}}(r)[1-\beta] + \Sigma_{s_{g',g}}(r)]\phi_{g'}(r,t) + \sum_{i=1}^{I}\chi_{g,i}\lambda_i C_i(r,t)$$

$g = 1,2,...,G$ (3.23)

$$\frac{\partial}{\partial t}C_i(r,t) = \beta_i\sum_{g=1}^{G}\nu\Sigma_{f_g}(r)\phi_g(r,t) - \lambda_i C_i(r,t)\,,$$

$i = 1,2,..., I$ (3.24)

where $\phi_g(r,t)$ is the scalar neutron flux (see Figure 3.4) in group $g, v_g$ mean velocity of the neutron in group $g$, $D_g(r)$ is the diffusion coefficient in group $g, \Sigma_{a_g}\phi(r)$ is the absorption cross-section in group $g, \Sigma_{f_g}(r)$ is the fission cross-section in group $g$, $\Sigma_{s_{g',g}}(r)$ is the scattering cross-section from group *g*' to group *g* such that ($\Sigma_{sgg'}(r) = 0$ from $g' > g$), *v* is the mean number of fission neutrons, $\chi_g$ is the spectrum of prompt neutrons in group *g*, $\chi_{g,i}$ is the spectrum of i-group delayed neutrons in group *g*, $\beta_i$ is the fraction of delayed neutrons in group *i*, and $\beta = \sum_{i=1}^{I}\beta_i$ is the total fraction of delayed neutrons.

Neutron diffusion equation can be obtained by the approximation of the neutron transport equation. The main assumptions which lead to that are as follows:

- angular flux varies sufficiently slowly with angle;
- neutron sources, including fission, are isotropic;
- the current density varies slowly, relative to the collision frequency.

The first assumption is very stringent and comparisons with solutions from transport theory show that is invalid in the following cases:

- in the vicinity of localized sources;
- in highly absorbing media;
- near external boundaries of the domain, and near interfaces for which properties change suddenly.

For these reasons codes solving neutron diffusion equation are inappropriate for fine core modelling (inter alia due to the strongly absorbing regions such as the fuel and the control rods). However, that type of codes can be used freely to calculate the macroscopic flux distribution in the reactor, with using material properties obtained by homogenizing (in neutron transport lattice codes) unit cells with dimensions much greater than the neutron mean free path (e.g. of the size of a fuel assembly).

As was mentioned earlier, reactor core behaviour depends strongly on different physical processes coupled with feedback effects between them. Among others the most important dependences exist between neutronics and thermal-hydraulics and are caused by changes of reactor coolant flow conditions and changes of the fuel rod temperatures and densities. In the past the calculations for the analysis of reactor core behaviour and the whole plant transients were performed separately. The problems related to the feedback effects were handled by including in thermal-hydraulic and neutronic codes simplified models describing the necessary relations. For example point kinetic model (significant simplification of neutron diffusion model) was widely implemented in all thermal-hydraulic system codes. Recently, there is a great interest in performing such calculations by coupling 2D and 3D neutronic codes with thermal-hydraulic 3D and system codes (Leppänen 2012) (Figure 3.4). It is impossible for now to solve the full-scale neutron transport problem, especially with considering the coupling to thermal-hydraulic systems.

For this reason modelling and simulation of the operating nuclear reactor includes several approximations and is based on a two-stage calculation scheme:

1) homogenization at fuel assembly level done usually by neutron transport lattice code;
2) calculations performed by coupled thermal-hydraulic and neutron diffusion codes.

Neutron transport for reactors is modeled with a multi-level approach.

Level 1: Single Pincell

- High-fidelity 1-D space on a small domain
- High-fidelity in energy
- Approximate BCs and state
- Up-scale data to a coarser scale
- Provide “homogenized” or “effective” data

Level 2: Single Lattice

- Moderate-fidelity 2-D space on a larger domain
- Moderate-fidelity in energy
- Approximate BCs and state

Level 3: Full Reactor Core

- Low-fidelity for the full 3-D spatial domain
- Very low-fidelity in energy
- True BCs
- Coupled with other physics for true state.

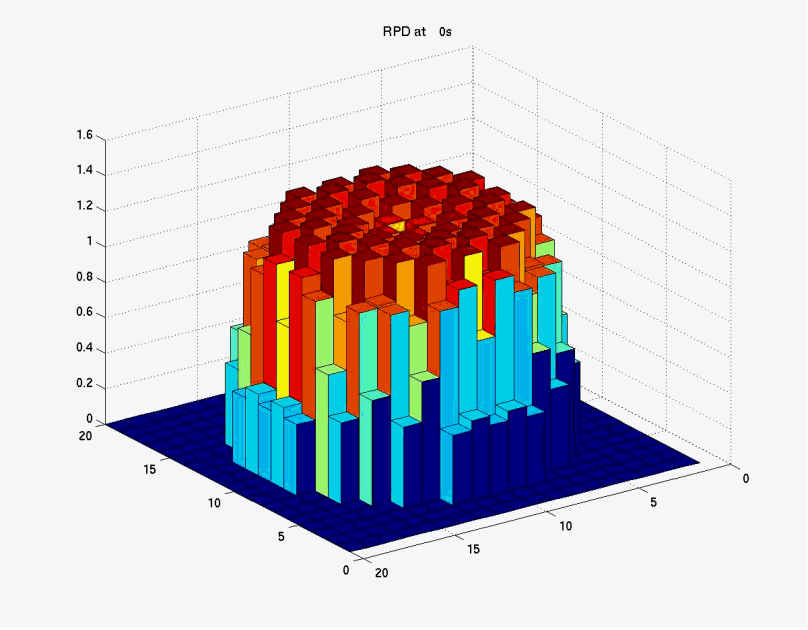


Figure 3.4 Steady state spatial distribution of neutron flux in PWR reactor core calculated by PARCS code. Source [38].

The main challenge for the simulation lies in the first stage of the presented scheme because expressing physical neutron interactions with simplified parameters without losing to much important information is required. This can be achieved by preserving physical quantities such as reaction rate balance and leakage currents over boundaries as well as by tracking the isotopic changes in materials occurring during whole reactor operation period. Most of the neutronic codes include additional physical models allowing that kind of fuel depletion calculations (solving Bateman nuclide depletion equation). Further information on burnup calculations can be found for example in (Marleau 2001; Šmuc).

Over the next few years deterministic methods will remain the main computing tool in reactor core modelling and simulation with MC methods as benchmarking tools. In the intermediate future (5 to 10 years from now) MC methods probably will be used with deterministic methods as a hybrid tool with multi-physics coupling to thermal-hydraulics codes. In the distant future (more than 10 years from now) multi-physics codes using non-orthogonal grids will become complete, high-accuracy design tools, fully integrated into problems of reactor core design and operation.

# 10. Feature and performance of the computational neutron transport methods

## 10.1. Monte Carlo methods

Monte Carlo methods do not suffer, in principle, from the approximations related to the treatment of the energy variable, even if unresolved and resolved resonance treatments require appropriate methodologies. To this latter purpose codes like NJOY providing a capability to work with nuclear data libraries all over the world, are used to preprocess the basic data libraries for subsequent use in Monte Carlo codes. In theory, with unlimited computing power, because of the flexibility in treating complex geometries, and with a rigorous continuous energy treatment of the energy variable, the Monte Carlo codes should be able to achieve an extremely accurate solution. While this is true for a fixed source problem without multiplication, on the contrary for an eigenvalue problem, due to the stochastic nature of the algorithm, it seems that an intrinsic limit of accuracy exists. Moreover, when interested in local quantities, in order to achieve very low standard deviations, unreasonable number of neutron histories could be required.

In the realm of the Monte Carlo codes, the Los Alamos MCNP (X-5 Monte Carlo Team 2003) is the widespread reference (Blomquist 2002) from ANL, and the French Code TRIPOLI (Both et. al. 1994) are among other very well known

Monte Carlo codes.

While Monte Carlo codes are widely used, running these codes efficiently is problematic for complex problems. In addition to specifying the physical problem, the user must also specify the problem-dependent biasing parameters, and this can be a formidable task.

## 10.2. Deterministic methods

Deterministic methods are characterized by the discretization of the neutron transport equation to obtain an algebraic system of equations for the scalar flux. The primary limitation in deterministic methods is the number of unknowns that can be stored in memory. The errors in deterministic methods decrease as the various grids decrease in size (and the number of unknowns increases). Therefore, the size of available computer memory and computational performance can limit the accuracy of deterministic calculations.

The spatial discretization of the transport equation consists of dividing the system domain into a structured or unstructured grid. “Homogenization” of materials within a cell is often performed in order to reduce the number of spatial unknowns, computational cost and memory requirements.

The angular, or direction-of-flight variable $\Omega$ is generally discretized in one of two ways: *discrete-ordinates,* or *collocation* (or $S_N$) methods, and *spherical harmonic* (or $P_N$) methods. $S_N$ methods are more commonly used because the structure of the resulting discrete equations is more closely linked to the innate physical interpretation of particle transport. (In Cartesian geometries, $S_N$ methods can be interpreted as ones in which particles travel only in a finite, specified set of directions $\Omega_m$.) However, $S_N$ and $P_N$ methods have characteristic errors. In particular, $S_N$ methods have *ray effects,* which are most apparent in problems with strong absorption and localized sources. For problems whose solutions have a strong direction- dependence, such as neutron streaming through a voided channel, it is necessary to use a very high-order angular quadrature set. $P_N$ methods also have angular truncation errors, but of a different nature. Like $S_N$ methods, $P_N$ methods cannot easily describe an angular flux with a complicated direction-dependence. Also, the $P_N$ equations have a form and structure that are more difficult (than the $S_N$ equations) to interpret in terms of the physics of particle transport.

The diffusion approximation can also be used by integrating the transport equation to yield the balance equation. Use of the diffusion approximation is limited to problems in which leakage, absorption rates, and flux gradients are small. When these circumstances do not apply, diffusion theory is not accurate.

Of all the independent variables in the transport equation, the energy variable $E$ is the most problematic. The reason for this is that typically, the material cross sections, and hence the particle flux itself, have an extraordinarily complex energy-dependence. If the simple rule of thumb is followed that an energy grid should be chosen for which the solution varies in energy from one grid point to the next by no more than about 15%, then for typical problems, *millions* of grid points in $E$ would be required. This constraint would render the solution of typical problems to be outside the range of possibility.

Energy discretization is the most complex and difficult step of a deterministic calculation. As previously alluded, the multigroup (MG) approximation is typically required. This approximation consists of partitioning the energy range into "groups" and condensing the continuous energy cross sections over each group with a weighting function. The subscript $g$ is used to denote a quantity that has been condensed over the $g^{th}$ energy group: $E_g < E < E_{g-x}$. In order to rigorously preserve reaction rates, the exact angular flux must be applied as the weighting function. This technique eliminates the energy dependence of the cross section but introduces angular dependence of the resulting multigroup cross section. While this approach has become the standard for energy discretization in deterministic methods, it can incur unacceptable errors when the true flux is *not* separable in angle and energy, or when the spectrum is inadequately computed. Refining the group structure mitigates these errors, but computational expense and memory limitations prevent the use of an arbitrarily fine group structure. The consistent $P_N$ and extended transport approximations are alternatives to using an isotropic weighting function, but these techniques require angularly-dependent spectrum calculations.

In addition to the difficulties presented by the multigroup approximation, the spatial and angular discretization schemes introduce truncation errors. These errors are reduced as the grids are refined, but the grid size is often limited by computational resources. The number of unknowns for a typical fission reactor problem can quickly become intractable even on supercomputers. In addition, it is difficult to optimize the grid parameters *a priori.* Despite the difficulties in discretization and multigroup cross section generation, most commercial neutron transport codes are based on deterministic methodologies.

After preparation of the multigroup cross sections, the transport equation can be discretized in angle and space, and the resulting algebraic system of equations can be solved on a computer. For fixed source problems, the transport equation reduces to a matrix system, Hy = q . For fission source problems, the transport equation is formulated as an eigenvalue problem, $\mathbf{Af} = 1/\mathbf{k}\,\mathbf{f}$, where $\mathbf{f}$ is the fission source.

In practical neutron/photon transport problems, the total number of unknowns can be extraordinarily large. To minimize the number of unknowns, computer codes have been written for 3-D problems with 1-D or 2-D spatial symmetry.

However, a fundamental difficulty remains at the heart of deterministic calculations: the costly and time-consuming task of obtaining adequate multigroup cross sections for a specified difficult problem. This aspect of deterministic simulations remains the most significant obstacle to obtaining useful, accurate deterministic solutions of practical transport problems in a reliable, efficient, and user-friendly manner.

As noted above deterministic methods utilize numerous approximations to discretize the exact transport equation into a set of linear equations solvable on a computer. Sometimes the resulting numerical solution differs from the true solution because the true physics cannot be accurately modeled. The physics that cannot be accurately modeled without an ultra- fine space-angle-energy grid are referred to as *transport effects.* For example, at some material interfaces, the angular flux exhibits a strong correlation between energy and angle. These "transport effects" are difficult to capture using conventional deterministic methods due to the limitations of the multigroup approximation. Transport effects are only associated with deterministic methods, since Monte Carlo methods model the exact physics and geometry. These effects can be described by refining the spatial, energy, and angular grids, but several calculations may be necessary to determine the required level of refinement.

It is important to address the issue of transport effects in computational modeling because candidate future nuclear reactors, such as the Very High Temperature Reactor, have new geometries and materials (i.e. voids, streaming regions, steel reflectors) that cause transport effects not well modeled by existing numerical techniques.

## 10.3. Hybrid Monte Carlo/Deterministic methods

In the last 10-15 years, it has become understood that the most challenging aspect of difficult Monte Carlo simulations - the determination of problem-dependent biasing parameters - can be done efficiently by a deterministic simulation.

The advantages to this procedure are that (i) it removes from the code user the burdensome task of calculating the biasing parameters, and (ii) the resulting computer-generated biasing parameters are usually much more efficient at reducing the Monte Carlo variance than the biasing parameters obtained by human trial and error (Smith and Wagner 2005).

The principal disadvantage is that two separate codes (Monte Carlo and deterministic) must be set up to run the same geometric problem, and the results of the deterministic code must be processed, formatted properly, and then input to the Monte Carlo code. This process can be unwieldy unless a suitable investment has been made in the computing infrastructure, enabling the process to occur automatically.

Most public particle transport codes are either Monte Carlo or deterministic, but a small number of user-friendly hybrid codes are now available. For example, the recent SCALE 6.0 package from Oak Ridge National Laboratory contains software that enables, with one geometric input deck, deterministically generated multigroup $S_N$ solutions to be calculated then used in Monte Carlo simulations (Haghighat and Wagner 2003; Smith and Wagner 2005).

To date, the term "hybrid" has implied a method in which a deterministic simulation is used to assist - through the calculation of biasing parameters - a Monte Carlo simulation. However, deterministic and Monte Carlo techniques can be merged in different advantageous ways. For example, it has been demonstrated that for source-detector problems, an adjoint calculation can be used to *actively* modify the physical scattering process, so that Monte Carlo particles are encouraged to scatter into directions and energies that will bring them from regions of low importance to regions of greater importance (Turner and Larsen 1997). In addition, recent work on the *functional Monte Carlo* method has shown that even more accurate estimates of eigenvalues and eigenfunctions can be obtained by a hybrid method in which the Monte Carlo simulation is *not* used to obtain estimates of the flux, but rather to obtain estimates of certain *nonlinear functionals*, which are then used to obtain estimates of the flux (Larsen and Yang 2008).

Convergence of the fission source is a significant computational burden in Monte Carlo criticality calculations. For large systems, the dominance ratio = the ratio of the second to first eigenvalue) is close to unity. In these cases, the higher-order eigenfunction modes decay slowly, and the true eigenfunction is poorly resolved for a long time. The Monte Carlo estimate of the fission source is unstable, and in some cases never fully converges. Slow fission source convergence is an inherent undesirable property of standard Monte Carlo calculations, and it can cause significant uncertainty in the true power distribution of a reactor.

A remedy on weakness of Monte Carlo and determenistic methods for solving neutron transport problem could recently developed hybride metthods, in particular Functional Monte Carlo (FMC) or Coarse Mesh Finite Difference (CMFD)-Accelerated Monte Carlo. Larsen and Yang first proposed the use of

the method FMC to accelerate Monte Carlo convergence of the fission source iteration. In FMC, Monte Carlo is used to estimate nonlinear functionals, which are ratios of space-angle-energy moments of the angular flux, resembling Eddington factors. The functionals are used in quasi-diffusion-like equations with no truncation errors to estimate the eigenvalue and eigenfunction.

Larsen and Yang demonstrated that FMC estimates of the eigenvalue and eigenfunction are more accurate. The principal difficulty with deterministic methods is the laborious calculation of multigroup cross sections. If continuous-energy Monte Carlo simulations could be efficiently run, to automatically determine (problem-dependent) multigroup cross sections, then this would be a way in which Monte Carlo simulations could significantly influence deterministic solutions. Promising work in this area has recently been reported (Wolters et al. 2009; Yang and Larsen 2009).

## Acknowledgement

The presented work was supported by the EU and MSHE grant no POIG.02.03.00-00-013/09.

## References

[1] DOE-HDBK-1019/1-93 (1993). DOE FUNDAMENTALS HANDBOOK: NUCLEAR PHYSICS AND REACTOR THEORY U.S. Department of Energy.

[2] Adams ML Larsen EW (2002) Fast iterative methods for discrete-ordinates particle transport calculations. Prog Nucl Energy 40:3 [Review article]

[3] Carlson BG, Lathrop KD (1968) Transport theory - the method of discrete ordinates. In:

[4] Carter LL, Cashwell ED (1975) Particle transport simulation with the Monte Carlo method. TID- 26607, National Technical Information Service, U.S. Department of Commerce Case KM, Zweifel PF (1967) Linear transport theory.

[5] Haghighat A, Wagner J (2003) Monte Carlo variance reduction with deterministic importance functions. Prog Nucl Energy 42:25 [Review article]

[6] American Nuclear Society, La Grange Park Kalos MH, Whitlock PA (1986) Monte Carlo meth-ods. Wiley, New York

[7] Larsen EW (1992) The asymptotic diffusion limit of discretized transport problems. Nucl Sci Eng 112:336 [Review article]

[8] Becker TL, Larsen EW (2009) The application of weight windows to "global" Monte Carlo prob-lems. In: Proceedings of the 2009 international conference on advances in mathematics, compu-tational methods, and reactor physics, Saratoga Springs, New York 3-7 May 2009
[9] Lewis EE, Miller WF (1993) Computational methods of neutron transport. American Nuclear Society, Lagrange Park
[10] Lux I, Koblinger L (1991) Monte Carlo particle transport methods: neutron and photon calculations. CRC Press, Boca Raton Marchuk GI
[11] Sanchez R, McCormick NJ (1982) A review of neutron transport approximations. Nucl Sci Eng 80:481 [Review article]
[12] Spanier J, Gelbard E (2008) Monte Carlo principles and neutron transport problems. Dover, New York. Originally published by Addison-Wesley, Reading (1969)
[13] X-5 Monte Carlo Team, "MCNP — a general Monte Carlo n-particle transport code, version 5, volume I: Overview and theory" Technical Report LA-UR-03-1987, Los Alamos National Laboratory, Los Alamos, NM, April 24, 2003
[14] G. Marleau (2001). DRAGON THEORY MANUAL, Ecole Polytechnique de Montreal.
[15] Le Mouel C., Soldevila M., APOLLO2 BEGINNER'S TRAINING DOCUMENTATION, RAPORT DM2S, SERMA/LTSD/RT/06-3967/A
[16] T. Downar et. al., PARCS v2.6 U.S. NRC Core Neutronics Simulator: USER MANUAL, RES / U.S. NRC.
[17] A.-M. Baudron et. al., CRONOS2.7: USER'S GUIDE, RAPPORT DM2S, SERMA/LENR/RT/06-3978/A.
[18] D. Rozon, Introduction to Nuclear Reactor Kinetics, Éditions de l'École Polytechnique de Montréal.
[19] Richard Sanchez, Prospects in deterministic three-dimensional whole-core transport calculations, Nuclear Engineering and Technology, Volume 44, Issue ,2, 2012, pp.113-150
[20] Borysiewicz M, Stankiewicz R (1979 A) Weak solution and approximate methods for the transport equation, Journal of Mathematical Analysis and Applications, Vol. 68, No.1
[21] Borysiewicz M, et al. (1981) Fundamentals of Neutron Transport Theory; Transport Theory and Advanced Reactor Calculation, Chap. I, IAEA, TECDOC-254, IAEA, p.7-57.
[22] Borysiewicz M (1981) Stiff variational problem in linear transport theory, Progress in Nuclear Energy, 1981, Vol.8, pp.117-125.

[23] Larsen EW, Morel JE (2009) Advances in discrete- ordinates methodology. In: Azmy YY, Sartori E (eds) Nuclear computational science: a century in review. Springer, Berlin [Review article]
[24] Azmy YY (1992) Arbitrarily high order characteristic methods for solving the neutron transport equation. Ann Nucl Energy 19:593
[25] Duo JI, Azmy YY (2007) Error comparison of diamond difference, nodal, and characteristic methods for solving multidimensional transport problems with the discrete ordinates approximation. Nucl Sci Eng 156:139
[26] Adams ML, Wareing TA, Walters WF (1998) Characteristic methods in thick diffusive problems. Nucl Sci Eng 130:18 Alcouffe RE (1977) Diffusion synthetic acceleration methods for the diamond-differenced discrete- ordinates equations. Nucl Sci Eng 64:344
[27] Azmy YY (1998) Impossibility of unconditional stability and robustness of diffusive acceleration schemes. In: Proceedings of the ANS topical meeting on radiation protection and shielding, Nashville, 19-23 April 1998, vol 1, p 480
[28] Faber V, Mantueffel TA (1989) A look at transport theory from the viewpoint of linear algebra. In: Nelson P et al (eds) Transport theory, invariant imbedding, and integral equations (Lecture notes in pure and applied mathematics), vol 115. Marcel Dekker, New York, p 37
[29] Borysiewicz M, Spiga G (1974) Smoothness of the solution in the twodimensional neutron transport equation, IAEA, Contract No. 1236/R1/RB
[30] Borysiewicz M, Kruszyńska N (1978) Smootness of the solution of the 2D neutron transport equation in the polygon region, Atomkernenergie - Kerntechnik Bd. 34 (1979) Lfg.1.
[31] Borysiewicz M (1970) Time dependent neutron thermalisation theory, Thesis, Institute of Nuclear Research, Świerk, Otwock, Poland.
[32] Borysiewicz M (1978), Solution to the critical problem for the neutron transport equation; Transport Theory and Statistical Physics, 7(4), 139-160
[33] Borysiewicz M, Mika J( 1969) Time behaviour of thermal neutrons in moderating media, Journal of Mathematical Analysis and Applications 26 (pp. 461.
[34] Borysiewicz M, Mika J( 1972) Existence and uniqueness of the solution to the critical problem in the multigroup neutron-transport theory; Transport Theory and Statistical Physics, 2(3), 243-270,
[35] Fynn Scheben (2011). Iterative Methods for Criticality Computations in Neutron Transport Theory, University of Bath, Department of Mathematical Sciences.

[36] Faisal A. Al-Malki, et. al., Numerical Techniques for the Neutron Diffusion Equations in the Nuclear Reactors, Adv. Studies Theor. Phys., Vol. 6, 2012, no. 14, 649 – 664.
[37] Jaakko Leppänen, Serpent Monte Carlo Neutron Transport Code, UC Berkeley, April 30, 2012.
[38] T. Kozlowski (KTH), Features and Limitations of nodal core simulator codes, NRS HOT presentation.
[39] T. Šmuc et. al., Demonstration of the Compact Depletion Models for Burnup Calculations, Rudjer Bošković Institute, Interfaculty Reactor Institute (IRI) Delft Univeristy of Tehnology.
[40] Blomquist R. N. Status of the VIM Monte Carlo neutron/photon transport code. In Proceedings of the 12th Biennial RPSD Topical Meeting, April 14-18, 2002. Santa Fe, NM.
[41] Both JP, Derriennic H, Morillon B, Nimal JC (1994) A Survey of TRIPOLI-4, Proceedings of the 8th International Conference on Radiation Shielding, Arlington, Texas, USA, 24-28 April 1994, pp. 373-380
[42] Sigmund P (1969) Theory of sputtering. I. Sputtering yield of amorphous and polycrystalline targets. Phys Rev 184:383 Smith HP, Wagner JC (2005) A case study in manual and automated Monte Carlo variance reduction with a deep penetration reactor shielding problem. Nucl Sci Eng 149:23
[43] Smith HP, Wagner JC (2005) A case study in manual and automated Monte Carlo variance reduction with a deep penetration reactor shielding problem. Nucl Sci Eng 149:23
[44] Turner SA, Larsen EW (1997) Automatic variance reduction for 3-D Monte Carlo simulations by the local importance function transform - Part I: Analysis. Nucl Sci Eng 127:22; Part II: Numerical results. Nucl Sci Eng 127:36
[45] Larsen EW, Yang J (2008) A “functional Monte Carlo” method for k-eigenvalue problems. Nucl Sci Eng 159:107
[46] Wolters ER, Larsen EW, Martin WR (2009) A hybrid Monte Carlo-S2 method for preserving neutron transport effects. In: Proceedings of the 2009 international conference on advances in mathematics, computational methods, and reactor physics, Saratoga Springs, New York, 3-7 May 2009

# CHAPTER 4

# Real-time on-line decision support systems for nuclear emergencies

Mieczysław Borysiewicz, Sławomir Potempski, Henryk Wojciechowicz,
Anna Wawrzyńczak, Piotr Kopka
National Centre for Nuclear Research (NCBJ)
Andrzeja Sołtana 7 Str., 05-400 Otwock, Poland
mieczyslaw.borysiewicz@ncbj.gov.pl

## Introduction

The Chernobyl accident had a profound effect on emergency preparedness and post-accident management worldwide and, in particular, in Europe. Deficiencies in arrangements dealing with an accident of this magnitude at both national and international levels (e.g., in world food trade) led to many problems of a practical and political nature. Many lessons have been learnt, and considerable resources have since been committed, to improve emergency preparedness and post-accident management in order to avoid similar problems in future. Improvements have been made at national, regional and international levels and have been diverse in nature. However, more needs to be done to ensure a timely and effective response to any future accident.

Emergency management, more generally, has received increased attention following the tragic events in the U.S. in September 2001. The Fukushima Daichi disaster after the earthquake and following tsunami in 2011 has shown that there is still room for improvement.

A number of requirements emerge from these considerations; they include:

- the need for a more coherent and harmonized response in Europe and during different stages of an accident (in particular, to limit the loss of public confidence in the measures taken by the authorities for their protection);
- exchanges of information and data in an emergency so as to enable neighbouring countries to take more timely and effective action; and
- the necessity to make better use of limited technical resources and avoid duplication.

The RODOS project was established to respond to these needs. It was launched in 1989 and increased in size through the European Commission's 3rd,

4th, 5th and 6th Framework Programmes. Significant additional funds have been provided by many national R&D programs, research institutions and industrial collaborators. In particular, the German Federal Ministry for the Environment, Nature Conservation and Nuclear Safety (BMU) contributed to the project financially with a special focus on early emergency response. Up to 40 institutes from some 20 countries in the European Union, Central and Eastern Europe and the Former Soviet Union were actively involved in the project [1].

As a result of these collaborative actions, a comprehensive decision support system (RODOS) has been developed which can be applied generally within and across Europe [2, 3]. It can be used in national or regional nuclear emergency centres, providing coherent support at all stages of an accident (i.e., before, during and after a release), including the long term management and restoration of contaminated areas. The system is able to support decisions about the introduction of a wide range of potentially useful countermeasures (e.g., sheltering and evacuation of people, distribution of iodine tablets, food restrictions, agricultural countermeasures, relocation, decontamination, restoration, etc.) mitigating the consequences of an accident with respect to health, the environment, and the economy. It can be applied to accidental releases into the atmosphere and into various aquatic environments. Appropriate interfaces exist with local and national radiological monitoring data, meteorological measurements and forecasts, and for adaptation to local, regional and national conditions in Europe.

The current version of the system (RODOS version PV 7.0) has been, or is being, installed in national emergency centres in several European countries for (pre-operational) use (Germany, Finland, Spain, Portugal, Austria, the Netherlands, Poland, Hungary, Slovakia, Ukraine, Slovenia, Bulgaria, Romania, Russia and the Czech Republic). Installation is foreseen or under consideration in Switzerland, Greece and for the second time Ukraine within the next few years. Installation in the CEE and FSU has been achieved with support from the European Commission's ECHO, PHARE and TACIS programs, respectively. Installation of the system for (pre-operational) use in many national emergency centres is indicative of the success of the system and its potential for achieving more coherent and effective responses to future accidents which may affect Europe.

The description of the RODOS system presented here is basically taken from the RODOS brochure and was possible due to courtesy of colleagues from the Karlsruhe Institute of Technology, Germany, in particular Dr Wolfgang Raskob, whom we acknowledge.

# 1. Structure and functions of the RODOS system

From the beginning, the RODOS system has been designed as a comprehensive system, that:

- incorporates state-of-the-art methods, models and data bases for assessing, presenting and evaluating the consequences of a nuclear accident,
- can be applied at all distances from the release site,
- takes account of the most important emergency actions and countermeasures,
- can be used from the moment that an accident threatens, through to long-term actions implemented months or years after an accident.
- provides information ranging from largely descriptive reports (Levels 0-2, see Table 4.1) to a detailed evaluation of the benefits and disadvantages of various strategies and their ranking according to the societal preferences expressed by the decision makers (Level 3, see Table 4.1).

Table 4.1 Levels of decision support systems.

| |
|---|
| Level 0: Acquisition and checking of radiological data and their presentation, directly or with minimal analysis, to decision makers, along with geographical and demographic information. |
| Level 1: Analysis and prediction of the current and future radiological situation (i.e. the distribution over space and time in the absence of countermeasures) based upon monitoring data, meteorological data and models, including information on the radioactive material released to the environment. |
| Level 2: Simulation of potential countermeasures (e.g. sheltering, evacuation, issue of iodine tablets, relocation, decontamination and food-bans, restoration), in particular, determination of their feasibility and quantification of their benefits and disadvantages. |
| Level 3: Evaluation and ranking of alternative strategies by balancing their respective benefits and disadvantages (i.e. costs, averted doses, reduction of stress and anxiety, socio-psychological aspects, political acceptability, etc.) taking account for judgements and preferences of decision makers. |

The system should be capable of coping with differences in site and source term characteristics, in the availability and quality of monitoring data, and in national regulations and emergency plans. In addition, the use of RODOS for

training and education in radiological protection and emergency management has been one of the major objectives from the beginning. Another important requirement was that the system uses meteorological and radiological monitoring data and field measurements to improve the accuracy of its simulations of atmospheric and hydrological dispersion and radio-ecological processes.

Due to the complex requirements on the RODOS system, during planning and development only minor benefit could be taken of the experience gained with existing systems. Therefore, from the beginning the iterative "prototyping" concept was pursued, which led step by step to the completion and continuous improvement of the system. However, the operational version RODOS PV 7.0 released end of 2010 has to be considered as the final release of the Linux based RODOS system. A further JAVA based RODOS system will be the basis for any further development of RODOS. The JRODOS called system is described in [13]. The computational kernel of both version is nearly identical, therefore the description presented is also valid for the JAVA based RODOS version.

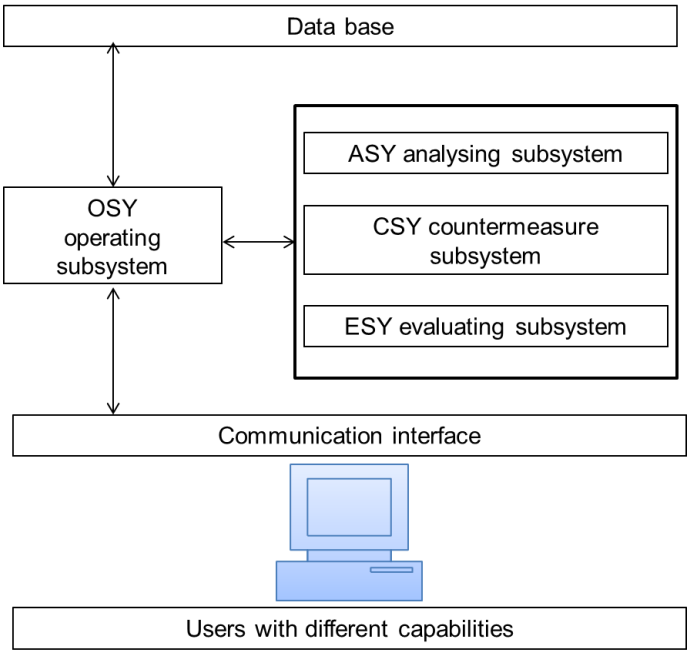


Figure 4.1 Conceptual structure of the RODOS system.

The basic concept and design of RODOS were specified and agreed upon by participants at the outset of the project. The conceptual RODOS architecture (see Figure 4.1) is split into three distinct subsystems, which are denoted by Analysing Subsystem, Countermeasure Subsystem and Evaluating Subsystem. Each subsystem consists of a variety of modules developed for processing data and calculating endpoints belonging to the corresponding level of information processing. The modules are fed with data stored in three different databases, comprising real-time data with information coming from regional or national radiological and meteorological data networks, geographical data defining the environmental conditions, and program data with results obtained and processed within the system. The interconnection of program modules, the input, transfer and exchange of data, the display of results, and the interactive and automatic modes of operation are all controlled by the specially designed RODOS Operating System.

The dialogue between RODOS and a user is organised in two different modes. In the so-called "automatic mode" the system automatically presents all information which is relevant to decision making and quantifiable in accordance with the current state of knowledge in the real cycle time. For this purpose, all the data entered into the system in the preceding cycle (either on-line or entered by the user) are taken into account in the current cycle. Interaction with the system is limited to a minimum amount of user input necessary to characterise the current situation and adapt models and data.

The diagnostic calculations are performed in the automatic mode with cycle times of 10 min. Prognostic calculations and simulations of emergency actions together with consequence assessments are repeated typically every 30 min. The automatic mode is limited to the near range around the nuclear facility, defined by an area of 160 km × 160 km; it is terminated after the cloud has left the calculation area and thus when “stable” conditions are reached (see Figure 4.2). Either in parallel to the automatic mode or alone, RODOS can be operated in the "interactive mode". In particular, all calculations at distances outside the 160 km × 160 km area are performed interactively.

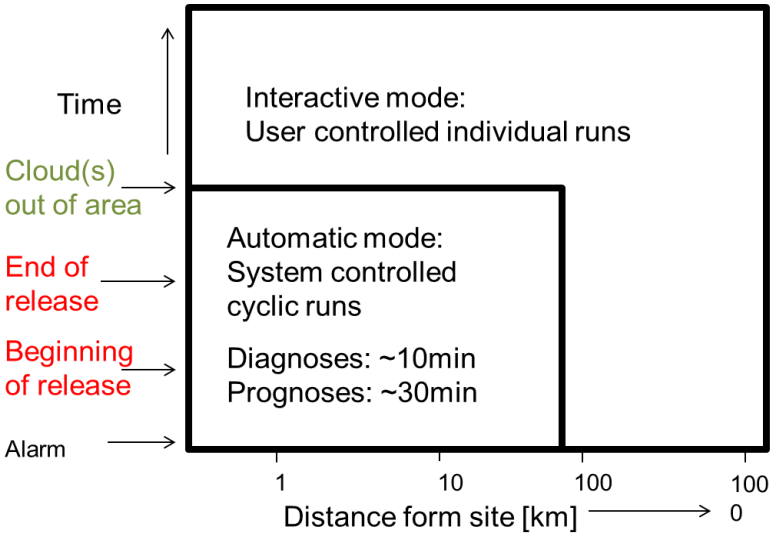


Figure 4.2 Operation of RODOS in different time scales and distances.

The dialogue between RODOS and a user is performed via various user-interfaces tailored to the needs and qualification of the user. The access rights of different user groups determine the type of user-interface, which allows increasing access to models, data and system parameters in a hierarchical structure. At the lowest level of access, there is an easily understood but very limited interface; at the highest, the full spectrum of interface tools is available for system administrators and operators familiar with the system's content and structure.

## 2. Interfaces to plant safety, radiological monitoring data and meteorological information

The RODOS system offers appropriate interfaces to plant safety, radiological and meteorological networks:

- flexible input of source term information,
- accident source term data base for nuclear power plants, such as PWRs, BWRs, VVER440 and VVER1000,
- radiological real-time data,
- stack emission data,
- local monitoring data,

- national monitoring data (incl. EURDEP, the European Data Exchange Platform),
- site meteorological data (multiple meteorological stations),
- meteorological forecasts of numerical weather models of national weather services,
- prognostic long range atmospheric dispersion calculations performed externally.

Parallel to the development of the RODOS system, prototype software tools have been developed within the STEPS/ASTRID and STERPS projects (Schulte et al., 2002) which, in the event of an emergency situation in a light water reactor, allow following up the progression of an accident from the moment it is detected, and to forecast the future behaviour of the reactor and potential releases. The source term, thus evaluated faster than in real time, can be used to predict with RODOS the potential and/or real radiological consequences. On the basis of the results of these prognostic calculations, decisions about precautionary emergency action can be initiated in a timely manner. Appropriate interfaces exist to directly transfer to the RODOS system the source term data estimated with the software packages mentioned above.

## 3. Diagnosis and prognosis of the radiological situation

RODOS provides continuously updated fast and comprehensive assessments of the radiation exposure of the population following accidental releases of radioactive material (or the threat of such a release) into the atmosphere and/or the aquatic environment. Calculations can be performed:

(1) either with the incoming on-line meteorological data and prognosticated meteorological fields,

(2) or with historic and/or user defined meteorological information.

The case (1) corresponds to the typical real-time operation of the system. In the automatic mode, diagnostic calculations can be performed without time limitations, the 30 min interval prognostic calculations extend over a time period of 24 hours. In the interactive mode, the time period of the prognostic calculations is limited by the duration of the available meteorological forecasts.

In the case (2), RODOS is used for calculating complete episodes of past or artificial accident situations with known information about meteorology and source term. These episodes can extend over a time period of up to 47 days. The

main purpose of this kind of application is to educate and train current and future RODOS operators and users and to support the preparation and performance of local, national, regional or international exercises.

The dispersion and deposition of material released into the atmosphere is predicted by means of a nested chain of models. The models consistently simulate dispersion and deposition processes over two distinct ranges, the local scale within an area of 160 km × 160 km, and the far range up to several thousands of kilometres. The models included in RODOS were selected from among the many models available as those best able to meet the operational demands of the system.

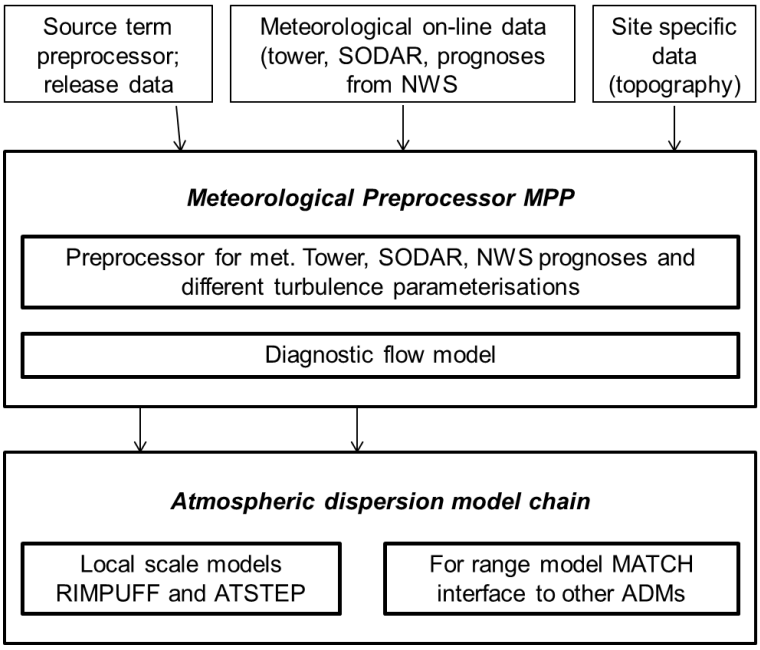


Figure 4.3 Local scale model chain and long range atmospheric dispersion model chain [2].

The local scale model chain comprises the local-scale Meteorological Pre-Processor MPP [3], the puff dispersion model RIMPUFF [2, 4] and the elongated puff model ATSTEP [2] (see Figure 4.3). MPP provides the local-scale system with actual and forecast local scale wind fields and local boundary layer variables by intensive pre-processing of the meteorological input data; if need be, a diagnostic flow model can be used. The state of the atmospheric turbulence can be characterised by different parameterisation schemes

(Karlsruhe-Jülich, Mol, German-French modelling [5]). Estimates of the current cloud position (diagnosis) are automatically updated every 10 minutes, the situation after cloud passage (prognosis) is recalculated typically every 30 minutes.

Weather data and forecasts are provided in real-time via on-line connections to local meteorological observations (from on-site meteorological towers or SODARs) or via network connections to national or international meteorological services (NWS). Prognoses of ground-level air, dry and wet deposited concentrations including dose rates in half hour steps can be produced on the local scale for the time period, for which forecasted meteorological data are available.

The applicability to farther distances is mainly a result of the integrated far range atmospheric dispersion model MATCH [6] with an interface for accessing meteorological data of the Danish forecast model HIRLAM [7]. Through its coupling to the near range model chain, a complete model chain is realised and consistent dispersion calculations are possible from the near range to large distances in the European scale. However, interfaces exist to other numerical weather prediction models, such as those from the German Weather Service (DWD) and the ALADIN model [8].

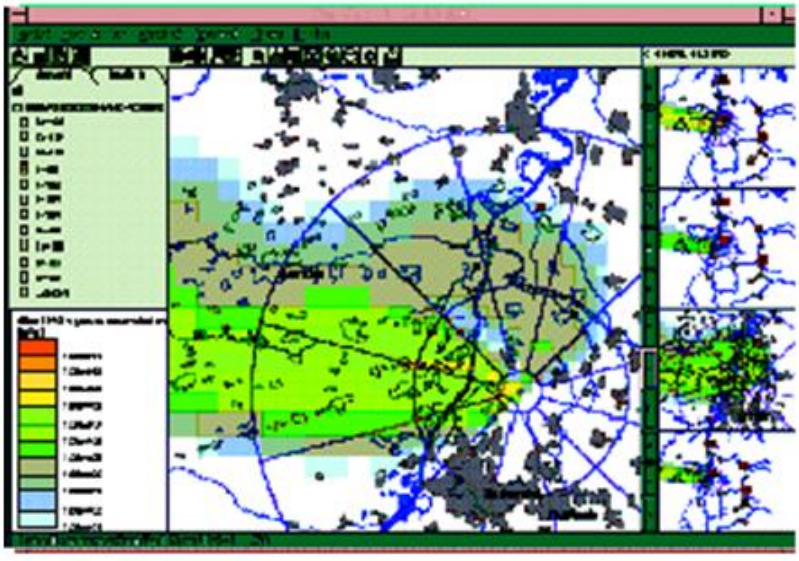

Figure 4.4 Example presentation of activity concentrations on ground surface.

The hydrological model chain in RODOS is comprehensive [9], covering the dispersion of material released into and through most aquatic environments (e.g., rivers, reservoirs, lakes, estuaries, coastal waters, seas, etc). In addition, transfer to various water bodies of material deposited from the atmosphere (e.g., by run-off from catchments) is modelled. Many models in the system have different levels of complexity and detail, thus enabling users to choose the most appropriate one, depending on the application and the desired output.

## 4. Exposure pathways and dose calculations

Exposures from all pathways of potential importance are assessed both during and after passage of a radioactive cloud (e.g., external irradiation from a radioactive cloud, external irradiation from material deposited on the ground and on the skin and clothing, and internal irradiation from the inhalation of airborne material and ingestion of contaminated food).

The transfer of radionuclides from the cloud to terrestrial foods as well as the resulting radiation exposure are modelled in the Terrestrial Food Chain and Dose Module, FDMT, which comprises the Food Chain Modules and the Dose Modules (see Figure 4.5). Activity concentrations on soil, plants and other surfaces as input to FDMT are calculated in the Deposition Module DepoM. Activity intake by animals is considered using season dependent feeding practices. The products considered in the Food Chain Module can be adapted to the specific situation in the different parts of Europe; the default list of products presently comprises 21 feedstuffs (17 based on plants, 4 based on animal products) and 33 foodstuffs (17 plant products, 16 animal products).

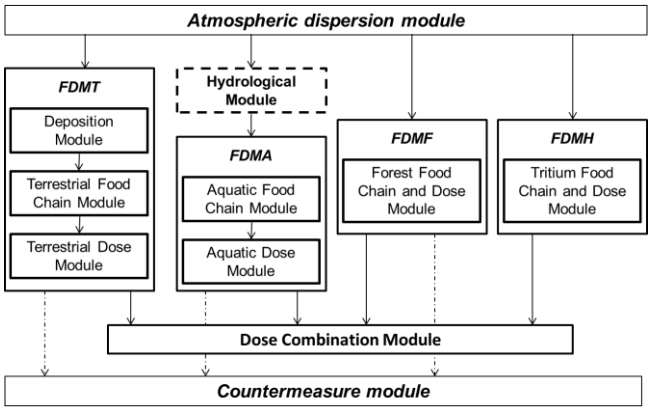


Figure 4.5 Food chain and dose modules integrated in RODOS [2].

The relatively large number of products results from the need to reflect properly the diversification of plant species in reality. The estimation of doses is performed via all external and internal exposure pathways of importance during and after the passage of the radioactive cloud; the endpoints are collective and individual organ doses for people of different ages.

## 5. Data assimilation

Another main focus of development was to implement data assimilation methods into the RODOS system. Data assimilation in general is the concept of combining measured data with model predictions for improving the diagnostic and prognostic results. The aim is to smoothly change from pure model output to a description of the radiological situation mainly based on monitoring data and measurements. Particularly, data assimilation is important for the food chain and dose modules of RODOS, since output of these modules is the main source of information for deciding on emergency actions and long-term countermeasures (see Figure 4.6).

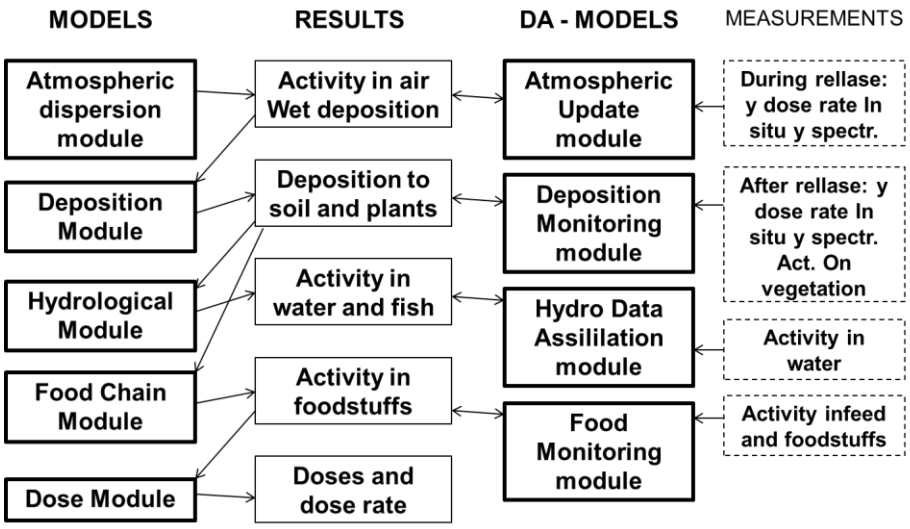


Figure 4.6 Data assimilation in RODOS [2].

Data assimilation methods, including uncertainty handling, have been developed which are ‘primed’ either with the concentrations in air or the depositions predicted by atmospheric dispersion models, or with food contamination from the food chain modules, and update their diagnoses and

prognoses as monitoring data (e.g. gamma dose rates, ground deposition or food contamination) arrive. The times after the cloud has passed are covered by techniques which allow estimates of contamination and of uncertainties to be made purely on the basis of databases of radiological monitoring data and measurements. Uncertainty handling and data assimilation have also been introduced in the river models to update the predictions of contamination downstream of measurements made upstream. Theoretical investigations exist for the other parts of the hydrological model chain.

Prototype real-time data assimilation modules have been introduced into RODOS version PV7.0 to improve the predictions for deposition onto different types of plants and for foodstuff contamination by assimilation of measurements.

## 6. Customisation

The transfer of radioactive material to food (both commercial and natural) and, subsequently, to man is modelled with seasonal variations (e.g., state of crop growth) taken into account; special tools allow topical databases to be used in emergencies, thus improving the predictive power of the models. Differences in agricultural practice and climatic and soil characteristics are considered by adapting the databases of the models applied to various regions in Europe. This makes RODOS a unique tool in a consistent approach to dose assessment on a multinational level. Comparable models are used to assess exposures from radioactive material in different aquatic environments (e.g., drinking water, crop irrigation, fish consumption, etc.). Estimates are made of exposures of individuals (with average and special habits) and the population as a whole.

As the models for food chain transfer have been originally developed for Central Europe, an important task in connection with the customisation of RODOS for use in other regions of Europe is the adaptation of the many model parameters in the food chain and dose module FDMT. The selection of appropriate radio-ecological regions, with relatively uniform radio-ecological conditions, is predominantly determined by prevailing agricultural production regimes, growing periods of plants, harvesting times, feeding regimes for domestic animals, human consumption habits, etc. Typically, a country is subdivided into 1 to 5 such radio-ecological regions. Radio-ecological regions have been defined for Czech Republic, Hungary, Poland, Romania, one part of Russia, Slovak Republic, and Ukraine and the collection of the radio-ecological data has been completed to a large degree.

For several regions in Northern and Eastern Europe or in parts of the Alps, an additional specialised radio-ecological model has been developed for semi-natural (forest) pathways, FDMF. It considers transfer of radionuclides to mushrooms, berries and game and quantifies the internal and external exposure from contaminated forests. After reviewing the present status of tritium modelling for emergency response purposes, a simple module describing the transfer of tritium through food-chains, FDMH, has also been developed. The dose combination module, DCM, combines results from these and the FDMT food chain and dose modules.

In case of Poland 7 radio-ecological regions for which the same set of model parameters can be used [11]. The selection of the radio-ecological regions to major extent follows agroclimate conditions and the long experience in Poland in collecting statistical agriculture data for those regions, taking also into account information from digital maps of soil.

The following works have been carried out in that area [11]:

- Identification of 7 radio-ecological regions (Figure 4.7, Table 4.2), based on agriculture, vegetation and intensive growth periods.
- Development of the algorithm for calculating radionuclide dependent and radionuclide independent data for different radio-ecological regions related to the different groups of plants.
- Development of databases containing:
  - plant production, vegetable production, fruit production, animal products;
  - detailed data on agriculture types of land use, various cultivated plant areas and plant production, cattle, animal production, building categories, pipelines for potable water use;
  - country averaged components of the human diet per day/ month/year and animal diet (cows, pigs, poultry );
  - leaf area index (LAI) as a function of vegetation period for various plants specific for Poland, representing different groups identified in FDMT.
- Making use of available measured data for the leaf area indices of grass, winter wheat, potatoes, beet experts of the Faculty of Plant Physiology of the Agriculture Academy in Warsaw developed functions presenting LAI vs. time, taking into account various vegetation cycles for 7 agroclimate regions of Poland, plant and soil library of properties.

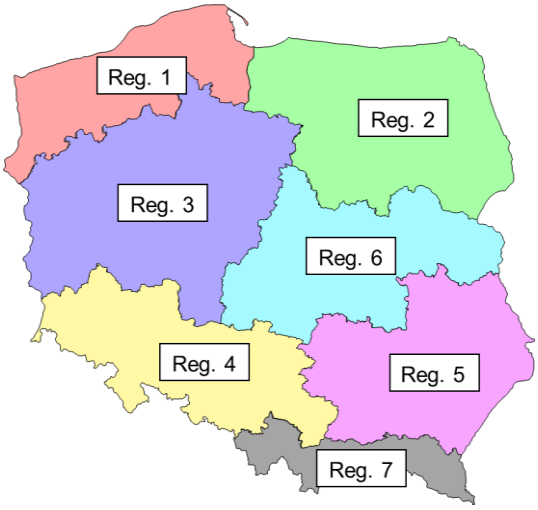


Figure 4.7 Radio-ecological regions in Poland.

Table 4.2 Simple characteristics of radio-ecological macro-regions in Poland.

| | Macro-regions | | | | | | |
|---|---|---|---|---|---|---|---|
| Parameter | 1 | 2 | 3 | 4 | 5 | 6 | 7 |
| Mean soil bonitation index | 0.80 | 0.68 | 0.84 | 0.83 | 0.91 | 0.67 | 0.88 |
| Mean annual precipitation [mm] | 540 | 572 | 500 | 566 | 550 | 515 | 620 |
| Mean annual temperature [°C] | 9.5 | 7.9 | 9.5 | 9.0 | 8.5 | 9.0 | 8.6 |
| Mean annual length of vegetation period [days] | 298 | 271 | 293 | 291 | 275 | 286 | 276 |

# 7. Extent and implications of emergency actions and countermeasures

The RODOS system, in a coherent and comprehensive approach, simulates and estimates the timing and the extent and duration of all countermeasures which can be implemented to limit the health and environment impact of an accident. Intervention strategies adopted in various European countries can be implemented. All information available about the types of intervention listed below have been integrated and synthesized in the corresponding models and the databases associated with them:

- sheltering,
- distribution of stable iodine tablets,
- evacuation,
- decontamination of inhabited areas,
- temporary and permanent relocation, plus these agricultural countermeasures:
- banning foods, which may imply food disposal or stopping food production,
- food processing and storage,
- changes in the feed composition of grazing animals; factors for evaluation include the effect of supplying clean feed for a certain period after deposition, changes in the proportion of contaminated feed in the diet, and the use of different feedstuffs,
- administration of sorbents or boluses,
- soil treatment, such as the addition of fertilizer,
- change of crop varieties or crop species grown,
- change in land use from agriculture to forestry,
- decontamination of agricultural land by plowing and soil removal.

The areas of early emergency actions and later countermeasures defined by intervention dose criteria can be modified by the user via the graphical user interface and fed back into the system for repeated calculations. This is of importance particularly in countries with regulations concerning the size or extension of areas in which measures are to be implemented. For example, prescribed emergency planning zones and sectors necessitate the projection of the areas defined by isolines onto these fixed geometric areas. The same holds for countries, where decisions on agricultural countermeasures would only be taken for areas defined by administrative borderlines (districts). Software tools for automatically presenting RODOS results for administrative units will be available in the next RODOS version.

Measures to reduce radioactivity concentrations in freshwater fish and drinking water are also analysed for situations when streams, rivers and lakes have been contaminated. Measures range from changing the sources of drinking water supply to processing fresh fish to applying fertilisers to lakes in order to reduce the uptake of radionuclides by fish feeding in these lakes.

The relative merits and disadvantages (e.g., avoidable doses, health risks, costs, effort) of individual or combinations of emergency action and countermeasure can be assessed (e.g., sheltering indoors and taking iodine tablets as against immediate evacuation) and presented to those responsible for emergency management. In particular, the doses that would potentially be received by workers implementing countermeasures can be assessed for decontamination in inhabited areas, relocation of the population and agricultural countermeasures.

In order to explore the effectiveness of combinations of agricultural countermeasures, selected combinations of two options can also be considered for each food; however, with the underlying constraint that the combination is broadly feasible. For decontamination, the effect on the extent and duration of relocation and the need for, and duration of, food restrictions can be considered. In the case of relocation, the implications of relocation on the further use of agricultural land in the relocated area can be studied.

For agricultural countermeasures, a ‘decision mode’ has been defined to provide information on a number of countermeasure options and combinations of these options for a single food to the evaluating subsystem of RODOS to enable countermeasure strategies to be evaluated using a wide range of information including effectiveness, costs, health effects and feasibility considerations.

A database of technical information on decontamination and agricultural measures has been compiled for use in RODOS within Europe based largely on experience following the Chernobyl reactor accident in the Ukraine and other experimental research. This allows information about the costs of implementation, the manpower resources needed, and the quantities of waste produced to be estimated as well as the effectiveness in reducing contamination levels in the environment and radiation doses to members of the population. Technical, logistic and radio-ecological information pertinent to the implementation of countermeasures in individual countries has been collected. This has made it possible to give constructive guidance in the use of the RODOS

database on countermeasure effectiveness and technical feasibility for specific areas of Europe.

## 8. Evaluation of countermeasure strategies

Whenever there is an option of two or more countermeasure strategies, a choice has to be made by the emergency management team. Evaluation techniques may support this task of the decision maker by proposing those courses and/or combinations of countermeasures, which are practicable under the actual or future conditions, and which are ranked by balancing of benefits and effort.

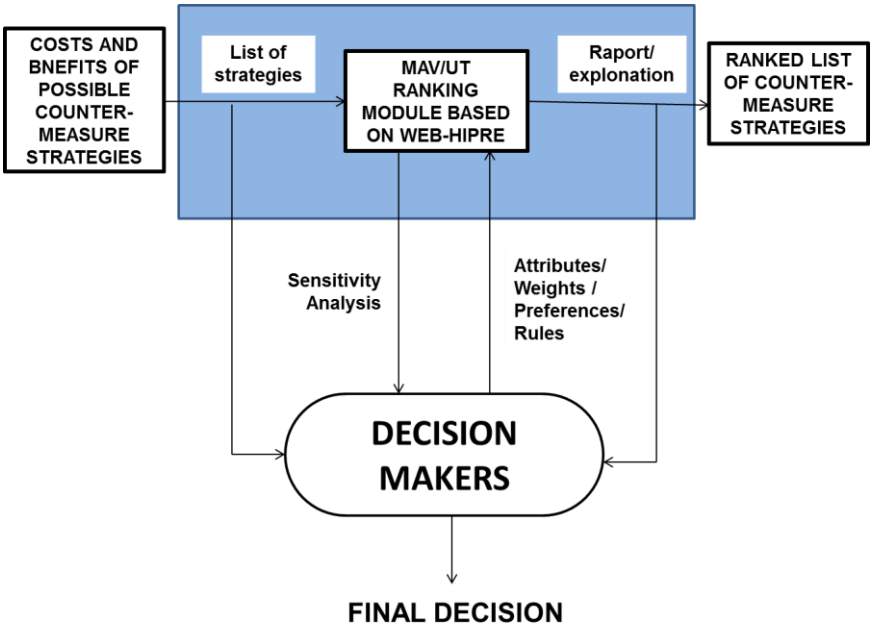


Figure 4.8 Evaluation of countermeasure strategies [2].

The MAV/UT-based software package, WebHipre [10], has been integrated in RODOS to enable users to compare and evaluate the benefits and drawbacks of different countermeasure strategies (e.g., risks, costs, feasibility, public acceptance, perceptions, social, psychological and political implications, and preferences or value concepts of decision-makers, etc). Rules, weights, and preference functions are encoded and applied to a list of alternative countermeasures providing a ranked shortlist to decision-makers together with

the rules and preferences which determined the order of the list. Intuitive justifications of choices and underlying uncertainties inherent in the predictions are also provided. The evaluation software assists users in modifying rules, weights, and preferences and other model parameters as well as exploring the consequences of each change. The importance of this exploration cannot be emphasized too strongly. Any decision support systems helps decision-makers not by making the decision itself, but by enhancing the decision-makers' understanding of the problem, the issues before them, and their value judgments. Because of this improved understanding, they are then better able to make decisions (see Figure 4.8).

More detailed information on the RODOS system, in particular Java version can be found in the special issue of Radioprotection [12].

## 9. Bayesian inference in stochastic event reconstruction in the case of the localization of the atmospheric contamination source

One of the most difficult problems in crisis management arises when there is not at all or only a little data on the source of the release available. Basing on the information coming from the monitoring network one must sometimes find a location of the release or estimate characteristics of the emission like the amount of radionuclides released. This is a typical the so-called inverse problem, which is ill posed, and therefore special techniques must be applied in order to solve it. For this purpose stochastic approach is often utilised as it in natural way, allows also for estimation of uncertainties. Basing on the measurements of the concentration of dangerous substance obtained from the network of sensors one can try to estimate the most probable location or values of parameters of the source of the release. Depending on the situation in which detected concentrations of the released material were found the problem can be considered at the continental, regional or local scale.

Given concentration measurements and knowledge of the wind field and other atmospheric air parameters, finding the location of the source and its parameters is ambiguous. The problem has no unique solution and can be considered in the probabilistic frameworks. In the case of gas dispersion, the unknowns to be determined are the gas source distribution of strengths and locations; given the measured gas concentrations at measurement locations for the associated wind field and other weather data (e.g. weather stability pattern). However, to create the model realistically reflecting the real situation based only

on a sparse point-concentration data is not trivial. This task requires specification of set of models' parameters, which depends on the applied model.

In general, aim is to find the source distribution that will generate predicted concentrations closest to those actually measured. To do this a dynamic data-driven event reconstruction model which couples data and predictive models through Bayesian inference to obtain solution to the inverse problem has to be developed. In this context the combination of Bayesian inference with stochastic sampling methodologies provides a powerful approach. Bayesian methods reformulate the event reconstruction problem into searching for a solution based on efficient sampling of an ensemble of simulations, guided by comparisons with data. This methodology provides probabilistic estimates, which in turn are used to produce a forward model, which is necessary to obtain data to compare with real observations.

A comprehensive literature review of past works on solutions of the inverse problem for atmospheric contaminant releases can be found in [13]. Ref. [14] implemented an algorithm based on integrating the adjoint of a linear dispersion model backward in time to solve a reconstruction problem. Refs. [15, 16] introduced dynamic Bayesian modeling, and the Markov chain Monte Carlo (MCMC); [17, 18] sampling approaches to reconstruct a contaminant source for synthetic data. In Refs. [19, 20] the authors used a sampling procedure with the Metropolis-Hastings algorithm to obtain the posterior distribution P(M|D) of the source term parameters given the concentration measurements at sensor locations. This way they completely replace the Bayesian formulation with a stochastic sampling procedure to explore the model parameters' space and to obtain a probability distribution for the source location.

### 9.1. Bayesian formulation

A good introduction to Bayesian theory can be found in [17]. Bayes' theorem, as applied to an emergency release reconstruction problem, can be stated as follows:

$$P(M \mid D) \propto P(D \mid M)P(M), \tag{4.1}$$

where $M$ represents possible model configurations or parameters and $D$ are observed data. For the event reconstruction problem, Bayes' theorem describes the conditional probability $P(M|D)$ of certain source parameters (model configuration $M$) given observed measurements of concentration at sensor locations ($D$). This conditional probability $P(M|D)$ is also known as the posterior

distribution and is related to the probability of the data conforming to a given model configuration *P(D|M)*, and to the possible model configurations *P(M)*, before taking into account the sensors' measurements. The probability *P(D|M)*, for fixed *D*, is called the likelihood function, while *P(M)* is the prior distribution [17].

Value of likelihood for a sample is computed by running a forward dispersion model with the given source parameters *M*. Then the model predicted concentrations *M* in the points of sensors location are compared with actual data *D*. The closer the predicted values are to the measured ones, the higher is the likelihood of the sampled source parameters. This function is taken as:

$$\ln[P(D \mid M)] = \ln[\lambda(M)] = \frac{\sum_{i=1}^{N} [\log(C_i^M) - \log(C_i^E)]^2}{2\sigma_{rel}^2}, \qquad (4.2)$$

where λ is the likelihood function, $C_i^M$ are the predicted by the forward model concentrations at the sensor locations *i*, $C_i^E$ are the sensor measurements, $\sigma^2_{rel}$ is the standard deviation of the combined forward model and measurement errors, *N* is the number of sensors.

The posterior probability distribution (4.1) is computed directly from the resulting samples defined by the algorithm described above and is estimated with:

$$P(M \mid D) \equiv \breve{\pi}^N(M) = \frac{1}{N} \sum_{i=1}^{N} \delta(M_i - M) \qquad (4.3)$$

which represents the probability of a particular model configuration *M* giving results that match the observations at sensors locations. Equation (4.3) is a sum over the entire samples set of length *N* of all the sampled values $M_i$. Thus $\delta(M_i - M) = 1$ when $M_i = M$ and 0 otherwise. In the case of MCMC parts interpretation is as follows: if a Markov chain spends several iterations at the same location value of *P(M/D)* increases through the summation (increasing the probability for those source parameters).

## 9.2. Example of the stochastic contaminant source localization procedure at local scale

The procedure of the contaminant source localization with use of the Bayesian approach will be presented based on the synthetic example. The stochastic models based on the MCMC sampling will be implemented to find the contamination source location based on the concentration of given substance registered by the 10 sensors distributed over 15 km × 15 km area during 1.5 h with 15 min time interval (Figure 4.9). The testing concentration data (Figure 4.9, right panel) were generated with use of the atmospheric dispersion second-order Closure Integrated PUFF Model (SCIPUFF) [21]. In this experiment the contamination source was located at $x$ = 2 km, $y$ = 5 km, $z$ = 50 m within the domain (Figure 4.9, left panel), the release was continuous with rate $q$ = 500 g/s and started one hour before first sensors measurements. The wind was directed along $x$ axis with speed 5 m/s.

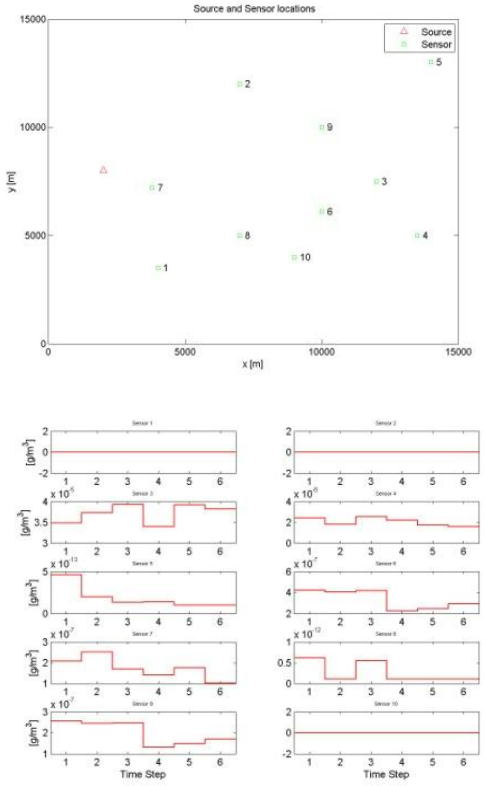


Figure 4.9 Top panel - the location of the stationary release source along with the 10 sensors. Botton panel - the synthetic concentration at the 10 sensor in 6 time step during 1.5 hour.

The effectiveness of different version of the MCMC algorithms and its modification to estimate the probabilistic distributions of atmospheric release parameters will be presented. The presented algorithms in different ways use the source location parameters probability distributions obtained based on the to date measurements to update the marginal probability distribution of considered parameters with use of the newly received information (subsequent measurements).

As the sampling procedure an MCMC with the Metropolis–Hastings algorithm will be used to obtain the posterior distribution $P(M|D)$ of the source term parameters given the concentration measurements at sensor locations [17, 18]. This way the Bayesian formulation was completely replaced with a stochastic sampling procedure to explore the model parameter space and to obtain a probability distribution for the source location and release rate. The Markov chains were initialized by taking samples from the prior distribution (in different ways presented below). To lower the computational cost, searching for the source coordinates was limited to the two dimensional space fixing the vertical position constant both for the source and sensors location at 50 m.

In the Bayesian inference approach to achieve rapid-response event reconstructions based on the successively arriving information about concentration of given substance registered by distributed sensor network a forward model is needed to calculate the concentration $C^M$ at the point of sensor locations for the tested set of model parameters at each Markov chain step (eq. 4.2). In emergency situations one have to face up during the dangerous substance releases from unknown source the time of response is crucial. Thus as the forward model the fast-running Gaussian plume dispersion model [11] was chosen. To summarize, in the presented example the scanned model parameter space is

$$M = (x, y, q, \zeta_1 \zeta_2) \tag{4.4}$$

where $x$ and $y$ are spatial location of the release, $q$ release rate and $\zeta_1$, $\zeta_2$ are stochastic terms in the turbulent diffusion parameterization.

It is assumed that the information from the sensors arrives subsequently every 15 minutes during 1.5 hour, i.e. in six time steps. However, searching for the source location ($x$, $y$), release rate ($q$) and model parameters $\zeta_1$, $\zeta_2$ starts after first concentrations' registration by sensors (based on the data in time $t$ = 1, see Figure 4.9 right panel). Thus, scanning algorithm was run with obtaining the first measurements from the sensors (Figure 4.9, right panel). Based on this

information one obtain the probability distributions of the searched parameters (6) starting from the randomly chosen set of parameters *M* (i.e. start from the 'flat' priori). In the subsequent time intervals (subsequent time steps) different version of MCMC algorithms that use (or not) the probability distributions obtained based on information from previous measurements as the priori distribution in (4.1) and update the marginal probability distribution with use of the newly arrived measurements were investigated. The resulting probability distribution was averaged over all time steps and all Markov chains.

To begin the iteration process forward dispersion calculation, from the initial location of the Markov chain, are performed to provide the initial data for comparison with observed data from the sensors. First the models parameters *M* (eq. 4.4) are chosen randomly with uniform distribution within interval [0.15 km] for *x* and *y*, [0.10000 g/s] for *q* and [0, 0.4] for $\zeta_1$, $\zeta_2$.

This assumption reflects lack of knowledge about the release, i.e. the flat prior *P(M)* in (4.1). The forward calculations are performed for the actual state of *M* and likelihood function $\lambda$ (eq. (4.2)) is calculated. Then random walk procedure "moving" Markov chain to the new position is applied.

Precisely, each model *M* parameter is changed by the value draw from the Gaussian distribution with the variance $\sigma_2^2$ equal 200 for *x* and *y*, 100 for *q* and 0.02 for $\zeta_1$, $\zeta_2$. Based on proposal state forward calculation the likelihood function $\lambda_{prop}$ is again estimated. Then comparison of this two values $\lambda$ and $\lambda_{prop}$ is performed:

$$\frac{\ln(\lambda_{prop})}{\ln(\lambda)} \geq RND(0,1) \ , \tag{4.5}$$

where $\lambda_{prop}$ is the likelihood value of the proposal state, $\lambda$ is the previous likelihood value, and RND(0, 1) is a random number generated from a uniform distribution in the interval (0, 1).

If the comparison is more favorable than the previous chain location, the proposal is accepted (Markov chain moves to the new location). If the comparison is 'worse', new state is not immediately rejected. Bernoulli random variable (a "coin flip") is used to decide whether or not to accept the new state of chain. This random component is important because it prevents the chain from becoming trapped in a local minimum.

The number of iteration $n$ for each Markov chain $n$ = 10000. This number was chosen based on the numerical experiments as the number of iteration needed to reach convergence for each sampled model parameters (6). Statistical convergence to the posterior distribution is monitored by computing between-chain variance and within-chain variance [19, 20].

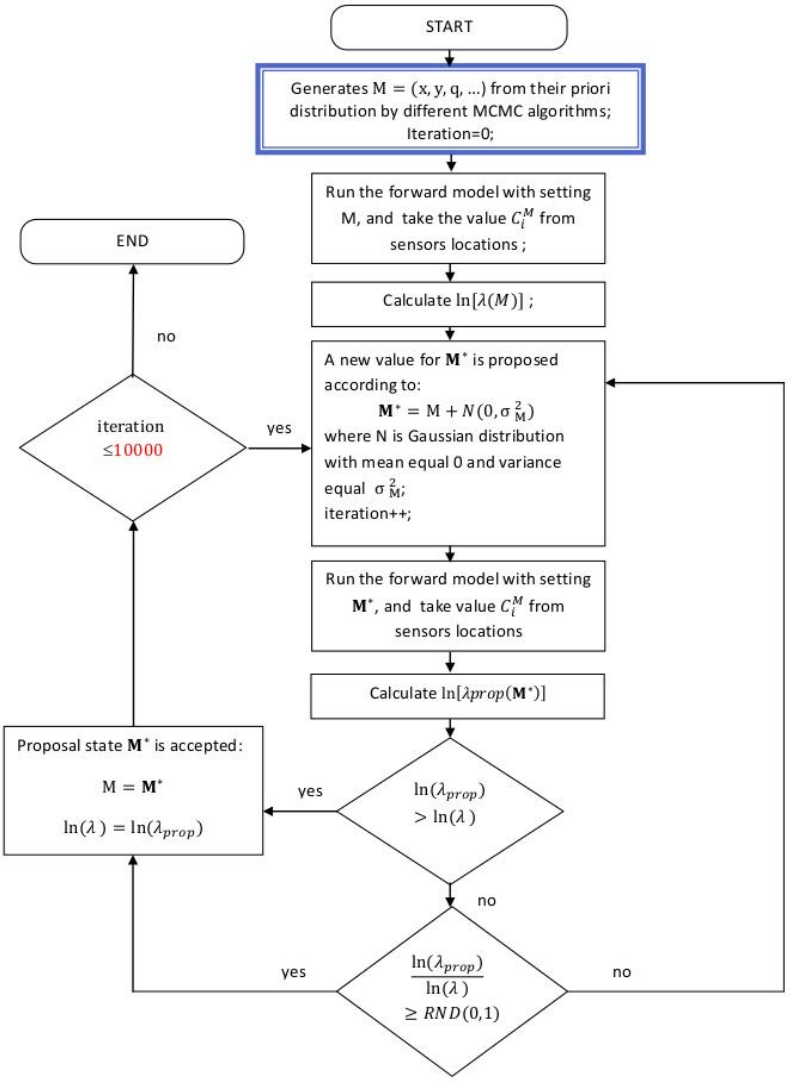


Figure 4.10 Block diagram of one time step of the algorithms.

The algorithm is presented in Figure 4.10. In this calculation 10 Markov chains in each time step were used. The traces of five independent Markov chains in the location space are presented in Figure 4.11, the source location is marked by triangle and the sensors by squares.

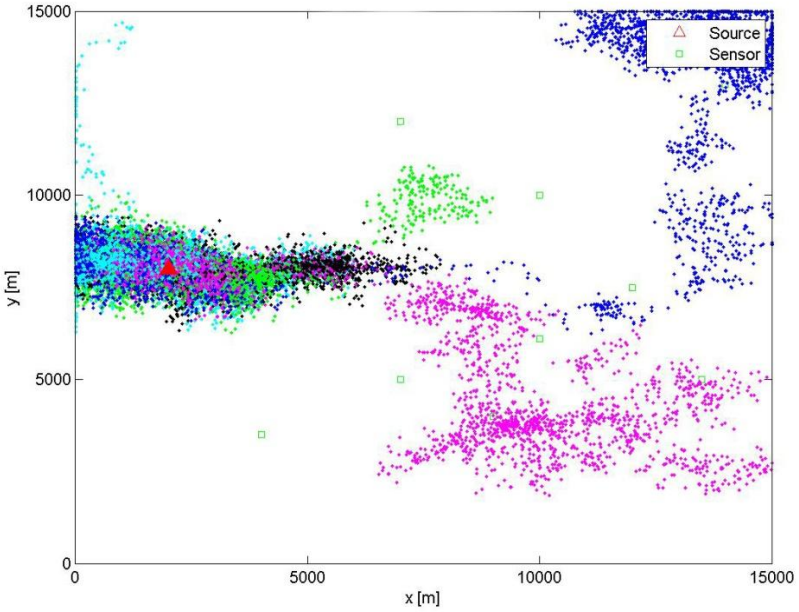


Figure 4.11 The traces of five Markov chains in the location space. The source location is marked by triangle and the sensors by squares. The samples came from results -Standard MCMC algorithm in time step $t$=1, first 5 chains.

The scanning algorithm can (or not) take the advantage from the MCMC realizations from previous time step in different ways. Each type of algorithms has unique properties that have an impact on various aspects of the reconstruction of events. In this paper are presented the following MCMC algorithms:

Standard MCMC

In this algorithm, the parameter space scan in each time step $t$ is independent form the previous ones. So, in this case we don't use information from past calculations.

MCMC Max Likelihood

This algorithm uses the results obtained in the previous time step to run calculation with use of the new measurements. As the first location of Markov chain is selected the set of $M$ parameters for which likelihood function in previous time step was the highest. So, for $t$>1:

$$M_0^t \sim = \underset{M \in \{M_0^{t-1}, \ldots M_n^{t-1}}{\arg\max} \ln[\lambda(M)] \tag{4.6}$$

With this approach, one always start with the best values of the model (previously found) and correct the result with new information from sensor.

MCMC via Rejuvenation and Extension

This algorithm as the first location of Markov chain $M_0^t$ at the time $t$ >1 chooses the set of parameters $M$ selected randomly from previous realization $t$-1 with use of the uniform distribution:

$$M_0^t \sim U(M_0^{t-1}, M_1^{t-1}, ..., M_n^{t-1}) \text{ a uniform distribution } \{1,\ldots,n\} \tag{4.7}$$

Applying the new knowledge (new measurements) the current chain is "extended" starting from selected position with use of the new data in the likelihood function calculation.

MCMC Standard

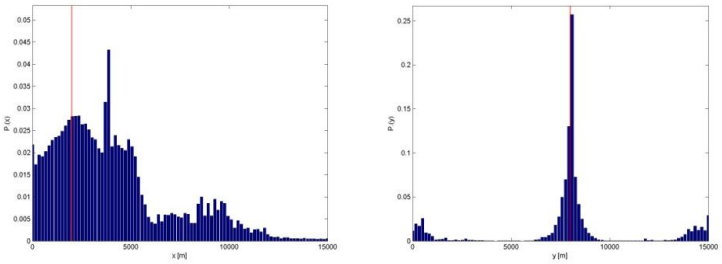

MCMC Max Likelihood

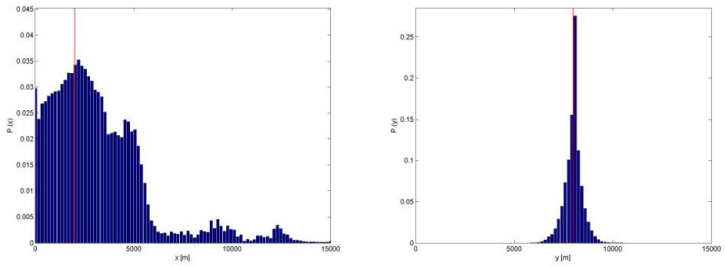


MCMC Rejuvenation and Extension

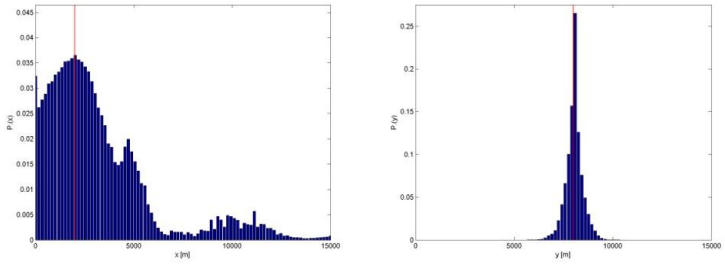


Figure 4.12 Posterior distribution as inferred by the Bayesian event reconstruction all applied algorithms for *x* and *y* parameters. Vertical lines represent the true values for *x* and *y* selected in creating the testing data.

Figures 4.12 and 4.13 present the results of calculation with use of all three above described MCMC algorithms. Presented marginal probability distributions were calculated based on the scanning algorithms results from all time steps and all Markov chains. Figure 4.13 shows the marginal probability distribution for *x* and *y* coordinates of source location within the considered domain. The exact location set up in creation of the testing data is marked by the vertical line. One can see that all algorithms found, with high probability, the contamination source location in the crosswind *y* direction. The high peek in the histogram is justified by the sensitivity of the used forward dispersion model to this parameter. Another situation is with the *x* coordinate of the source. The Standard MCMC algorithm do not show the right source *x* position, instead $x = 2000$ m it points out the $x \approx 4000$ m as the location with the highest probability. At the same time for the two another algorithms the synthetic true answer lies within a region of high posterior probability. It is worth to mention that these algorithms

(MCMC Max Likelihood, MCMC via Rejuvenation and Extension) use the probability distributions obtained based on information from previous measurements to update the distribution with use of the new data. This methodology is more effective in location the most probable value of considered parameters. On the other hand, Figure 4.13 shows that none of the methods found the correct release rate $q$. This is caused by the simplicity of the applied forward dispersion model and its relatively small sensitivity to this parameter within the searched interval.

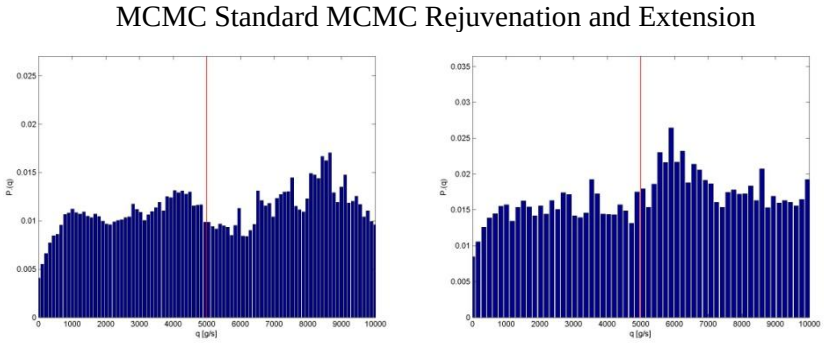


Figure 4.13 Posterior distribution as inferred by the Bayesian event reconstruction two applied algorithms for $q$ parameter. Vertical lines represent the true values for $q$ in creating the testing data.

The presented methodology allows reconstruction a source of contamination based on a set of measurements. The method combines Bayesian inference with Markov chain Monte Carlo sampling and produces posterior probability distributions of the parameters describing the unknown source. Developed dynamic data-driven event reconstruction model, which couples data and predictive models through Bayesian inference, successfully found the solution to the stated inverse problem i.e. having the downwind concentration measurement and knowledge of the wind field algorithm found the most probable location of the source both on the continental and local scale.

## Acknowledgments

The presented work was supported by the EU and MSHE grant no POIG.02.03.00-00-013/09.

## References


[1] E.-H. Schulte, G. N. Kelly, C. A. Jackson, Decision Support for Emergency Management and Environmental Restoration, European Commission, Luxemburg, Report EUR 19793, 2002

[2] J. Ehrhardt, A. Weis (eds), RODOS: Decision Support System for Off-site Nuclear Emer-gency Management in Europe. European Commission, Brussels, Report EUR 19144, 2000

[3] J. Ehrhardt, (ed.), Migration of RODOS to Practical Applicability, Forschungszentrum Karlsruhe, Report FZKA-7015, 2004

[4] Mikkelsen, T., Larsen, S. E., Thykier-Nielsen, S.: Description of the RISO Puff Model. Nuclear Technology 76(1984)56

[5] AtmosphärischeAusbreitungbeikerntechnischenNotfällen; Stellungnahme der Strahlen-schutzkommission, Berichte der SSK des Bundesministeriumsfür Umwelt, Naturschutz und Reaktorsicherheit, Heft Nr. 5 (1996), Gustav Fischer Verlag, Stuttgart, ISSN 0948-308X

[6] Langner, J., Persson, C. and Robertson, L. 1995. Concentration and deposition of acidifying air pollutants over Sweden: Estimates for 1991 based on the MATCH model and observations. Water Air and Soil Pollution 85, 2021-2026.

[7] Gustafsson, N. HIRLAM 2 Final Report. Norrköping, March 1993.

[8] http://www.cnrm.meteo.fr/aladin/scientific/scientif.html

[9] W. Raskob, R. Heling, M. Zheleznyak, Is There a Need for Hydrological Modelling in Decision Support Systems for Nuclear Emergencies? Rad. Prot. Dos., vol. 109, No. 1-2, p. 111, 2004

[10] R. P. Hämäläinen, J. Mustajoli, Web-HIPRE - Java-applet for Value Tree and AHP Analysis, Computer Software, System Analysis Laboratory, Helsinki University of Technology, Finland, http://www.hipre.hut.fi/WebHipre

[11] M. Borysiewicz, S. Potempski and R. Żelazny, Implementation of pre-operational version of RODOS System in the Center for Radiological Events of the National Atomic Energy Agency in Poland, J. of Technical Physics, vol. 43, no 2, 2002

[12] Enhancing nuclear and radiological emergency management and rehabilitation: Key Results of the EURANOS European Project, Radioprotection, vol. 45 - Issue 05, 2010

[13] Keats, A., E. Yee, and F.-S. Lien, (2007): Bayesian inference for source determination with applications to a complex urban environment. Atmos. Environ., 41, 465–479.

[14] Pudykiewicz, J. A., (1998): Application of adjoint tracer transport equations for evaluating source parameters. Atmos. Environ., 32, 3039–3050.
[15] Johannesson, G. et al., (2005): Sequential Monte-Carlo based framework for dynamic data-driven event reconstruction for atmospheric release., Proc. of the Joint Statistical Meeting, Minneapolis, MN, American Statistical Association and Cosponsors, 73–80.
[16] Johannesson, G., W. Hanley, and J. Nitao, 2004: Dynamic Bayesian models via Monte Carlo—An introduction with examples, Lawrence Livermore National Laboratory Tech. Rep. UCRL-TR-207173, 53
[17] Gilks, W., Richardson, S., Spiegelhalter, D. : Markov Chain Monte Carlo in Practice, 1996; Chapman & Hall/CRC.
[18] Gelman, A., J. Carlin, H. Stern, and D. Rubin, (2003): Bayesian Data Analysis. Chapman & Hall/CRC, 668 pp.
[19] Borysiewicz, M., Wawrzynczak A., KopkaP.Stochastic algorithm for estimation of the model's unknown parameters via Bayesian inference, Proceedings of the Federated Conference on Computer Science and nformation Systems; 2012; pp. 501-508.
[20] Borysiewicz, M., Wawrzynczak A., Kopka P. S Bayesian-Based Methods for the Estimation of the Unknown Model's Parameters in the Case of the Localization of the Atmospheric Contamination Source, Foundations of Computing and Decision Sciences; 2012; 37(4);pp.253-270.
[21] Sykes, R.I., S.F. Parker, D.S. Henn, C.P. Cerasoli and L.P. Santos, (1998). PC-SCIPUFF Version 1.2PD Technical Documentation. ARAP Report No. 718. Titan Corporation, Titan Research & Technology Division, ARAP Group, P.O. Box 2229, Princeton, NJ, 08543-2229.

# CHAPTER 5

# Applying IRIDM to the nuclear safety authority activities

Mieczysław Borysiewicz, Karol Kowal, Sławomir Potempski, Piotr Prusiński
National Centre for Nuclear Research (NCBJ)
Andrzeja Sołtana 7 Str., 05-400 Otwock, Poland
mieczyslaw.borysiewicz@ncbj.gov.pl

## Introduction

The primary issue of the modern nuclear power engineering is facing to ensure safety and security of the nuclear facilities and to convince people that the risks associated with this type of installations are much lower than the risks to life and health arising from everyday lives. Therefore, the main task when a nuclear power plant (NPP) is designed, operated or dismantled is to carry out its safety assessment. The results of such an analysis are then included into the Safety Assessment Report (SAR) for a specific plant or installation. For many years, the SARs were based on the Deterministic Safety Assessment (DSA) with use of results of experiments and conservative simulations, covering thermal-hydraulic issues, structure mechanics, neutron kinetics, and radiation protection. However, such reports should also contain both qualitative and quantitative risk assessment.

The risks, generated by the nuclear facilities, can be analyzed in details (both qualitatively and quantitatively) by making use of the PSA (Probabilistic Safety Assessment) methodology, including identification of possible initiating events leading to the potential accident, specification of expected accident scenarios as well as an estimation of their probability and consequences. The PSA methodology has been elaborated in the 70's [1] and it is being used and developed until now. Nowadays, there is a general consensus that PSA has reached the status of methodology mature enough to strongly influence the design and operation of NPPs as an approach complementary to the traditional DSA analysis. Moreover, the results from the PSA studies are considered next to the deterministic aspects as an essential element of the risk informed decision making process on the nuclear facilities [2].

In general, the risk informed decision making can be applied by all stakeholders involved in the nuclear industry, i.e. the NPP operators, nuclear

technology vendors and the regulatory body – nuclear safety authority established to enforce the nuclear law within the country. However, while the regulatory body shall be guided firstly by the public safety, commercial activity of the NPP operators and technology vendors is focused on the economic aspects. Consequently, when a non-routine decision on a nuclear facility needs to be made a number of qualitatively different aspects, corresponding to different types of risk must be taken into account in order to obtain a balanced solution. Thus, the risk should be interpreted not only in terms of the potential hazards, which poses some threats to the environment or people, but also in the context of decrease in production efficiency or financial losses, leading to the suspension of the activity. This is the reason why the risk informed decision making process in the nuclear industry should be an integrated one.

In this chapter the methodology of an Integrated Risk Informed Decision Making (IRIDM) is described according to the recent documents of the International Atomic Energy Agency (IAEA) and U.S. Nuclear Regulatory Commission (U.S. NRC). The main features of IRIDM are presented in the context of relationship between the major stakeholders of the nuclear industry and with relation to the public perception of risks associated with the nuclear facilities. The advantages and limitations of this approach are also emphasized. Finally, the major factors influencing a formal implementation of the IRIDM methodology within the regulatory organization are indicated and discussed.

## 1. Nuclear safety authority responsibilities and functions

The major regulatory body responsibilities and functions can be briefly described as the authorization, review and assessment, inspection and enforcement, development of regulations and guides. Authorisation means granting a written permission by the regulator for an operator (utility) to perform specific nuclear activities, based on the national legislations, which includes, for example, necessary licensing, certification and registration. After the authorisation process, the operator of the nuclear facility is continuously supervised by the regulatory body, which determines whether the operator's activity ensures that the facility complies, throughout its life cycle, with the safety objectives, safety principles and safety criteria approved by the national regulations. The regulatory body conducts these inspections to check independently and satisfy itself that the operator stays in compliance with the requirements set out in the authorization and regulations. If non-compliance with conditions of the authorization is demonstrated then the regulatory body applies appropriate sanctions against the operator, including cancelation of the licence for the nuclear activity [3].

The regulatory body is also authorised to grant a licence for a usage of specific technology within the country. Since the decisions on nuclear installations shall be always guided by the public safety, the choice of the technology is also based mainly on the safety criteria. Therefore, the technology vendors are interested to convince both the regulatory body and the investor that their technology is safe. Moreover, that their technology is safer than the others. For this purpose they have to prepare appropriate safety analyses demonstrating that the safety criteria given by the regulations are met (Figure 5.1).

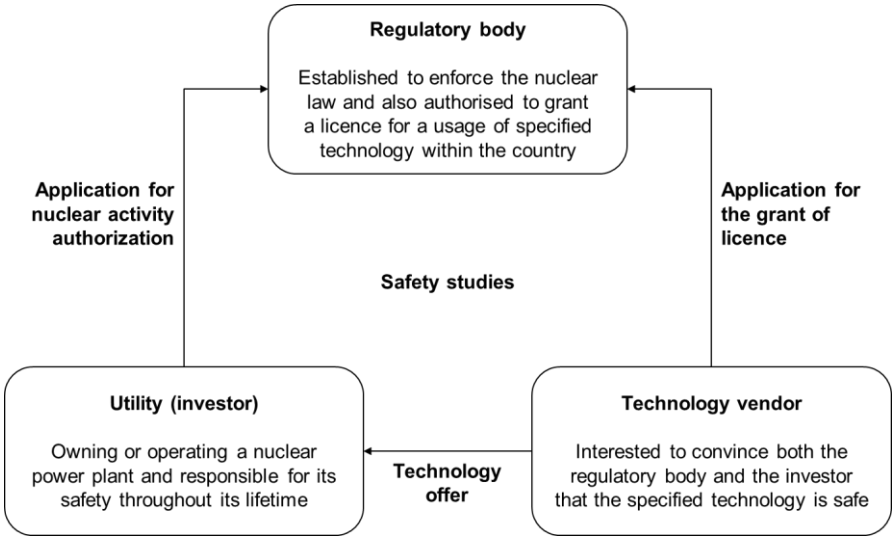


Figure 5.1 The major stakeholders of the nuclear industry and their relationships.

However, understanding the relationship between the major stakeholders of the nuclear industry, one can ask a question, how people can be sure that the results of safety studies presented by the vendor to the investor and to the regulatory body have been obtained in a right way. Since the results of the safety studies have an impact on the regulatory decisions, and the decisions have an impact on people safety, the regulatory body has to verify it. Although, the regulatory body usually has an internal group qualified to prepare some of the required safety analyses, it is a common practice to delegate the whole safety evaluation to the independent organization which, from now on, gains status of the Technical Support Organization (TSO).

However, in any case when the TSO performs safety studies on the request of the regulator, the final decision and ultimate responsibility always lies in the competences of the President of the regulatory organization. Thus, the regulatory

body never delegates its competences in the decision making on nuclear safety to any external organization including TSO.

The role of TSO can be played either by one or several institutions i.e. university laboratories, nuclear research centres and all other units qualified to perform regularly the comprehensive assessments of nuclear safety or even independent specialists in the relevant fields if necessary. Thus, the TSO model can be slightly different, depending on the country, while its main tasks in supporting the regulatory body usually stay the same all over the world. Besides of safety assessment, TSO can also assist in developing of nuclear regulations, conducting the technical inspections and, in case of an accident, it is expected to advice on the possible countermeasures [4].

All these activities are aimed to access and reduce the risk associated with the nuclear industry that focuses public attention all over the world. The main reason is that the long-term consequences of a nuclear accident can occur even far away from the location where it happened. Unfortunately, even meeting of all safety and security standards provided by national and international regulations does not reduce the risk to zero. Therefore, operation of nuclear facilities must ensure the probability of undesired consequences much lower than risks to life and health arising from everyday lives. Otherwise, it would not be accepted by the public opinion.

## 2. The nuclear risk perception and its acceptability

How people see risks and apply value judgments seems to be the most challenging factor of the decision making based on risk. The way we all treat risks depends on our perception of how they relate to us and the things we value. It has been found that there is a wide range of factors influencing this perception. Particularly important for man-made hazards are: how well the process (giving rise to the hazard) is understood, how equitably the danger is distributed and how good individuals can control their exposure and whether risk is assumed voluntarily. Many researchers argue that the concept of risk is strongly shaped by human minds and culture. It may include the prospect of physical harm and other factors, such as ethical and social considerations, and even the degree of trust in the ability of those creating the risk (or in the regulator) in ensuring that adequate preventive and protective measures are in place for controlling the risks. For many new hazards, high quality risk assessments by leaders in the field often fail to reassure people even using all available data and best science and technology. The other thing is that many of risk assessments cannot be

undertaken without making a number of assumptions such as the relative values of risks and benefits or even the scope of the study [5].

The studies have also show that hazards give rise to concerns which can be put into two broad categories: the individual and societal. The individual concerns relate to how individuals see the risk from a particular hazard affecting them and things they value personally. Individuals may be willing to live with a risk that they do not regard as negligible, if it secures them or society certain benefits, they would want such risks to be kept low and clearly controlled. Societal concerns cover the risks from hazards which impact on society and which, if realized, could have negative repercussions for the institutions responsible for putting in place the provisions and arrangements for protecting people, e.g. Parliament or the Government. This type of concern is often associated with hazards that give rise to risks which, were they to materialize, could provoke a socio-political response, e.g. risk of events causing widespread or large scale detriment or the occurrence of multiple fatalities in a single event. The typical example relates to the nuclear power generation.

In order to evaluate the risk associated with the nuclear power industry, one needs to express the definition of risk in more mathematical terms. The generally accepted definition of risk is described by the following equation:

$$R_i = P_i \cdot C_i , \tag{5.1}$$

where $R_i$ is the risk associated with an accident sequence $i$, while $P_i$ describes the probability of the sequence $i$ and $C_i$ specifies the magnitude of the consequences corresponding to its occurrence. However, when the consequences from an accident sequence $i$ can be specified by a continuum of outcomes between $x$ and $x + \Delta x$, the risk density $R_i(x)$ of magnitude $C_i(x)$ can be defined. In such a case usually more important becomes the risk of damages exceeding the acceptable magnitude $C_i(X)$. This is the complementary cumulative distribution function for accident sequence $i$:

$$R_i(\geq X) = P_i \sum_j \int_X^\infty C_{ij}(x) dx , \tag{5.2}$$

where $C_{ij}(x)$ includes a variety of predicted consequences of type $j$ caused by the event sequence $i$ [6].

## 3. Risk informed regulation of the nuclear facilities

Many regulatory bodies all over the world are currently revising their regulations according to the risk informed concept, where risk insights are considered together with other factors to establish requirements that focus licensee and regulatory attention on design and operational issues in a way that is commensurate with their importance to public health and safety. It may be useful to specify the way in which a regulatory body should carry out its activities. It is also believed that the use of risk insights can result in both improved safety and reduction of unnecessary regulatory burdens [2].

As an example, the risk informed process of the nuclear regulations improvement can be considered with accordance to the diagram depicted in Figure 5.2.

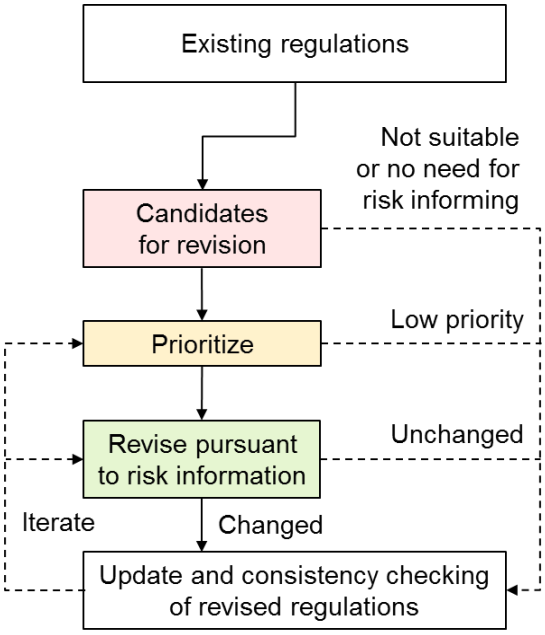


Figure 5.2 Risk informed process of improvement of the nuclear regulations [cf. 2].

First, the existing regulations should be reviewed in the terms of possible changes potentially leading to the safety improvement. As a result the list of requirements, that are candidates to be modified, can be developed. From that list, those elements, for which the risk informed approach is suitable, should be

identified and prioritized according to the risk information. It means that the regulatory body can assess the importance of the proposed changes based on their impact for safety as well as time and resources needed for their full implementation. Different options for modification of particular requirement can be also considered and scored. The last step aims to verify whether the approved modification of specific requirement is not in contrary to the other regulations. Since this is the iterative process one can back to the previous steps and select another regulation to be checked for possible improvements.

However, to use risk insights in the decision making processes in an adequate manner, it is very important to establish a structural approach that integrates in a sound, transparent and justifiable manner all the elements needed. The real difficulties arise when trying to identify all the relevant safety contributors (inputs) and especially to assign the relative weight of each of them to decision making. Particular difficulties are experienced when determining the necessary quality of the IRIDM inputs and treating large uncertainties [2].

## 4. IRIDM – the structural approach to the decision making

According to the basic framework, describing the IRIDM process (Figure 5.3), the clear and unambiguous definition of issue to be resolved is crucial to identify which elements or information are relevant to make a decision. The issue characterization should provide additionally its necessity evidence as well as an impact on the facility operation and safety, which covers required design changes, security arrangements, organizational model, internal procedures, man-machine interactions and other factors, that potentially might be dependent on the decision making process.

After defining the problem, consideration must be given to the requirements of both regulatory body and licensee in order to draft a preliminary set of options, which potentially could solve the issue. However, to make the final decision and choose one from the preliminary set of options, specified inputs must be established, namely the standards and good practices, operating experience, deterministic and probabilistic considerations, organizational and security systems and other factors such as research or economic insights. Relative importance of each element depends upon the decision to be made and should be weighted either qualitatively or quantitatively. This process leads to evaluation and to reduction of the preliminary set of options. Finally one of them should be chosen, implemented and monitored. If the performance of just implemented decision is not satisfactory corrective actions should be undertaken and the list of options needs to be redefined.

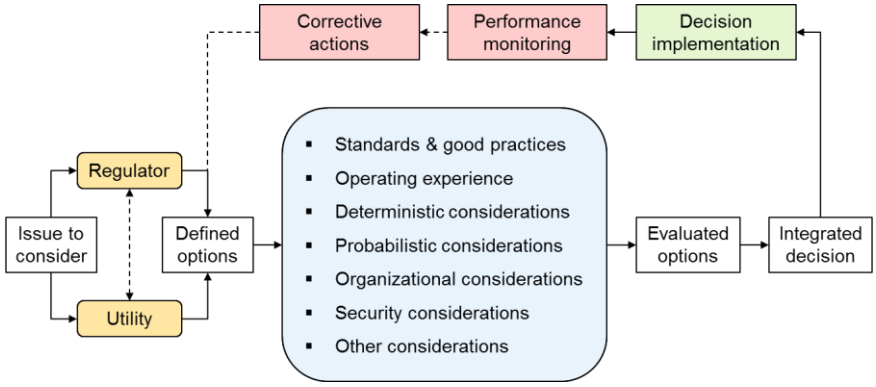


Figure 5.3 Basic framework and key elements of the IRIDM process [cf. 7].

The DSA principles, that underlie the safety design and operation of nuclear facilities, require firstly the definition of safety criteria to be meet, secondly the appropriate level of defence in depth (DID) to be guaranteed and finally large safety margins to be ensured.

The safety criteria mean a set of values, describing parameters and performance of the nuclear installations, in compliance with which its safety is justified e.g. maximum acceptable peak cladding temperature of the fuel rods. These requirements cover also the limits of the radiological doses, which cannot be exceeded [8].

The DID ensures that there are multiple safety systems and barriers to preventing core damage, containment failure and consequently release of radioactive material outside the plant. Therefore, the redundancy of safety systems must be guaranteed. It is also a good practice to use different physical processes in the alternative systems intended to perform certain safety function [9, 10].

Safety margins describe the difference between the limiting values of the parameters crucial for safety and their current values. However, the precise determination of safety margins is often very hard to obtain. It is because, in many cases, both the limiting values of the parameters and their current values are provided by computer simulations with some uncertainties. Thus, there are two ways to assess appropriate level of them. First one bases on conservatism in calculations. This approach is assumed to determine the safety margins much lower than they actually are which is not optimal from the economic point of view, because it needs some additional resources to balance the pessimistic

assumptions. Therefore, the second solution, leading to the best estimation of safety margins, is more and more commonly applied (Figure 5.4). This approach, based on realistic assumptions, is additionally supplemented by the uncertainty analysis. As a result the actual value of a particular parameter is estimated by the calculated one including the upper bound of its uncertainty [11].

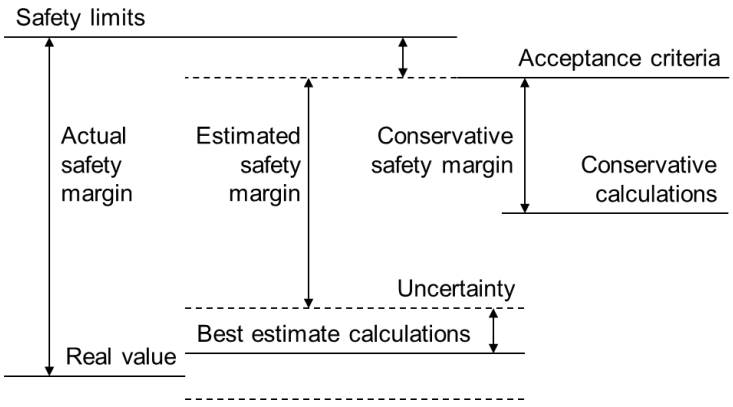


Figure 5.4 Different approaches to the assessment of safety margins [cf. 11].

Probabilistic analysis is intended to complement the DSA approach by identification of all contributions to the risk in an integrated model that otherwise may be overlooked. The outcomes from these considerations include both quantitative and qualitative insights to the IRIDM process. Probabilistic Safety Assessment is an essential element of IRIDM because it provides relevant information on all possible initiating events, internal hazards (including fires and floods), external hazards (including seismic events), system failures and human errors, that would potentially lead to a nuclear accident.

Various sequences of the accident progress can be identified by the PSA methods depending on the success or failure of the safety systems designed to prevent the accident or mitigate its consequences. These sequences are then depicted in a form of an event tree (Figure 5.5).

Since the reliability of particular safety systems can be obtained based on probabilities of basic equipment failures and human errors, the identified accident sequences can be evaluated quantitatively as well. In order to quantify the event tree, it is necessary to develop a fault tree for each relevant safety system, by identification of basic events, i.e. equipment failures and human

errors, and their relations. Moreover, the frequency of each basic event has to be assessed based on operational experience or external database. It makes this approach capable of calculating the frequency of each accident sequence, and especially those leading to the reactor core damage [12].

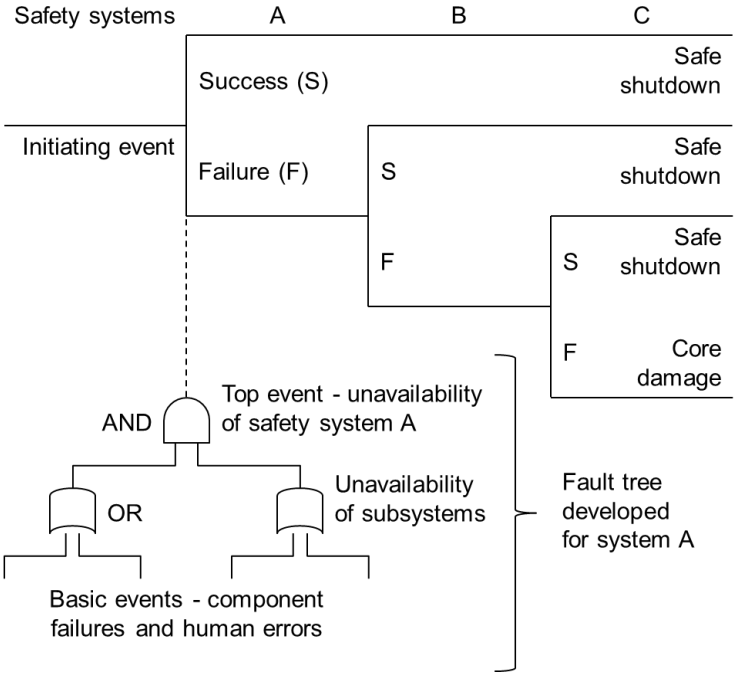


Figure 5.5 The event tree and fault tree construction.

After preparing the safety studies (including DSA and PSA analysis) appropriate integration of different IRIDM elements is needed. First of all, it must be demonstrated that the essential requirements are satisfied for each element separately. For that purpose an implementation of some additional safety measures could be required, but these improvements must not affect adversely the other IRIDM inputs. However, since all key elements of IRIDM are somehow depended on each other, the integration process should be an iterative one and consideration should be given to all inputs again after one of them has been changed. If the proposed improvements leading to meet one of the safety factors adversely affect at least one another, it is necessary to consider an implementation of alternative safety measures to ensure the acceptability of all relevant factors.

Figure 5.6 depicts the combination of the deterministic and probabilistic elements, which is only a part of the overall IRIDM integration process. The deterministic considerations answer question, if the safety systems are able to meet their design intent properly and if the other requirements like DID or safety margins are ensured. The PSA, instead, investigates all possible sources of equipment failures, human errors, as well as internal and external hazards, which could lead to unavailability of safety systems or breach of the safety barriers. There are also some interfaces between these two elements. It is enough to mention that deterministic calculations are used to specified the success criteria for each safety system, that are required as an input to the PSA analysis. These success criteria mean the minimum conditions, under which the designed safety system is recognized to be sufficient to perform its functions properly, even if there are some failures of its single components. Basing on these criteria, the total system unavailability or severely limitation of its functionality can be defined, which is crucial for system reliability assessment under accident conditions. On the other hand, the PSA considerations are able to indicate additional initiating events, which should be included into the deterministic studies.

Moreover, the PSA methodology is used in prioritising of the events in order to focus more intensively on those cases that are more probable. It is also applicable to define assumptions for the so-called risk informed best estimate deterministic calculations, which are more and more commonly applied instead of conservative ones. The DSA results are then compared with appropriate acceptance criteria given by the regulatory body, while the PSA insights are assessed in the context of risk minimization. Only when the requirements of both are satisfied the IRIDM option can be implemented.

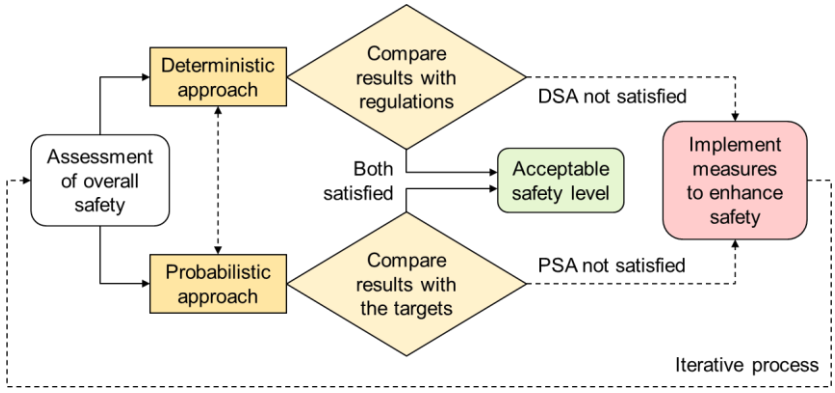


Figure 5.6 Integration of DSA approach and PSA insights [cf. 7].

Nevertheless, the major challenge of the integration process is to assess the relative importance of various qualitative and quantitative inputs, not only the DSA and PSA insights. It aims to determine the weights to be attributed to each of the inputs in the IRIDM process. However, the weighting scale for the inputs needs to be established first. The weighting scale describes the range of values for weighting factors assigned for particular types of risk. In practise there are two general ways for the factors assessment. Qualitative or quantitative approach can be applied to achieve it. The first one is to divide the inputs into three categories according to their significance for the considered issue: high, medium and low. The alternative way is to assign for each input $j$ the numerical value $w_j$ from 0 – negligible impact, up to 10 – the highest impact on the decision. During this process one needs to remember that the factors $w_j$ are to specify the relative importance of each input $j$ in relation to the others. Moreover, the weights assigning is quite subjective, based on the engineering judgment and dependent on the particular issue being addressed.

As a result of the weighting process the inputs can be ranked by their relative significance for the considered problem. Then one can determine the impact of the various IRIDM options on the particular inputs. Usually at the beginning the qualitative impact assessment is performed. It means each option needs to be analyzed in the context whether it has a positive or negative impact on each particular input. After that the score can be assigned for each option in the range of values from -10 (the highest negative impact) through 0 (no impact) up to 10 (the highest positive impact). It allows us to evaluate the option $i$ by the total weighted score ($S_i$) described by the following equation:

$$S_i = \sum_j w_j \cdot s_{ij} \,, \tag{5.3}$$

where $w_j$ is the weighting factor of the input $j$ and $s_{ij}$ is the impact of option $i$ on the input $j$ based on the scoring approach.

Consequently, all initially proposed options can be ranked by the $S_i$ factor and the best solution can be selected. The recommendation is given for that option which has the highest positive impact or, if all are negative, the lowest one.

Having selected option, final documentation of the IRIDM process and its results should be prepared. This documentation is essential for the IRIDM implementation while making it traceable and reproducible. On this basis, formal application for approval of the selected solution can be addressed to the

President of the regulatory body, which has the necessary authority to its acceptance, rejection or to request additional revisions.

While performing the safety analyses that significantly affect the decision-making process, one needs to remember about the uncertainties associated with such kind of studies. In the deterministic analyses based on computer simulations the sources of uncertainties are as follows: simplifications of the modelled geometry, lack of data from measurements and conservative assumptions [8]. Moreover, the numerical calculations itself are to obtain the approximate but never the exact values.

Another issue is the expected resolution of the results. The more complex geometry needs to be mapped in details, the lower scale of mesh elements is required, which leads to increase of the computational domain. This is because the appropriate calculations are performed for each element in the volume mesh of a higher density. It provides the higher resolution of the results, but also the high performance computing is needed, which implies additional limitations related to computation time and availability of hardware resources.

The uncertainty assessment is even more integrated with the PSA approach. It is because its methodology is used in modelling of such processes and phenomena, which can be described only statistically. Consequently, the initiating events, system failures and human errors, considered by the PSA studies, have an inherent random nature which implies the aleatory uncertainty in such kind of studies. This type of PSA uncertainty cannot be reduced neither by further studies nor even by enlarging of the data set.

Another type of the PSA uncertainties is the epistemic one that arises when making statistical inferences from the data, due to a lack of complete knowledge about systems, processes and modelled phenomena. In contrast to the aleatory uncertainties, the epistemic ones may be reduced over time, by additional measures, testing and analyses, leading to increase the data set and the knowledge. The identification, well understanding and appropriate consideration of this type of uncertainties are crucial for the comprehensiveness of PSA study and consequently for the overall IRIDM process [13, 14].

## 5. Implementation of IRIDM within the regulatory organization

The major factors influencing the implementation of the IRIDM methods within the specified organizational structure are as follows: relevant infrastructure, competence base and computational codes. Therefore the existing

organizational structure, employees' competencies, computational resources as well as the management system itself should be adjusted to carrying out the formal IRIDM process before its first implementation.

Since the organizational changes may cause many complex issues the detailed IRIDM implementation programme needs to be developed within the organization in order to resolve them all in the structured manner. The programme for the IRIDM implementation should indicate the potential fields of its applicability. It means that the range of issues should be defined by the regulatory body and shared between the stakeholders. Then one needs to provide and develop the whole infrastructure suitable to perform and review the analyses covering the specified IRIDM inputs. This infrastructure then should be capable to understand the conclusions from that process. It requires the identification of the expertise areas to be covered and the assessment tools to be provided.

Another important issue is the division of responsibilities regarding IRIDM between individuals within the organization. It is a common practice in the industries, where various risks for the public exist, to train a group of leaders responsible for different types of them. Moreover, there are also specialists for financial risk assessment, responsible for minimization of the financial losses or bankruptcy probability. Thus, the risks associated with the industry should be interpreted not only in terms of the potential hazards, which poses some threats to the environment or to the people, but also in the context of decrease in production efficiency or financial losses, leading to the suspension or even cessation of the activity. This is the reason why the risk informed decision making process in the industry as a whole should be an integrated one.

The same approach is applicable in the nuclear industry through the explicit IRIDM implementation. First, the special IRIDM team needs to be established within the organization. Since the IRIDM process covers a wide range of issues, from technical, through economic up to the psychological ones, it is essential for the team to be multidisciplinary, which means its members should be specialists in their fields. It is also a good practice to extend the team with external experts when the issue under consideration and options defined require a specific expertise.

Then the leaders, responsible for different IRIDM inputs, corresponding to various risks, should be selected from the team members. The leaders, however, are expected to be interdisciplinary, which means capable to understand and evaluate the significance of conclusions coming from different inputs, in the light of that type of risk, which has been assigned to them.

It is essential that the final decision maker in the organization performing the IRIDM (plant director, chairmen of regulatory authority, chief designer, etc.) is included in the IRIDM team in order to assure that the decision option identified in the IRIDM process will not be rejected at later stages on the basis of any additional considerations not taken into account by the IRIDM team [15].

To fulfil its mission, the team needs to be intensively trained, i.e. by implementing the IRIDM methodology into the real problems. However, while the understanding of the IRIDM principles is relatively simple, their practical application is usually very difficult. Therefore, besides of the general IRIDM training for the team as a whole, some specialised courses on various fields are necessary to be provided systematically for each group, according to its activity area within the team.

Moreover, the knowledge gained from the trainings and from experience as well should be documented in a form of guidelines describing the best practices for the IRIDM implementation. On that basis, some internal procedures and tools can be developed for the teamwork improvement. After that it is recommended to carry out the pilot project in order to test the IRIDM methodology, review the team capability and verify the guidance and procedures in a realistic, but small scale preliminary study.

## Conclusions

Making a complex decision should always be a structured process, not just an act, especially when it comes to the people safety. The risk management in the field of the nuclear industry is even more demanding due to the social concerns after such events like the Chernobyl and Fukushima accident. Therefore the decision making process on nuclear facilities and activities should be transparent and auditable. In order to meet this challenge the IRIDM methodology has been developed.

This approach to the decision making assumes an integration of qualitatively different inputs including deterministic and probabilistic insights as well as other aspects like economic factors and results of scientific research. Many advantages and benefits of the IRIDM process were indicated in this chapter e.g. complementary approach to the deterministic and probabilistic considerations, transparency, balance, logic and consistency of that approach. Implementation of IRIDM within the nuclear safety authority organization leads to improve the effectiveness, efficiency and realism in the decisions and practices increasing

public confidence and reducing unnecessary burden on the operators without compromising safety.

However, the integration process itself is usually quite subjective and based mainly on the engineering judgment. This is actually the main disadvantage of the overall IRIDM methodology that needs to be improved. Moreover, one needs to take into account the uncertainties associated with both the DSA and PSA calculations that may affect the decision making process. Practical implementation of the IRIDM methodology within the regulatory organization may be also limited by such aspects like unavailability of adequate codes and hardware resources. It seems, however, that the most difficult task is to build a suitable base of competence and create the multidisciplinary IRIDM team, qualified in a wide range of issues covering all aspects considered within the IRIDM process.

## Acknowledgements

The presented work was supported by the EU and MSHE grant no POIG.02.03.00-00-013/09.

## References

[1] U.S. Nuclear Regulatory Commission: *Reactor Safety Study - An assessment of accident risks in U. S. commercial nuclear power plants*. U.S. NRC, Washington D. C. 1975.
[2] International Atomic Energy Agency: *Risk informed regulation of nuclear facilities: Overview of the current status*. IAEA, Vienna 2005.
[3] International Atomic Energy Agency: *Training the staff of the regulatory body for nuclear facilities: A competency framework*. IAEA, Vienna 2001.
[4] Govaerts P.: *Roles, functions and value of TSOs*. Proceedings of an International Conference on Challenges Faced by Technical and Scientific Support Organizations in Enhancing Nuclear Safety, Aix-en-Provence 2007, pp. 49-54.
[5] Health and Safety Executive: *Reducing Risks, Protecting People: HSE's decision-making process*. HSE Books, Norwich 2001.
[6] Lee J.C., McCormick N.J.: *Risk and Safety Analysis of Nuclear Systems*. John Wiley & Sons Inc., Hoboken 2011.
[7] International Atomic Energy Agency: *A Framework for an Integrated Risk Informed Decision Making Process*. IAEA, Vienna 2011.
[8] International Atomic Energy Agency: *Deterministic Safety Analysis for Nuclear Power Plants*. IAEA, Vienna 2009.

[9] International Atomic Energy Agency: *Assessment of Defence in Depth for Nuclear Power Plants*. IAEA, Vienna 2005.
[10] International Atomic Energy Agency: *Defence in Depth in Nuclear Safety*. IAEA, Vienna 2005.
[11] International Atomic Energy Agency: *Safety Margins of Operating Reactors*. IAEA, Vienna 2003.
[12] International Atomic Energy Agency: *Development and Application of Level-1 PSA*. IAEA, Vienna 2010.
[13] Volkanovski A., Čepin M.: *Implication of PSA uncertainties on risk-informed decision making*. Nuclear Engineering and Design 241/2011, pp. 1108-1113.
[14] United States Nuclear Regulatory Commission: *Guidance on the Treatment of Uncertainties Associated with PRAs in Risk-Informed Decision Making*. US NRC, Washington 2009.
[15] Lyubarskiy A., Kuzmina I., El-Shanawany M.: *Advances in Risk Informed Decision Making – IAEA's Approach*. Proceedings of the Nordic PSA Conference, Gottröra 2011, pp. 1-14.

# CHAPTER 6

# Application of Mössbauer Spectroscopy to Study Metamict Minerals as Potential Forms for the Immobilization of High-Level Nuclear Waste

Dariusz Malczewski
University of Silesia, Faculty of Earth Sciences,
Będzińska 60 Str., 41-200 Sosnowiec, Poland,
dariusz.malczewski@us.edu.pl

Elżbieta Jartych
Lublin University of Technology, Faculty of Electrical Engineering and Computer Science, Nadbystrzycka 38A Str., 20-618 Lublin, Poland
e.jartych@pollub.pl

## 1. Introduction

The stabilization and immobilization of high-level nuclear waste (HLW) in a solid form is an important problem in the nuclear industry. In most cases, HLW is immobilized by homogeneously distributing it inside glass waste forms [1]. In potentially crystalline nuclear waste forms, such as oxides, silicates, and phosphates structures, radionuclides can occupy specific atomic positions within these periodic structures as dilute solid solutions. Some of the coordination polyhedra in each phase exhibit specific size, charge, and bonding characteristics, thereby making it possible to incorporate the radionuclides into the structures [2]. Metamict minerals are a class of natural amorphous materials that were initially crystalline [3]. These specific minerals contain radioactive elements that degrade their crystal structures. The metamictization (amorphization) process is primarily caused by progressive overlapping nuclear recoil collision cascades from the $\alpha$-decays of $^{238}U$, $^{232}Th$, $^{235}U$ and their daughter products. The average range of $\alpha$ particles that are emitted (4-8.8 MeV) is about 20 $\mu$m, whereas recoil lengths of the recoil nuclei (70-168 keV) ranges from 0.01 to 0.05 $\mu$m. In many cases, the metamictization process may be reversible under high temperature annealing in an inert atmosphere. Allanite $(Ca,REE)_2(Al,Fe^{3+})_3(SiO_4)_3(OH)$, gadolinite $REE_2Fe^{2+}Be_2Si_2O_{10}$, monazite $(Ce,La,Nd,Th)PO_4$, thorite $(Th,U)SiO_4$, titanite $(Ca,REE)TiSiO_4$ and zircon $(Zr,REE)SiO_4$, in which REE means rare earth elements, as well as yttrium, uranium and thorium, are good examples of such minerals. Because of the

natural occurrence of uranium and thorium in metamict minerals, they serve as natural analogs for radiation effects in high level nuclear waste over extremely long time periods ($10^8$-$10^9$ years). For example, because Pu can readily substitute for Zr in the zircon structure, zircon is a proposed host phase for plutonium and monazite, which is a suggested waste form for high-level nuclear waste [2]. The preferred potential actinide-bearing phases in a single or multiphase crystalline form are provided in Table 6.1.

Table 6.1 Potential actinide-bearing phases. In pyrochlore structure A - Na, Ca, U, Th, Y and REE; B - Nb, Ta, Ti, Zr, $Fe^{3+}$ [2].

| **Structure type** | **Composition** |
|---|---|
| **Oxides** | |
| Fluorite | $PuO_2$; $UO_2$ |
| Pyrochlore | $A_2B_2O_7$; $REE_2Ti_2O_7$; $CaPuTi_2O_7$ |
| Zirconolite | $CaZrTi_2O_7$ |
| Perovskite | $CaTiO_3$ |
| Zirconia; Ceria | $ZrO_2$; $CeO_2$ |
| **Silicates** | |
| Zircon | $ZrSiO_4$ |
| Titanite | $CaTi(SiO_4)O$ |
| **Phosphates** | |
| Monazite | $CePO_4$ |
| Apatite | $Ca_{4-x}REE_{6+x}(SiO_4)_{6-y}(PO_4)_yO_2$ |
| NZP | $NaZr_2(PO_4)_3$ |

The most important quantity that characterizes metamict minerals is the absorbed α-dose (α-events), *D*, as expressed in α-decay/mg or α-decay/g, which is given by the following expression:

$$D = 8 \cdot N_{238}\left[\exp\left(t\lambda_{238}\right)-1\right] + 7 \cdot N_{235}\left[\exp\left(t\lambda_{235}\right)-1\right] + 6 \cdot N_{232}\left[\exp\left(t\lambda_{232}\right)-1\right], \quad (6.1)$$

where $N_{238}$, $N_{235}$ and $N_{232}$ are the present number of atoms of $^{238}U$, $^{235}U$ and $^{232}Th$ per milligram, $\lambda_{238}$, $\lambda_{235}$ and $\lambda_{232}$ are the decay constants of $^{238}U$, $^{235}U$ and $^{232}Th$, and $t$ is the geologic age.

Most silicates, such as zircon and gadolinite, become metamict after a cumulative α-dose of about $10^{16}$α-decay/mg, whereas for metamict oxides, the amorphization dose is higher than $10^{17}$α-decay/mg [4, 5].

Many experimental techniques have been applied in order to characterize the amorphous state in metamict minerals, e.g., X-ray diffraction, EXAFS (extendent X-ray absorption fine structure), XANES (X-ray absorption near edge structure), DTA (differential thermal analysis), EPR (electron paramagnetic resonanse), HRTEM (high-resolution transmission electron microscopy), SEM-EDS (scanning electron microscopy-energy dispersive X-ray spectrometry), infrared spectroscopy, Raman spectroscopy and NMR (nuclear magnetic resonance). The purpose of the section is to present the recent research findings of representative metamict oxides (columbite, davidite and samarskite) and silicates (allanite, gadolinite and perrierite) using $^{57}Fe$ Mössbauer spectroscopy. In this case,$^{57}Fe$ Mössbauer spectroscopy is a probe of the local structure around the $Fe^{2+}$ and $Fe^{3+}$ positions, and indirectly provides information on the ordering of the adjacent polyhedra that are occupied by large cations such as U, Th and REE during the metamictization/recrystallization processes of the iron-bearing metamict phases that are examined.

Mössbauer spectroscopy is particularly useful technique for detecting small amounts of iron in materials due to the high resolution of this method. Because of its sensitivity to the nearest neighbor coordination and oxidation state of iron ions, Mössbauer spectroscopy is very well suited to studying the amorphous state of metamict phases and the transformation from a metamict state to the original crystalline state after high-temperature annealing. The Mössbauer spectrum is characterized by the hyperfine interactions parameters, i.e., the isomer shift, hyperfine magnetic field and quadrupole splitting (or shift). In a case in which the Mössbauer spectrum is a superposition of a few component subspectra, the relative contribution of the components can be estimated from the area of the spectral lines.

## 2. Basics of Mössbauer spectroscopy

In 1957 Rudolf L. Mössbauer, a German physicist, discovered the effect of recoilless emission and absorption of γ radiation by the nuclei in solids [6, 7]. He carried out experiments using the $^{191}Ir$ isotope, which emits γ quanta with energy

of 129 keV. The Mössbauer effect is based on the nuclear resonance. For typical nuclear transitions in Mössbauer spectroscopy with energy of about $10^4$-$10^5$ eV, the value of the recoil energy is of the order of $10^{-3}$-$10^{-2}$ eV, while the natural half width of the excited nuclear levels is about $10^{-9}$-$10^{-7}$ eV. For this reason, it is not possible to measure the resonance absorption for a free nucleus. The situation is different when a nucleus with its own atom is built into the crystalline lattice. During the emission of γ radiation, the recoil energy can be transferred for the creation of zero, one or more phonons. When the average value of recoil energy is comparable or lower than the energy of phonon excitation in the crystalline lattice, with the finite probability during emission and absorption of γ quanta, the recoil energy is taken over by the whole crystal. The process that has no creation of phonons but with a transfer of momentum into the crystal is called the recoilless emission and absorption of γ radiation, i.e., the Mössbauer effect.

The probability of the Mössbauer effect, *f*, i.e., the ratio of the recoilless photons that are emitted to the total number of photons, is determined as the Lamb-Mössbauer factor:

$$f = \exp(-k^2 < x^2 >), \tag{6.2}$$

where $k = 2\pi/\lambda$ and $<x^2>$ denotes the square average value of the amplitude of atom oscillations in the direction of the quantum momentum that is emitted. The value of the *f* factor strongly depends on the temperature and the energy of the transition of the nucleus from an excited to a ground state. Thus, the probability of the Mössbauer effect increases with a decrease in the measurement temperature and is larger for low energy transitions. The Mössbauer effect has been observed for many nuclides, i.e., for the isotopes of elements from periods 4, 5 and 6 of the table of elements and the majority of lanthanides and actinides. However, in the case of the value of the *f* factor, the most popular Mössbauer nuclides are $^{57}$Fe, $^{119}$Sn, $^{151}$Eu, $^{155}$Gd and $^{161}$Dy. The value of $f = 0.75$ for isotope $^{57}$Fe at room-temperature for energy E = 14.4 keV. Fortunately, the iron is prevalent in nature and materials, and in all of the samples that contain iron, the relative concentration of $^{57}$Fe isotope is equal to 2.17 %. In measurements, $^{57}$Co is used as the source of γ radiation. During electron capture, $^{57}$Co decays to $^{57}$Fe with a half-decay time of 270 days. A narrow emission line with energy of 14.4 keV that is used in measurements arises during the transition from an excited state with nuclear spin $I = 3/2$ to a ground state with $I = 1/2$.

The main idea of Mössbauer spectroscopy is the motion of the source (Figure 6.1). The movement of the source relative to the absorber (the

investigated sample) causes a change in the energy of γ quanta in accordance with the Doppler effect:

$$\Delta E = \frac{V}{c} E_{\gamma}, \tag{6.2}$$

where Eγ is the energy of the γ quantum and *V* denotes the velocity of the source relative to the absorber. For γ radiation with energy of 14.4 keV, the change of velocity by 1 mm/s causes a change of energy by 48 neV. This modulation allows the Mössbauer spectrum to be registered, i.e., the possible shifts and splittings of the absorption lines.

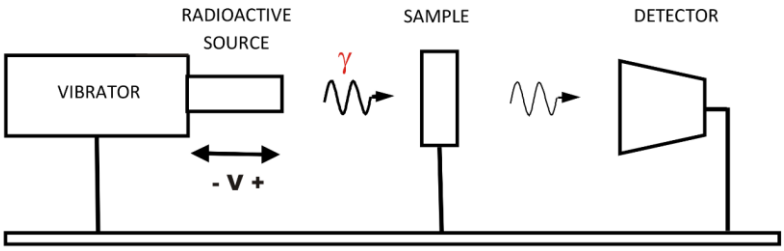


Figure 6.1 Schematic diagram of an experimental setup for Mössbauer spectroscopy in transmission geometry.

Two popular techniques are used to measure Mössbauer spectra. The first is transmission geometry in which the sample is placed between the mobile source and the detector. In this case, the absorber should be made of ten mg/cm$^2$ thick foil. The most effective technique for investigating thin and ultrathin films and surface layers of materials is Conversion Electron Mössbauer Spectroscopy – CEMS in which the sample is placed inside a conversion electrons counter that is filled with a calibration mixture of methane and helium. The sensitivity of Mössbauer spectroscopy is one of the highest in experimental physics. The uncertainty of the determination of energy for $^{57}$Fe is about $10^{-10}$ eV. The most important problem is to precisely determine the movement of the source with the constant acceleration. The range of the source motion that is selected is dependent on the composition of the material.

## 2.1. Hyperfine interactions

### Isomer shift

Mössbauer spectroscopy is a technique that can be used to investigate hyperfine interactions. These are interactions of the electromagnetic moments of the nuclear probe (i.e., $^{57}$Fe isotope) with the electric and magnetic fields that originate from its own electron shells as well as from the nearest neighborhood of the probe. The Hamiltonian of the hyperfine interactions consists of several components; three of them are the most important:

$$H = H_{E0} + H_{M1} + H_{E2} + .... \qquad (6.4)$$

The first term of the Hamiltonian, $H_{E0}$, describes the monopoly electrostatic interaction between the positive charge of the atomic nucleus and the *s*-type electrons. The shift of the nuclear levels occurs during the interaction. The energy of this shift is very small (of the order of $10^{-9}$ eV) and it is not possible to directly measure such a low value. However, changes in the energy of $\gamma$ radiation can be registered using a comparative method, i.e., a Mössbauer spectrometer with the accuracy of $10^{-10}$ eV, which acts as a calibration unit, can record the changes in energy during the transitions of the nucleus from an excited to a ground state in the absorber and source (Figure 6.2 a). In the Mössbauer spectrum, the absorption line is always shifted relative to the velocity $V = 0$ (Figure 6.2 b) because the nearest chemical neighborhood of the nuclear probe in the sample is different than that for the analogous nucleus in a standard source.

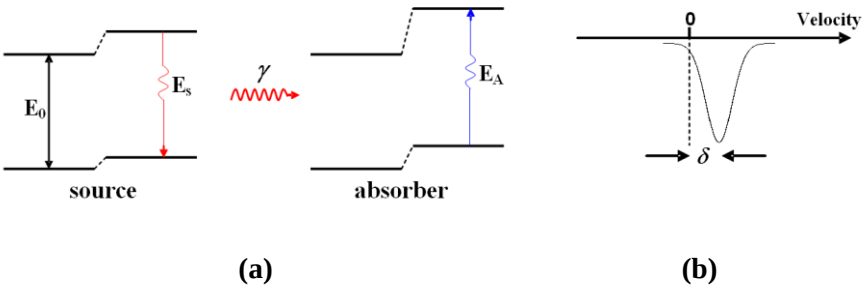


Figure 6.2 (a) Shift of the nuclear levels in the source and absorber. (b) Shift of the absorption line in an experimental Mössbauer spectrum.

The value of the shift, $\delta$, which is called the isomer shift (or chemical shift), is described by the formula:

$$\delta = E_A - E_s = \frac{2\pi}{5} Ze^2 \left[ \left|\Psi_A(0)\right|^2 - \left|\Psi_s(0)\right|^2 \right] \left( \langle R_{exc}^2 \rangle - \langle R_{ground}^2 \rangle \right), \quad (6.5)$$

where $Z$ denotes the atomic number, $e$ – the charge of the electron, $\left|\Psi_A(0)\right|^2$ and $\left|\Psi_s(0)\right|^2$ – the probability density of founding of the *s*-type electrons in the volume of the absorber nucleus and source nucleus, respectively, $\langle R_{exc}^2 \rangle$ and $\langle R_{ground}^2 \rangle$ – the average square radius of the nucleus in an excited and ground state, respectively. The term that is connected with the radii of the nucleus in both states is the constant value for the given isotope - for $^{57}$Fe it equals $14.3 \cdot 10^{-3}$ fm$^2$. The measured value of the isomer shift gives direct information about the density of the *s*-type electrons in the volume of the nucleus in the given chemical surrounding.

**Quadrupole splitting**

The second electric interaction, which is described by the third term of the Hamiltonian $H_{E2}$, is the interaction between the quadrupole electric moment of the nucleus and the electric field gradient that is generated by the surrounding electrons. During this interaction, the nuclear levels are split according to the rules of quantum mechanics. In the case of $^{57}$Fe, the ground state (spin $I$ = ½) is not split and the excited state, which has a spin $I$ = 3/2, is split into two sublevels, which are degenerated because of the magnetic quantum number $m_I$. Two transitions between the excited and ground state are possible according to the rules of choice $\Delta m_I$ = 0, ± 1 (Figure 6.3 a). The difference between the energy of these transitions, $\Delta E_Q$, that is called quadrupole splitting, is described by the formula:

$$\Delta E_Q = \frac{1}{2} e^2 q Q \left[ 1 + \frac{\eta^2}{3} \right]^{1/2}, \quad (6.6)$$

where $V_{zz} = eq$ denotes the „z" component of the diagonalized tensor of the electric field gradient, $eQ$ – the internal quadrupole moment of nucleus and the $\eta$ – asymmetry parameter, which is defined as:

$$\eta = \frac{V_{xx} - V_{yy}}{V_{zz}}, \tag{6.7}$$

where $V_{xx}$ and $V_{yy}$ are the „x" and „y" components of the electric field gradient. In an experimental Mössbauer spectrum, the absorption spectral line is split in two lines, i.e., a doublet (Figure 6.3 b).

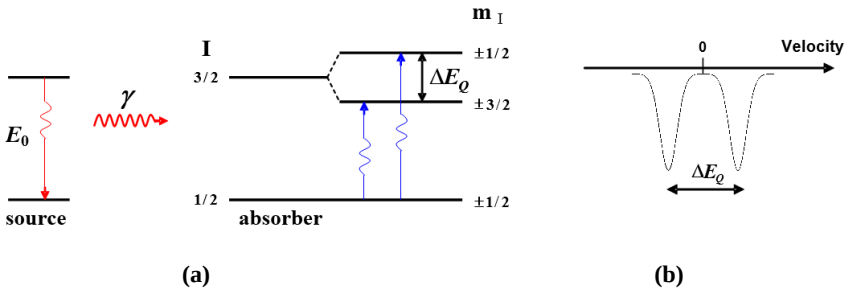


Figure 6.3 (a) The splitting of the nuclear levels of $^{57}$Fe for η = 1. (b) The splitting of the absorption line in an experimental Mössbauer spectrum.

It is worth emphasizing that in a case in which the magnetic interaction occurs in the material, the quadrupole interaction, which is called a quadrupole shift, can be treated as a small disturbance. In the samples with a cubic structure, the value of the quadrupole shift is practically zero for the nuclear probes that are placed in the lattice sites. However, most materials have no ideal structure and in strongly defected samples, the quadrupole splitting or quadrupole shift may reach high values. The measured value of the quadrupole splitting together with the known value of the quadrupole nuclear moment gives information about the $V_{zz}$ component of the electric field gradient and about the electron configuration of the surrounding ligands.

**Magnetic dipole interaction**

The next term of the Hamiltonian, $H_{M1}$, describes the interaction between the magnetic moment of the nucleus, $\vec{\mu}_I$, and the magnetic field inside the nucleus, $\vec{H}$, which is mainly produced by the *s*-type electrons. The explicit form of $H_{M1}$ describes the formula:

$$H_M = -\vec{\mu}_I \cdot \vec{H} = -g_N \mu_N \vec{I} \cdot \vec{H}, \tag{6.8}$$

where $g_N$ denotes the nuclear gyromagnetic coefficient, $\mu_N$ – the nuclear magneton and $\vec{I}$ – the nuclear spin. During the interaction of the nuclear magnetic moment with the internal magnetic field, the nuclear levels are split into $2I + 1$ sublevels, i.e., a nuclear Zeeman effect occurs (Figure 6.4). In the case of $^{57}$Fe the ground level is split into two sublevels within $\delta E_M$, while the excited level is split into four sublevels, which lie from each other by $\Delta E_M$. According to the rules of choice $\Delta m_I = 0, \pm 1$, six transitions are possible (Figure 6.4).

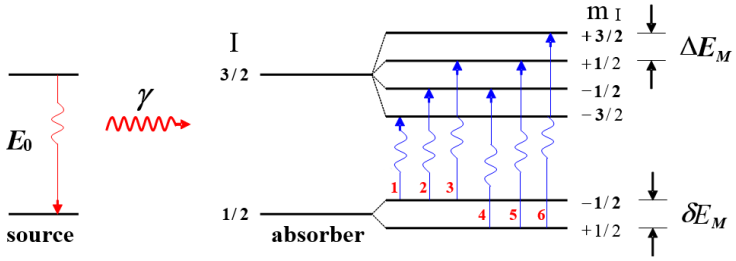


Figure 6.4 The hyperfine magnetic splitting of the nuclear ground and the excited levels of $^{57}$Fe.

In the Mössbauer spectrum a six-line pattern is observed in the case of the existence of magnetic interactions in the investigated sample (Figure 6.5). The distance between the most external spectral lines, i.e., 1 and 6, reflects the magnitude of the hyperfine magnetic field which is very sensitive to the changes in the local environment of the nuclear probe $^{57}$Fe. The values of the hyperfine magnetic field induction, $B_{hf}$, are of the order from tens to hundreds T; for pure iron $B_{hf} = 33$ T.

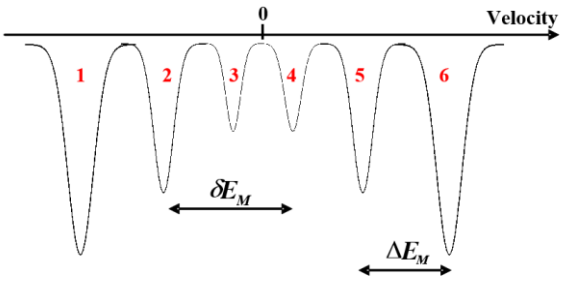


Figure 6.5 The shape of an experimental Mössbauer spectrum in the case of a hyperfine magnetic interaction in $^{57}$Fe.

In general, all of the interactions that are described above can occur simultaneously in the investigated material. The possible shifts and splitting of nuclear levels are reflected in the Mössbauer spectrum that is registered. The numerical fitting of the experimental spectrum together with the structural information, for example from the XRD patterns, allows the phase composition of the material to be recognized and its magnetic properties to be determined. The fitting procedure is performed until the best fitting parameter, Chisq ($\chi^2$), is achieved. The hyperfine interactions parameters that are determined from the spectra are as follows: *IS* – the *I*somer *S*hift relative to α-iron (*IS* = $\delta$), *QS* – the *Q*uadrupole *S*hift of the magnetically split spectra or the *Q*uadrupole *S*plitting of the paramagnetic doublet (*QS* = $\Delta E_Q$), $B_{hf}$ – hyperfine magnetic field, $\Gamma$– half width at half maximum of the spectral lines. All of the parameters are determined with an accuracy of about 0.01 mm $s^{-1}$, which translates into an accuracy of the determination of the hyperfine interaction energy of the order of $10^{-10}$ eV. The electric quadrupole interactions that arise from the interaction between the nuclear quadrupole moment and the electric field in which nuclei occur, produce characteristic quadrupole doublets in the Mössbauer spectra. For high-spin $^{57}$Fe ions, these doublets are usually characterized by large isomer shifts, which generally range from 0.7 to 1.40 mm/s with respect to the α-Fe foil. The doublets also have large quadrupole splitting values that range from 0.7 to 3.7 mm/s [8, 9]. The interaction of the electric field gradient with high-spin $Fe^{3+}$ ions in the octahedral positions is reflected in the Mössbauer spectrum by characteristic doublets that have relatively small isomer shifts (0.20 to 0.60 mm/s) and quadrupole splitting that averages from 0.20 to about 2.10 mm/s. Unlike $Fe^{2+}$, high quadrupole splitting for $Fe^{3+}$ ions imply an increasing distortion of the coordinated octahedral.

## 3. Results of $^{57}$Fe Mössbauer study of selected metamict minerals

The samples of metamict minerals were ground into powder and prepared in the shape of a thin disc absorber. The Mössbauer transmission spectra were recorded at room temperature (RT) using a constant acceleration spectrometer, a multichannel analyzer with 512 channels and a linear arrangement of a $^{57}$Co/Rh source (of 50 mCi activity) absorber and detector. All Mössbauer spectra were numerically analyzed using the Recoil fitting software and MEP. The X-ray powder diffraction (XRD) patterns were obtained using a PHILIPS X'Pert diffractometer in the $\Theta - 2\Theta$ system and Cu Kα radiation in scan mode with a step size of $0.02^{\circ}$.

## 3.1. Silicates

### Allanite

Allanite belongs to the epidote group (a type of sorosilicate) [5]. The epidote group can be represented by the ideal formula $A_2M_3Si_3O_{13}H$, where A indicates a large cation that has a high coordination number such as Ca, REE, U or Th, and the M sites are occupied by octahedrally coordinated trivalent and divalent cations such as $Al^{3+}$, $Fe^{3+}$, $Fe^{2+}$, $Mn^{3+}$ and $Mg^{2+}$ [10]. The structure of allanite contains chains of the edge-sharing $MO_6$ octahedra of two types, a single chain of M(2) octahedra that are completely occupied by $Al^{3+}$ and a multiple chain that is composed of a central M(1) (less distorted) and a lateral M(3) (more distorted) octahedra. Iron ions are unequally distributed between the M(1) and M(3) sites and 83% of the total Fe is in the M(3) site.

A sample of allanite from Reno (ALR) was collected in Washoe County, Nevada [11]. Crystal sections of the dimensions 0.3 to 2.5 cm were present in the rock matrix. The black crystals showed several good facies (Figure 6.6). A sample of allanite from Franklin (ALF) was collected in Sussex County, New Jersey [12]. Black aggregates of the dimensions 0.2 to 2.5 cm were scattered in a pale greenish microcline matrix with minor quartz (Figure 6.6). The basic characteristics of all samples are given in Table 6.2. The two allanite samples are good examples of the impact of an increasing absorbed $\alpha$-dose on hyperfine interactions parameters for the same mineral species.

Figure 6.6 (left) A sample of allanite from Reno – black fragments. (right) A sample of allanite from Franklin - black aggregates.

Table 6.2 Ages, Fe, Th and U concentrations and calculated α-doses of the allanite samples that are used.

| | ALR | ALF |
|---|---|---|
| Age (Ma) | 145-200 [a] | 986(4) [b] |
| Fe (wt%) | 11.90 | 13.43 |
| Th (ppm) | 3917 | 2245 |
| U (ppm) | 89 | 49 |
| Calculated total dose (α-decay/mg) | 5.8(8) x $10^{14}$ | 1.95(2) x $10^{15}$ |
| Calculated dose from $^{232}$Th (α-decay/mg) | 5.3(7) x $10^{14}$ | 1.77(1) x $10^{15}$ |

[a][11], [b][12].

The Mössbauer spectra of the allanite samples with the corresponding X-ray powder diffraction (XRD) patterns are shown in Figure 6.7. The hyperfine interactions parameters that were derived from the fitting procedure for each of the five samples are summarized in Table 6.3.

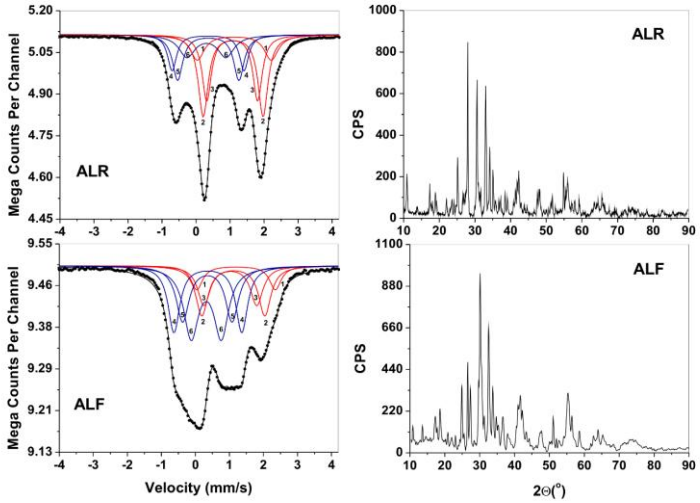


Figure 6.7 (left) $^{57}$Fe Mössbauer spectra at RT of the allanite samples. Solid dots – experimental data; solid line – fitted curve; red solid line – fitted $Fe^{2+}$ doublets; blue solid line – fitted $Fe^{3+}$ doublets. (right) XRD patterns.

Table 6.3 Hyperfine interactions parameters from the $^{57}$Fe Mössbauer spectra (Figure 6.7) for the allanite samples that were investigated. Isomer shift values *(IS)* are given relative to the α-Fe standard at RT.

| Sample | Doublet no. | $\chi^2$ | *IS* (mm/s) | *QS* (mm/s) | $\Gamma$ (mm/s) | Assignment (CN)* | Intensity (%) |
|---|---|---|---|---|---|---|---|
| ALR | | 1.5 | | | | | |
| | 1 | | 1.12 | 2.17 | 0.25 | $Fe^{2+}$ (6) M1 | 12 |
| | 2 | | 1.09 | 1.76 | 0.17 | $Fe^{2+}$ (6) M3 | 28 |
| | 3 | | 1.06 | 1.49 | 0.16 | $Fe^{2+}$ (6) M3 | 21 |
| | 4 | | 0.35 | 2.11 | 0.16 | $Fe^{3+}$ (6) M3 | 11 |
| | 5 | | 0.36 | 1.80 | 0.18 | $Fe^{3+}$ (6) M3 | 16 |
| | 6 | | 0.31 | 1.15 | 0.28 | $Fe^{3+}$ (6) M1 | 12 |
| ALF | | 1.4 | | | | | |
| | 1 | | 1.19 | 2.31 | 0.23 | $Fe^{2+}$ (6) M1 | 10 |
| | 2 | | 1.09 | 1.82 | 0.21 | $Fe^{2+}$ (6) M3 | 16 |
| | 3 | | 1.03 | 1.52 | 0.21 | $Fe^{2+}$ (6) M3 | 10 |
| | 4 | | 0.36 | 1.99 | 0.21 | $Fe^{3+}$ (6) M3 | 20 |
| | 5 | | 0.35 | 1.45 | 0.22 | $Fe^{3+}$ (6) M3 | 18 |
| | 6 | | 0.32 | 0.88 | 0.26 | $Fe^{3+}$ (6) M1 | 26 |

* CN - Coordination number.

As expected, the Mössbauer spectra of the allanites show doublets that represent $Fe^{2+}$ in the M(1) and M(3) octahedral sites. Ion $Fe^{2+}$ in the M(1) site is represented by doublet no. 1 in all of the spectra, as is labeled in Figure 6.7 and Table 6.3. Ion $Fe^{2+}$ in the M(3) site in the spectra of ALR and ALF, is represented by doublets 2 and 3 (Figure 6.7, Table 6.3). Doublet no. 3 which has lower IS and QS values, can be interpreted as representing the most distorted octahedra of the M(3) site, whereas doublet no. 2 represents the less distorted positions of $Fe^{2+}$ in the M(3) site [13]. These two samples differ markedly in the absorbed α-dose. The sample ALR is characterized by more than a three-fold lower absorbed α-dose than the sample ALF, which is reflected in both the Mössbauer spectra and corresponding XRD patterns (Figure 6.7). Figure 6.8 shows the weighted averages of the line widths and weighted averages of the quadrupole splittings all of the $Fe^{2+}$ components as a function of the α-dose. The average line widths (Figure 6.8a) and quadrupole splittings (Figure 6.8b) increase with the absorbed α-dose. The isomer shift values of $Fe^{2+}$ components do not show any noticeable changes. The average IS values range from 1.09(1) mm/s for the sample ALR to 1.10(1) mm/s for ALF [13].

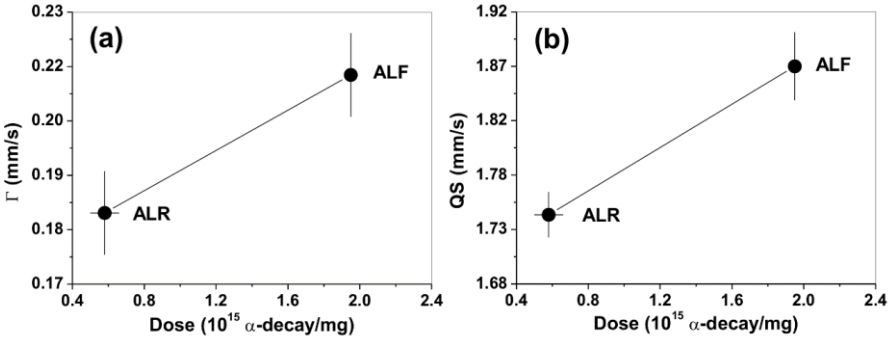


Figure 6.8 (a) Average line widths of the $Fe^{2+}$ doublets vs. the absorbed α-dose. (b) Average of the quadrupole splittings of the $Fe^{2+}$ doublets vs. the absorbed α-dose.

The weighted averages of the line widths of $Fe^{3+}$ components vs. the total α-dose are shown in Figure 6.9a. Similarly to the $Fe^{2+}$ components, the average line widths of the $Fe^{3+}$ doublets increased slightly with the absorbed α-dose.

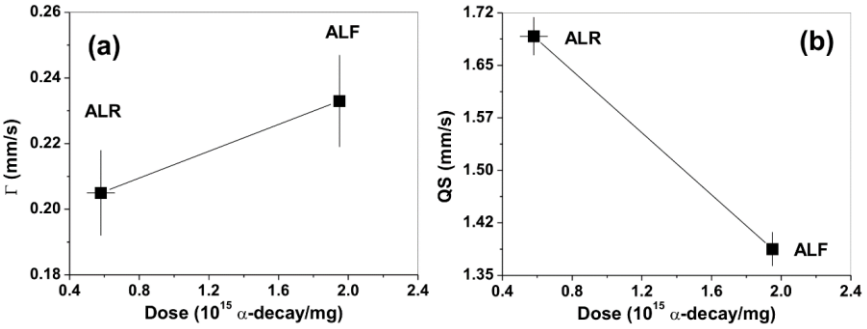


Figure 6.9 (a) Average line widths of the $Fe^{3+}$ doublets vs. the absorbed α-dose. (b) Average of the quadrupole splittings of the $Fe^{3+}$ doublets vs. the absorbed α-dose.

Figure 6.9b shows that the weighted averages of the quadrupole splittings for the $Fe^{3+}$ components decreased with the increasing absorbed α-dose.

## Perrierite

The group of perrierite-chevkinite minerals (sorosilicates) can be represented as $A_4BC_2Ti_2O_8(Si_2O_7)_2$ where A = REE, B = $Fe^{2+}$ and $Mg^{2+}$, and C = $Fe^{3+}$ and

$Al^{3+}$ [14]. Many substitutions are possible. The massive black mat perrierite was collected near Amherst, Bedford Co., Virginia (Figure 6.10).

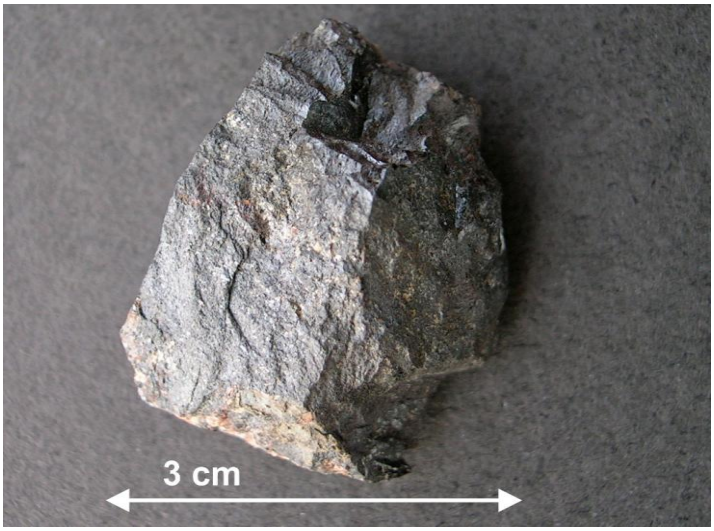


Figure 6.10 The sample of perrierite from Amherst, Virginia.

The age of the sample, Fe, Th and U concentrations and the estimated α-dose are given in Table 6.4. The $^{57}Fe$ Mössbauer spectrum and XRD pattern are shown in Figure 6.11.

Table 6.4 Age, Fe, Th and U concentrations and the calculated α-dose of the perrierite sample.

| Age (Ma) | Fe (wt.%) | Th (wt.%) | U (wt.%) | Calculated α-dose (α-decay/mg) |
|---|---|---|---|---|
| 1000-1200 [a] | 5.0 | 0.26 | 0.03 | $3.4 \times 10^{15}$ |

[a]Mesoproterozoic granitoids

The Mössbauer spectrum of perrierite is complex (Figure 6.11, Table 6.5). The peaks can also be fitted to four doublets that represent the $Fe^{2+}$ (no. 1 and 2) and $Fe^{3+}$ (no. 3 and 4) components in two different octahedral sites [15]. Doublets 1 and 4 can be interpreted as representing the less distorted octahedral sites relative to doublets 2 and 3. As can be seen in Table 6.5, the relative contribution of $Fe^{2+}$ is high and equals 71.3 %.

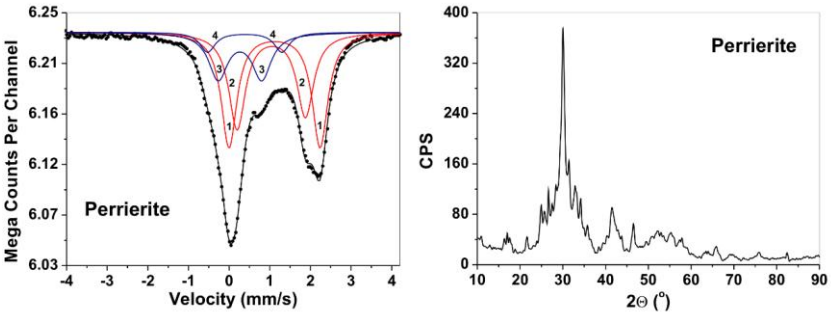


Figure 6.11 (left)$^{57}$Fe Mössbauer spectrum of the perrierite sample. Solid dots – experimental data; black solid line – fitted curve; red solid line – $Fe^{2+}$ doublets; blue solid line – $Fe^{3+}$ doublets. (right) XRD pattern.

Table 6.5 Hyperfine interactions parameters for the $^{57}$Fe Mössbauer spectrum for the perrierite sample that was investigated. Isomer shift values (*IS*) are given relative to the α-Fe standard at RT.

| Sample | Doublet no. | $\chi^2$ | *IS* (mm/s) | *QS* (mm/s) | $\Gamma$ (mm/s) | Assignment (CN)* | Intensity (%) |
|---|---|---|---|---|---|---|---|
| Perrierite | | 1.5 | | | | | |
| | 1 | | 1.13 | 2.24 | 0.23 | $Fe^{2+}$ (6) | 38.3 |
| | 2 | | 1.04 | 1.69 | 0.24 | $Fe^{2+}$ (6) | 33.0 |
| | 3 | | 0.38 | 1.79 | 0.22 | $Fe^{3+}$ (6) | 6.5 |
| | 4 | | 0.28 | 1.03 | 0.30 | $Fe^{3+}$ (6) | 22.2 |

* CN - Coordination number

The corresponding XRD pattern of perrierite shows a very high degree of metamictization (Figure 6.11). It seems probable that an α-dose of 3.4 x $10^{15}$α-decay/mg is near the critical dose for the metamictization (amorphization) of this mineral species.

## Gadolinite

Structurally, gadolinite $REE_2Fe^{2+}Be_2Si_2O_{10}$, in which REE means the rare earth elements, yttrium, uranium, and thorium, is composed of sheets of $SiO_4$ and $BeO_4$ tetrahedra that are interconnected by layers of distorted iron octahedra and eight-coordinated REE ions [16]. A sample of fully metamict gadolinite (GYT) was collected from Ytterby in central Sweden. The sample was massive and pitch black with conchoidal fracture (Figure 6.12). The age of the sample, Fe, Th and U concentrations and the estimated α-dose are given in Table 6.6.

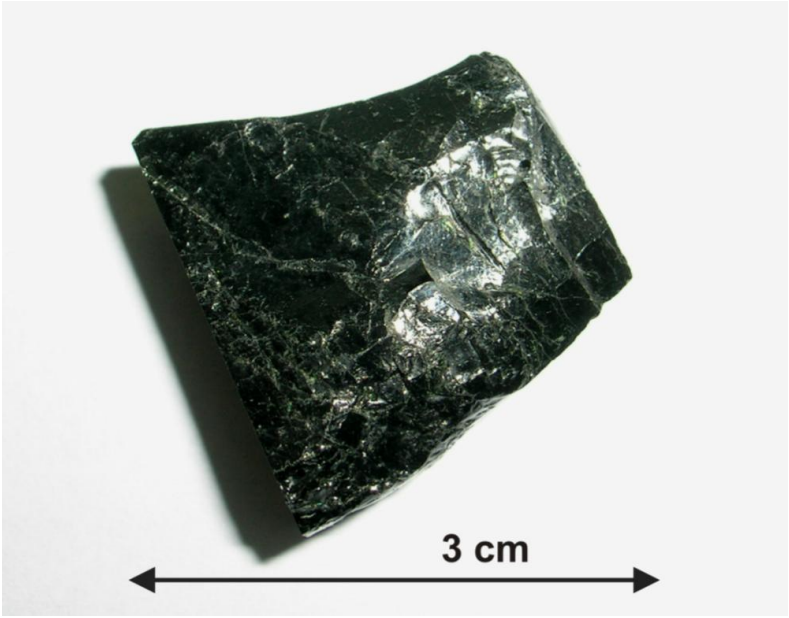


Figure 6.12 A photograph of fully metamict gadolinite from Ytterby (Sweden).

Table 6.6 Age of the sample, Fe, U and Th concentrations and the calculated α-dose.

| Age (Ma) | Fe (wt.%) | Th (wt.%) | U (wt.%) | Calculated α-dose (α-decay/mg) |
|---|---|---|---|---|
| 1795(20)[a] | 6.65 | 0.258 | 0.097 | $1.07(3) \times 10^{16}$ |

[a] Reference [17]

The $^{57}$Fe Mössbauer spectra and XRD patterns of an untreated gadolinite sample and a sample that was annealed in argon at 1373 K are shown in Figure 6.13. The hyperfine interactions parameters that were derived from the fitting procedure for each annealed sample are summarized in Table 6.7. Based on the quadrupole splitting distribution, the Mössbauer spectrum of the untreated sample can be fitted to two $Fe^{2+}$ doublets labeled 1 and 2 (Figure 6.13, Table 6.7) [18]. Doublet no. 1, which has an *IS* = 0.94 mm/s, represents the $Fe^{2+}$octahedra that have undergone a contraction during metamictization, while doublet no. 2, which has an *IS* = 1.06 mm/s, represents the $Fe^{2+}$octahedra that have undergone an expansion during metamictization. The XRD pattern of the untreated sample (Figure 6.13) had a complete lack of long range structural order.

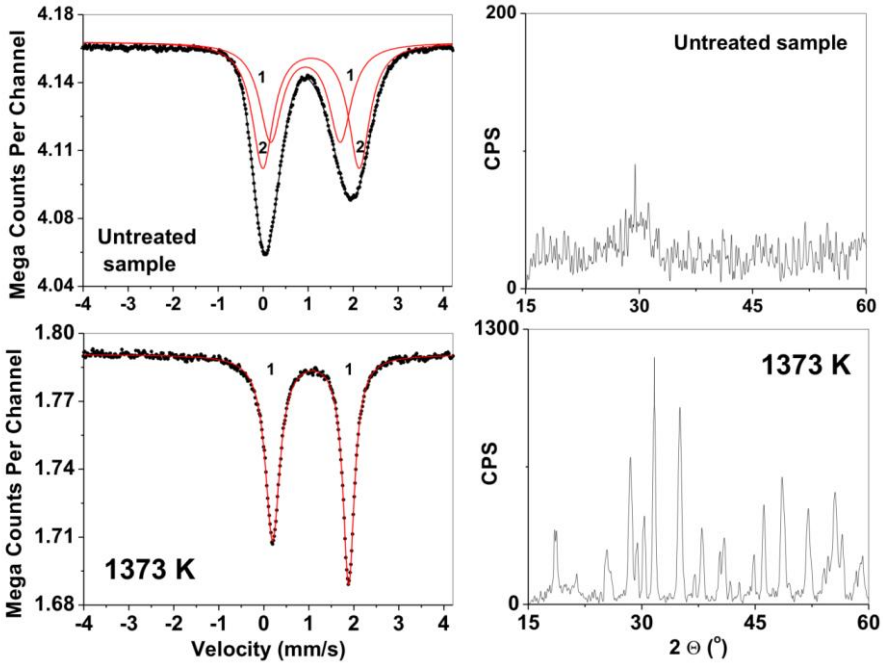


Figure 6.13 (left) The $^{57}$Fe Mössbauer spectra at RT of the untreated gadolinite sample and a sample after one-hour annealing at 1373 K. Solid dots – experimental data; solid line – fitted curve; red solid line – fitted $Fe^{2+}$ doublets. (right) Corresponding XRD patterns.

Table 6.7 Hyperfine interactions parameters for the $^{57}$Fe Mössbauer spectra for the untreated sample GYT and the sample that was annealed at 1373K (Figure 6.13). Isomer shift values *IS* are given relative to the α-Fe standard at RT.

| *T* (K) | Doublet no. | $\chi^2$ | *IS* (mm/s) | *QS* (mm/s) | $\Gamma$ (mm/s) | Assignment (CN)* | Intensity (%) |
|---|---|---|---|---|---|---|---|
| Reference | | 1.5 | | | | | |
| sample | 1 | | 0.94 | 1.55 | 0.30 | $Fe^{2+}$ (6) | 45 |
| | 2 | | 1.06 | 2.14 | 0.28 | $Fe^{2+}$ (6) | 55 |
| 1373 | | 1.0 | | | | | |
| | 1 | | 1.04 | 1.69 | 0.20 | $Fe^{2+}$ (6) | 51 |
| | | | | | 0.15 | | 49 |

*CN - coordination number

The sample that was annealed at 1373 K shows one asymmetric $Fe^{2+}$ doublet that is labeled with no. 1 (Figure 6.13). The corresponding XRD pattern in Figure 6.13 indicates that the GYT sample became completely crystalline after annealing at 1373 K. The recrystallization process was accompanied by a narrowing of the spectral lines along with a reverse of the amplitude ratios of the high energy peak to the low energy peak. The strong asymmetry of the $Fe^{2+}$ absorption peaks in doublet no. 1 was due to the Goldanskii-Karyagin effect from the non-isotropic vibrations of $Fe^{2+}$ in the crystalline structure of the gadolinite. The same isomer shift and asymmetry of absorption lines were reported for synthetic gadolinite [19]. This fact indicates that the chemical composition of the GYT sample did not change despite the metamictization process over 1.8 x $10^9$ years and an absorbed α-dose of 1.07(3) x $10^{16}$α-decay/mg.

## 3.2. Oxides

**Davidite**

Davidite (multiple oxides) - $(La,Ce,Ca,Th)(Y,U,Fe)(Ti,Fe,Mn)_{20}(O,OH)_{38}$ is isostructural with the crichtonite – group minerals and has a structure that is based on a close – packed anion framework with the mixed stacking sequence ABCBCACABA with rare earth elements REE M(0), and occupies a site in the anion framework and five cation sites M(1)-M(5) [20]. The davidite samples that were investigated, massive, grayish black with vitreous-metallic luster, were collected from a Permian granitoid massif Bektau-Ata, Kazakhstan (Figure 6.14). The basic characteristics of the sample of davidite are given in Table 6.8.

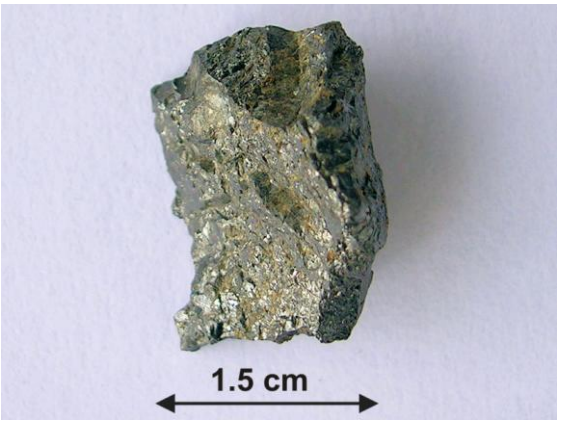


Figure 6.14 A sample of davidite from Bektau-Ata (Kazakhstan).

Table 6.8 The basic characteristics of the davidite sample.

| Age (Ma) | Fe (wt.%) | Th (wt.%) | U (wt.%) | Calculated α-dose (α-decay/mg) |
|---|---|---|---|---|
| 270(20) [a] | 19.0 | 0.25 | 0.83 | $8.1(8) \times 10^{15}$ |

[a] Permian granitoid massif

The $^{57}$Fe Mössbauer spectra of the untreated sample and a sample after one-hour annealing in argon at 1273 K and corresponding XRD patterns are shown in Figure 6.15. The hyperfine interactions parameters that were derived from the fitting procedure are given in Table 6.9.

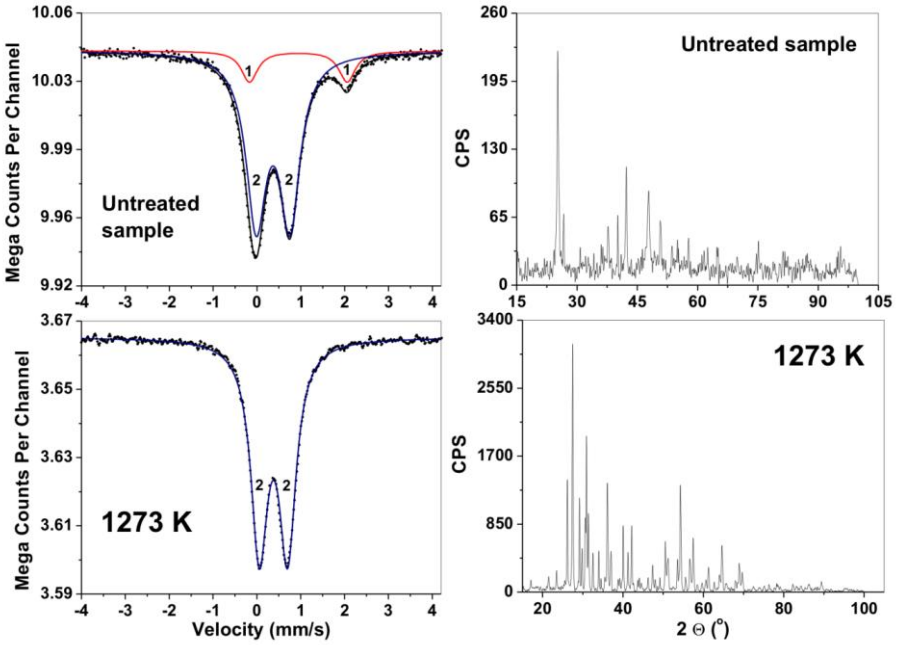


Figure 6.15 (left) The $^{57}$Fe Mössbauer spectra of the untreated davidite sample and the sample after one-hour annealing at 1273 K. Solid dots – experimental data; solid line – fitted curve; red solid line – fitted $Fe^{2+}$ doublets; blue solid line – fitted $Fe^{3+}$ doublets. (right) Corresponding XRD patterns.

Table 6.9 Hyperfine interactions parameters for the $^{57}$Fe Mössbauer spectra for the untreated sample of davidite and sample annealed at 1273 K (Fig. 6.15). Isomer shift values *IS* are given relative to the α-Fe standard at RT.

| T (K) | Doublet no. | $\chi^2$ | *IS* (mm/s) | *QS* (mm/s) | $\Gamma$ (mm/s) | Assignment (CN)* | Intensity (%) |
|---|---|---|---|---|---|---|---|
| Untreated sample | | 1.0 | | | | | |
| | 1 | | 0.94 | 2.23 | 0.22 | $Fe^{2+}$ (6) | 13.1 |
| | 2 | | 0.37 | 0.77 | 0.28 | $Fe^{3+}$ (6) | 86.9 |
| 1273 | | 1.1 | | | | | |
| | 2 | | 0.37 | 0.64 | 0.23 | $Fe^{3+}$ (6) | 100 |

* CN - Coordination number

The Mössbauer spectrum of davidite (Figure 6.15, Table 6.9) can be fitted to two quadrupole doublets that are assigned to $Fe^{2+}$ (doublet no. 1) and $Fe^{3+}$ (doublet no. 2) in octahedral positions. From crystalline structure of davidite one can result that these doublets correspond to $Fe^{2+}$ and $Fe^{3+}$ in octahedral M(3) site [21]. As can be seen in Figure 6.15, the corresponding XRD pattern shows an intermediate degree of the amorphization (metamictization) of this mineral. This ferrous component completely vanishes after heating (annealing) at 1273 K. A similar behavior of an $Fe^{2+}$ component was observed in an extensive study of α-decay damage in titanite [22]. Similarly to metamict titanite, the damage process in metamict davidite is accompanied by a reduction of the $Fe^{3+}$ to $Fe^{2+}$ that resides in the aperiodic domains. These damaged regions can incorporate much more hydrogen (as $OH^-$) than is contained in crystalline state, presumably as a result of the post-damage diffusion of H into the structure. Conversely, the recrystallization process is accompanied by intense dehydroxylation (as $H_2O$) with the simultaneous oxidation of $Fe^{2+}$ to $Fe^{3+}$.

## Columbite

Columbite-tantalite minerals (multiple oxides) have the general formula $AB_2O_6$, where A = $Fe^{2+}$, $Mn^{2+}$ and $Mg^{2+}$ and B = $Nb^{5+}$ and $Ta^{5+}$, with minor substitutions of $Sn^{4+}$, $W^{6+}$ and $Fe^{3+}$ [23]. The samples of columbite were collected in Chester Co, Pennsylvania (Figure 6.16). The basic characteristics of the sample are given in Table 6.10.


Figure 6.16 Irregular black assemblages of columbite in a rocky fragment.

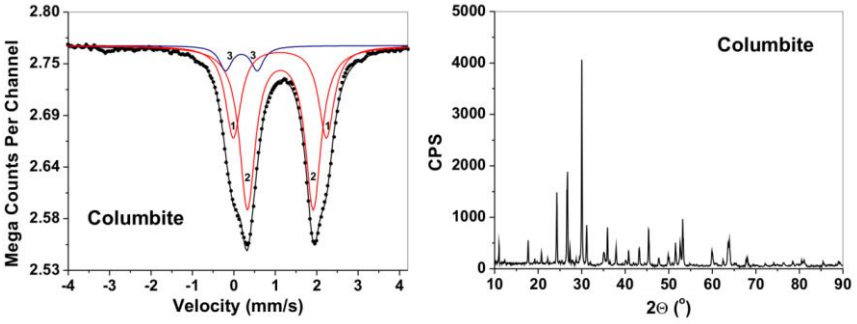


Figure 6.17 (left) The $^{57}$Fe Mössbauer spectrum of a columbite sample. Solid dots – experimental data; black solid line – fitted curve; red solid line – $Fe^{2+}$ doublets; blue solid line – $Fe^{3+}$ doublet. (right) XRD pattern.

Table 6.10 Age, Fe, Th and U concentrations and the calculated α-dose of the columbite sample that was used in this study.

| Age (Ma) | Fe (wt.%) | Th (wt.%) | U (wt.%) | Calculated α-dose (α-decay/mg) |
|---|---|---|---|---|
| 876-1009[a] | 19.0 | 0.05 | 0.54 | 1.9(2) x $10^{16}$ |

[a] Reference [24]

The Mössbauer spectrum of columbite (Figure 6.17, Table 6.11) is fitted to two doublets that are assigned to $Fe^{2+}$ in the octahedral coordination and one narrow $Fe^{3+}$ doublet with IS = 0.18 mm/s in the octahedral coordination (no. 3, Table 6.11). The outer $Fe^{2+}$ doublet (no. 1) represents a less distorted octahedral site, whereas the inner doublet (no. 2) represents another strongly distorted octahedral site [15].

Table 6.11 Hyperfine interactions parameters for the $^{57}Fe$ Mössbauer spectrum for the columbite from Chester Co, Pennsylvania (Figure 6.17). Isomer shift values (*IS)* are given relative to the α-Fe standard at RT.

| Sample | Doublet no. | $\chi^2$ | *IS* (mm/s) | *QS* (mm/s) | $\Gamma$ (mm/s) | Assignment (CN)* | Intensity (%) |
|---|---|---|---|---|---|---|---|
| Columbite | | 2.3 | | | | | |
| | 1 | | 1.11 | 2.25 | 0.22 | $Fe^{2+}$ (6) | 33.2 |
| | 2 | | 1.12 | 1.59 | 0.23 | $Fe^{2+}$ (6) | 59.7 |
| | 3 | | 0.18 | 0.76 | 0.18 | $Fe^{3+}$ (6) | 7.1 |

* CN - Coordination number

Despite a relatively high absorbed α-dose, the XRD pattern in Figure 6.17 shows that the sample is still highly crystalline. This observation suggests that the columbite phase is mostly unaffected by radiation damage at least up to an α-dose of 1.9 x $10^{16}$α-decay/mg.

## Samarskite

Samarskite is a complex niobium tantalum titanium oxide. Samarskite has a structural formula of $ABO_4$, where A = Ca, Ti, $Fe^{2+}$, $Fe^{3+}$, REE, U and Th, and B = Nb and Ta [25]. Analysis of the average site charges and cation radii indicated that both the A and B sites have octahedral coordination. A large, massive, metallic brownish-black sample of samarskite (SCC) was collected in pegmatites in Centennial Cone, Colorado (Figure 6.18). The basic characteristics of the sample are given in Table 6.12.

Table 6.12 Age, Fe, Th and U concentrations and the calculated α-dose of the samarskite sample.

| Age (Ma) | Fe (wt.%) | Th (wt.%) | U (wt.%) | Calculated α-dose (α-decay/mg) |
|---|---|---|---|---|
| 1400-1700 [a] | 5.9 | 1.7 | 11.4 | 7.1(8) x $10^{17}$ |

[a] Reference [26]


Figure 6.18 A fragment of the samarskite sample from Centennial Cone, Colorado.

The hyperfine interactions parameters that were derived from the fitting procedure are summarized in Table 6.13.

The Mössbauer spectrum of the samarskite sample and the corresponding XRD pattern are shown in Figure 6.19. The Mössbauer spectrum of the sample SCC is fitted to three quadrupole doublets that were assigned to $Fe^{2+}$ (labeled with a number 1 in Figure 6.19) and $Fe^{3+}$ (labeled 2 and 3) in octahedral positions with a total relative $Fe^{2+}$contribution of 24 %.

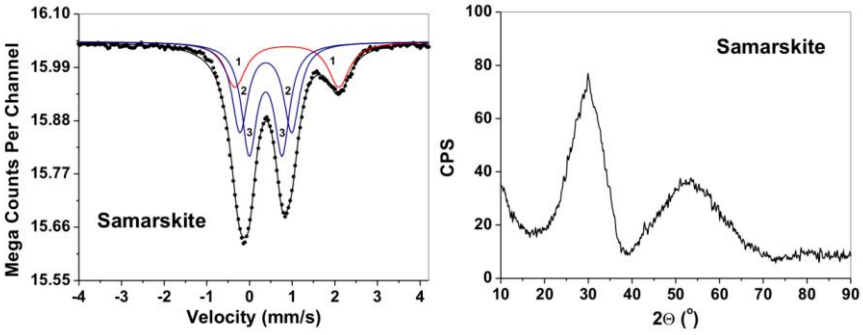


Figure 6.19 (left) The $^{57}Fe$ Mössbauer spectrum of the samarskite sample. Solid dots – experimental data; black solid line – fitted curve; red solid line – $Fe^{2+}$ doublet; blue solid line – $Fe^{3+}$ doublets. (right) XRD pattern.

Table 6.13 Hyperfine interactions parameters for the $^{57}$Fe Mössbauer spectrum (shown in Figure 6.19) for the metamict samarskite that was investigated. Isomer shift values (*IS)* are given relative to the α-Fe standard at RT.

| Sample | Doublet no. | $\chi^2$ | *IS* (mm/s) | *QS* (mm/s) | $\Gamma$ (mm/s) | Assignment (CN)* | Intensity (%) |
|---|---|---|---|---|---|---|---|
| Samarskite | | 1.6 | | | | | |
| (SAM1) | 1 | | 0.88 | 2.43 | 0.30 | $Fe^{2+}$ (6) | 24 |
| | 2 | | 0.38 | 1.21 | 0.22 | $Fe^{3+}$ (6) | 35 |
| | 3 | | 0.38 | 0.77 | 0.21 | $Fe^{3+}$ (6) | 41 |

*CN - Coordination number

Due to the high absorbed α-dose, the XRD pattern of samarskite showed a complete lack of long range structural order. The samarskite sample was fully metamict. Based on annealing experiments, it appeared that nearly the entire content of $Fe^{2+}$ in SCC was a result of the metamictization process.

## 4. General trends of the $Fe^{2+}$ components vs. absorbed α-dose

Detailed studies of brannerite, cerite, columbite, perrierite and samarskite showed that isomer shift values of the $Fe^{2+}$ components decrease with an increasing absorbed α-dose (Figure 6.20a) [15]. An increase in the line widths vs. absorbed α-dose for these $Fe^{2+}$ doublets was also observed (Figure 6.20b).

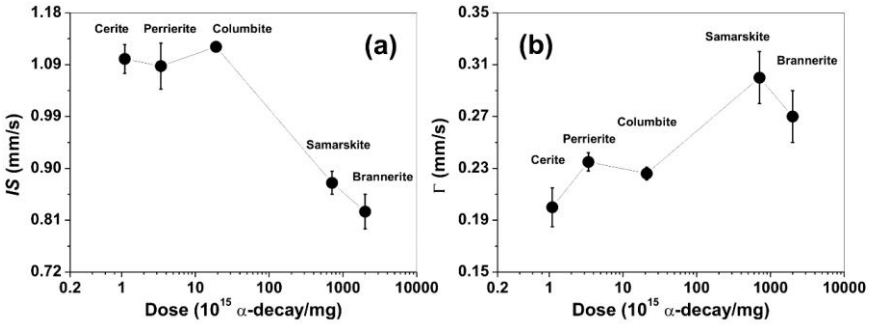


Figure 6.20 Averaged values of **(a)** isomer shifts and **(b)** line widths ($\Gamma$) of the $Fe^{2+}$ components vs. the absorbed α-dose.

Positive correlations between the average isomer shifts of the $Fe^{2+}$ doublets and increasing crystallinity (logarithmic growth, Figure 6.21a) were also reported in the same paper [15].

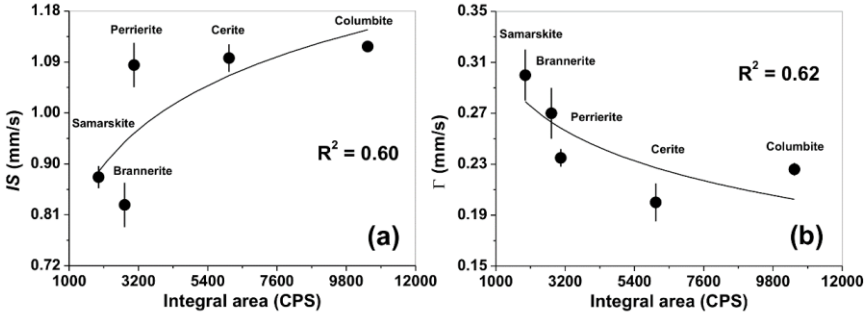


Figure 6.21 Averaged values of **(a)** the isomer shifts and **(b)** line widths ($\Gamma$) of $Fe^{2+}$ components versus the integrated area under the X-ray diffraction peaks. The solid lines represent the logarithmic regressions: (IS) = 0.152 x ln(integral area) - 0.26, and ($\Gamma$) = - 0.045 x ln(integral area) + 0.624. $R^2$- multiple regression coefficients.

Unlike the IS values, the average line widths of these $Fe^{2+}$ components decreased with increasing crystallinity (logarithmic decay, Figure 6.21b). As can be seen in Figure 6.21, there are good correlations between the average *IS* and $\Gamma$ values for the $Fe^{2+}$ doublets and the degree of crystallinity of the samples.

## Conclusions

The Mössbauer spectra of all of the metamict minerals that were investigated showed features that can only be explained by assuming octahedral coordinations for both the $Fe^{2+}$ and $Fe^{3+}$ ions. In other words, the coordination number of the iron ions was the same in the crystalline and metamict states, despite the high absorbed alpha dose which ranged from $10^{15}$ to ~$10^{18}$ alpha-decays per milligram. This result was rather unexpected and it suggested that the main mechanism of the metamictization process involved the rotation and translation of tetrahedra, octahedra and other coordination polyhedra as a whole, rather than the production of point defects. The application of the Mössbauer effect has great potential for the future of this field. Due to the mechanical and chemical durability over geologic time scale, three of the metamict phases that were presented above such as columbite, samarskite and gadolinite seem to be suitable candidates for potential forms for immobilization of HLW.

## References


[1] W.J. Weber, R.C. Ewing, C.A. Angell, G.W. Arnold, A.M. Cormack, J.M. Delaye, D.L. Griscom, L.W. Hobbs, A. Navrotsky, D.L. Price, A.M. Stoneham, and M.C. Weinberg, J. Mater. Res. 12 (1997) 1434.

[2] W.J. Weber, R.C. Ewing, C.R.A. Catlow, T. Diaz de la Rubia, L.W. Hoobs, C. Kinoshita, H. Matzke, A.T. Motta, M. Nastas, E.K.H. Salje, E.R. Vance, and S.J. Zinkle, J. Mater. Res. 13 (1998) 1946.

[3] R.C. Ewing, Nucl. Instr. and Meth. in Phys. Res. B91 (1994) 22.

[4] J.A. Woodhead, G.R. Rossman, L.T. Silver, Am. Mineral. 76 (1991) 74.

[5] D. Malczewski, A. Grabias, G. Dercz, Hyperfine Interact. 195 (2010) 88.

[6] R.L. Mössbauer, Z. Physik 151 (1958) 124.

[7] R.L. Mössbauer, Naturwissenschaften 45 (1958) 538.

[8] F.C. Hawthorne, Reviews in Mineralogy 18 (1988) 255.

[9] E. Murad, J. Cashion, Mössbauer spectroscopy of environmental materials and their industrial utilization, Kluwer Academic Publishers, New York, 2004.

[10] W.A. Dollase, Am. Mineral. 566 (1971) 447.

[11] A. Volborth, Econ. Geol. 57 (1962) 209.

[12] R.A. Volkert, R.E. Zartman, P.B, Moore, Precambrian Res. 139 (2005) 1.

[13] D. Malczewski, A. Grabias, Acta Phys. Pol.A 114 (2008) 1683.

[14] G.C. Parodi, G. Della Ventura, A. Mottana, M. Raudsepp, Mineral. Mag. 58 (1994) 607.

[15] D. Malczewski, A. Grabias, Hyperfine Interact. 186 (2008) 75.

[16] R. Miyawaki, I. Nakai, K. Nagashima, Am. Mineral. 69, (1984) 984.

[17] R.I. Romer, S.A. Smeds, Precambrian Res. 67 (1994) 141.

[18] D. Malczewski, A. Molak, J. Nucl. Mater.412 (2011) 239.

[19] J. Ito, S.S. Hafner, K. Nagashima, Am. Mineral. 59, (1984) 984.

[20] B.M. Gatehouse, I. E. Grey, P.R. Kelly, Am Mineral 64 (1979) 1010.

[21] D. Malczewski, J.F. Frąckowiak, E.V. Galuskin, Nukleonika 52 (2007) S81.

[22] F.C. Hawthorne, L.A. Groat, M. Raudsepp, N.A. Ball, M. Kimata, R. Gaba, N.M. Halden, G.R. Lumpkin, R.C. Ewing, R.B. Greegor, F.W. Lytle, T.S. Ercit, G.R. Rossman, F.J. Wicks, R.A. Ramik, B.L. Sherriff , M.E. Fleet, C. McCammon, Am Mineral (1991) 76 370.

[23] M. Wenger,T. Armbruster, C.A. Geiger, Am. Mineral. 76 (1991) 1897.

[24] J.M. Pyle, GSA Philadelfia Annual Meeting, Paper No. 80-4, 2006.

[25] J.K. Warner, R.C. Ewing, Am. Mineral. 78 (1993) 419.

[26] B. Bryant, L.W. McGrew, R.A. Wobus, Geologic map of the Denver Map I-1163, U.S. Geological Survey Miscellaneous Investigations, 1981.

# CHAPTER 7

## Safety requirements for storage and disposal of radioactive waste in Poland

Zbigniew Surowiec
Institute of Physics, Maria Curie-Skłodowska University,
M. Curie-Skłodowskiej 1 Sq., 20-031 Lublin, Poland
zbigniew.surowiec@poczta.umcs.lublin.pl

Radioactivity is a natural phenomenon. The use of radioactive materials and radiation sources leads to the production of radioactive waste. Radioactive waste is hazardous to most forms of life and the environment but radiation and radioactive substances have many beneficial applications in many fields ranging from power generation to uses in medicine, industry, and agricultural and scientific research. The permanent increase in the applications of radioactive isotopes in different areas of science and industry caused an urgent need to solve the problem of radioactive waste management. To satisfy this need, a professional institution dealing with waste management was created under the name the Radioactive Waste Centre – an auxiliary establishment in the former Institute for Nuclear Research and the Central Radioactive Waste Management Repository.

Treatment and disposal of radioactive waste require reducing its production, segregating the waste, decreasing its volume, solidifying and packaging it in a manner that guarantees that all the undertaken measures and barriers effectively isolate waste from humans and the biosphere.

The objective of radioactive waste management is to control and account for radioactive waste to protect human health and the environment now, but also to make sure we do not leave unnecessary burdens for future generations.

The question of radioactive waste management appeared in Poland in 1958, when the first research reactor Ewa was put to operate in the Institute for Nuclear Research in Świerk near Warsaw. Since that time, several research reactors have been working for isotope production and research.

## 7.1. Fundamental principles of radioactive waste management

The use of radioactive materials and radiation sources in science, medicine, and industry and, in particular, in the field of nuclear energy leads to the production of radioactive waste. Radioactive waste might be dangerous through its negative influence on the environment, including human health and life; therefore, it requires an appropriate way of treatment.

The radioactive waste management involves the treatment, conditioning, transportation, storage, and disposal of all categories of radioactive wastes, including administrative, operational, and safety-related activities. To ensure an adequate level of safety in management of radioactive waste and spent nuclear fuel, the international community had to determine the appropriate proceeding of dealing with radioactive waste. The principles for the management of nuclear waste were published first time in 1995 by the International Atomic Energy Agency (IAEA ) [1]. These principles show the need for global and long-term consideration of radioactive wastes [2].

**Principle 1:** Protection of human health

Radioactive waste shall be managed in a way to secure an acceptable level of protection for human health. The management of nuclear waste should be part of the justification of the whole activity that produces nuclear waste. A special feature of radioactive waste is the threat posed due to ionizing radiation. Particular attention should be paid to the control of routes of exposure. It must be ensured that such an exposure will be maintained within the limits set in the country requirements. Establishing the acceptable levels of protection should usually be based on the recommendations of the International Commission of Radiological Protection – ICRP and IAEA. In the radioactive waste management, the principle of justification, optimization, and dose limitation should apply.

The principle of "justification" means a principle, as a result of which the radioactive waste should be taken only when the benefits of this activity outweigh the inconvenience caused by the formation of waste.

The optimization principle means that, at a reasonable consideration of economic and social factors, the number of people exposed in the process of dealing with radioactive waste will be as small as possible, and those receiving a radiation dose will be small as possible.

The principle of limiting the doses means adherence to the established system of dose limits.

**Principle 2:** Protection of the environment

Radioactive waste shall be managed in such a way to provide an acceptable level of protection of the environment. Safe treatment of waste ensures release of radioactive substances into the environment at the lowest level possible, in all stages of the proceedings. Methods for compaction and transfer of waste into dilution and dispersion sites in the environment should be preferred. However, it is possible to remove radioactive substances into the environment within the accepted limits. The release of radioactive substances into the environment may lead to exposure of not only humans but also other living organisms to ionizing radiation, and this exposure should be taken into account. Locally, radioactive waste can have negative consequences for the long-term availability or use of resources, for instance woods, water, land. The management of radioactive waste has to limit these consequences to minimize the impact to a practically reachable one.

**Principle 3:** Protection beyond national borders

Radioactive waste shall be managed in a way to assure that possible effects on human health and the environment beyond national borders will be taken into account. This principle was derived from the ethical care for the health of people and environment in foreign countries. It assumes that a country has the duty to prevent foreign countries from suffering the consequences that are unacceptable for its own society.

**Principle 4:** Protection of future generations

Radioactive waste shall be managed in such a way that predicted impacts on the health of future generations will not be greater than relevant levels of impact that are acceptable today.

Since it is not possible to isolate completely radioactive waste for a very long time, such security should be sought in order to avoid adverse effects on human health in the considered time. This is possible to achieve by application of the multibarrier system consisting of the engineered and natural barriers. Ensuring adequate natural barriers usually occurs in the process of object location. In addition, possible future exploitation of natural resources that could potentially affect adversely the insulation value of the landfill should be considered.

**Principle 5:** Burdens on future generations

Radioactive waste shall be managed in such a way that it will not impose undue burdens on future generations. The care for future generations is of fundamental importance in the management of nuclear waste. This principle is based on the ethical consideration that generations benefiting from an activity also have the responsibility to manage the waste. The responsibility of the present generation implies the development of technology, building and operation of storage sites, and provision of funds. As far as possible, the management should not be based on long-term institutional regulations, although future generations might decide to do so. On the other hand, the IAEA states: restricted activities, like ongoing institutional control, may be shifted to future generations.

**Principle 6:** National legal framework

Radioactive waste shall be managed within an appropriate national legal framework.

The national legal system should identify the responsibility at every stage of waste treatment.

It should establish an independent regulatory body.

**Principle 7:** Control of radioactive waste generation

Generation of radioactive waste shall be kept to the minimum practicable level of both the activity and the volume by the use of appropriate design solutions and practices during operation and decommissioning. This includes selection and control of materials, recycling, and implementation of appropriate operational procedures.

**Principle 8:** Radioactive waste generation and management interdependencies

Interdependencies among all steps in radioactive waste generation and management shall be appropriately taken into account. For instance, the choice for reprocessing implies that nuclear waste is generated with certain properties, with a certain production of heat that has an influence on the method of storage.

**Principle 9:** Safety of facilities

The safety of facilities for radioactive waste management shall be appropriately assured during their lifetime. In designing, building, operating, and dismantling of installations and storage sites, safety must have high priority. That means preventing accidents and limiting consequences when accidents do happen. The appropriate level of quality assurance, personnel training, and competence should be maintained throughout the period of operation of the object.

## 7.2. Radioactive waste classification scheme proposed by IAEA safety standards

Radioactive waste is generated in different kinds of facilities and it may arise in a variety of physical and chemical characters and a wide range of concentrations of radionuclides. Each type of radioactive waste requires an individual treatment. There are many ways for processing waste and for short-term or long-term storage prior to disposal. Similarly, there are various alternatives for the safe disposal of waste, ranging from near surface disposal in engineered vaults or trenches to disposal in engineered facilities located in stable underground geological formations at depths of several hundred meters.

The general indicative criteria for classification of radioactive waste are presented in Table 7.1.

Table 7.1 Factsheet of general criteria for classification of radioactive waste

| | |
|---|---|
| Radiation character | alfa emitter |
| | beta-gamma emitter |
| | neutron emitter |
| Activity | low level waste |
| | intermediate level waste |
| | high level waste |
| Half-life | very short life $T_{1/2}$<90 days |
| | short life $T_{1/2}$<30 years |
| | long life $T_{1/2}$>30 years |
| Form | solid |
| | liquid |
| | biological |
| Sources | open sources |
| | sealed sources |
| Heat emission | no heat emission |
| | heat emission |

Source: Own elaboration on the basis of [3-5].

The IAEA, which publishes the Radioactive Waste Safety Standards (RADWASS), plays a significant role in introduction of classification of radioactive waste to national laws. In accordance with the IAEA safety standards [3-8], six classes of radioactive waste are derived and used as the basis for the classification scheme:

- **Exempt waste (EW):** Waste that meets the criteria for exemption from regulatory control for radiation protection purposes.

- **Very short-lived waste (VSLW):** Waste that can be stored for decay over a limited period of up to a few years and subsequently exempted from regulatory control according to arrangements approved by the relevant regulatory authority, for uncontrolled disposal, use, or discharge. This class includes waste containing primarily radionuclides with very short half-lives often used for industrial, medical, and research purposes.

- **Very low-level waste (VLLW):** Waste that does not meet the criteria of EW, but does need a moderate level of containment and isolation and therefore is suitable for disposal in a near surface, industrial or commercial, landfill type facility with limited regulatory control. Such landfill type facilities may also contain other hazardous waste. Typical waste in this class includes soil and rubble with low activity concentration levels. Concentrations of longer-lived radionuclides in VLLW are generally very limited.

- **Low-level waste (LLW):** Waste that is above exemption levels, but with limited amounts of long-lived radionuclides. Such waste requires robust isolation and containment for periods of up to a few hundred years and is suitable for disposal in engineered near surface facilities. This class covers a very broad range of waste. Low-level waste may include short-lived radionuclides at higher activity concentration levels and long-lived radionuclides, but only at relatively low activity concentration.

- **Intermediate-level waste (ILW):** Waste that, because of its content, particularly of long-lived radionuclides, requires a greater degree of containment and isolation than that provided by near surface disposal. However, ILW needs little or no provision for heat dissipation during its storage and disposal. Intermediate-level waste may contain long-lived radionuclides, in particular alpha emitting radionuclides, which will not decay to an activity concentration acceptable for near surface disposal during the time for which institutional controls can be relied upon. Therefore, waste

in this class requires disposal at greater depths, in the order of tens of meters to a few hundred meters.

- **High-level waste (HLW):** Waste with activity concentration levels high enough to generate significant quantities of heat by the radioactive decay process or waste with large amounts of long-lived radionuclides that need to be considered in the design of a disposal facility for such waste. Disposal in deep, stable geological formations usually several hundred meters or more below the surface is the generally recognized option for disposal of HLW. Quantitative values of allowable activity content for each significant radionuclide will be specified on the basis of safety assessment for individual disposal sites.

A conceptual illustration of the waste classification scheme is presented in Figure 7.1. The vertical axis represents the activity content of the waste and the horizontal axis represents the half-lives of the radionuclides contained in the waste. In some cases, the total activity, rather than activity concentration, may be used to determine the class of the waste. For example, waste containing only very small amounts of certain radionuclides (e.g. low-energy beta emitters) may be excluded or exempted from regulatory control.

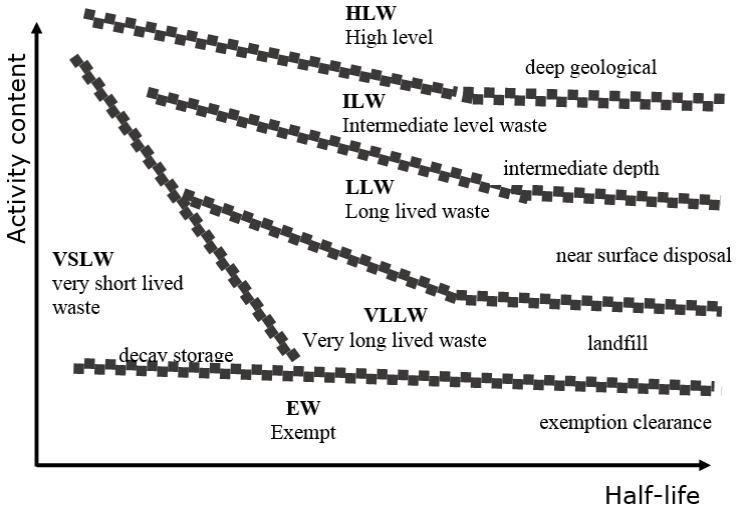


Figure 7.1 Conceptual illustration of the waste classification scheme (adapted from GSG-1). Source: Own elaboration on the basis of [3].

## 7.3. Radioactive waste classification in Polish law

According to the Act of the Polish Parliament: Atomic Law of 11 November 2000 (with subsequent amendments) and Regulation of the Council of Ministers of 3 December 2002 on radioactive waste and spent nuclear fuel, radioactive waste, with respect to its activity level or surface dose rate, shall be classified into the following categories: low, medium, and high-level radioactive waste [9,10]. These categories may be further subdivided into sub-categories with respect to the half-lives of radioactive isotopes contained in the waste or to the thermal power of the waste.

Spent sealed radioactive sources shall constitute an additional radioactive waste category.

Spent sealed radioactive sources, according to the level of their activity, shall be classified into the following sub-categories of spent sealed radioactive sources: low, medium, and high activity, which shall be further subdivided according to the half-lives of contained radioactive isotopes into short-lived and long-lived sub-categories. Qualification into the sub-category of sealed radioactive sources shall be done on the basis of their calculated activities or measurements of ionizing radiation emitted by these sources (Figure 7.2).

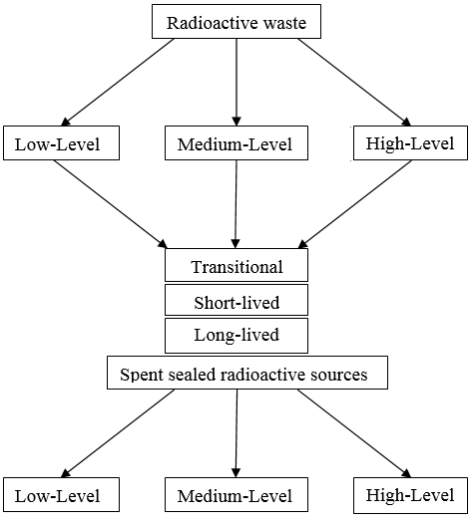


Figure 7.2 Scheme of radioactive waste classification in Polish law. Source: Own elaboration on the basis of [9].

**Low-Level Waste (LLW)**

Radioactive waste shall be qualified into the low-level waste category if the radioactive isotope concentration in this waste exceeds the value established in Annex 1 to the Regulation, but no more than ten thousand times. In the case of radioactive waste containing various radioactive isotopes, such waste shall be qualified into the low-level waste category if the sum of radioactive isotope concentration ratios for each isotope in this waste to the values established in Annex 1 to the Regulation exceeds 1, but does not exceed 10 000.

Liquid waste containing a single isotope, in which the radioactive isotope concentration does not exceed the value established in Annex 1 to the Regulation and which was generated in a period not longer than 30 days as a result of activities involving exposure to ionizing radiation, provided that the activity of this isotope exceeds more than thousand times the activity established in Annex 1 to the Regulation, shall also be qualified into the low-level radioactive waste category.

Liquid waste containing more than one isotope, in which the sum of radioactive isotope concentration ratios for each isotope to the values established in Annex 1 to the Regulation does not exceed 1, and which was generated in a period not longer than 30 days as a result of activities involving exposure to ionizing radiation, provided that the sum of isotope activity ratios to the activity values established in Annex 1 to the Regulation exceeds 1 000, shall also be qualified into the low-level waste category.

Earth or rock masses, removed or transferred in relation to an investment or mining of useful minerals containing natural radioactive isotopes, including their processing, shall not be qualified into the low-level radioactive waste category if the sum of the maximal concentration ratios of these isotopes, resulting from inhomogeneity of the waste, to the values established in Annex 1 to the Regulation does not exceed 10 for a representative 1 kg waste sample.

**Medium -Level Waste (LLW)**

Radioactive waste shall be qualified into the medium-level radioactive waste category if the radioactive isotope concentration in this waste exceeds the value established in Annex 1 to the Regulation more than ten thousand times, but no more than ten million times. In the case of waste containing various radioactive isotopes, this waste shall be qualified into the medium-level radioactive waste category if the sum of radioactive concentration ratios for each isotope in this

waste to the values established in Annex 1 to the Regulation exceeds 10 000, but does not exceed 10 000 000.

**High -Level Waste (HLW)**

Radioactive waste shall be qualified into the high-level radioactive waste category if the radioactive isotope concentration in this waste exceeds the value established in Annex 1 to the Regulation more than ten million times. In the case of waste containing various radioactive isotopes, this waste shall be qualified into the high-level radioactive waste category if the sum of radioactive concentration ratios for each isotope in this waste to the values established in Annex 1 to the Regulation exceeds 10 000 000.

Low-, medium- and high-level radioactive waste shall be divided into the three subcategories:

- Transitional waste – if the radioactive isotope concentration in this waste at the moment of generation thereof is such that in a 3-year-period it shall fall below the values determined for low-level waste;

- Short-lived waste – if it contains short-lived isotopes, and the average radioactive isotope concentration of long-lived isotopes in this waste does not exceed 400 kBq/kg and the maximal radioactive isotope concentration of long-lived isotopes in this waste, resulting from material inhomogeneity in a representative 1 kg sample, does not exceed 4 MBq;

- Long-lived waste – if the average radioactive isotope concentration of long-lived isotopes in this waste exceeds 400 kBq/kg.

Qualification to a category or division into sub-categories of radioactive waste shall be done on the basis of measurements of ionizing radiation emitted from the waste and calculations of the radioactive isotope concentration in the waste transferred for storage, processing, or disposal.

## 7.4. Storage conditions for radioactive waste and spent nuclear fuel

The storage conditions for radioactive waste and spent nuclear fuel are determined in the Regulation of the Council of Ministers of 3 December 2002 on radioactive waste and spent nuclear fuel and the Act of the Parliament of 29 November 2000 on Atomic Law.

The radioactive waste and spent nuclear fuel shall be stored in a way ensuring protection of humans and environment under normal conditions and in radiation emergencies, including protection against waste spilling, dispersal, or release. The radioactive waste shall be stored under conditions that facilitate segregation thereof according to the categories and sub-categories.

### 7.4.1. Warehouse for radioactive waste

The radioactive waste shall be stored in a facility or on premises (radioactive waste warehouse) outfitted with equipment for mechanical or gravitational ventilation and for cleansing the air removed from these premises, appropriate fire resistance, and protection against flooding.

The outer walls and ceilings of the radioactive waste warehouse and of the storage facility for spent nuclear fuel shall prevent the members of the general public from receiving an annual effective dose from all exposure pathways in excess of 0.1 mSv.

The radioactive waste warehouse and spent nuclear fuel storage facility shall be equipped with dosimetric equipment, appropriate for the type of emitted ionizing radiation and permanent or movable radiation shields.

The warehouse for radioactive waste that does not generate gases shall be equipped with ventilation preventing precipitation forming on the packaging surfaces and on the warehouse walls. However, the warehouse for radioactive waste that does generate gases or can cause radioactive contamination of the air shall be equipped with mechanical ventilation that facilitates reduction of the concentration of generated gases or contamination to a level negligible from the radiological protection viewpoint.

Facilities that have a special sewage system for liquid radioactive waste shall be equipped with at least two tanks ensuring the continuity of radioactive waste reception.

### 7.4.2. Packaging for radioactive waste storage

Packaging designed for radioactive waste storage (steel, concrete or plastic tanks or containers, drums or foil sacks) shall be adapted to the radioactive waste aggregation state and physicochemical properties. Packaging material cannot enter into chemical reactions with the radioactive waste.

Solid radioactive waste shall be stored in steel, concrete or synthetic plastic containers, drums or foil sacks of synthetic plastics with thickness exceeding 0.5 mm. Low-level wastes can be stored in plastic sacks. Storage of radioactive wastes classified into different categories and in a different state of aggregation, in the same packaging shall be inadmissible.

Liquid radioactive waste shall be stored in steel tanks with inner chemo-resistant coating, in concrete tanks with insides sealed and with chemo-resistant coating, or in laminated synthetic plastic tanks. In facilities that are not equipped with a special sewage system, liquid radioactive waste can be stored in containers or tanks of stainless steel or of synthetic plastic, with volumes that do not exceed 100 $dm^3$, and in glass or ceramic containers protected against mechanical damage, with volumes not exceeding 25 $dm^3$. The container or tank for radioactive waste storage shall be placed in a steel or concrete tub, covered from inside with chemo-resistant coating, with capacity not smaller than the volume of the container or tank placed in this tub.

Radioactive waste that contains alpha-radioactive isotopes and/or isotopes with half-lives not exceeding 65 days shall be stored separately from other liquid radioactive waste, in separate tanks or containers.

Liquid radioactive waste that contains organic solvents, extrahents and oils, or detergents in a concentration exceeding 10 $mg/dm^3$, or complex-forming substances in a concentration exceeding 10 $mg/dm^3$, or dissolved substances and deposits with content of dry residue exceeding 10 $g/dm^3$ shall be stored separately from each other.

### 7.4.3. Storage conditions for spent nuclear fuel

Spent nuclear fuel, after the cooling period in the reactor pool, shall be stored in a wet storage facility (aqueous environment) or in a dry storage facility under conditions ensuring that the temperature on the surface elements of spent nuclear fuel, permissible for a given type of nuclear fuel, shall not be exceeded and preventing the occurrence of self-sustaining nuclear fission reaction (preservation of sub-criticality). In calculations demonstrating the preservation of sub-criticality, it shall be admissible to take into account the burn-up level of stored spent nuclear fuel.

Preservation of sub-criticality shall be ensured in particular by maintaining an appropriate distance between individual spent nuclear fuel elements or by using neutron absorbers.

In the case of wet storage, the facility for spent nuclear fuel shall be subject to inspection, which will consist in verification of the quantity and arrangement of the fuel, water level in the storage facility, leak-tightness of the storage facility and water parameters such as a specific activity, temperature, chemical composition, and electric conductivity.

Moreover, the ionizing radiation dose rate and radioactive contamination in the storage facility and its surroundings shall be observed.

In the case of dry storage, the facility for spent nuclear fuel shall be subject to inspection, which will consist in verification of the fuel quantity and arrangement, leak-tightness of the containers enclosing spent nuclear fuel elements, temperature of spent nuclear fuel elements, and the ionizing radiation dose rate and radioactive contamination in the storage facility and its surroundings.

## 7.5. Requirements for surface and deep repositories

Deep and surface radioactive waste repositories shall be sited in areas, where the natural environment is subject to gentle evolution, and the conditions shaped by this evolution can be reliably forecasted for the periods of 500 years and 10 000 years for surface and deep repositories, respectively [11].

### 7.5.1. Selection of location

Site selection for deep and surface radioactive waste repositories shall be preceded by the investigation of considered sites from the viewpoint of social and economic conditions, including demographic conditions, site planning, ownership structure, and cultural and aesthetic values. Other important factors are geographic and natural conditions such as the geological structure and its evolution, geomorphology and its evolution, presence and importance of natural resources, hydro-geological conditions, including geochemical, hydrological, meteorological, and climatic conditions, threats to permanent stability of the site area arising from natural processes and those related to economic activity.

Deep geological radioactive waste repository cannot be sited in the areas of occurrence, or possible occurrence, of violent phenomena, including floods with probability higher than that for a 500-year water, increased seismic activity, normal or induced by human activities, increased tectonic activity or in the fault zone, and mass movements of grounds or rocks.

Unacceptable is location of a deep radioactive waste repository in the areas of occurrence of ground settlement or subsidence, karts phenomena or erosion landslide phenomena, and intensive linear or surface water and wind erosion. Furthermore, waste repositories should not be sited within areas of city agglomerations and concentrated settlements, in areas of higher social value (cultural, recreational and sanitary), protective zones for water intakes and protective areas for inland reservoirs, feeding zones of main and used reservoirs of underground waters, as well as in areas where activities consisting in mining useful minerals from deposits are conducted or deposits of useful minerals have been documented.

A surface repository for radioactive waste cannot be sited in areas defined for the deep radioactive waste repository and additionally below the ground water level and in territories where permanent or periodic inundation of repository elements can occur, in regions characterized by short water circulation pathways, which cause fast pollution migration to the biosphere or into used reservoirs of underground waters, below the water level of rivers or lakes in the vicinity, and in regions threatened by inundation, flooding by melting snow, or rainstorm water.

A deep repository shall be sited in geological formations ensuring the necessary thickness and expanse for the elements of the repository and for protective pillars.

The design and conduct of geological works and the preparation of geological documentation shall be regulated by the provisions of the geological and mining law. The results of geological, hydrological, environmental, social, economic, and other required investigations shall serve as the basis for nuclear safety and radiological protection analyses for a given repository [12].

### 7.5.2. Exploitation and repository closure

The packages in the repository facilities should be placed in a way to prevent damage thereof under their own weight. The reflux should be collected and purified, if required.

The nuclear waste should be disposed of in separate facilities in accordance with the classification:

- Short-lived low- and medium level radioactive waste,
- Low- and medium level disused sealed radioactive sources,
- High-level disused sealed radioactive sources

Additionally, environmental monitoring should be ensured. In particular, it should include measurements of the radioactive substance content:

- in surface waters present in the repository surroundings,
- in ground waters on the repository site, in drainage waters, and in ground waters in the repository surroundings,
- in tap water on the repository site and in its surroundings,
- in the air on the repository site,
- in grass and soil on the repository site and in its surroundings.

Additional monitoring includes measurements of the gamma dose rate on the repository site and in its surroundings, radioactive contamination on the repository site and on the surface of roads in the repository surroundings. Hydrological observations should comprise measurements of the ground water level on the repository site and in its surroundings and measurements of the

magnitude of atmospheric precipitation on the repository site and in its surroundings.

The surface radioactive waste repository, when its operation has been terminated, shall be closed up in a way that secures it, in particular, against infiltration of precipitation water into the repository, unintentional penetration by humans, and a destructive impact from the vegetation and animals.

### 7.5.3. Multibarrier concept

Safety barriers are physical and natural barriers preventing the release and spread of radioactive substances (Figure 7.3). These barriers are multistage:

- a chemical barrier - a soluble chemical compound (concentrate) binding radioactive isotopes;

- a physical barrier - a binding material (bonding agent), which causes waste fixation, prevents dispersion, spray and leaching of the radioactive material. The binder can be concrete, bitumen, and organic polymers;

- a first engineering barrier – waste packaging. The packaging protects against mechanical damage, atmospheric agents, and contact with water. Solid or solidified wastes are generally closed in metal containers or concrete, and in this form they are transported, stored, and disposed of;

- a second engineering barrier constitutes a concentrate storage construction. This is the additional protection against atmospheric agents waste, prevents corrosion of the packaging and migration of radioactive substances from the disposal place;

- a geological/natural barrier - a geological structure of the site. This barrier determines the choice of a place of the storage location. The ground must be primarily aseismic, unsinkable (e.g. at the time of the flood), little useful economically and away from clusters of human.

The multi-stage nature of the barrier system is an essential condition of its effectiveness in protection against spilling, dispersion, spraying, and leaching of radioactive substances, and thus, in prevention of their migration in the repository and its surroundings. Artificial and natural barriers should always be seen as complementary systems creating a multi-barrier system that provides effective protection.

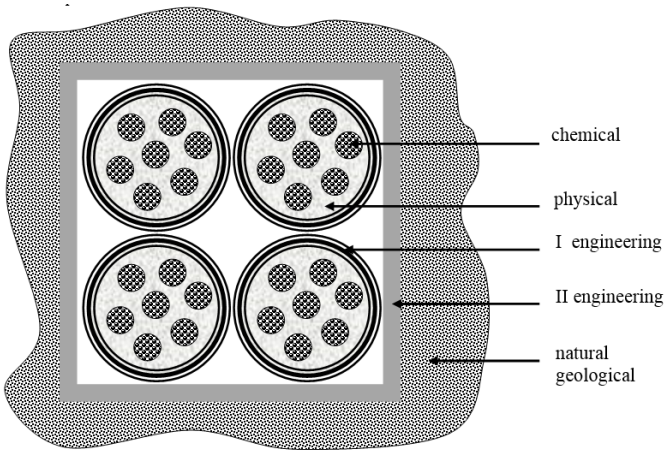


Figure 7.3 Multibarrier system for disposal of radioactive waste. Source: Own elaboration on the basis of [13].

## 7.6. Nuclear waste sources and quantities in Poland

Radioactive waste in Poland arises from research reactors and from applications of radioisotopes in industry, medicine, and science. There is no waste from operation of power reactors or spent fuel reprocessing activities in Poland. The pool-type research reactor Maria, which is used mainly for material testing and production of radioisotopes, has been in operation since 1976 at the National Centre for Nuclear Research in Świerk. Waste is both of solid and liquid form. The group of liquid waste constitutes mainly radioactive substances such as water solutions and suspensions. Solid waste group includes spent sealed radioactive sources, personal protection items polluted with radioactive substances (rubber gloves, protective clothing, footwear), laboratory material and equipment (glass, components of instruments, lignin, cotton wool, foil), used tools and elements of technological equipment as well as used sorptive and filtering material applied in the purification of radioactive solutions or air released from reactors and isotope laboratories (used ionites, post-fallout sludge, filters input etc.) [14].

The Radioactive Waste Management Plant (RWMP) is responsible for collection, transport, processing, and disposal of waste generated by radioactive waste users in Poland. The supervision over safety of waste management, including supervision over safety of waste disposal by the RWMP, is performed by the NAEA President.

The RWMP operates facilities situated within the territory of the Świerk center, which are fitted with equipment for radioactive waste conditioning.

The National Radioactive Waste Repository (NRWR) at Różan near the Narew River (ca. 90 km from Warsaw) is the site of radioactive waste disposal in Poland. According to the IAEA classification, the NRWR is a surface type repository dedicated for disposal of short-lived, low- and intermediate-activity radioactive waste (where the half-life period of radionuclides is less than 30 years). It is also used to store long-lived, mainly alpha radioactive waste, and spent sealed radioactive sources that are waiting to be placed in a deep repository (otherwise referred to as a geological or underground repository). The Różan repository has been in operation since 1961 and is the only facility of this type in the country. Since the disposal space is running short, it is scheduled to be closed down in 2020 [15, 16].

The amount of collected waste is relatively not very big because in Poland there is no nuclear power industry. The quantities of radioactive waste collected and processed over the last 8 years by the RWMP (including waste generated at the RWMP own premises) are shown in Table 7.2.

Table 7.2 Quantity of radioactive waste collected by the RWMP in 2007 – 2014

| **Waste sources** | 2007 | 2008 | 2009 | 2010 | 2011 | 2012 | 2013 | 2014 |
|---|---|---|---|---|---|---|---|---|
| | **Solid waste [$m^3$]** | | | | | | | |
| Outside Świerk centre (medicine, industry, research) | 17.27 | 12.68 | 9.21 | 21.27 | 14.87 | 8.9 | 18.1 | 7.4 |
| Radioisotopes Centre at the NCNR | 6.20 | - | 13.60 | 22.00 | 24.23 | 32.3 | 8.8 | 19.7 |
| MARIA reactor operation | 5.50 | 6.76 | 3.00 | 3.00 | 3.80 | 4.8 | 10.8 | 4 |
| Radioactive Waste Management Plant | 1.51 | 3.35 | 4.11 | 5.05 | 5.19 | 10.4 | 7 | 8.6 |
| In total: | 30.48 | 22.79 | 29.92 | 51.32 | 48.09 | 56.3 | 44.7 | 39.7 |

| Waste sources | 2007 | 2008 | 2009 | 2010 | 2011 | 2012 | 2013 | 2014 |
|---|---|---|---|---|---|---|---|---|
| | Liquid waste [$m^3$] | | | | | | | |
| Outside Świerk centre (medicine, industry, research) | 0.48 | 2.59 | 0.84 | 0.55 | 0.12 | 0.56 | 1 | 0.78 |
| Radioisotopes Centre at the NCNR | 0.02 | 0.05 | 0.04 | 0.04 | 0.04 | 0.1 | 0.4 | 0.15 |
| MARIA reactor operation | 84.00 | 29.00 | 53.00 | 25.50 | 22.00 | 22 | 27 | 20 |
| Radioactive Waste Management Plant | 0 | 6.00 | 6.03 | 10.00 | 4.00 | 26 | 0 | 0 |
| In total: | | 37.64 | 59.91 | 36.09 | 26.16 | 48.7 | 28.4 | 20.9 |

Source: Own elaboration on the basis of [17-23].

As regards the waste type and category according to the classification, the inventory of solid and liquid waste collected in 2001-2014 is presented in Figure 7.4.

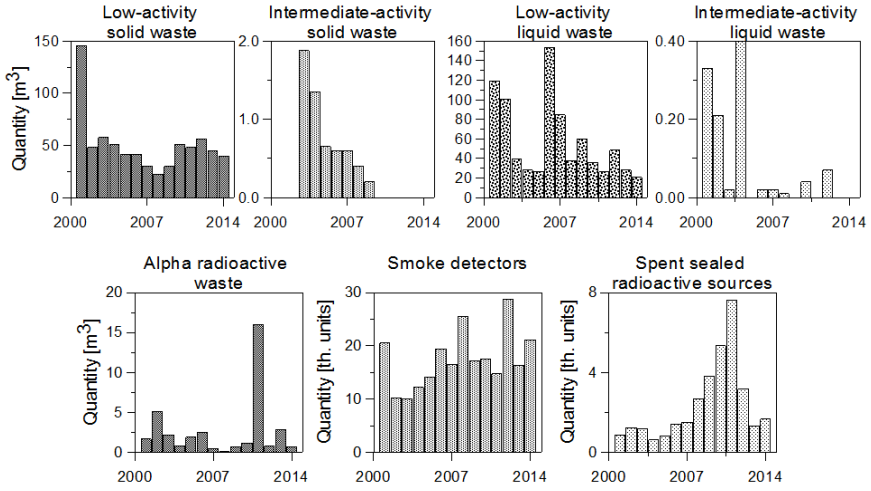


Figure 7.4 Radioactive waste type and category according to the classification. Source: Own elaboration on the basis of [17-23].

The data presented in Table 7.2 show systematically decreasing amounts of solid and liquid waste. This is due to the introduction of the new, improved technology of production of isotopes, proper exploitation of nuclear facilities, as well as a decline in the interest in the use of radioactive isotopes.

Given the forecast of total filling up of the NRWR by 2022, there is a need for building a new near surface radioactive waste repository for low- and intermediate-activity radioactive waste. It should be noted that the need to create such an object is independent of the acceptance of the Nuclear Energy Program or the construction of the nuclear power plant in Poland [24].

In 2009, the Ministry of Economy started preparation of the National Plan of Radioactive Waste and Spent Nuclear Fuel Management.

## References


[1] IAEA Safety Standards Series No. 111F, The Principles of Radioactive Waste Management, International Atomic Energy Agency, Vienna 1995

[2] IAEA Safety Standards Series No. Sf-1, Fundamental Safety Principles, Safety Fundamentals, International Atomic Energy Agency, Vienna 2006

[3] IAEA Safety Standards series no. GSG-1, Classification of radioactive waste, General Safety Guide, Guide International Atomic Energy Agency Vienna 2009.

[4] IAEA Safety Standards Series No. WS-R-1, Near surface disposal of radioactive waste, Requirements, International Atomic Energy Agency, Vienna 1999.

[5] IAEA, Technical, economic and institutional aspects of regional spent fuel storage facilities, IAEA-TECDOC-1482, International Atomic Energy Agency, Vienna 2005.

[6] IAEA, Multilateral Approaches to the Nuclear Fuel Cycle, INFCIRC/640, International Atomic Energy Agency, Vienna 2005

[7] IAEA, Safety of Radioactive Waste Disposal, Proceedings of an International Conference on the Safety of Radioactive Waste Disposal, International Atomic Energy Agency Vienna 2006.

[8] Radioactive Waste Repositories: Infrastructural Framework and Scenarios of Cooperation, IAEATECDOC-1413, International Atomic Energy Agency, Vienna 2004.

[9] Act of Parliament of 29 November 2000 Atomic Law.

[10] Regulation of the Council of Ministers of 3 December 2002 on radioactive waste and spent nuclear fuel.

[11] Geological Disposal Steps towards implementation Nuclear Decommissioning Authority Report no. NDA/RWMD/013, March 2010
[12] Developing multinational radioactive waste repositories: Infrastructural framework and scenarios of cooperation, IAEA, IAEA-TECDOC-1413, Vienna, 2004.
[13] Roger D. Spence, Caijun Shi, Stabilization and Solidification of Hazardous, Radioactive, and Mixed Wastes, CRC press, 2004.
[14] Report from I Workshop in Poland, IPPA FP7-269849, Project Deliverable 6.3, 2012.
[15] Implementing Public Participation Approaches in Radioactive Waste Disposal FP7-269849 Deliverable 6.6 (2.9), Katarzyna Szczygłów, Grażyna Zakrzewska, Institute of Nuclear Chemistry and Technology. Report summarizing hearing in Poland, 2013.
[16] Poland's National Report on compliance with the obligations of the joint convention on the safety of spent fuel management and on the safety of radioactive waste management, National Atomic Energy Agency, May, 2003.
[17] Działalność Prezesa Państwowej Agencji Atomistyki oraz ocena stanu bezpieczeństwa jądrowego i ochrony radiologicznej w Polsce w 2008 roku, Państwowa Agencja Atomistyki, Warszawa, czerwiec 2009 r.
[18] Działalność Prezesa Państwowej Agencji Atomistyki oraz ocena stanu bezpieczeństwa jądrowego i ochrony radiologicznej w Polsce w 2009 roku, Państwowa Agencja Atomistyki, Warszawa, czerwiec 2010 r.
[19] Działalność Prezesa Państwowej Agencji Atomistyki oraz ocena stanu bezpieczeństwa jądrowego i ochrony radiologicznej w Polsce w 2010 roku, Państwowa Agencja Atomistyki, Warszawa, czerwiec 2011 r.
[20] Działalność Prezesa Państwowej Agencji Atomistyki oraz ocena stanu bezpieczeństwa jądrowego i ochrony radiologicznej w Polsce w 2011 roku, Państwowa Agencja Atomistyki, Warszawa 2012 r.
[21] Działalność Prezesa Państwowej Agencji Atomistyki oraz ocena stanu bezpieczeństwa jądrowego i ochrony radiologicznej w Polsce w 2012 roku, Państwowa Agencja Atomistyki, Warszawa 2013 r.
[22] Działalność Prezesa Państwowej Agencji Atomistyki oraz ocena stanu bezpieczeństwa jądrowego i ochrony radiologicznej w Polsce w 2013 roku, Państwowa Agencja Atomistyki, Warszawa 2014 r.
[23] Działalność Prezesa Państwowej Agencji Atomistyki oraz ocena stanu bezpieczeństwa jądrowego i ochrony radiologicznej w Polsce w 2014 roku, Państwowa Agencja Atomistyki, Warszawa 2015 r.
[24] National report of Republic of Poland on compliance with obligations of the Joint Convention on the Safety of Spent Fuel Management and on the Safety of Radioactive Waste Management, Polish 5th national report as referred to in Article 32 of the Joint Convention, NAEA 2014.